Craniofacial gracilisation within *Homo sapiens* and its relationship to masticatory loading

Kira L. Crabtree

MSc by Thesis

The University of Hull and The University of York

Hull York Medical School

September 2023

Thesis Word Count: 47, 983

Abstract

It is frequently proposed that differences in craniofacial form are selectively and plastically driven by dietary differences, with species that consume mechanically challenging items having adaptations that increase bite force and optimise gape capacities, while also reducing strains experienced under masticatory loading. Paleoanthropologists commonly describe the crania of ancestral *Homo* species (such as *Homo ergaster*) as more robust that the crania of modern *Homo sapiens*. Interestingly, one area of increased robusticity in *H. ergaster* is the zygoma region, a key structure of the masticatory apparatus. Whether this zygoma region morphology is more optimal for consuming a mechanically challenging diet (relative to the morphology of *H. sapiens*) has yet to be investigated, nor have the global impacts of having a more robust zygoma region on craniofacial strains.

This thesis uses finite elements analysis to investigate the impact of simulating different masticatory loads, and changes in zygoma region morphology on craniofacial strains in a *H. sapiens* cranium. This involved constructing a *H. sapiens* cranial finite element model and subsequently using virtual anatomy techniques to create a hypothetical model containing *H. ergaster*-like zygoma regions. By comparing craniofacial strains, the efficiency of the jaw-elevator muscles, and bite force predictions in both models, the functional significance of the *H. ergaster*-like zygoma region is explored.

It is demonstrated that the zygoma region morphology of *H. ergaster* may be an adaptation to increase bite force and to reduce strains locally during bites at large gapes, however its importance in lowering strains during all masticatory loading scenarios remains questionable. It is therefore concluded that the gracile zygoma region of *H. sapiens* may be less of direct product of a release on selective pressures maintaining traits that reduce craniofacial strains, but consequential to less frequently performing bites at large gapes and reduced selective pressures on having large jaw-elevator musculature.

List of Contents

List of Figures

List of Tables

Author's Declaration

I confirm that this work is original and that if any passages or diagrams have been copied from academic papers, books, the internet, or any other sources these are clearly identified by the use of quotation marks and the references is fully cited. I certify that, other than where indicated, this is my own work and does not breach the regulations of HYMS, the University of Hull or the University of York regarding plagiarism or academic conduct in examinations. I have read the HYMS Code of Practice on Academic Misconduct, and state that this piece of work is my own and does not contain any unacknowledged work from any other sources.

Acknowledgements

Firstly, I would like to thank my supervisor, Dr. Laura Fitton, for her support through all stages of research behind this project and the writing of this thesis.

I am also deeply appreciative of the institutions and individuals who provided access to data that facilitated this research. Firstly, I would like to thank the New Mexico Decedent imaging database for access to the CT scan of a modern *Homo sapiens* individual. I would also like to thank the Department of Earth Sciences of the National Museum of Kenya for providing access to the CT scan of KNM-ER 3733. Thanks should also be given to Thomas Baird for kindly sharing his mandibular kinematic data.

1. Chapter 1: Introduction and Literature Review

Modern *Homo sapiens* have a distinct craniofacial configuration compared to extant primates and fossil hominin species. Compared to ancestral *Homo* species, the cranium of *H. sapiens* is said to be gracile, having a smaller facial skeleton, smaller teeth and muscles of mastication (Figure 1; Lieberman et al 2002; Demes and Creel 1988; Anton 1990; Brace 1991; Trinkaus 2003; O'Connor et al. 2005; Lieberman 2011; Eng et al. 2013; Oeschger et al. 2020). Alongside this increase in craniofacial gracilisation, the complexity of the extra-oral food processing behaviours of hominins has increased, developing from grinding, pounding and slicing raw plant and animal resources with stone tools, into the use of fire to cook foods, and subsequently into the diverse food preparatory behaviours used by modern *H. sapiens* populations today (Zink et al. 2014; Zink and Lieberman 2016). This combination of factors has led many researchers to suggest that modern *H. sapiens* have a reduced masticatory capabilities compared to earlier *Homo* species, having skulls that are poorly adapted to generate and withstand high masticatory forces (Demes and Creel 1988; Eng et al. 2013; Ledogar et al. 2016a; Godinho et al. 2018). As such, investigating relationships between craniofacial form and masticatory performance may be important in understanding the morphological variation apparent between modern *H. sapiens* and other members of the genus *Homo*.

However, the skull is a complex structure that hosts many different functional systems and features that co-develop and evolve, i.e. they are integrated, meaning changes to one structure or system can impact another (Cheverud 1982; Smith 1996; Lieberman et al. 2000; Mitteroecker and Bookstein 2008; Jung et al. 2023). Thus, understanding how alterations in craniofacial form impact masticatory performance and the mechanical loading of the skull could shed light on the mechanisms driving these morphological differences between *H. sapiens* and earlier members of our genus. Recent advancements in virtual anatomy and biomechanical modelling techniques offer ways to address such form-function questions (Rayfield 2007; O'Higgins et al. 2011). This review will therefore explore the functional anatomy of the masticatory apparatus within modern humans and fossil hominins, the evolution of food extra-oral processing technologies within hominins, how dietary differences

influence craniofacial form, and how the response of the cranium to masticatory loading can be investigated. Following this the aims and objectives this thesis will be outlined.

Figure 1. Lateral view of the crania of *Homo erectus*, *Homo heidelbergensis*, *Homo neanderthalensis* and *Homo sapiens* (left to right). *Image source: https://www.nhm.ac.uk/discover/homo-erectus-our-ancient-ancestor.html*

1.1. The functional anatomy of the masticatory system

The masticatory system is responsible for the breakdown of food in the oral cavity (Lucas 2004). The key elements of the system (Figure 2) include the upper and lower jaws, the dentition they contain, and the jaw-elevator musculature that attach to the mandible and cranium, including the temporalis, masseter and medial pterygoid muscles (Hylander 2006). The mandible and the cranium are articulated bilaterally at the temporomandibular joint (TMJ), which is a synovial joint containing a fibrocartilage disc that separates its articular surfaces (Alomar et al. 2007). Both the maxilla and mandible contain sets of dentition which contact food within the oral cavity, and are anchored to the alveolar bone via the periodontal ligament (Lucas 2004; de Jong et al. 2017).

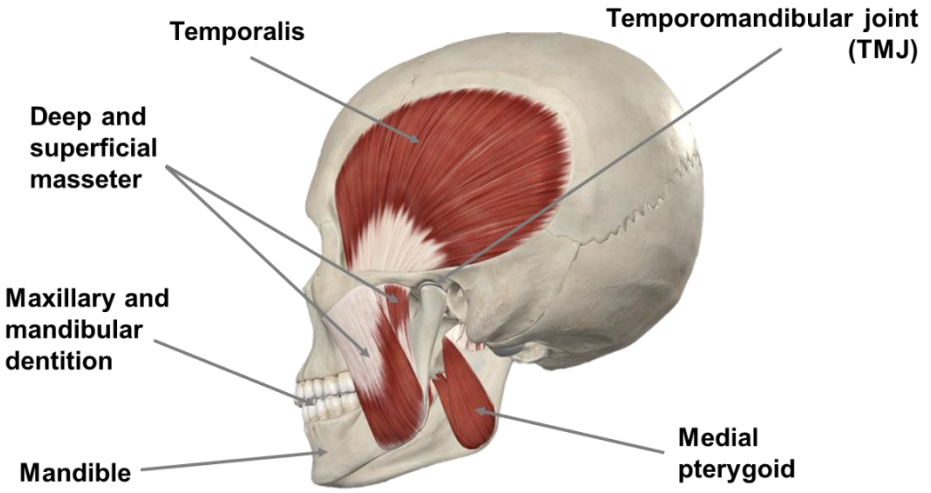

Figure 2. Anatomy of the masticatory system, demonstrating the origin and insertions of the jaw-elevator musculature (the masseter, temporalis, and medial pterygoid) on the crania and mandible, the articulation of the crania and mandible at the temporomandibular joint, and the maxillary and mandibular dentition.

The jaw-elevator muscles function to elevate the mandible, occluding the teeth and producing a bite reaction force, thus causing the breakdown food objects (Smith 1978; Weijs 1989; Hylander 2006; Koc et al. 2010). Bite force can be defined as the magnitude of force exerted by the jaw-elevator muscles on the occlusal surface of the teeth (Gu et al. 2021). The bite force magnitude an individual can produce varies due to the internal properties of the jaw-elevator muscles, as well as their spatial position in relation to both the TMJ and dentition (Hannam and Wood 1989; Raadsheer et al. 1999; Bonakdarchian et al. 2009; Custodio et al. 2011; Quiudini et al. 2017). Additionally, factors including the position of the bite along the dental row (Spencer 1999, 1998) and the extent to which the jaw is opened when the jaw-elevator muscles exert their force (Pröschel et al. 2008; Koc et al. 2012) also influence the bite force magnitude an individual can produce. While producing a bite force is essential to fracturing food objects, the resources an organism consumes need to first be placed and fit in the oral cavity between the occlusal surfaces. Therefore, another important determinant of the performance of the masticatory system is the extent to which the mouth can be opened, or gape (Smith 1984; Terhune et al. 2015a; Fricano and Perry 2019).

1.1.1. The Muscles of Mastication

The primary muscles of mastication are the masseter, temporalis and medial pterygoid (van Eijden et al 1997; Hylander 2006), and their combined function is the elevation of the mandible and the production of a bite reaction force (Hylander 2006; Koc et al. 2010). The masseter is quadratic, with deep and superficial heads originating along the inferior border of the zygomatic arch and inserting along the mandibular ramus and angle (Gaudy et al. 2000). The temporalis is a fan shaped muscle, originating in the temporal fossa on the lateral walls of the skull and inserting on the coronoid process and anterior border of the ramus of the mandible (Gaudy et al. 2002; Sedlmayr et al. 2009). Owing to its wide origins, the different fibres of temporalis perform different functions, with the anterior most fibres being more responsible for mandibular elevation and posterior most fibres for mandibular retraction and stabilisation (Korfage and Eijden 1999; Gaudy et al. 2002). The medial pterygoid is a deep muscle, originating on the medial surface of the lateral pterygoid plate of the sphenoid bone and inserting on the medial surface of the mandibular ramus and angle (El Haddioui et al. 2007).

The internal architecture of skeletal muscle impacts its mechanical function and therefore varies significantly between muscles (Lieber and Fridén 2000). Generalised skeletal muscle is made up of a hierarchical structure, with each muscle belly being composed of bundles of muscle fibres called fascicles that attach to its tendon or aponeuroses (Lieber and Fridén 2000; Trotter 2008; Huang 2020). The individual fibres within fascicles and are in turn made up of thinner myofibrils (Huang 2020). These are chained structures composed of repeating units of contractile structures called sarcomeres (Figure 3), which contain actin and myosin protein myofilaments (Huang 2020).

During muscle contraction, the length of sarcomeres shortens as the myosin filaments move across the actin filaments, forming cross-bridges between them and producing force (Huxley and Hanson 1954; Huxley and Niedergerke 1954). The magnitude of force produced by a sarcomere is a result of the extent of overlap between the two myofilaments and the number of cross-bridges formed force (Figure 3; Huxley and Hanson 1954; Huxley and Niedergerke

1954). Variations in the length of a muscle fibre affects the number of cross-bridges created during contraction, meaning this can impact the force production capacity of the sarcomeres within it (Banus and Zetlin 1938; Gordon et al. 1966; Burkholder and Lieber 2001). This means that muscles have an optimum length for force production, i.e. a length at which muscle fibres can generate the maximum forces they are capable of during contraction; if a muscle is stretched beyond this or compressed below this, their force production capacity decreases (Figure 3; Banus and Zetlin 1938; Gordon et al. 1966; Burkholder and Lieber 2001). This is known as the length-tension relationship of skeletal muscle and is visualised by length-tension curves as shown in Figure 3, describing how the length of a muscle during its contraction interacts with its force production capacity.

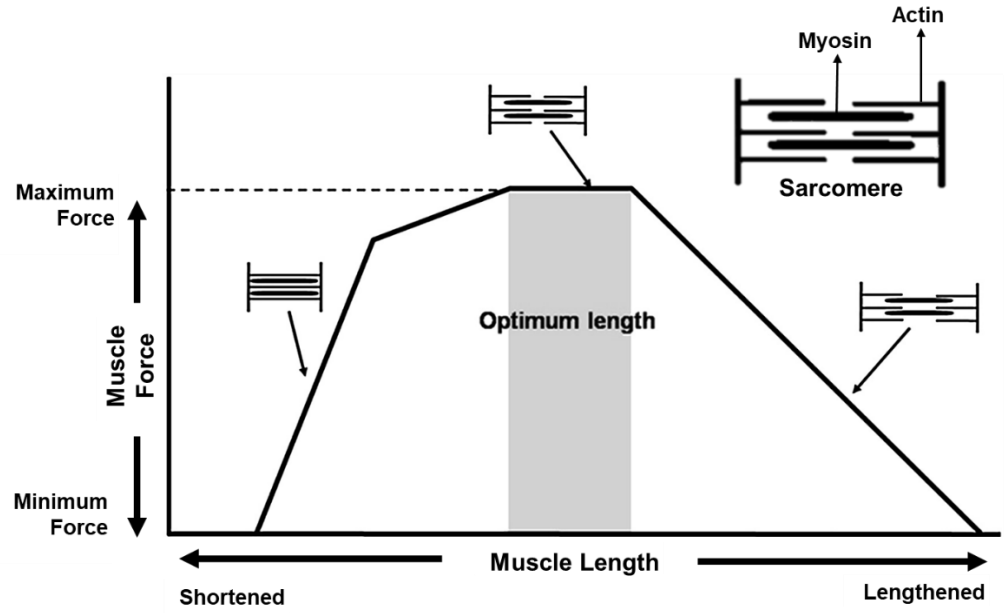

Figure 3. A generalised muscle length-tension curve, showing how increasing or decreasing the length of a muscle beyond its optimum length interacts with the cross-over of actin and myosin filaments in sarcomeres, and how this impacts the maximum force a muscle can produce. ***Image source: Tomioka et al. (2009).***

As mentioned, the macroscopic composition of individual muscles can also impact their mechanical function (Lieber and Fridén 2000). The maximum force a muscle can exert depends on the number of sarcomeres in parallel and the maximum excursion range of a muscle (i.e. the distances between maximum elongation to shortening) depends on the number of sarcomeres arranged in series (van Eijden et al. 1997; Lieber and Fridén 2000). These arrangements vary between muscles with different functions, and are determined by

the length of fibres within a muscle and its pennetion angle, or the angle at which fascicles attach to a tendon or aponeurosis of a muscle relative to its line of action (van Eijden et al. 1997; Lieber and Fridén 2000). Typically, muscles with high pennation angles function to produce maximal forces as the arrangement allows many sarcomeres to be arranged in parallel (van Eijden et al. 1997). However, this compromises on muscle fascicle length, and therefore muscle excursion, and velocity of contraction (van Eijden et al. 1997). Muscles with longer fascicle lengths allow a greater maximum excursion range and higher velocities of contraction as this configuration allows many sarcomeres to be arranges in series, while the maximal force they can produce is compromised (Lieber and Fridén 2000). The physiological cross-sectional area (PCSA) of a muscle is a measure the total area of the cross-sections perpendicular to the direction its muscle fibres, thus representative of the number of sarcomeres arranged in parallel and increases with pennation angle (van Eijden et al. 1997; Lieber and Fridén 2000). Anatomical dissections of the human masticatory musculature have demonstrated that compared to the jaw-depressor musculature, the jaw-elevators have larger PCSAs with larger pennation angles and shorter fibres lengths, demonstrating their architectural features are more suited to force production (van Eijden et al. 1997).

The force produced by a muscle can also vary depending on the activity it is performing. During the range of different biting tasks performed by the jaw-elevator musculature different patterns of muscle activation are apparent within each muscle and between the functional group (Hylander 2006). This refers to the distribution and number of fibres recruited by the central nervous system to perform a task within one muscle, as well as the relative degree of activation between muscles within one functional group and the symmetry of activation of paired muscles (Herring et al. 1979; Moore 1993; Merletti and Farina 2016). Within modern humans, *in vivo* data has demonstrated that the activation patterns of the masticatory musculature varies depending on a range of factors including the extent of jaw opening during biting, the location of a bite along the dental row and the magnitude of bite force required, among others (e.g Lindauer et al. 1993; Paphangkorakit and Osborn 1997; Spencer 1998; Miyawaki et al. 2001; Farella et al. 2008); similar findings have also been demonstrated by research performed on non-human primates and other mammals (e.g Herring 1976; Hylander and Johnson 1985; Hylander et al. 2005; Williams et al. 2007; Vinyard et al. 2008). Some of

these differences in muscle activation are due to how variability in the biting point impacts the lever mechanics of the masticatory system (see **Error! Reference source not found.**), and due to how jaw opening impacts the length-tension relationships of the masticatory musculature (see above).

1.1.2. The Lever Mechanics of the Masticatory System

In many biomechanical models of the masticatory system, mandibular elevation is modelled as a third-class lever. Here, the force produced by the jaw-elevator musculature functions as the effort force required to rotate the mandible about the TMJ, which functions as the fulcrum of the system, producing a bite at a specific tooth, which is the load of the system (Figure 4; Hylander 1975; Greaves 1978; Spencer 1999). This means that the bite force magnitude an individual can produce is a product of the spatial relationships between the masticatory musculature, TMJ and dentition (Hannam and Wood 1989; Raadsheer et al. 1999; Bonakdarchian et al. 2009; Custodio et al. 2011; Quiudini et al. 2017). This is because the ratio between the length of the in-lever (distance between the fulcrum and the applied effort) to the length of the out-lever (distance between the fulcrum and the point of applied load) determines the mechanical advantage (MA) of a lever system (Throckmorton et al. 1980; Norconk et al. 2009). Therefore, the MA of the jaw-elevator musculature can be improved by reducing the distance between the biting point and TMJ (the out-lever of the system) and by increasing the distance between the TMJ and the line of action of the jaw-elevators (the in-lever), allowing a higher bite force to be produced for a given input muscle force (Spencer 1999; Noback and Harvati 2015a).

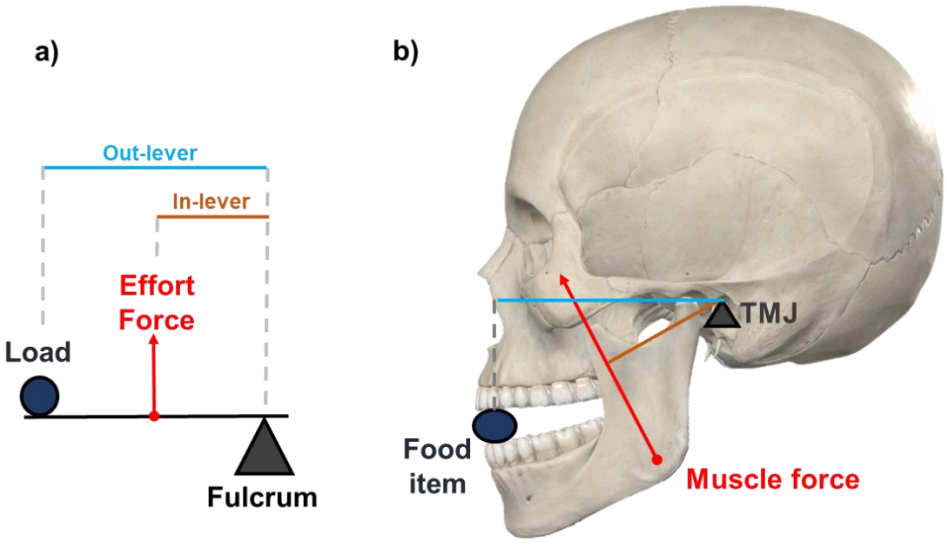

Figure 4. The lever mechanics of the masticatory system. a) Diagram of a generalised third-class lever system containing the fulcrum (dark grey), effort force (red), load (dark blue), as well as in-lever and out-lever distances (orange and light blue respectively). b) Visualisation of how mandibular elevation is modelled as a third-class lever for a modern human (where the TMJ serves as the fulcrum, the muscle force as the effort force and the bite point is the load) and the measures of in-lever and out-lever distances. The same colour correspondences are used between a) and b) to demonstrate how the different elements of the masticatory system function as the components of a third-class lever.

The maximum bite force an individual can produce also varies depending on where the bite is performed along the dental row. This is partially explained by the lever mechanics of mandibular elevation as moving the bite point posteriorly along the dental row will continually decrease the distance between the bite point and TMJ, thus increasing the MA of the masticatory muscles (Hylander 1975). However, *In vivo* bite force data recorded from modern humans indicate that this is not reflective of biological reality, as individuals typically produce maximal bites forces at the M^1, not the M^2 or M^3 (Edmonds and Glowacka, 2020). This is explained by the constrained lever model of jaw biomechanics (Greaves 1978; Spencer 1999), predicting that during the posterior-most bites, the resultant vector of the jaw-elevator muscles lies outside of a triangle of support of produced by the two TMJs and the biting point (Greaves 1978). This causes the working joint (the joint on the same side of the crania as the biting tooth) to be loaded in tension. To prevent this, the activation of the balancing side musculature is reduced, shifting the resultant back into the triangle of support and preventing the working joint from being loaded in tension, but causing bite forces to decrease at the posterior-most bites along the dental row (Greaves 1978; Spencer 1999, 1998).

Species known to consume mechanically challenging diets are suggested to produce high bite forces, through having large, mechanically advantageous jaw-elevator musculature with large PCSAs (Wright 2005; Wroe and Milne 2007; Santana, Dumont and Davis 2010; Campbell and Santana 2017; Ledogar et al. 2018; Taylor et al. 2018). Through examining morphological variability in the size and position of the masticatory apparatus in hominin fossils, high bite force capacities have been inferred for fossil hominins species. The anteriorly positioned zygomatic root of the australopithecines is hypothesized to be an adaptation for increasing the MA of the masseter (Rak 1983, 1988; Ward and Molnar 1980; Rak and Marom 2017). Furthermore, australopithecine fossils are noted to have laterally flaring zygomatic arches, sagittal crests and pronounced temporal lines indicative of large muscles of mastication (Robinson 1962a, 1962b; Wolpoff 1974; Du Brul 1977; Rak, 1978, 1983; Kimbel and Rak 1985; Rak and Marom 2017). These factors indicate that these hominins could produce high bite force magnitudes, and this is frequently argued to indicate adaptations to the consumption of a mechanically demanding diet (Robinson 1962b; Rak 1983; Walker et al. 1997; Wood and Strait 2004; Strait et al. 2013).

1.1.3. The functional trade-off between bite force and gape

When the jaw is opened within humans and most primates, the mandibular condyles rotate and anterior-inferiorly translate over the articular eminences, and onto the preglenoid plane during maximal opening (Wall 1999; Hylander 2006; Terhune 2011b). This causes the distance between the upper and lower dentition (i.e. gape) to increase (Smith 1984; Iriarte-Diaz et al. 2017; Fricano and Perry 2019). While this allows larger food objects to be placed between the occlusal surfaces, a functional compromise exists between the extent of jaw gape and maximal bite force capacity. In non-human mammalian taxa, *in vivo* bite force data has demonstrated that as gape increases, bite force decreases (Herring and Herring 1974; Dumont and Herrel 2003; Santana 2016). This is because as the jaw opens, the muscles of mastication are stretched beyond their optimum lengths, reducing the force they can produce (see section **Error! Reference source not found.** and Figure 5; Herring and Herring 1974; Terhune et al. 2015; Laird et al. 2023). The available *in vivo* bite force data for *H. sapiens* follow similar trends,

with the decrease in muscle force production that occurs during bites at wider gapes being compensated by an increase in muscle activation (Manns et al. 1979; Mackenna and Turker 1983; Paphangkorakit and Osborn 1997; Koc et al. 2012). It has been suggested that condylar translation within primates and other mammals is a kinematic adaptation to reduce jaw-elevator muscle stretch, thus maintaining more optimal lengths for these muscles during jaw opening (Carlson 1977; Hylander 1978; Wall 1999; Terhune 2011b). As such in many primate taxa that frequently perform bites at larger gapes are reported to have a relatively anteriorly-posteriorly elongated joint to increase mandibular translation allowing bite force to be retained at higher gapes (Terhune 2011a, 2013; Terhune et al. 2022). Other adaptations to this include having a low TMJ relative to the occlusal plane (Herring 1972; Herring and Herring 1974; Vinyard et al. 2003; Fricano and Perry 2019) and increasing muscle fibre length although this can compromise maximum bite force capacity (see section **Error! Reference source not found.**; van Eijden et al 1997; Taylor et al. 2009; Terhune et al. 2015; Hartstone-Rose et al. 2018; Taylor et al. 2018).

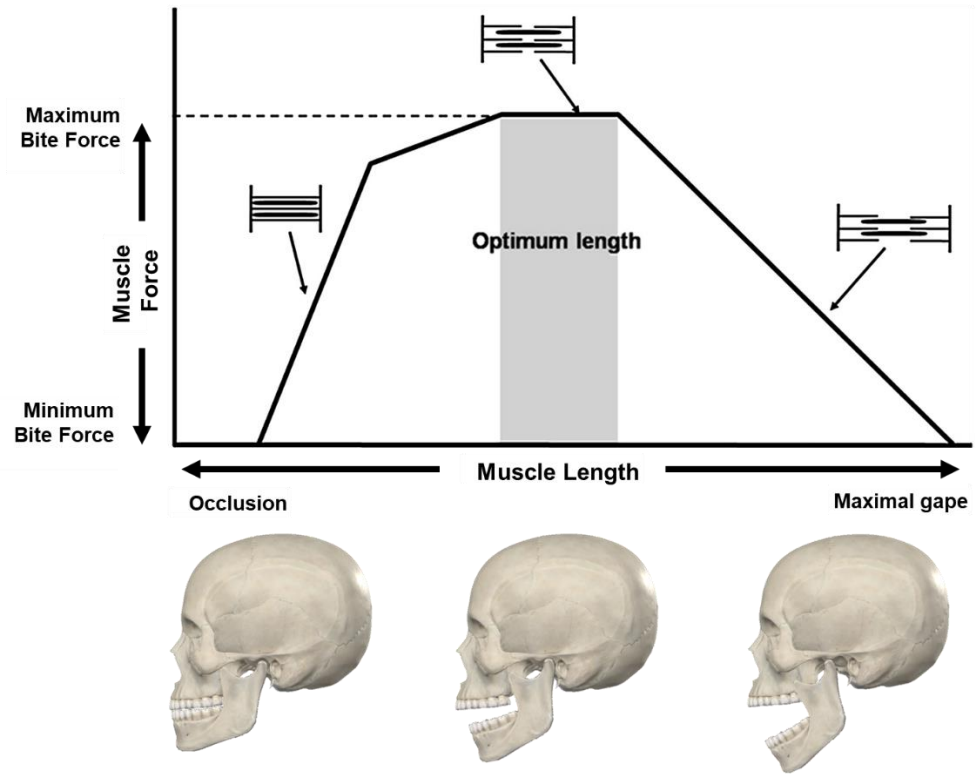

Figure 5. The generalised muscle length-tension curve from Figure 3, adapted to demonstrate how increasing and decreasing jaw gape interacts with bite force production due to the impact that changing the length of a muscle has upon force production. ***Image source: Tomioka et al. (2009).***

Behavioural and anatomical adaptations that facilitate wider gapes can also compromise bite force capacity. Gape capacities can be increased through moving the bite point further away from the fulcrum, either by performing bites on the anterior dentition and or through adaptively increasing the length of the dental arcade via increasing subnasal prognathism and mandibular length (Smith 1984; Terhune et al. 2015a; Fricano and Perry 2019). Further adaptations associated with producing large gapes include more posteriorly positioned jaw-elevator muscles origins relative to the dentition, which reduces muscle stretch for all the jaw-elevator muscles but particularly the masseter during jaw opening (Herring and Herring 1974; Terhune et al. 2015a; Fricano and Perry 2019). While more posteriorly positioned jaw elevator muscles facilitate higher gapes, this decreases their MA compromising bite force production, as does engaging in more anterior bites and increasing subnasal prognathism (Smith 1984; Spencer 1999; Vinyard et al. 2003; Terhune et al. 2015a; Godinho et al. 2018). Interestingly, bony adaptations that facilitate larger gapes are apparent within hominin fossils. For example the reduction in the height of the canines and increased subnasal prognathism of the australopithecines (Hylander 2013), as well as the retromolar gap (space between the

mandibular ramus and the distal border of the M_3), posteriorly positioned zygomatic root, and relatively low height of the coronoid process of *Homo neanderthalensis* (Rak and Hylander 2003). Therefore, how a species feeds, what is feeds on, its maximum performance capacities, and its anatomy are all interrelated, however the mechanical demands of the masticatory apparatus are not the only thing the cranium has to adapt to.

1.1.4. The Mechanical Loading of Bone

When an object is mechanically loaded with an external force, stresses (applied force per unit area; σ) and strains (the ratio between the change in length to the original length; ε) are induced within an object due to its deformation under load (Currey 2006). The type of stress and strain experienced by an object under load depend on the axis of loading and whether an object is loaded in compression, tension, shear etc (Currey 2006). As increased force is applied to an object, the resulting deformation and subsequent stresses and strains it experiences increase proportionately until the yield point of an object its reached (Currey 2006). The yield point of a material is the extent to which it can be elastically deformed, meaning it will return to its original dimensions if the loading is halted (Figure 6; Currey 2006). When objects deform or recover proportionately to the stresses and strains they experience during elastic loading, they are described as linearly elastic (Currey 2006), however as most biological objects contain a high-water content meaning that when deformed elastically they do not recover to their original dimensions instantaneously, and are referred to as visceoelastic (Currey 2006). The deformation of linearly elastic objects, and resulting stresses and strains, under load is proportional to the magnitude of force applied to them; this relationship between stress, strain and applied force in linearly elastic materials is described by Hooke's Law (Vinckier and Semenza 1998; Giuliodori et al. 2009). Further, when objects are linearly elastic and are strained, the ratio of the change in width per unit of an object compared to its change in length per unit can be expressed as its Poisson's ratio, which denotes the deformation of a material in the direction perpendicular to an axis of loading (Lucas 2004; Berthaume 2016). The stiffness of a material is a measure of how able it is to resist elastic deformation, and this is quantified as the Young's Modulus (*E*) of a material, which is calculated as the gradient of the

slope of a material's stress-strain curve within the zone of elastic deformation, prior to its yield point (Figure 6; Berthaume 2016).

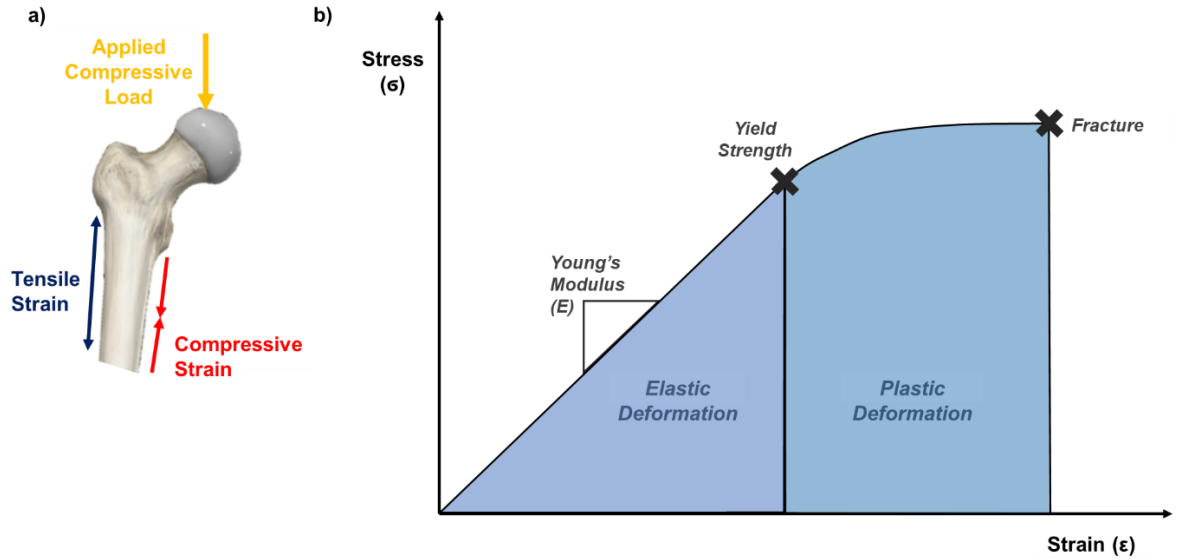

Figure 6. The mechanical loading of biological objects. a) The simplified, theoretical tensile (blue) and compressive (red) strains experienced by a proximal femoral shaft when the head is loaded in compression (orange). b) The hypothetical stress-strain curve of the femur showing its Young's Modulus (E), yield strength, failure point, and its behaviour during both elastic (purple graph area) and plastic deformation (blue graph area).

If an object is loaded beyond its yield point, irreversible changes occur to an object, which is referred as plastic deformation, and when an object is loaded beyond plastic deformation, it will eventually fracture and fail (Currey 2006). Different materials behave differently under plastic deformation. Some materials can withstand considerable deformation beyond their yield point before they fracture, i.e. they are ductile. Others fracture immediately after reaching their yield point, i.e. they are brittle (Currey 2006). For an object to fail entirely initiated fractures must be propagated through it, and the 'toughness' of a material is a measure of a materials resistance to crack propagation following fracture (Currey 2006). Such materials are often termed 'displacement-limited' meaning they fail after considerable displacement, as opposed to high stresses (Berthaume 2016; Lucas 2004). Other materials can be described as 'stress-limited', meaning high stresses are required to initiate fracture (Lucas 2004; Berthaume 2016), and these require high force to initiate fracture as stress is proportionate to applied force (as described by Hooke's law, see above).

In reality, biological objects are made up of multiple different tissues containing materials with a range of mechanical properties (Lucas 2004; Berthaume 2016). The term 'heterogeneous' can be used to described materials with spatially variable mechanical properties; homogeneity is the opposite of this where mechanical properties of a material are the same throughout (Berthaume 2016). Furthermore, the mechanical properties of a material can depend on the axis of loading, such material are called anisotropic (Currey 2006). Isotropy is the opposite state, meaning that the properties of a material are consistent in all axis of loading (Currey 2006). On a gross scale, the physical size and shape of objects can also impact how they respond to mechanical loading.

1.1.5. The physiological response of bone to mechanical loading

During feeding, the cranium experiences stresses and strains through the transmission of bite reaction forces into food objects, the maxillary dentition, and the facial skeleton, and through the contractile force of the masticatory musculature (Endo 1965; Hylander et al. 1991; Herring et al. 2001). Craniofacial strains under masticatory load in a range of species have been predicted and recorded, through biomechanical models and *in vivo* strain gauge experiments (see section 1.4). The masticatory apparatus, and the cranium as a whole, therefore needs to be adapted to withstand the mechanical loads it is routinely exposed to, meaning it needs to be strong enough to resist fracture while not wasting energy by being excessively massive (Currey 2003b, 2003a, 2012). This is controlled by both genetic and epigenetic processes (Currey 2003b, 2006). On a selective level, this may lead to the selection for features associated with reducing masticatory strains.

As with all biological objects, when bone is mechanically loaded through muscle contractions and reaction forces, it deforms and experiences stresses and strains. The forces and subsequent strains that bone experiences during loading create areas of microdamage, which are though to be detected by specialised bone cells called osteocytes (Lanyon 1993; Katsimbri 2017). Following this, cells specialised to remove bone tissue, osteoclasts, are activated and

attach to bone and begin resorption in micro-damaged areas (Currey 2006; Katsimbri 2017). To fill the cavity left by the resorption of bone, osteoblasts secrete collagen and bone matrix, which is subsequently mineralised to form new bone (Currey 2006; Katsimbri 2017). This process of bone resorption and formation underpins its modelling and remodelling. Bone modelling is the process through which the form of bone can change in response to mechanical loads (and physiological influences) and is the predominant process in shaping bones during their growth in childhood (Katsimbri 2017). During modelling bone resorption and formation are not tightly coupled, allowing bones to increase in size and change shape (Katsimbri 2017). On the other hand, during bone remodelling resorption and formation are more tightly coupled, with old bone being replaced with newly deposited matrix, functioning to maintain bone strength, and is the predominant process shaping bone in adulthood, although bone remodelling does occur during childhood (Katsimbri 2017). Combined, these processes prevent the accumulation of microdamage and maintain the structural integrity of bone during mechanical loading, as well as allowing changes to the shape of a bone during the lifetime of an individual.

It is theorised that changes in the mechanical environment of bone induce changes to the architecture of bone, allowing the suitable resistance of routinely applied loads. The 'mechanostat' theory of bone adaptation to mechanical loading predicts that bone can detect changes to the strains regimes they routinely experience, and that their strength is adapted accordingly by changing their microstructure, mass and form to withstand habitually applied loads without failing (Frost 1987, 2003; Pearson and Lieberman 2004; Ruff et al. 2006). Accordingly, in areas where strains over a particular threshold are experienced, bone formation increases to provide reinforcement, thus reducing the strains experienced under load (Skerry 2008; Rucci 2008; Mellon and Tanner 2012). Alternatively, in areas where strains experienced are lower than a given threshold, bone resorption increases to decrease bone mass and reduce energy wastage (Skerry 2008; Rucci 2008; Mellon and Tanner 2012). These principles have been affirmed from *in vivo* experiments on a range of animals dedicated to investigating the response of bone to mechanical loading (Meakin et al. 2014). This research has demonstrated that the increased bone formation due to increase mechanical loading is a product of dynamic rather than static loading, that the rate of formation is most closely

correlated with peak strain magnitude and strain rate during loading and unloading (Lanyon and Rubin 1984; Judex et al. 2007; Meakin et al. 2014).

When the response of the craniofacial skeleton mechanical load is investigated, dietary differences between organisms are repeatedly reported to impact craniofacial growth and bone modelling (see section 1.3; Lieberman et al. 2004; Ravosa et al. 2008; Menegaz et al. 2010; Spassov et al. 2017). Within hominin palaeontology, many suggest that the anterior nasal pillars of gracile australopithecines are associated with reducing strains induced by premolar loads (Rak 1983; Strait et al. 2009; Ledogar et al. 2017). The laterally expanded, straight and deep zygomatic roots in australopithecines are also suggested to be important in the reduction of masticatory strains induced by bite reaction forces and the contraction of the masseter (Rak 1983; Demes 1987; Ledogar et al. 2017). Furthermore, many have suggested that both robust supraorbital features and midfacial projection of archaic *Homo* (particularly *H. neanderthalensis*) represent adaptations to reducing strains during anterior bites (Oyen et al. 1979; Russell et al. 1985; Rak 1986; Demes 1987; Endo and Adachi 1988; Hilloowala and Trent 1988; Spencer and Demes 1993). Therefore, the form of the masticatory system locally and the craniofacial skeleton globally is impacted by both selective and plastic processes associated with the generation and resistance of mechanical forces.

1.2. Food material properties, dietary adaptations and the evolution of the genus *Homo*

As with all biological objects, food objects vary in their physical and mechanical properties, which impacts how they deform and fracture when they are clenched between the occlusal surfaces of an organism by the jaw-elevator muscles (see section 1.1.4 for more details surrounding the mechanical properties of biological materials). It is common for displacement-limited materials to be described as 'tough' food objects, whereas stress-limited materials are often described as 'hard' food objects (Lucas 2004; Berthaume 2016). Therefore, hard objects (e.g. Figure 7) require high bite forces to initiate fracture (Lucas 2004; Berthaume 2016). Tough food items (e.g. Figure 7), however, require multiple chewing cycles for fractures

to be initiated and cracks to be propagated (Lucas 2004; Berthaume 2016). Food objects can also vary in their physical size, meaning that an organism may need to perform bites at a range of gapes depending on. Thus, feeding on different dietary resources impacts how the cranium is mechanically loaded and places different selective requirements on the form of the masticatory system. As such, the considerable changes that have occurred to the craniofacial skeleton during the evolution of the hominin lineage (Figure 8) may have been fuelled by dietary differences between species and by the intensification of extra-oral food processing within the genus *Homo*.

Figure 7. Examples of hard and tough foods. The leaves (left) are a tough food and the nuts (right) are a hard food. ***Image sources (from left to right):*** ***https://www.bigplantnursery.co.uk/shop/plants/flowers-and-grasses/setaria-palmifolia-chb-2017/*** ***and*** ***https://www.ohnuts.com/buy.cfm/bulk-nuts-seeds/brazil/in-shell*****.**

The genus *Homo* first appears in the fossil record in the form of a mandible fragment from the site of Ledi-Geraru, dated to between 2.8-2.5 million years ago (Villmoare et al. 2015). The Ledi-Geraru specimen demonstrated that a divergence from the australopithecine masticatory anatomy was a key phase in the evolution of *Homo* (Villmoare et al. 2015). Compared to *Homo*, the australopithecines (4.2-2.9 million years ago; Alemseged 2023) have small endocranial volumes, projecting midfacial skeletons, large masticatory muscles, pronounced subnasal prognathism, as well as large and robust mandibles that host large, thickly enamelled dentition (Figure 8; Kimbel et al. 1984; Grine 1988; Lieberman 2011;

Alemseged 2023). Having anteriorly positioned and large muscles of mastication, as well as large facial skeletons containing traits proposed to reduce masticatory strains, these species are frequently described as to being well adapted to generating and withstanding high bite forces indicating the consumption of mechanically challenging diets (Robinson 1962b; Wolpoff 1974; Du Brul 1977; Ward and Molnar 1980; Rak 1983; Kimbel et al. 1984; Kimbel and Rak 1985; Rak and Marom 2017). With the emergence of the genus *Homo*, endocranial volume and neurocranial globularity increased, reducing the projection of the smaller, more vertically oriented midfacial skeleton, with smaller masticatory muscles, less pronounced subnasal prognathism and smaller dentition (Figure 8; Lieberman 2011; Lacruz et al. 2019). These anatomical changes indicate significant dietary changes between australopithecines and early *Homo* (Robinson 1962a; Walker et al. 1997; Wood and Strait 2004; Ungar 2006; Ungar and Sponheimer 2011; Strait et al. 2013; Teaford et al. 2023).

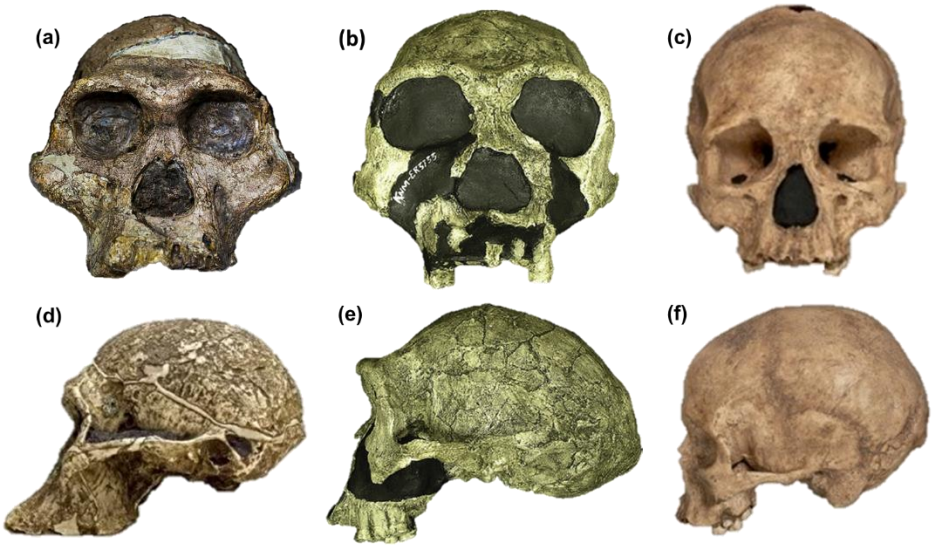

Figure 8. Frontal and lateral view of hominin crania including *Australopithecus africanus* (a and d), *Homo ergaster* (b and e) and *Homo sapiens* (c and f). *Image sources (from left to right by species): https://www.prints-online.com/t/164/australopithecus-africanus-cranium-sts-5-8595745.jpg.webp and https://ccschmitt.github.io/STS%205%20%28Mrs.%20Ples%29.html; (Simpson, 2015); and https://www.nature.com/articles/nature.2017.22114*

Compared to ancestral *Homo,* the facial skeleton of *H. sapiens* is small in all anatomical dimensions, as is the maxillary and mandibular dentition (Brace 1991; Lieberman 2011; Lacruz

et al. 2019; Oeschger et al. 2020). First appearing in the fossil record approximately 315,000 years ago at Jebel-Ihroud (Hublin et al. 2017; Richter et al. 2017), the facial skeleton is retracted under the anterior cranial fossa of a globular neurocranium with a large endocranial capacity (Lieberman et al. 2002). This gives *H. sapiens* an orthognathic (non-projecting) facial profile compared to earlier hominin species, where the facial skeleton projects forwards from the anterior cranial fossa (Enlow and Mcnamara 1973; Lieberman 1998; Lieberman et al. 2000; Lieberman et al. 2002; Lieberman et al. 2004; Bastir et al. 2008; Bastir and Rosas 2016). This orthognathic facial profile is accentuated by the reduction in the anterior projection of the premaxillary region, or subnasal prognathism (Norman 1999; Spoor et al. 2005; Laird et al. 2016; Lesciotto et al. 2016). Most cranial superstructures including large supraorbital tori and sagittal keels are comparatively diminished (Lahr and Wright 1996; Lieberman 2011) and the infraorbital profile is concave due to the presence of a canine fossa (Maddux and Franciscus 2009; Trafí et al. 2022). Through measurements of their bony attachments, it has been shown that the jaw-elevator musculature of *H. sapiens* is smaller than that of earlier hominins (Demes and Creel 1988; Anton 1990; Antón 1996; O'Connor et al. 2005; Eng et al. 2013). This combination of features lead to the description of the facial skeleton of *H. sapiens* as gracile (Trinkaus 2003; Lieberman et al. 2002; Lieberman 2011; Ledogar et al. 2016a; Godinho et al. 2018), resulting in suggestions that *H. sapiens* is poorly configured to withstand high bite forces and not adapted to the consumption of a mechanically challenging diet (Lieberman 2011; Ledogar et al. 2016a; Godinho et al. 2018).

1.2.1. The evidence for extra-oral food processing in the genus *Homo*

The use of fire to cook dietary resources is hypothesized to have been imperative to the evolution of increased cranial volume and reduced masticatory apparatus of the genus *Homo* (Wrangham et al. 1999). The emergence of African *Homo erectus*, or *Homo ergaster*, the earliest species who's status in the genus is relatively uncontested (Wood 1992; Wood and Collard 1999b, 1999a), at 1.9 million years ago has been specifically connected to the habitual use of fire to cook food resources (Wrangham et al. 1999; Wrangham 2017). While there is evidence to connect traces of burning events and hominin activity from the FxJj20 complex at Koobi Fora (1.5 million years ago; Hlubik et al. 2019), the earliest evidence for habitual fire usage dates to 350,000 years ago from Tabun Cave in the Levant in the form of stratified

sequences of burnt flint (Shimelmitz et al. 2014). However, this does not mean that *H. ergaster* did not use extra-oral food processing technologies at all (Zink et al. 2014).

There is archaeological evidence suggesting that *H. ergaster* used stone tools to process carcasses and plant materials (Keeley and Toth 1981; Diez-Martin et al. 2010; Pobiner et al. 2008; Ferraro et al. 2013; Plummer and Bishop 2016; Semaw et al. 2020; Yravedra et al. 2020). The shape edges on hand axes and scrapers (Figure 9) could have been used to slice food items, and tools like hammerstones and anvils (Figure 9) could have been used as pounding or grinding instruments (Zink et al. 2014). These suggestions are supported by cutmarks on carcasses and polishes on stone tools (Keeley and Toth 1981; Pobiner et al. 2008; Ferraro et al. 2013; Yravedra et al. 2020). Furthermore, paleodietary proxies (dental microwear and carbon isotopes from enamel bioapatite) indicate that *H. ergaster* consumed a diet including both hard and tough objects from animal and plant sources (Lee-Thorp and Sponheimer 2006; Ungar et al. 2006; Ungar and Sponheimer 2011; Teaford et al. 2023). Therefore, while the archaeological evidence that *H. ergaster* habitually used fire to cook foods is limited (Attwell et al. 2015; Chazan 2017), this species was likely engaging in other extra-oral food processing technologies that may have released selective pressures upon the robusticity and force production capabilities of the masticatory system (Eng et al. 2013) and facilitated encephalisation (Aiello and Wheeler 1995).

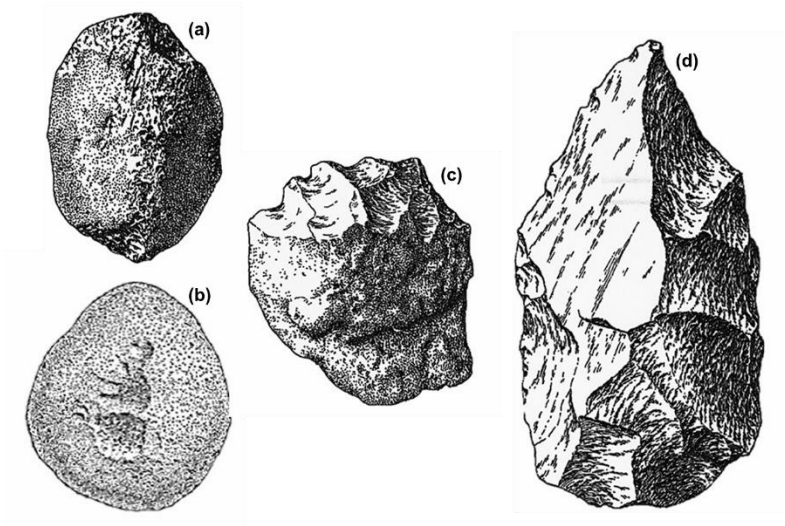

Figure 9. Diagrams of a selection of Oldowan and acheulean stone tools. (a) hammerstone. (b) anvil. (c) scraper. (d) handaxe. *Image source Favreau (2023).*

1.2.2. Food mechanical properties and extra-oral processing techniques

The changes in mechanical properties of ancestral hominin dietary resources following the intensification of extra-oral food processing technologies have been speculated to explain craniofacial gracilisation in *H. sapiens* (Lieberman 2011; Zink et al. 2014; Ledogar et al. 2016a; Zink and Lieberman 2016). Previous research has addressed how the mechanical properties of food objects are impacted by basic food processing behaviours (e.g. grinding, pounding, slicing etc) and more complex food processing behaviours (e.g. cooking; Dominy et al. 2008; Zink et al. 2014). Additional research has addressed the impacts that the chewing foods processed in these ways has upon the masticatory effort (i.e. number of chews and muscle activation) of *Homo sapiens* individuals (Zink and Lieberman 2016; Van Casteren et al. 2022). Dominy et al. (2008) and Zink et al. (2014) both found that the toughness of plant tubers decreased following cooking, while the toughness of the muscle fibres of meat increased (Zink et al. 2014). Subsequently, Zink and Lieberman (2016) found that following both cooking and pounding, tubers required less muscle recruitment to chew due to their decreased toughness, and slicing reduced the muscle recruitment required to chew meat (Zink and Lieberman 2016). It was therefore concluded that a reduction in masticatory robusticity was likely facilitated by increased used of basic food processing techniques within early *Homo*, but not exclusively through cooking (Zink and Lieberman 2016).

Interestingly, the chewing of cooked of tubers has been reported to reduce masticatory muscle recruitment by 15% within *H. sapiens* individuals, which would facilitate selection for a 14% reduction in molar area (Zink and Lieberman 2016), a value similar to the reduction in dental size between *Homo sapiens* and *Homo ergaster* (McHenry 1994). The temporal proximity for the first evidence of habitual fire usage (350,00 years ago; Shimelmitz et al. 2014) and the emergence of anatomically modern *H. sapiens* (315,000 years ago; Hublin et al. 2017; Richter et al. 2017) may point to an association between the increase in craniofacial gracilisation between *H. sapiens* and *H. ergaster* and the habitual use of cooking to prepare dietary resources. This could be a product of both a reduction on selective pressures maintaining the size of the masticatory muscles and robusticity of the facial skeleton (Zink et al. 2014; Zink and Lieberman 2016), as well as due a reduction in craniofacial strain impacting bone formation within the facial skeleton (Ravosa et al. 2008; Lee and Moon 2012).

While these authors discuss how craniofacial gracilisation within *Homo* may be a product of a reduction in masticatory effort following the habitual use of food processing technologies (Zink and Lieberman 2016; Van Casteren et al. 2022), the impacts that this may have had upon food object size, and subsequently the form of the facial skeleton are less explicitly discussed. Yet, these basic food processing behaviours reduce the size of a food item form its unprocessed form (Zink et al. 2014), also potentially altering the mechanical environment of the cranium. Firstly, this change to the size of dietary objects could have reduced selective pressures on features like subnasal prognathism that increase gape capacities for large object feeding (Rak and Hylander 2003a; Hylander 2013). Secondly, this would allow food objects to be compressed between the more mechanically advantageous posterior dentition (Strait et al. 2009), meaning less muscle force would be required to produce the necessary stresses required to fracture an item, potentially reducing the selective pressures upon maintaining large jaw-elevator muscles (Wroe et al. 2010). Both may have contributed to craniofacial gracilisation within *H. sapiens.*

1.3. The influence of dietary differences on craniofacial form

Theoretically, the consumption of a harder and or tougher diet will increase the frequency and magnitude of craniofacial strains, leading to increased craniofacial growth. This has been demonstrated through controlled feeding studies where extant samples of small mammals are divided into two groups, with one being fed a control diet, and the other fed an artificially softened, hardened, or toughened diet (Beecher et al. 1983; Kiliaridis et al. 1985; Kiliaridis 1986; Engström et al. 1986; Ito et al. 1988; Ciochon et al. 1997; He 2004; Lieberman et al. 2004; Menegaz et al. 2010; Spassov et al. 2017). Following this, the influence that dietary differences between groups have upon global craniofacial growth and muscle internal architecture are analysed (Menegaz et al. 2010; Lieberman et al. 2004; Spassov et al. 2017). Typically, the populations consuming softer diets exhibit lower rates of craniofacial growth, increased rates of malocclusion and a reduction in the force production capabilities of the masticatory musculature (Kiliaridis 1986; Ciochon et al. 1997; Beecher et al. 1983; He 2004; Menegaz et al. 2010; Spassov et al. 2017). These studies demonstrate how dietary differences impact the mechanical loading of the cranium, and thus its phenotypical plasticity (Beecher et al. 1983; Kiliaridis 1986; Ciochon et al. 1997; Menegaz et al. 2010; Spassov et al. 2017).

One limitation of these studies is that the differential craniofacial growth between groups is not quantified in relation to *in vivo* strain data (Lieberman et al. 2004). As such, Lieberman et al. (2004) integrated *in vivo* strain data with the analysis of how the consumption of a cooked diet impacts with craniofacial growth in the rock hyrax (*Procavia capensis*). This species was chosen for use within this research as it is retrognathic, defined by the authors as a facial shape where the post-canine dentition is situated inferiorly to the orbits rather than the rostrum (Lieberman et al. 2004). As this is a trait shared with *Homo sapiens*, inferences into how dietary differences may impact craniofacial strain and growth could be made from this research (Lieberman et al. 2004). It was found that the rock hyrax crania experienced higher strain magnitudes when consuming raw foods versus cooked foods, and that individuals raised on cooked foods had reduced craniofacial growth compared to their raw food fed counterparts, concluding that advancements in food processing techniques may have resulted in decreased craniofacial growth in *H. sapiens* (Lieberman et al. 2004). However, conducting similar experiments upon *H. sapiens* is difficult for methodological and ethical reasons (see section 1.4). To this end, previous researchers have correlated histological observations of

bone remodelling to *in silico* predictions of masticatory strains (see section 1.4.1) to elucidate relationships between masticatory loading and craniofacial form in *H. sapiens* (Brachetta-Aporta and Toro-Ibacache 2021). Others have analysed form differences in the crania of *H. sapiens* populations assumed to consume different diets to quantify the impacts this may have has upon craniofacial form (see section 1.3.2; Varrela 1990, 1992; Spencer and Ungar 2000; Sardi et al. 2004; 2006; Pinhasi et al. 2008).

1.3.1. Craniofacial variation within fossil hominins and its relationship to diet

As discussed, craniofacial form varies significantly within the hominin lineage. The australopithecines are known for having robust features while increasing craniofacial gracilisation within *Homo* is argued to be a product of the increasing complexity of food processing behaviours throughout the evolution of the genus (Zink et al. 2014; Zink and Lieberman 2016). Interestingly Demes and Creel (1988) predicted that *Homo ergaster* could produce bite forces comparable to the australopithecines, while bite force predictions for *Homo sapiens* were lower. It was therefore suggested that craniofacial form in earlier hominin species was heavily influenced by the need to generate and dissipate high masticatory forces, primarily through large jaw-elevator muscles and posterior dentition (Demes and Creel 1988). On the contrary, *H. sapiens* was found to have smaller jaw-elevator muscles, but with high mechanical advantage (MA; Demes and Creel 1988), leading to conclusions that the use of cooking in modern humans released selective forces on large dentition and jaw-elevator musculature (Demes and Creel 1988). This is consistent with Godinho et al. (2018) who demonstrated that the jaw elevator musculature of *Homo sapiens* has a higher MA than *Homo heidelbergensis,* concluding this is a secondary consequence of the retraction of the facial skeleton of *H. sapiens* under the anterior cranial fossa rather than a product of direct selection. Eng et al. (2013) also suggested that selection for larger masticatory muscles was the most influential mechanism through which the hominin masticatory system was adapted to produce high bite forces as variation in their bite force predictions were most explainable through differences in muscle force estimates. However, these authors also found that *H. ergaster* produced bite forces lower than predicted for their molar area (Eng et al. 2013). From this, the authors suggested that the reduction in bite force capabilities occurred before the habitual use of fire for cooking, hypothesizing instead that this was facilitated by increased

reliance upon basic food processing technologies (Eng et al. 2013). The interpretations made by these authors emphasise the selective importance that extra-oral food processing technologies have had upon the form and force production capabilities of the masticatory system throughout human evolution.

1.3.2. Craniofacial variation within *Homo sapiens* and its relationship to diet

Within *Homo sapiens* populations, the relationship between craniomandibular form and differences in mechanical loading are highlighted by morphological differences between populations with diverging subsistence strategies (Menéndez et al. 2014; von Cramon-Taubadel 2011, 2014; Galland et al. 2016; Katz et al. 2017; von Cramon-Taubadel 2017; May et al. 2018). It is proposed that the diets of agriculturalist populations are less mechanically challenging relative to hunter-gatherers owing to their use of more complex food processing technologies like the use of pottery for cooking, the use of grind stones for processing grains etc (Brace et al. 1987). Therefore, comparison of craniofacial form between the crania of hunter-gatherer and agriculturalist populations (dating to periods where there is compelling evidence for this subsistence transition) are frequently used as proxies to investigate how dietary difference influence craniofacial anatomy in *H. sapiens* (Carlson and Van Gerven 1977; Sardi et al. 2006; Pinhasi et al. 2008; Paschetta et al. 2010; Galland et al. 2016; May et al. 2018).

The analysis of cranial remains from lower-Nubian archaeological record is example of this (Carlson and Van Gerven 1977; Galland et al. 2016). The first to investigate the impacts of dietary difference on craniofacial form in this sample were Carlson and Van Gerven (1977), and more recently Galland et al. (2016) have corroborated their findings to demonstrate that hunter-gatherer populations had wider midfacial skeletons and zygomatic regions, more pronounced subnasal prognathism, more robust supraorbital features, among other changes to the cranial vault and mandible (Figure 10), with the Nubian agriculturalist populations having both smaller dentition and temporomandibular joints (Brace et al. 1987; Hinton and Carlson 1979). The results of this research led to the proposition of the 'Masticatory function hypothesis', suggesting that these craniofacial differences were selectively driven by dietary

differences, resulting in hunter-gatherers having a more robust cranium containing adaptations to increase bite force via the size and mechanical advantage of the jaw-elevator musculature (Carlson and Van Gerven 1977; Paschetta et al. 2010; Galland et al. 2016). The initial proponents of this hypothesis suggested it could explain some of the changes that have occurred to the facial skeleton during human evolution (Carlson and Van Gerven 1977)

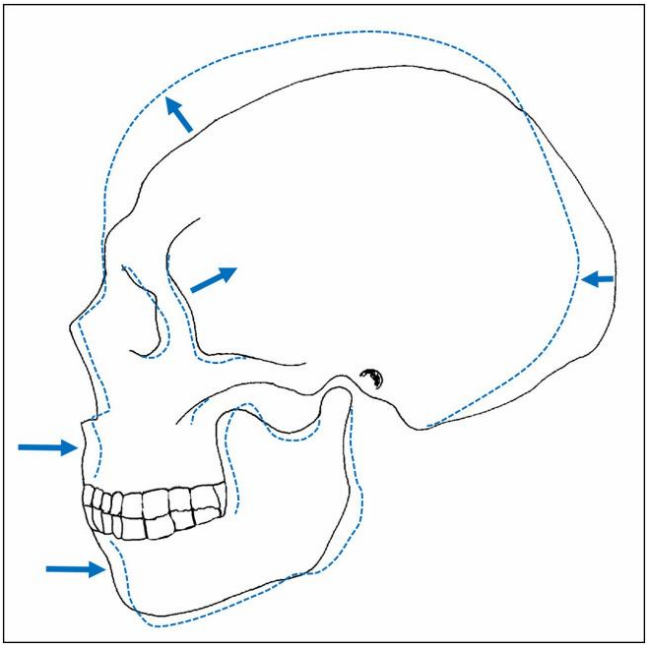

Figure 10. Visual representation of the differences in cranial shape between hunter-gatherers (black solid outline) and agriculturalists (blue dashed outline) from the agricultural transition of lower Nubia. ***Image source: von Cramon-Taubadel (2017).***

Similar research has been conducted on the South American osteological record, which has instead revealed the impact that differences in masticatory loading have upon the phenotypical plasticity of the cranium (González-José et al. 2005; Paschetta et al. 2016; Eyquem et al. 2019). For example, González-José et al. (2005) identified differences in the form of the masticatory apparatus of hunter-gatherer and agriculturalist populations, attributable to phenotypical plasticity caused by differential masticatory loading environments. Similarly, Menéndez et al. (2014) found that dietary differences between populations explained differences in craniofacial form, but cautioned against assuming that agriculturalist populations of *H. sapiens* consume a less mechanically challenging diets than hunter-gatherer populations as both may use similar food processing technologies (Menéndez et al. 2014; Katz et al. 2017). Contrary to this, Eyquem et al. (2019) found that dietary

differences had no clear influence upon craniofacial shape in modern urban populations, and that covariation between the upper face and the maxilla decreases with the intensity of masticatory loading (Eyquem et al. 2019). These authors therefore concluded that the large variation in craniofacial shape in modern *H. sapiens* is a consequence of reduced functional demands on the masticatory system with the consumption of less mechanically challenging diets (Eyquem et al. 2019). Similar conclusions were reached by Paschetta et al. (2016) from the analysis of craniofacial variability within South and North American populations.

Variation between craniofacial form in hunter-gatherer and agriculturalist populations from across the world have also been studied. Research into the relationships between craniofacial robusticity (typically defined by the expression of some of the features depicted within Figure 11) and increased masticatory loading demonstrate weak correlations between the form of the masticatory system and the expression of such features (Baab et al. 2010). The expression of these features instead demonstrates stronger correlations to overall cranial size (Lahr and Wright 1996). Investigations surrounding covariation within the masticatory apparatus, between this and overall craniofacial shape, and subsistence strategies in *H. sapiens* populations have produced more concrete findings. Katz et al. (2017) report that agriculturalist populations have smaller masticatory muscle attachment sites, but highlight the paradoxical combination of the more orthognathic faces of agriculturalist populations increasing the leverage of smaller jaw-elevator muscles (Katz et al. 2017). This supports suggestions this is increased mechanical advantage is not a primary adaptation to producing high bite forces within modern *H. sapiens* (Ledogar et al. 2016a; Katz et al. 2017; Godinho et al. 2018).

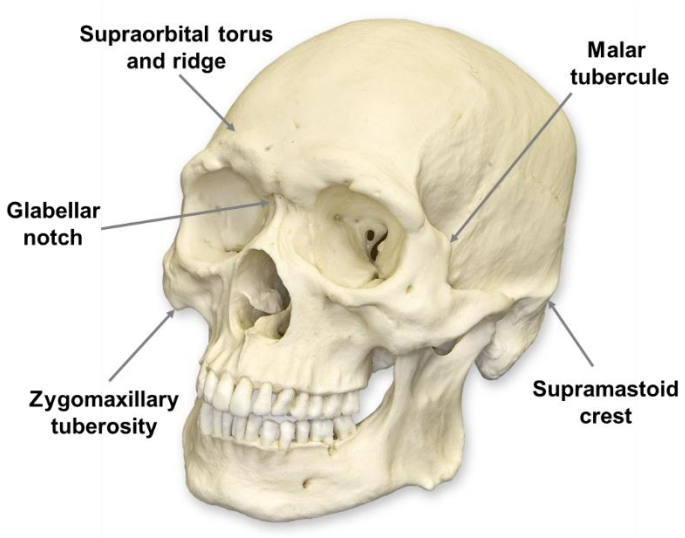

Figure 11. Some examples of visceocranial and neurocranial features frequently used as indicators of craniofacial robusticity. ***Image source: https://www.skullsunlimited.com/products/replica-human-male-asian-robust-skull-bc-287.***

In two publications, Noback and Harvati (2015a; 2015b) investigated patterns and magnitudes of covariation between the shape of the dental arch and attachments of the masticatory musculature in fifteen modern *H. sapiens* populations, and how subsistence patterns contribute to differences in craniofacial shape on a global scale. Similarly to Eyquem et al. (2019) and Paschetta et al. (2016), these authors found higher rates of covariation within the form of the masticatory apparatus in populations that consume more mechanically demanding diets (Noback and Harvati 2015a). This research also showed that traits previously suggested to be adaptations for generating high bite forces covary with one another, being the anterior-posterior position of the temporalis and masseter attachments, and the width of the zygomatic regions and the infratemporal fossae (Noback and Harvati 2015a). These authors reported that agriculturalist populations typically have smaller, shorter and more posteriorly positioned muscle attachments, but different covariation patterns existed for populations more reliant upon fishing and hunting compered to populations more reliant upon gathering (Noback and Harvati 2015b). However, both the covariation patterns identified are suggested to reflect adaptations that aid the resistance elevated masticatory strains and improve bite force capabilities (Hylander 1977; Wang et al. 2010a; Noback and Harvati 2015a).

The subtle morphological differences identified between populations emphasises how craniofacial variation within *H. sapiens* are small compared to the differences between *H. sapiens*, other members of the genus *Homo,* and earlier hominins (Katz et al. 2017). These small-scale differences between *H. sapiens* populations may be associated with the use of sophisticated food processing technologies (e.g. cooking with pottery) preceding the emergence of farming, easing the functional demands on the masticatory system on all *H. sapiens* populations (Katz et al. 2017). The larger differences in craniofacial form between modern *H. sapiens* and earlier *Homo* may be a product of only *H. sapiens* habitually engaging in complex food processing technologies (Brace et al. 1987; Katz et al. 2017). As such, the larger facial and dental dimensions, increased craniofacial robusticity, larger and more anteriorly positioned jaw-elevator muscle attachments of *H. ergaster* compared to *H. sapiens* (Howells 1980; Rightmire 1988, 1992; Lieberman 1995; Antón 2003; Harvati et al. 2010; Freidline et al. 2012; Antón and Middleton 2023), may be both plastic and selective adaptations to the consumption of a more mechanically demanding diet (Pope 1991; Lieberman 2008, 2011). Therefore, comparing the strain regimes experienced by *H. ergaster* and *H. sapiens* under masticatory loads may be important in investigating craniofacial gracilisation during human evolution.

1.4. Predicting craniofacial strains caused by masticatory loads

Given the connections between mechanical loading and craniofacial form, much research has been conducted to predict strain regimes in the cranium during masticatory loads. Traditionally, this been predicted by simplifying the cranium into a series of beams, cylinders, buttresses and pillars (Greaves 1985; Rak 1983; Russell et al. 1985; Rak 1986; Demes 1987; Endo and Adachi 1988; Prado et al. 2016; Rak and Marom 2017). Beam and cylinder models simplify the geometry of the cranium to predict patterns of stress and strain (Chalk et al. 2011). These models predict that during incisive bites, the face undergoes bending in the sagittal plane, due to the superior components of bite and joint reaction forces, and the inferiorly directed muscle force (Figure 12; Hylander et al. 1991). This is predicted to subsequently cause compressive strains in the facial skeleton and tensile strains through the hard palate (Hylander et al. 1991). Similar mechanisms are used to conceptualise bending of the face in a frontal view during incision (Figure 12; Endo and Adachi 1988) and the behaviour

of the supraorbital region, which is tensed laterally by muscle forces and compressed medially by bite reaction forces (Figure 12; Russell et al. 1985). When bites are away from the midline, it is predicted that the face twists about an anterior-posterior axis (Figure 12), as a unilaterally positioned bite force compresses the biting side of the face, while the contralateral side of the face is tensed due to the inferiorly directed muscle forces (Greaves 1985). The buttress and pillar models describe the cranium as a rigid frame constituted of vertical pillars that transmit bite forces from the dentition to the neurocranium as axial compressive stresses, and are reinforced from bending by a series of transverse buttresses (Figure 13; Endo and Adachi 1988; Prado et al. 2016).

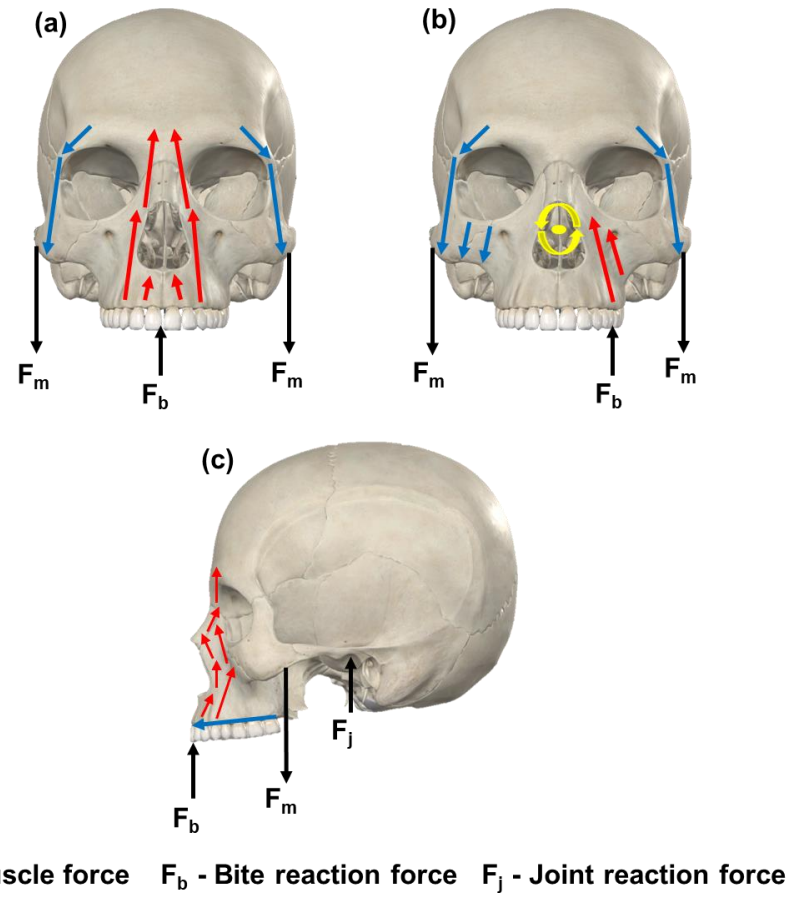

Figure 12. Beam and cylinder models that predict strains in the cranifacial skeleton under masticatory loading. Compressive strains are represented by the red arrows, tensile strains are represented by the blue arrows, and masticatory forces (muscle forces, bite force and joint reaction forces) are represented by the black arrows. (a) Bending in the frontal plane. (b) Torsion about an anterior-posterior axis (represented by the yellow arrrows and circle). (c) Bending in the sagittal plane.

These biomechanical models have been employed frequently to provide functional explanations of the craniofacial anatomy of fossil hominins (Demes 1982; Hylander and Johnson 2002). For example, it has been hypothesized that the anterior nasal pillars of the gracile australopithecines are hypothesized to provide support against compressive strains during premolar loading (Rak 1983; Strait et al. 2009; Ledogar et al. 2017). Furthermore, using beam and cylinder modes Rak (1986) concluded that the sagittal orientation of the Neanderthal infraorbital region improves resistance against sagittal bending during forceful incision. Although Demes (1987) utilised a different framework to predict stresses under masticatory load, the same conclusions as Rak (1986) were reached.

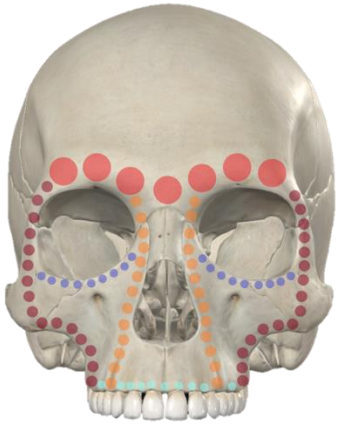

Figure 13. Pillar and buttress models of the craniofacial skeleton of *Homo sapiens*. The pillars include the canine frontal pillar (orange dots) and the zygomaticomaxillary pillar (maroon dots). The buttresses include the hard palate (light blue dots), the infraorbital rims (purple dots) and the frontal bar (red dots).

Unfortunately, experimental strain gauge analysis in a range of non-human primates indicate that these models poorly predict the craniofacial strains during masticatory loading (Chalk et al. 2011; Hylander et al. 1991). This research involves directly recording strains on the surface of bones in living animals during masticatory loading, or on the surface of *ex vivo* specimens (Rayfield 2007). Strain gauge analysis comes with experimental limitations, especially when performed *in vivo* due to the limitations of where gauges can be placed, notwithstanding the ethical concerns with invasive research on living animals (Rayfield 2007; Toro-Ibacache et al. 2016). While *ex vivo* strain gauge analysis can increase the range sampled locations and has less ethical concerns, realistic loads can be difficult to simulate therefore strain recordings are non-physiological (Ross and Hylander 1996; Gupta et al. 2004; Bright and Rayfield 2011; Cuff et al. 2015; Godinho et al. 2017). Hylander et al. (1991) reported that the supraorbital regions

of *Macaca fascicularis* and *Papio anubis* do not strain as predicted by Endo (1970) and Russell et al. (1985), concluding that simple beam models poorly approximate the response of the primate supraorbital region to mechanical loads. Further research demonstrated that this is also observable in the zygomatic arch of macaques (Hylander and Johnson 1997). Additionally, Prado et al. (2016) demonstrated that predictions of strain regimes derived from pillar and buttress models are mostly inaccurate, upon reviewing *in silico* and *in vivo* strain data from humans and non-human primates. Clearly, the reduction of the geometrically complex primate skull into simple mechanical models to predict global deformation patterns leads to imprecise predictions of strain distributions under masticatory loads (Ross and Hylander 1996; Ross 2001; Hylander and Johnson 2002; Chalk et al. 2011).

1.4.1. *In silico* predictions of strain: finite element analysis

The previous discussions identified that recording and predicting strains under masticatory load is an important in understanding form-functional relationships of the cranium, yet traditional biomechanical models and the strain regimes they predict correspond poorly to *in vivo* and *ex vivo* strain gauge data (Hylander and Johnson 2002; Chalk et al. 2011). More accurate predictions of strain regimes can be produced by *in silico* methods, such as finite element analysis (FEA; Chalk et al. 2011). Frequently used within engineering, FEA is mathematical methodology capable of reconstructing patterns of deformation in structures under complex loading regimes, providing predictions of strains, stresses and reaction forces (Richmond et al. 2005; Ross 2005; Rayfield 2007). Finite element (FE) models of biological specimens are frequently constructed from medical and micro computed tomography (CT) imaging (Marcián et al. 2021), as volumetric images allow both the surface morphology internal geometry of biological specimens to be represented within FE models, both of which are influential in regulating their response to mechanical load (Chamoli and Wroe 2011; Parr et al. 2013). To construct a FE model from a CT scan, the raw data format (e.g. a DICOM stack) is converted into a volumetric image from which the geometry of the biological object is segmented by applying a threshold to the voxels in a CT stack which differentiates them based on their grey values, thus separating the volumetric image into different materials and reconstructing its geometry (Mazonakis and Damilakis 2016).

Following this, digital models are converted into a FE mesh, i.e. they are sub-divided into a finite number of geometrically simple, uniform shapes that are connected via nodes at their corners (Richmond et al. 2005; Rayfield 2007). Depending on the choice of FEA software, models can be constructed from either surface-geometry or voxel-based conversions (Lengsfeld et al. 1998). Surface based geometry converts digitised 3D objects in wireframe formats, which are subsequently converted into triangular elements (Dumont et al. 2005). Direct voxel conversion converts volumetric data in to a FE mesh by converting voxels into cubic elements, offering a time-effective method to generate geometrically accurate FE models (Keyak et al. 1990; van Rietbergen et al. 1995; Fagan et al. 2007; Rayfield 2007; Liu et al. 2012). The elements within a FE mesh can be ascribed elastic properties, including Young's modulus and Poisson's ratio values (see section 1.1.4; Richmond et al. 2005; Rayfield 200). Force vectors are applied to nodes on the surface of a FE mesh, and others are defined as constraints to prevent rigid body movement of the model under the applied forces (Richmond et al. 2005; Rayfield 2007); collectively these are referred to as loading and boundary conditions (see section 2.1 for more details; Rayfield 2007).

Following this, a model is solved. This generates a series of simultaneous equations that are solved to calculate nodal displacements of a model based on the material properties of its elements, and its loading and boundary conditions (Richmond et al. 2005; Rayfield 2007). These nodal displacements are used to interpolate strain values, which are subsequently used to calculate stresses in combination with the Young's modulus values ascribed to individual elements (Richmond et al. 2005; Rayfield 2007). In FEA post-processing software, these predictions can be displayed as colour maps, which visualise global distributions of stresses and strains in a model following its solving. Figure 14 visualises the finite element method (FEM).

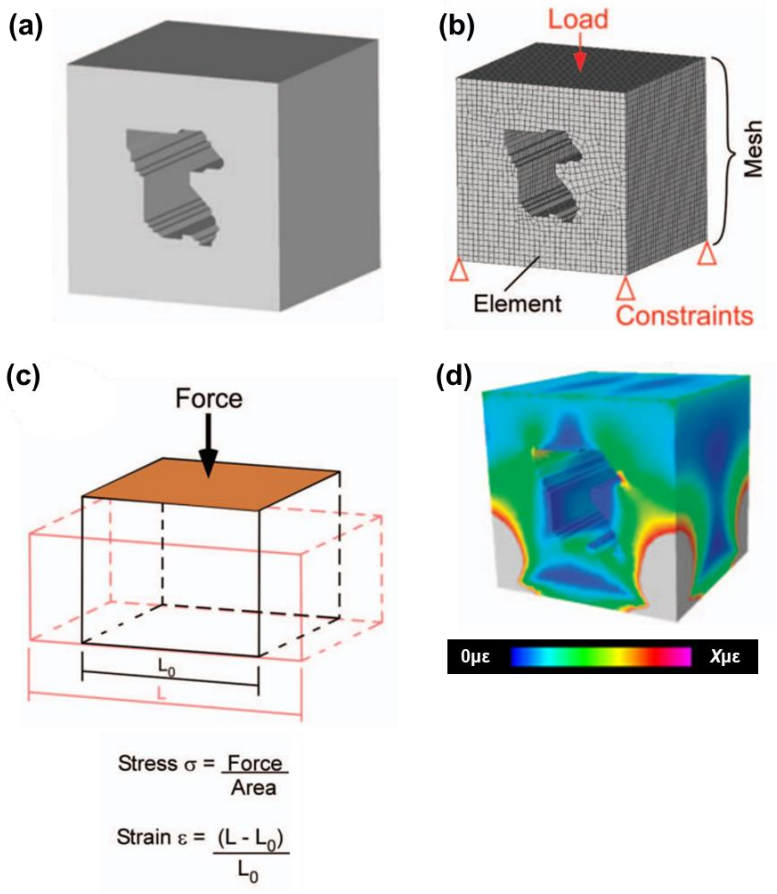

Figure 14. Visualisation of the steps of the FEM. (a) Digitisation of the object to be modelled. (b) Creation of a FE mesh and application of loading and boundary conditions. (c) The prediction of nodal displacements under the loading and boundary conditions during the solution phase. (d) The visualisation of global strain predictions. *Image source: Bright (2014)*.

As with all models, loading scenarios simulated by FEA represent a simplification of biological reality (Anderson et al. 2011), therefore once models are created it is important to assess how closely their predictions reflect reality, and how sensitive they are to error in how input parameters are modelled (Rayfield 2007; Bright and Rayfield 2011). Typically, FE models are validated by comparing the predictions of the model to *in* or *ex vivo* strain data, through a process of altering the input parameters of a model until its predictions are as consistent with strain gauge data as necessary (Ross 2005; Bright and Rayfield 2011). Whether absolute predictions of magnitudes are required of an FE model depends on the research it is being constructed for (e.g. this is necessary if a model is being used to predict breaking stresses; Bright 2014).

Validation studies of FE models are often accompanied by sensitivity studies, which is process of altering the input parameters of a model and quantifying the impacts of this upon its predictions (Ross 2005; Rayfield 2007; Bright 2014). These are of importance for paleontological studies utilising FEA, as many important input parameters are absent for fossil specimens (Bright 2014). Therefore, understanding how the predictions of validated models respond to changes in input parameters is informative towards model constructions decisions and in understanding the margins of error of paleontological models (Bright and Rayfield 2011). Many validation and sensitivity studies of biological FE models have been performed on *Macaca fascicularis* cranial and mandibular models, owing to the large body of *in vivo* and *ex vivo* strain data available to researchers to validate their models against (Ross 2005; Kupczik et al. 2007; Ross et al. 2011). Attempts have been made to validate models of other primate species including *Pan troglodytes* (Smith et al. 2015a), and other mammal species such as *Sus domesticus* (Bright and Rayfield 2011; Bright and Gröning 2011). Outside of Mammalia, models of reptiles (e.g. *Alligator mississippiensis*; Metzger et al. 2005) and avians (e.g. *Struthio camelus*; Cuff et al. 2015) have been subject to validation studies.

FE models of *Homo sapiens* crania have also been the subject of validation and sensitivity studies (Szwedowski et al. 2011; Toro-Ibacache et al. 2016; Ledogar et al. 2016a; Godinho et al. 2017). Recognising the difficulty of sourcing and producing experimental data to validate human FE models against, Toro-Ibacache et al. (2016) and Godinho et al. (2017) aimed to validate a model construction approach, and to assess the sensitivity of *H. sapiens* craniofacial FE models to variations in this. This modelling approach has subsequently been used to build other *H. sapiens* craniofacial FE models that have been used to investigate relationships between muscles force, craniofacial morphology and deformations under masticatory loads (Toro-Ibacache et al. 2016), and to correlate regions of high tensile and compressive strains to areas of bone apposition and resorption in osteological specimens (Brachetta-Aporta and Toro-Ibacache 2021). While these FEA sensitivity and validation studies will be reviewed in more detail later in the thesis (see section 2.1), a key take away is that while models with simplified input parameters fail to accurately predict absolute strain magnitudes, they still produce accurate predictions of regions of high and low strains, or relative strain distributions (Ross et al. 2005; Strait et al. 2005; Cox et al. 2011; Bright and Rayfield 2011; Fitton et al. 2012; Fitton et al. 2015; Toro-Ibacache et al. 2016; Godinho et al. 2017). This points to the

robusticity of FEA as an analytical tool to investigate patterns of global deformations within biological specimens and lends credibility to paleontological models where many of the input parameter necessary to make accurate predictions of magnitude are absent (Bright 2014).

A significant amount research has utilised finite element analysis (FEA) in investigations of craniofacial and masticatory biomechanics, in a wide range of extinct and extant taxa (Rayfield et al. 2001; Dumont et al. 2005; Ferrara et al. 2011; Cox, et al. 2015; Smith et al. 2021; Chatar et al. 2022). Masticatory function is simulated on craniofacial FE models through the deformation of a model onto constraints placed on the maxillary dentition and temporomandibular joints via force vectors applied to nodes within the attachment sites of the jaw-elevator muscles on the model's surface which oriented to the insertion of each respective muscle, simulating their line of action (Dumont et al. 2005; Strait et al. 2005). Theoretically, these loading and boundary conditions simulate the contact between the mandibular condyle, articular disc, and the glenoid fossa during jaw-elevation, and the compression of an object between the mandibular and maxillary dentition by the jaw elevator muscles (Dumont et al. 2005; Strait et al. 2005). Chalk et al. (2011) examined whether simple geometrical models (see section 1.4) provide accurate predictions of craniofacial strain under masticatory load, using a model of a *Macaca fascicularis* crania. These authors concluded that these simplified models do not produce accurate predictions of craniofacial strain under masticatory load (Chalk et al. 2011). This is consistent with previous observations of strain gauge data (Hylander and Johnson 1997; Hylander et al. 1991; Ross 2001; Prado et al. 2016), and indicates that FE models should be preferentially used to predict strains within masticatory biomechanical research (Chalk et al. 2011).

1.4.2. Finite element analysis in Hominin Palaeontology

In hominin palaeontology FEA is a popular analytical tool to investigate the feeding adaptations of fossil specimens (e.g. Strait et al. 2009; Wroe et al. 2010; Smith et al. 2015b; Ledogar et al. 2016b; Wroe et al. 2018; Godinho et al. 2018; Cook et al. 2021; Ledogar et al. 2022). The first use of the finite element method (FEM) in hominin palaeontology involved the construction of models *Australopithecus africanu*s (Strait et al. 2009, 2010). Currently, there are FE models of a range of australopithecine species including: *Australopithecus*

afarensis (Ledogar et al. 2022), *Australopithecus sediba* (Ledogar et al. 2016b), and *Paranthropus boisei* (Smith et al. 2015b). The examples of the FEM being used to investigate craniofacial biomechanics in *Homo* species have focused on modern *Homo sapiens* and middle and late Pleistocene species, such as *Homo neanderthalensis*, *Homo heidelbergensis*, and *Homo floresiensis* (Wroe et al. 2010; Ledogar et al. 2016b; Wroe et al. 2018; Godinho et al. 2018; Godinho et al. 2018; Godinho and O'Higgins 2018; Cook et al. 2021). However, currently no FE models of early *Homo* fossils have been made.

Contrasting previous lever-mechanical and geometric models that predict Neanderthal specimens are well adapted to producing and withstanding heavy incisive bites (Rak 1986; Demes 1987; Spencer and Demes 1993), Wroe et al. (2018) found that their Neanderthal FE models predicted comparable strains to contemporary *H. sapiens* specimens during anterior bites, and produced the lowest bite forces when compared to models of *H. sapiens* and *H. heidelbergensis*. These authors therefore concluded that Neanderthals were not suited to withstanding or generating high anterior loads (Wroe et al. 2018). These conclusion are consistent with some lever-mechanical analyses of the Neanderthal masticatory system (Anton 1990; O'Connor et al. 2005), but not others (Spencer and Demes 1993), or beam and cylinder models (Rak 1986; Demes 1987). This demonstrates that FEA may be a more reliable method to predict bite force capabilities and strain regimes under masticatory loads in fossil specimens.

Comparisons of the performance and dietary adaptations of *H. sapiens* to hominin fossils and extant great apes have produced conflicting results. For example, Wroe et al. (2010) suggested that *H. sapiens* are highly efficient producers of bite force and possess craniomandibular morphologies effective for withstanding high stresses. These authors concluded that masticatory reduction in *H. sapiens* could be explained through reduced stresses owing to the increased mechanical advantage of the masticatory musculature (Wroe et al. 2010). These results are contrary to other comparative FEA studies (Ledogar et al. 2016a; Godinho et al. 2018; Cook et al. 2021). For example, Godinho et al. (2018) demonstrated that a *H. sapiens* FE model predicted higher bite forces than a *H. heidelbergensis* model loaded with the same

muscle forces, however the *H. sapiens* model predicted higher strain magnitudes through most of the facial skeleton. This supported the conclusion that the efficient bite of *H. sapiens* was not directly selected for (see section 1.3.1; Godinho et al. 2018). These interpretations are supported by the findings of Ledogar et al. (2016a), who also demonstrated that *H. sapiens* are efficient producers of bite force, while experiencing high strain magnitudes during forceful bites. These authors also concluded that increased bite force efficiency is secondary to other evolutionary processes, while the habitual use of complex food processing behaviours may have released selective pressures on features associated with the resistance of forceful bites, explaining the small and gracile faces of *H. sapiens* (Ledogar et al. 2016a).

Despite the importance of extra-oral food processing in reducing the size of dietary objects, few researchers have directly addressed the impact that changes in gape requirements may have had on the strains experienced by hominin crania during masticatory loading using FEA. Although bites at a range of gapes have been simulated on FE models of different taxa including other primates (Dumont et al. 2011), rodents (McIntosh and Cox 2016), and carnivores (Bourke et al. 2008; Chatar et al. 2022), bites at different gapes have yet to be simulated on FE models of hominin crania. However, many researchers have emphasised the adaptive capabilities of hominin specimens to consume large hard objects when interpreting the predictions of their FE models (Strait et al. 2009, 2010; Smith et al. 2015b; Ledogar et al. 2016b; Cook et al. 2021). The predictions of a FE model of Sts 5 led Strait et al. (2009, 2010) to conclude that hard object feeding was an important dietary strategy for *Australopithecus africanus* (Strait et al. 2009), although it was not stated whether the simulated bites were at large gapes. Others have tested the adaptation of hominin crania to consume hard objects, with less explicit references to food object size (Smith et al. 2015b; Ledogar et al. 2016b; Cook et al. 2021). Both Cook et al. (2021) and Ledogar et al. (2016) report that their muscle force vectors were determined with the mandible in a depressed position with the condyles translated over the articular eminence to account for how muscle force vectors change with jaw-opening, although the extent of mouth opening modelled is not stated. Therefore, the experimental design of many of these publications limits the strength of the conclusions made by the authors surrounding the adaptations of hominin fossil crania to consume large hard objects. However, this may have been an important adaptive strategy for early hominins, prior

to the habitual use of extra-oral food processing technologies that reduce the size of food objects (Zink et al. 2014; Zink and Lieberman 2016). As such, simulating bites at gape in FEA may be important in assessing adaptations within the hominin crania to large object feeding.

1.5. The functional importance of differences in zygoma morphology throughout human evolution

One interesting and key region of the masticatory apparatus is the zygoma region, including anatomical structures such as the zygomatic bones, the zygomatic arches, the zygomatic process of the maxilla, and the zygomatic root (see Figure 15; Weber and Krenn 2017; Oettlé et al. 2017; Rak and Marom 2017). Given that it hosts the attachment of the masseter on its inferior border (Gaudy et al. 2000), the spatial position of the zygoma region is influential in determining bite force capabilities owing to how this interacts with the mechanical advantage of this muscle (Ward and Molnar 1980; Ledogar et al. 2017; Rak and Marom 2017). Furthermore, as a part of the midfacial skeleton, the zygoma region is also important in resisting strains induced by both the contractile force of the masseter and bite reaction forces (Herring et al. 2001; Prado et al. 2016; Rak and Marom 2017). These factors demonstrate the importance of the form of the zygoma region to masticatory biomechanics.

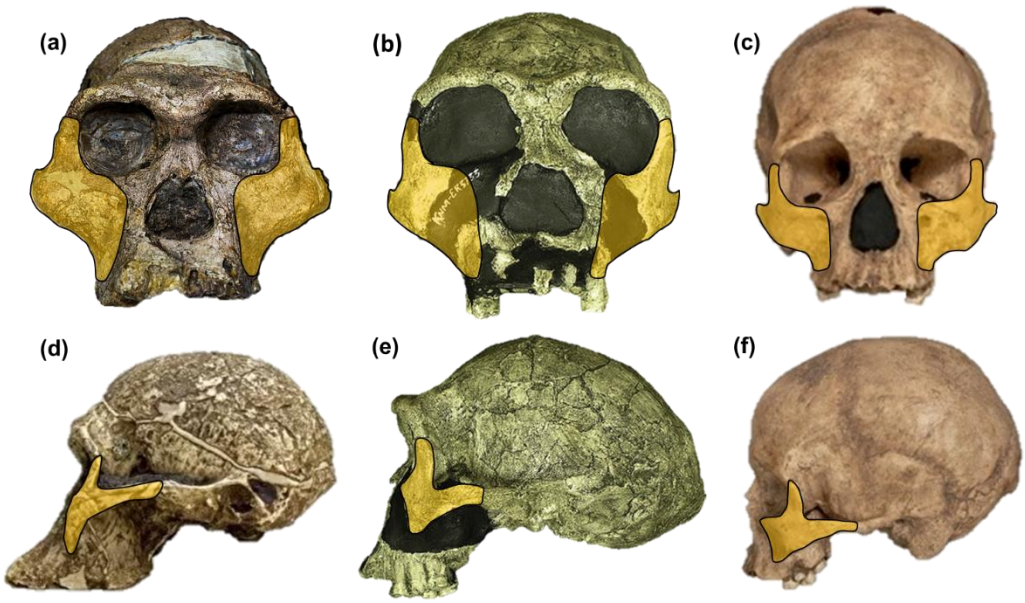

Figure 15. Frontal and lateral view of hominin crania Frontal and lateral view of hominin crania including *Australopithecus africanus* (a and d), *Homo ergaster* (b and e) and *Homo sapiens* (c and f), with the zygoma region highlighted in orange. *Image sources (from left to right by species): https://www.prints-online.com/t/164/australopithecus-africanus-cranium-sts-5-8595745.jpg.webp and https://ccschmitt.github.io/STS%205%20%28Mrs.%20Ples%29.html; (Simpson, 2015); and https://www.nature.com/articles/nature.2017.22114*

As such, changes to the form of the zygoma region during human evolution have frequently been suggested to reflect different dietary adaptations (Rak and Marom 2017). The laterally expanded, straight and deep zygomatic roots in australopithecines are suggested to reinforce the facial skeleton against high masticatory forces (Rak 1983; Ledogar et al. 2017). It is also commonly suggested that the laterally flaring zygomatic arch and anteriorly positioned zygomatic roots of the australopithecine species represents an adaptation to increasing the cross-sectional area and the mechanical advantage of the masseter (Du Brul 1977; Rak 1983; 1988; Rak and Marom 2017). *Paranthropus boisei* is an australopithecine species at the extremes of this morphological configuration (Rak 1983; Rak and Marom 2017), yet simplified geometric models indicate that these adaptations to optimise bite force production weaken the upper facial skeleton against the contraction of the masseter on a laterally flaring zygomatic arch, thus explaining the selection of the visor-like form of the zygoma to reinforce the facial skeleton (Figure 16; Rak 1983, 1988; Rak and Marom 2017).

The impacts that australopithecine zygoma region anatomy have upon craniofacial strains and bite force production has been investigated using finite element analysis in combination with virtual anthropological techniques that can manipulate the form of digitised specimens (see section 1.6; Fitton et al. 2009; Ledogar et al. 2017). Fitton et al. (2009) investigated the functional significance of differences in the form of the zygomaxillary region of *Au. africanus* (Sts 5) and *P. boisei* (OH 5), finding that the former improved the performance of the Sts 5 model of during incisive bites and the later improved performance during molar bites. Similarly, Ledogar et al. (2017) investigated the importance of the shape and position of the zygomatic root in producing and withstanding bite forces in *Au. africanus* (Sts 5) and *sediba* (MH 1), finding that while straight, deep and laterally expanded zygomatic roots decreased craniofacial strains in both models, increasing the anterior positioning of this structure increased bite force and thus craniofacial strain globally, thus explaining the presence of facial reinforcement features like anterior nasal pillars via plastic and selective processes. These studies demonstrate that changing features in isolation impact how the craniofacial skeleton responds globally to masticatory loads (Fitton et al. 2009; Ledogar et al. 2017). While not performed on a model of a hominin fossil, Smith and Grosse investigated the impacts of changing the cross-sectional shape of the zygomatic arch of *Pan troglodytes* model, finding that this only has local impacts on craniofacial strains (Smith and Grosse 2016). These author's instead emphasise the importance the global shape of the cranium in the resistance of masticatory forces (Smith and Grosse 2016). As argued by Rak (2014), the spatial position of the entire zygomatic arch may have more of a global impact upon craniofacial strains than changing the cross sectional shape of the structure.

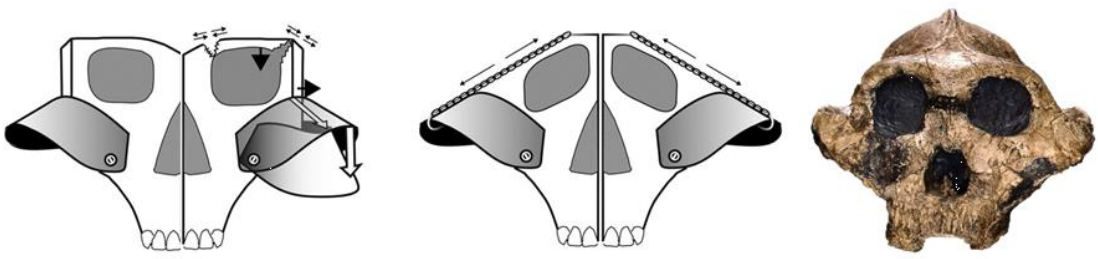

Figure 16. Schematic representation of how the visor-like zygoma region of *P. boisei* reinforces the facial skeleton against the pull of the masseter on a laterally flaring and anteriorly positioned zygomatic arch. *Image sources (left to right): Rak and Marmon (2017), and http://australianmuseum.net.au/image/Skull-cast-of-Paranthropus-boisei*

The zygoma region morphology of *Homo ergaster* differs from *Homo sapiens* (Figure 15). The infraorbital profile of *H. ergaster* is more vertically oriented and topographically flat than within *H. sapiens*, where this region is more posteriorly inclined and concave (Rightmire 1998; Antón 2003; Lieberman 2008, 2011; Harvati et al. 2010; Antón and Middleton 2023b). The zygomatic region of *H. ergaster* is larger, mediolaterally wider, superiorly-inferiorly taller, and more anteriorly projecting, than that of *H. sapiens* (Howells 1980; Rightmire 1988; Pope 1991; Rightmire 1992; Lieberman 1995; Freidline et al. 2012a), as is the rest of the facial skeleton (Rightmire 1998; Antón 2003; Lieberman 2008; Rightmire 2013; Antón and Middleton 2023). The frontal process of the zygoma of *H. ergaster* is more anteriorly-laterally oriented, whereas this is more laterally positioned in *H. sapiens* (Antón and Middleton 2023). The origin of the masseter is more anteriorly positioned in *H. ergaster* owing to its more anteriorly projecting zygoma (Pope 1991; Lieberman 1995; Rightmire 1998; Weber and Krenn 2017). The zygomatic root of *H. ergaster* is also positioned more superiorly in relation to the alveolar margin compared to *H. sapiens* (Pope 1991; Rightmire 1998; Weber and Krenn 2017). Multiple authors have described the zygomaxillary region and zygomatic arch of *H. ergaster* as more robust than *H. sapiens* (Howells 1980; Rightmire 1988, 1998). The previous sections of this chapter indicate that the craniofacial configuration of *H. ergaster* may be a product of both selective forces maintaining larger and more mechanically advantageous jaw-elevator muscles to optimise bite force production, and the consumption of a more mechanically demanding diet compared to *H. sapiens* increasing craniofacial modelling (Carlson and Van Gerven 1977; Demes and Creel 1988; Pope 1991; Lieberman 2008, 2011).

However, no previous research has investigated the distribution of strains under masticatory load in the facial skeleton of *H. ergaster.* Therefore, the functional significance of *H. ergaster* zygoma region morphology has yet to be addressed. As the zygoma region is important in both withstanding and producing masticatory forces, investigating how modifying the zygoma region of *H. sapiens* to resemble *H. ergaster* impacts global and local strains may provide insights into the relationship between craniofacial gracilisation and masticatory loading in *H. sapiens.*

1.6. Investigating the biomechanical consequences of form differences

Advances in virtual anthropological techniques have facilitated the construction of FE models of fossil hominins, as well as the modification digital specimens to test form-function hypotheses (O'Higgins et al. 2011; 2012; 2019). Finite element analysis (FEA) and geometric morphometrics (GMM) have been combined to investigate the biomechanical consequences of shape differences between biological structures. GMM studies frequently utilise thin plate spline (TPS) functions (Figure 17), which smoothly interpolate landmarks from a reference dataset to a target data set (Bookstein 1989; Bookstein et al. 2003), and can be used to produce deformed cartesian transformation grids that visualise shape differences between specimens (Figure 17; Bookstein 1989; Mitteroecker and Gunz 2009), or to produce a deformed version of a predetermined reference surface (Gunz et al. 2004, 2009; Mitteroecker and Gunz 2009; O'Higgins et al. 2011). This facilitates the generation of hypothetical digital specimens that can be used in functional analyses (O'Higgins et al. 2011, 2012; 2019). The first researchers to apply TPS deformations to FEA include Stayton (2009) and Sigal et al. (2008; 2010), who warped specimen-specific finite element (FE) meshes of a turtle shell and a rat caudal vertebra to the landmark configuration of target specimens. This research demonstrated that hypothetical FE models could be generated from one specimen-specific mesh, significantly reducing time and effort costs of constructing models, and expanding the investigative scope of FEA (Stayton 2009).

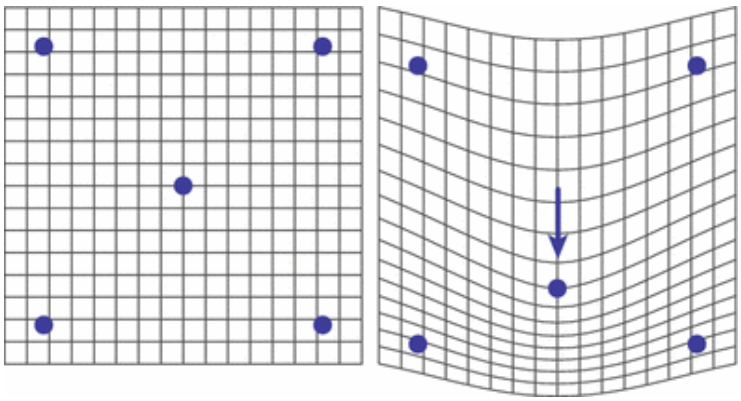

Figure 17. Example of a TPS deformed transformation grid. ***Image source: Mitteroecker and Gunz (2009).***

Developing this, O'Higgins et al. (2011) suggested two ways in which TPS warping could be used to produce hypothetical models for functional analyses. The first involves deforming

surfaces to extreme hypothetical landmark configurations, identified by linear regression, principal components or partial least squares analyses, allowing the investigation of the mechanical significance of shape differences (O'Higgins et al. 2011). These author's explored the functional relationship between cranial shape and post-canine area of plio-pleistocene hominins by deforming a surface of Sts 5 to the landmark datasets at the limits of a regression line and making FE models of these hypothetical forms (McHenry 1984; O'Higgins et al. 2011). Pierce et al. (2008) used a similar approach to investigate the significance of shape differences in crocodilian crania by constructing FE models from the hypothetical landmark configurations at the positive and negative most limits of four principal components. Others have adapted this approach to investigate the range of biomechanical performance within a sample by generating FE models of the specimens with the most extreme landmark configurations along principal components (Smith et al. 2015a; Ledogar et al. 2016a; Toro-Ibacache et al. 2016). Both approaches are important in form-function investigations, but do not provide inferences into the functional significance of altering one specific aspect of model geometry.

The second TPS warping method suggested by O'Higgins et al. (2011) facilitates such investigations by providing a framework to modify an isolated anatomical region of one digital specimen to contain the corresponding isolated feature of another (Figure 18; see section 3.1). This offers a controlled methodology to address form-functional hypotheses, as models can be produced where only one aspect of morphology differs between them (O'Higgins et al. 2011).

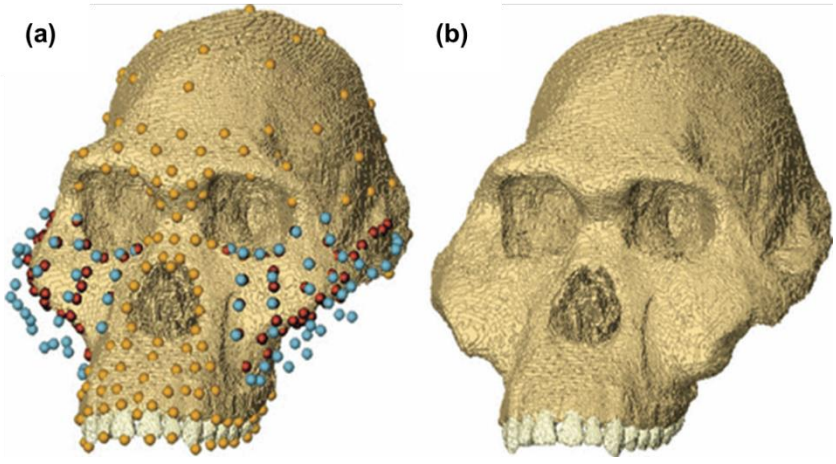

Figure 18. The use of TPSs to modify the zygomaxillary regions of Sts 5 (*Australopithecus africanus*) to contain the zygomaxillary form of OH 5 (*Paranthropus boisei*). (a) shows the undeformed reference surface and the landmarks used to perform the TPS warp. (b) shows the deformed surface produced by the TPS warping. *Image source: O'Higgins et al. (2011).*

Within hominin palaeontology, TPS warping has been used in combination with FEA to investigate the functional importance of variation in the zygoma region within australopithecines (see section 1.5; Fitton et al. 2009; Ledogar et al. 2017). This combination of methods has also been used examine the mechanical significance of *Homo sapiens* and *Homo neanderthalensis* mandibular symphyseal orientation and cross-sectional shape, as well as the presence or absence of a chin, demonstrating that the presence of this and vertical symphyseal morphology are closely mechanically interrelated (Gröning et al. 2011). While not using TPS warping, Godinho et al. (2018) and Godinho and O'Higgins (2018) virtually modified the internal and external morphology of the supraorbital region in *H. heidelbergensis* to address multiple form-function hypotheses, finding that their modifications had little impact upon craniofacial strains predicted by a FE model of the Kabwe 1 fossil, aside from minor differences local to the frontal bone. However, to date no research has used TPS warping on a *Homo* species to create models that test the impact of morphological changes in the zygoma region, or the impacts of simulating bites at a range of different gapes, on craniofacial strain and bite force production.

1.7. Thesis aims and objectives

This thesis aims to investigate how modifying the anatomy of a *Homo sapiens* finite element model to contain *Homo ergaster-like* zygoma region morphology impacts predictions of strain distribution and bite force under different masticatory loads, including bites at different gapes. It is predicted that a more archaic *Homo* like zygoma region would be more advantageous for resisting masticatory loads associated with a more mechanically challenging diet requiring higher bite forces and performing bites at larger gapes, whereas the zygoma region of a modern human should be less advantageous for resisting such loading conditions owing to the reduction in functional demands with the habitual use of complex food processing

technologies. Modifying the zygoma region in a controlled manner while keeping all other input-parameters identical allows a biomechanical investigation into how changes to the form (size and shape) of this region alter the mechanical advantage and force vector of the masseter, and impact craniofacial strains locally to the zygoma and more globally. Given the relationship between extra-oral food processing and food object size, it is assumed that archaic *Homo* would have a zygoma region better adapted to produce and withstand bites at larger gapes than modern *H. sapiens*. Therefore, bites at submaximal and maximal gapes will be simulated for both the *H. sapiens* FE model, and the model with the modified zygoma region.

To achieve this, a *H. sapiens* craniofacial FE model will firstly be constructed (objective 1 of the thesis; Chapter 2). The sensitivity of this model to changes in the input parameters necessary to simulate bites at gape will be assessed following its construction (objective 2 of the thesis; Chapter 2). To investigate the functional significance of the zygoma region, the geometry of the *H. sapiens* FE model will be modified using TPS warping to contain the zygoma region morphology reflective of a *H. ergaster* fossil (objective 3 of the thesis; Chapter 3). The performance of both models under the following loading conditions will then be compared: anterior and posterior bites, increasing the force applied to the masseter to reflect the likely higher masseter muscle force of *H. ergaster*, and bites simulating submaximal and maximal gapes (objective 4 of the thesis; Chapter 3).

2. Chapter 2: Creation, Validation and Sensitivity of a Finite Element Model of a modern *Homo sapiens* cranium

Predicting how the cranium strains in response to masticatory load is important for interpreting the functional significance of craniofacial form, due to the importance of strain regimes in driving plastic phenotypical variability, and for understanding the adaptive significance of morphological differences between specimens (O'Higgins et al. 2012). Finite element analysis (FEA) is a methodology that has been used in masticatory biomechanics research to predict how the crania of a range of extant and extinct species strain under masticatory loading regimes, hence its use within this thesis (see section 1.4.1 for a detailed review of FEA). A range of research surrounding the validity and sensitivity of FE models has occurred, involving assessing the accuracy of a models predictions of models against experimental strain data to ascertain which input parameters are necessary for inclusion and how they should be modelled (e.g. Strait et al. 2005; Ross et al. 2005; Cox et al. 2011; Tseng et al. 2011; Wood et al. 2011; Gröning et al. 2012; Fitton et al. 2012, 2015; Toro-Ibacache and O'Higgins 2016; Stansfield et al. 2018). While preferably models should be validated against experimental strain data to ensure their predictions are sufficiently accurate, this process is time and effort intensive, and impossible if the chosen specimen is paleontological or physically unavailable to a researcher (Bright 2014). In these instances, following previously experimentally validated protocols for constructing FE models is a prudent approach (Toro-Ibacache et al. 2016; Brachetta-Aporta and Toro-Ibacache 2021), alongside assessments of how error in defining unknown input parameters impacts the results of the model (Cox et al. 2015; Godinho et al. 2018).

2.1. Constructing craniofacial FE models

Biological FE models are constructed from the digitisation of the specimen of interest. This is achieved in multiple ways, e.g. through surface scanning or volumetric imaging modalities such as CT scanning (Rowe and Rayfield 2022). The geometry of a biological specimen is then segmented by applying thresholds which differentiate the voxels in an image based on their grey values (Mazonakis and Damilakis 2016). However, the boundaries between different materials in volumetric images can be difficult to discern due to partial volume averaging,

which is how the grey value of one voxel is an average of the attenuation of all the materials contained within that voxel (Kalisz et al. 2016). If lower resolution medical CT scanners are used to image a specimen to construct at FE model then simplifications to the geometry of a model are inevitable (Fitton et al. 2015; Toro-Ibacache et al. 2016). This can include omitting micro-anatomical features such as trabecular networks (Marcián et al. 2021), and artificially thickening fine cortical bone structures that in reality may be thinner than the resolution of one voxel (Toro-Ibacache et al. 2016). As such, previous FEA sensitivity analyses have been conducted to investigate impacts that errors in model construction can have upon their predictions. For example, when assessing the impacts that constructing a *Homo sapiens* cranial FE model to different resolutions (i.e. partial versus complete reconstruction of sinus walls), Toro-Ibacache et al. (2016) report that fully reconstructing nasal cavity and sinus walls produced the best predictions of overall strain distribution compared to their *ex vivo* experimental strain data. Therefore, manually reconstructing any fine cortical bone structures is a reasonable model construction decision to make for models created from low-resolution scans (Toro-Ibacache et al. 2016).

The cranium is made of multiple different materials, including cortical bone, trabecular bone, sutures etc. However, limits on computational powers, data availability, volumetric image resolution etc, prevent their combined inclusion into FE models (Gröning et al. 2012). Therefore, many sensitivity studies have addressed the impacts of including or excluding these different materials into cranial and mandibular FE models (e.g. Kupczik et al. 2007; Wang et al. 2010; Bright and Rayfield 2011; Reed et al. 2011; Bright 2012; Fitton et al. 2015; Toro-Ibacache et al. 2016; Godinho et al. 2017). Because many FE models are constructed from medical CT scans with resolutions too low to include trabecular networks (Gröning et al. 2012; Marcián et al. 2021), trabecular bone is frequently simplified and modelled as a bulk material (e.g. Strait et al. 2009, 2010; Bright and Rayfield 2011; Dumont et al. 2011). When the sensitivity of FE models to these simplifications are addressed, it has been reported on that models including trabecular bone as a bulk material with different material properties to cortical bone produce more accurate predictions of absolute strain magnitude than models that homogenise cancellous and cortical bone, when compared to experimental strain data (Bright and Rayfield 2011; Toro-Ibacache et al. 2016; Godinho et al. 2017). However, models

in which cancellous and cortical bone are homogenised into one bulk material still reasonably approximate relative strain distributions (Bright and Rayfield 2011; Godinho et al. 2017; Toro-Ibacache et al. 2016).

Research addressing the impact of including cranial sutures has produced more variable results. Wang et al. (2010) and Kupczik et al. (2007) investigated the impact of including sutures in *Macaca fascicularis* cranial FE models and independently produced similar results, demonstrating that while including sutures produced the most accurate predictions of absolute strain magnitude compared to their respective experimental strain data, omitting sutures from the models still produced broadly consistent predictions of strains distribution. Contrary to this, Bright (2012) reported that including sutures in a *Sus domesticus* model influenced both strain magnitude and distribution, but produces predictions less similar to their *ex vivo* data than models that excluded sutures.

Like the cranium, teeth are made of multiple materials including enamel, dentine, and pulp, and are anchored to alveolar bone by the periodontal ligament (PDL). As such, sensitivity studies have addressed the impacts of including or excluding these different materials into FE models (Marinescu et al. 2005; Wood et al. 2011; Gröning et al. 2012; Herbst et al. 2021). Herbst et al. (2021) investigated the impacts that modelling enamel, dentine and pulp as distinct or bulk materials in their reptilian mandible FE models, and demonstrated that this only influences strains local to the alveolar margin, but impacted predictions of bite force magnitude; the authors argue that comparison of the relative differences between specimens can still be achieved if model construction is consistent. Cox et al. (2011) performed similar research in investigating the impact of modelling dental tissues of the incisors in rodent cranial FE models as bulk or distinct materials, and also found that this only had localised impacts in the alveolar region.

However, research that has investigated the impacts of inclusion of the periodontal ligament (PDL) within cranial and mandibular FE models has produced discordant results. Wood et al.

(2011) reported that a model of a *Cecbus apella* crania is insensitive to the inclusion or exclusion of the PDL and variations in how it is modelled, with any differences in strain predictions being localised to the alveolar region. These authors argue that including the PDL is unnecessary, unless a model is constructed to predict accurate strain magnitudes in this region (Wood et al. 2011). On the contrary Gröning et al. (2011; 2012) report that their model of a *H. sapiens* mandible varied in both strain magnitude and distribution when the PDL is included or excluded, and that the models including the PDL produced the most accurate predictions based on their *ex vivo* validation data.

Therefore, if the goal of a model is to predict relative strain distributions, then it is reasonable for sutures, subcortical bone, the PDL, and dental tissues to be simplified. Including these variables is time, resource, and effort-intensive, and may be impossible for models constructed from low-resolution scans. The results of Godinho et al. (2017), Fitton et al. (2015), and Toro-Ibacache et al. (2016) affirm that modelling cancellous and cortical bone, as well as enamel and dentine, as separate bulk materials, while preserving major internal cranial cavities and sinuses produce acceptable approximations of strain distributions compared to experimental strain validation data. Indeed, this is a prudent approach when constructing models that cannot be validated, given the current lack of consensus surrounding how tissues such as the PDL and sutures should be represented within FE models and the impacts they have upon their predictions (Bright 2012).

2.1.1. Material properties

Research investigating the elastic properties of the human cranium report variation between neurocranial and facial bones, as well as within individual bones and between individuals (Peterson and Dechow 2002, 2003; Peterson et al. 2006). Simplifications of these variables within FE models are often unavoidable due to computational limitations, meaning that mechanical properties of objects are frequently modelled as linearly elastic, isotropic and homogenous within one material (Strait et al. 2005). Strait et al. (2005) investigated the impact the simplifications in modelling elastic properties had upon the predictions of a *M. fascicularis* model and reported that the most accurate predictions of strain magnitude were

produced when elastic properties varied regionally and were orthotropic. These authors recommend that the values given to the materials within a model should derive from a sensible source, as they found that the predictions from the *M. fascicularis* cranial model allocated the elastic properties of a human tibia were the least accurate compared to *in vivo* strain validation data (Strait et al. 2005). However, despite variability in the complexity to which elastic properties were modelled, all the models of Strait et al. (2005) produced similar predictions of relative strain distributions. Cox et al. (2011) reported similar observations for their sensitivity studies of rodent crania, in that although alterations to the Young's modulus value ascribed to cortical bone influenced global strain magnitudes, the relative distributions of strains across the crania remained consistent. Taken together, these studies also indicate that the elastic properties of models can be simplified to be homogenous across materials, and modelled as linearly elastic and isotropic, while still producing accurate predictions of global strain distributions.

2.1.2. Modelling muscle forces

Muscle forces are applied to FE models in the form of vectors, which have both a magnitude and direction (Grosse et al. 2007). The magnitude of force applied to these vectors represents the force produced by the jaw elevator muscles (Dumont et al. 2005; Strait et al. 2005), and is a product of their physiological cross sectional area (PCSA), muscle stress constant (the amount of force $1cm^2$ of muscle tissue can produce) and degree of activation (Maughan et al. 1983; Buchanan 1995; van Eijden et al. 1997; Fitton et al. 2012). The most optimal way of estimating muscle force is by calculating its PCSA, as the maximal force a muscle can produce is correlated to this (Maughan et al. 1983; van Eijden et al. 1997). PCSA can be calculated is through cadaveric dissection (e.g. Hartstone-Rose et al. 2012; Taylor and Vinyard 2013; Terhune et al. 2015; Taylor et al. 2018; Hartstone-Rose et al. 2018; 2019), allowing for specimen-specific measures of muscle mass, pinnation angle, fascicle length, and tissue density, all of which influence the force production abilities of a muscle (see section 1.1.1; van Eijden et al. 1997).

However, paleontological and archaeological specimens do not preserve soft tissue for dissection to calculate muscle PCSA. Therefore, some researchers opt to use PCSA estimates from previously published research when loading FE models of dry specimens. For example, Van Eijden et al. (1997) report PCSA for the masticatory musculature of eight cadaveric *H. sapiens* males, which have been used in the construction of models of the human masticatory apparatus (e.g. Ledogar et al. 2016a). Many workers producing FE models of hominin fossils, including Smith et al. (2015b) and Cook et al. (2021), use PCSA values calculated for a female chimpanzee, produced by Strait et al. (2009).

In the absence of PCSA data, other researchers have estimated muscle cross sectional area (CSA) from measures of their attachment sites on the cranium when working with dry specimens (i.e. calculating muscle CSA via bony proxies; Thomason 1991). Many lever-mechanical studies of the hominin masticatory apparatus have estimated muscle CSA in this manner (Demes and Creel 1988; Anton 1990; O'Connor et al. 2005; Eng et al. 2013). Unfortunately, Toro-Ibacache et al. (2015) report poor correspondences between muscle CSA estimates taken via bony proxies following the protocols used previously on hominin specimens compared to recordings of muscle CSA taken from the CT scans of the same *H. sapiens* individuals that visualised their jaw-elevator muscles. This suggests that estimates of muscle CSA based on bony proxies could be inaccurate, as such loading an FE model with muscle forces estimated in this manner need taking into careful consideration (Toro-Ibacache et al. 2015).

While estimates of muscle CSA taken via bony proxies correspond poorly to recordings of CSA taken from specimen-specific CT scans (Toro-Ibacache et al. 2015), previous research has demonstrated correlations between PCSA calculated via cadaveric dissection and CSA recorded from CT scans of human specimens for the jaw-elevator musculature (Weijs and Hillen 1984a). Muscle CSA calculated from medical imaging differs from PCSA as it is a measure of the area of a cross-section of a muscle approximately perpendicular to its longitudinal axis (Weijs and Hillen 1984). The results of Weijs and Hillen (1984a) demonstrate that using muscle CSA over PCSA to estimate muscle force is a valid methodology, when a

specimen is unavailable for cadaveric dissection required to calculate PCSA. This approach has previously been used to estimate muscle force magnitudes applied to FE models of human crania (Toro-Ibacache et al. 2016; Godinho et al. 2018).

Therefore, while using bony proxies to estimate muscle CSA should be used with caution, using previously published PCSA estimates or direct calculations of CSA via medical imaging both have their benefits and drawbacks. Ultimately the choice of variable used to estimate muscle force will depend on the data available to a researcher; as this thesis will construct a craniofacial FE model of a *H. sapiens* specimen from an anonymised CT scan that contains soft tissues (see section 2.3), recording muscle CSA from this is a justifiable approach.

2.1.2.1. Modelling muscle activation patterns

For a specific biting task, the activation patterns of the jaw-elevator muscles varies according to the degree of jaw opening, bite location, bite direction and magnitude of bite force required (see section 1.1.1; Manns et al. 1979; Hylander and Johnson 1985; Naeije et al. 1989; Ferrario et al. 1993; Lindauer et al. 1993; Paphangkorakit and Osborn 1997; Spencer 1998; Miyawaki et al. 2001; Ferrario et al. 2004; Farella et al. 2008). Patterns of muscle activation data during masticatory behaviours can be recorded *in vivo* using electromyographic (EMG) studies, which records the electrical activity of muscles performing a particular task (Reaz et al. 2006). Muscle forces applied to FE models simulating a particular bites are often scaled using EMG data to reflect muscle activation patterns in order to produce more accurate predictions of stress, strain and bite force magnitudes (Ross et al. 2005; Fitton et al. 2015). However, while EMG studies demonstrate that activation patterns of the jaw-elevator muscles vary between individuals and during different feeding tasks (Hylander and Johnson 1985; Spencer 1998), muscle activation patterns experimentally acquired for one individual are often used to scale muscle forces applied to FE models of different specimens (e.g. Ross et al. 2005; Strait et al. 2009; Kupczik et al. 2007), and muscle activation data is absent for paleontological specimens.

As such, several researchers have investigated the impact of error in modelling muscle activation patterns on the predictions of FE models (Fitton et al. 2012; Ross et al. 2005; Tseng et al. 2011; Toro-Ibacache and O'Higgins 2016). Ross et al. (2005) carried out a sensitivity study regarding error in modelling muscle forces on a *M. fascicularis* cranium, examining the impact of four different PCSA calculations and nine different methods of scaling force magnitudes to EMG signals. The authors found that the majority in variation in the predictions of the model was attributable to variation in the overall magnitude of deformation due to differences in magnitude of applied muscle force, while only 6% of variation in predictions attributable to differences the mode of deformation (Ross et al. 2005). Fitton et al. (2012) also altered the muscle activation patterns applied to another *M. fascicularis* cranial model based on predictions of muscle activation patterns made by a multibody dynamic analysis model. These authors found that although the bite force predictions were sensitive to changes in input force magnitude, varying the relative activation of muscles during a particular biting scenario has less impact on global strain distributions than varying the simulated bite point (Fitton et al. 2012). However, these authors also reported that the deformation of the zygomatic region is sensitive to changes in the magnitude of force applied to the superficial masseter (Fitton et al. 2012). Toro-Ibacache and O'Higgins (2016) investigated the impact that variability in applied muscle force had upon the predictions of FE model of a *H. sapiens* cranium and found that although strain and reaction forces magnitudes are proportionate to the magnitude of applied force, predictions of strain distribution are relatively insensitive to heterogeneity in muscle activation patterns. Again however, these authors noted the sensitivity of the zygomatic region to the magnitude of force applied to the masseter, as well as the sensitivity of strains and reaction forces predicted at the glenoid fossae to the symmetry of loading (Toro-Ibacache and O'Higgins 2016).

The results of these sensitivity studies have indicated that that some regions of the skull like the zygoma and temporomandibular joints are sensitive to how muscle activation patterns are modelled (Tseng et al. 2011; Fitton et al. 2012; Toro-Ibacache and O'Higgins 2016). However, it is also shown that as applied muscle forces vary, the most significant source of variation in the predictions of models is the overall magnitude of strain, while relative distributions remain more consistent (Ross et al. 2005; Toro-Ibacache and O'Higgins 2016).

As such, when FE models are created to predict relative distributions of strains, if muscle activation patterns as modelled reasonably and consistently, the error introduced through inaccuracies in modelling muscle activation patterns are minimal (Ross et al. 2005; Fitton et al. 2012; Toro-Ibacache and O'Higgins 2016). Indeed, Toro-Ibacache and O'Higgins (2016), suggest that when human craniofacial FE models are constructed for these purposes, applying symmetrical, maximal force estimates is a reasonable loading simplification. Many *H. sapiens* FE models have been loaded in this manner (Ledogar et al. 2016; Toro-Ibacache et al. 2016; Godinho et al. 2018; Brachetta-Aporta and Toro-Ibacache 2021).

2.1.2.2. Modelling muscle force orientation

To simulate masticatory loading on FE models, the nodes within the origin sites of the jaw-elevator muscles on the cranium are loaded with force vectors that have a line of action directed to their insertion on mandible (Dumont et al. 2005; Strait et al. 2005). Ideally force vector orientations should defined from the mandible and cranium of specimen used to construct a FE model for the most accurate representation of specimen-specific muscle lines of action (Gröning et al. 2012; Toro-Ibacache et al. 2016; Toro-Ibacache and O'Higgins 2016; Godinho et al. 2018). However, when working with palaeontological or archaeological material, the mandible of specimens may not always be available to researchers. As such, many have addressed the sensitivity cranial and mandibular FE models to error in muscle force vector orientation (Bright and Rayfield 2011; Tseng et al. 2011; Gröning et al. 2012; Cox et al. 2015; Godinho et al. 2018; Stansfield et al. 2018).

When this has been addressed on cranial FE models (Bright and Rayfield 2011; Godinho et al. 2018), it has been reported that varying the orientation of muscle force vectors have small impacts upon the strains predictions of models. As the Broken Hill fossil (*Homo heidelbergensis*) does not have a mandible, when constructing their FE model of this specimen, Godinho et al. (2018) defined muscle force vector orientations from a scaled version of a *Homo neanderthalensis* mandible, and assessed the sensitivity of their cranial FE model to 5 degree changes in the orientation of each muscle force vector in each anatomical direction. These authors reported that the largest impacts on strain magnitude and

distribution occurred when the muscle force vectors varied anterior-posteriorly, but that these were negligible (Godinho et al. 2018). Similarly, when assessing the sensitivity of a *Sus domesitcus* model to changes in temporalis and masseter orientation, Bright and Rayfield (2011) reported that aside from strains local to the zygomatic arch, differences of up to 10 degrees in the orientation of masseter and temporalis force vectors only resulted in differences in principal strain ratios on the order of 0.01. Thus, although previous sensitivity studies have indicated that error in the direction of muscle force vectors have little impacts upon the prediction of cranial FE models (Bright and Rayfield 2011; Godinho et al. 2018), understanding the impacts that error in muscle force vectors orientation have on the predictions of cranial FE models is important and their sensitive to changes in this input parameter should be addressed.

2.1.3. Constraining models

In craniofacial FE models simulating masticatory loading, the configuration of constraints and force vectors applied to a model simulate the reaction forces experienced at the temporomandibular joints during jaw-elevation, and at the maxillary dentition when an is compressed between the occlusal surfaces by the jaw elevator muscles (Dumont et al. 2005; Strait et al. 2005). However, protocols vary regarding the position of these constraints, which axes the joints and teeth are constrained in, and the number that should be placed on a model. For example the protocols of Ledogar et al. (2016) used to constrain FE models of *H. sapiens* crania vary considerably to that of Toro-Ibacache et al. (2016) and Godinho et al. (2018) with regards to the position (articular eminences versus glenoid fossae), the number (one node versus multiple) and axes of constraints at the joints (constraining each joint in different axes versus constraining each joint in all three axes). Although these differences are likely attributable to these models being constructed for use within different FEA software packages.

Many authors investigating the sensitivity FE models to these variables have conducted their studies upon models of mandibles, and demonstrate that predictions of strain magnitude, distributions and reaction forces are sensitive to errors in how models are constrained

(Marinescu et al. 2005; Tseng et al. 2011; Gröning et al. 2012; Stansfield et al. 2018). Similarly, Cox et al. (2011) report that overly constraining their models of rodent crania artificially increased stresses predicted local to both joints. Combined, these studies demonstrate that the way in which models are constrained can impacts their results and therefore determining appropriate loading and boundary conditions is important (Marinescu et al. 2005). For comparative studies, these variables need to remain consistent for results between models to ensure that differences in form are driving differences in results (Tseng et al. 2011; Stansfield et al. 2018). What is also clear from the above is that there is no standard practice for constraining models. As such, researchers constructing FE models of crania should conduct accompanying sensitivity studies regarding this to understand how modelling assumptions impact their results.

2.2. Chapter objectives

It is clear from the above that FE model construction and loading protocols will vary depending on the specimen being modelled, and the questions a model is being used to address. For this thesis, the aim is to create an FE model of a modern *H. sapiens* cranium to be used in form-function investigations. This raw data which is available to construct this FE models from is a medical CT scan with soft tissue included (sourced from the New Mexico Decedent Imaging Database; Edgar et al. 2020). This means that the dissection of the specimen to calculate muscle PCSA was not possible, nor was the collection of *in vivo* EMG data, or the collection of material properties of craniodental tissues. Different masticatory loading scenarios will be simulated (incisor versus molar bites, and bites at submaximal and maximal gapes), using Vox-Fe, a voxel-based software package (Fagan et al. 2007; Liu et al. 2012). These factors will impact how the model needs to be built, the material properties assigned to its elements, and how it is loaded and constrained. As the scale of the questions being asked in this thesis are broad, some large modelling assumptions can be made that may have a minimal impact to the overall interpretation of the results. Yet, these modelling assumptions may produce variations in results and this needs to be considered. As such, this chapter has three objectives:

1) Describe the construction protocol for the *H. sapiens* cranial FE model

2) Compare the performance of the model against previously validated *H. sapiens* cranial FE models and other biomechanical expectations

3) Assess the sensitivity of the model to alterations in a variety of input parameters necessary to simulate bites at submaximal and maximal gapes

The final model can then be used to investigate various biological questions regarding form and function (see Chapter 3).

2.3. Objective one: The construction of a *Homo sapiens* finite element model

This subsection details the methodologies used to construct and define the loading and boundary conditions of a finite element (FE) model of a *Homo sapiens* cranium, following the review of previously reported protocols (see section 2.1).

2.3.1. Selection of a suitable specimen

The New Mexico Decedent Image database (MNDID) was used to select a suitable specimen to construct the FE model to be used within this thesis, which is a free database that contains whole-body CT scans of human cadavers (Edgar et al. 2020). A young adult female individual with complete, healthy, well-occluded, dentition was preferred for inclusion. A female specimen was preferred as there is evidence that KNM-ER 7377 (the *Homo ergaster* fossil used in this thesis; see Chapter 3) was female (Rightmire 1998). As the anatomy of the *H. sapiens* specimen will be altered to contain the zygoma region morphology of this fossil, a female specimen was the most appropriate choice to minimize the impacts of sex-based differences in craniofacial form. Individuals who were the victims of craniofacial trauma, had previously undergone any facial surgeries or had any significant craniofacial deformities, were excluded from consideration as were individuals wearing any clothing or accessories that introduced significant scan artefacts. The chosen specimen was a 21-year-old Latinx female. Permission to use the imaging data of the cadaver was granted by the NMDID in line with sections B.1 & 3 of their database access, sharing and use agreement (https://nmdid.unm.edu/resources/data-use). Further ethical approval to conduct this research was granted by the Hull York Medical School (09/06/2023, grant number 22-23 55)

2.3.2. Constructing the 3D geometry of the model

The 3D geometry of the *Homo sapiens* cranium was reconstructed within Avizo 9.2.0 (FEI, Thermofisher Scientific), from the DICOM stack of a head and neck CT scan with a voxel resolution of 0.566507 x 0.566507 x 0. 566507 mm^3. The DICOM stack was saved as a volume file suitable for segmentation within Avizo and semi-automated thresholding was used to define the boundaries between bone, soft tissues, and air. Due to the resolution of this scan, some of the fine bony anatomical features of the cranium were poorly represented following semi-automatic thresholding (Figure 19). Because of this regional thresholds were applied to fully reconstruct these areas, as Toro-Ibacache et al. (2016) demonstrate not reconstructing thin cortical bone structures in the creation of the human craniofacial FE model can influence the predictions of global strain distributions. This process (Figure 20) involves lowering the threshold applied to the voxels within a specified material to reconstruct fine anatomical structures from lower resolution scans. When this still failed to fully reconstruct such features, voxels were manually segmented. Manual segmentation was also used to separate the mandible and the cervical vertebrae from the cranium (Figure 21).

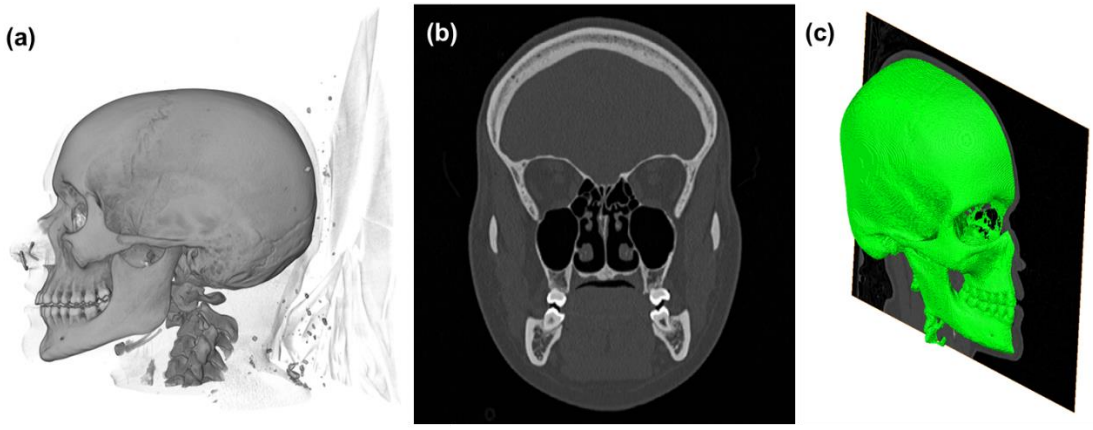

Figure 19. Volume rendering (a) and coronal slice (b) of the cadaveric CT scan prior to semi-automatic segmentation. The combination of a surface rendering of the cranium following semi-automatic segmentation and a sagittal CT slice demonstrates the fragmentary nature of the walls of the nasal cavity following semi-automatic segmentation (b).

The *H. sapiens* specimen was segmented into three materials: bone of the cranium (including both trabecular and cortical bone as one material) and the maxillary dentition (including enamel, dentine, and pulp as one material), and the mandible. While only the voxels segmented as the bone of the cranium and the maxillary dentition were used in the

construction of the FE model (see section 2.3.3), the mandible was also segmented as a bulk material to define specimen-specific loading and boundary conditions (see section 2.3.4). The air cells and paranasal sinuses were kept as hollow structures, to not overly stiffen the cranium (Parr et al. 2012; Fitton et al. 2015). The material representing the homogenisation of cranial cortical and trabecular bone will be referred to as 'bone' henceforth.

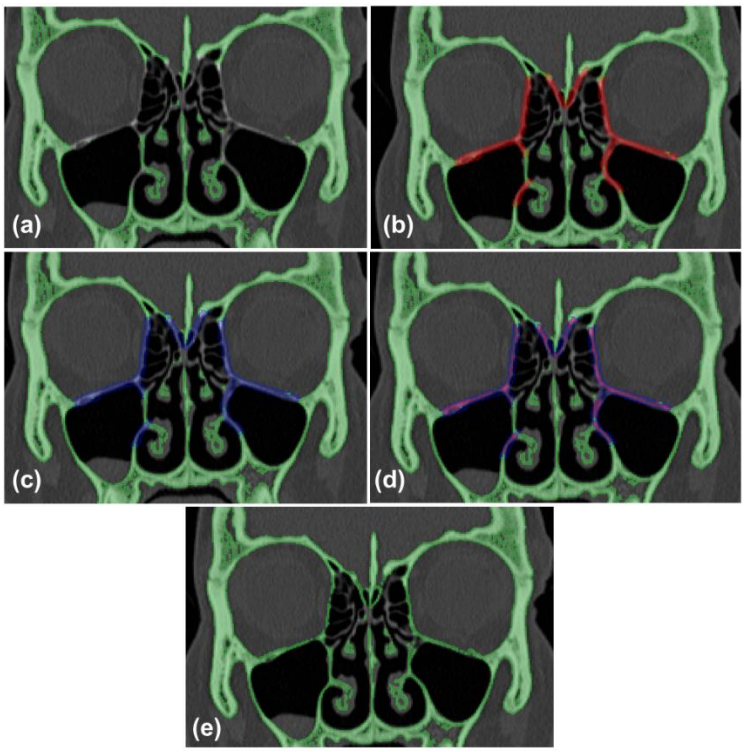

Figure 20. Regional segmentation of the nasal cavity and orbital walls. (a) The cranium following semi-automatic thresholding. (b) Selection of voxels to be regionally segmented. (c) The addition of the selected voxels to a new material. (d) The application of a regional threshold to this new material. (e) The cranium following the use of regional segmentation to reconstruct the nasal cavity and orbital walls.

The dental tissues were also modelled as a bulk material (i.e. homogenising the enamel, dentine, and pulp into one material) representing the crown and root morphology of the maxillary dentition (Figure 22). Previous sensitivity studies have demonstrated that this is a justifiable construction simplification if the aim of a model is to understanding global strain distributions, rather than predict absolute strain magnitudes local to the alveolar process (Cox et al. 2011; Herbst et al. 2021). The material representing the homogenised dental tissues of

the crown and root morphology of the maxillary dentition will henceforth be referred to as 'tooth'.

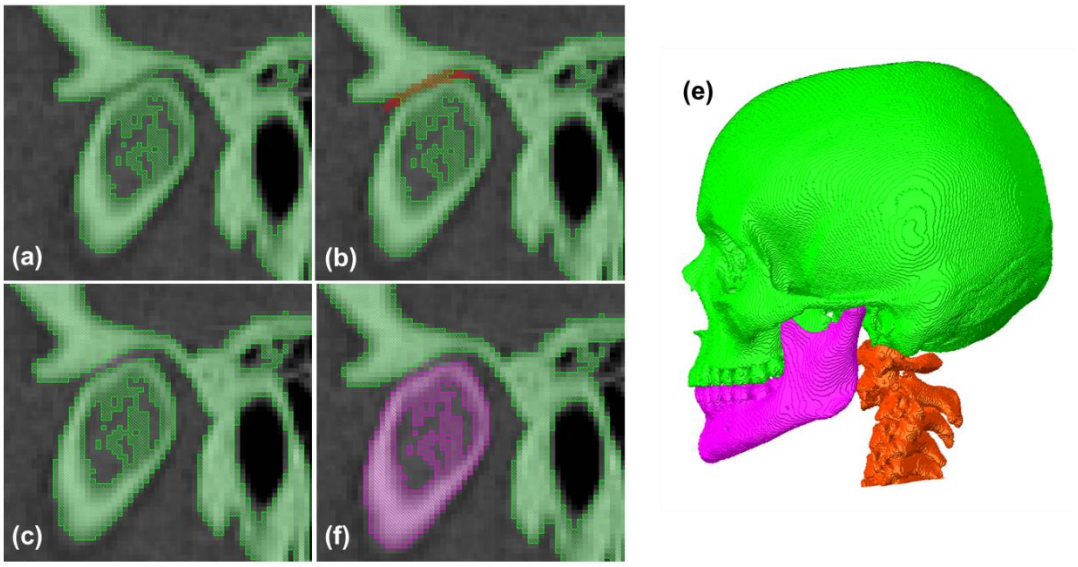

Figure 21. Manual separation of the cranium and mandible. (a) Articulation of the cranium and mandible following semi-automatic thresholding. (b) Manual selection of voxels to separate the cranium and mandible. (c) Separation of the cranium and mandible following manual segmentation. (d) Addition of the voxels representing the mandible into a new material (purple). (e) A surface rendering of the segmented cranium (green), mandible (purple), and cervical vertebrae (red).

Regional segmentation was also used to define the boundary between the tooth crowns and the surrounding air, as well as tooth roots from alveolar bone (Figure 22). To extract the morphology of the tooth crowns, voxels previously segmented via semi-automatic thresholding above the alveolar margin were selected and regionally segmented. Any voxels connecting adjacent tooth crowns were manually removed to ensure that the load applied to individual teeth during the solving of the model was transferred vertically into the cranium, rather than laterally between the teeth.

To extract the geometry of the tooth roots, voxels visually identified as to belonging to the tooth roots were added to a new material that was regionally segmented. The regional threshold applied was raised (compared to the initial semi-automatic threshold) to extract the denser cementum-covered tooth roots from the less dense alveolar bone. Because of this,

some voxels with lower grey values in the pulp cavity and alveolar bone were not selected. These voxels were manually added to either tooth or bone (Figure 22).

At this stage in the creation of the model, many assumptions and simplifications have been made. Section 2.1 outlined that previous sensitivity analyses have demonstrated that craniofacial FE models constructed in this manner will fail to accurately predict absolute strain magnitudes but provide acceptable predictions of relative strain distribution (Bright and Rayfield 2011; Fitton et al. 2015; Toro-Ibacache et al. 2016; Godinho et al. 2017). As this is acceptable for research purposes this model was constructed for no sensitivity analyses were conducted regarding the construction of the model.

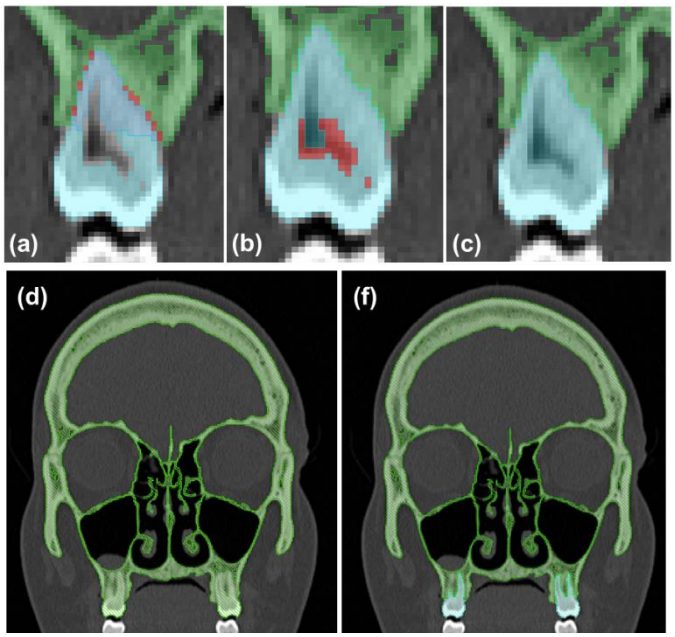

Figure 22. Manual addition of voxels to either bone or tooth following the regional segmentation of the maxillary dentition crown and roots. (a) Selection of voxels added to bone. (b) Selection of voxels added to teeth. (c) Fully segmented maxillary molar crown and root. (d) The cranium prior to the regional segmentation of the tooth crown and roots. (f) The cranium following the regional segmentation of the maxillary dentition.

2.3.3. Finite element mesh creation

Prior to converting the specimen into a finite element mesh, the label field containing fully segmented cranium and mandible was aligned to the Frankfurt horizontal. It was necessary to align the model to a defined orientation as the constraints within the FEA software used within this thesis (Vox-FE) are orientation dependent and prevent movement in the axis

ascribed to them (Fagan et al. 2007). The label field (containing the segmented cranium and mandible) was also re-aligned so that the cranial midline was perpendicular to the global Z-axis. Following this, a surface file of the mandible of the specimen was created in order to define some of the loading and boundary conditions of the model (see section 2.3.4), and then the voxels segmented as the mandible were then deleted, leaving only bone and teeth in the label field. This label field was then exported as a .bmp stack and converted into a finite element mesh suitable for use within Vox-Fe, a voxel-based FEA pre and post processing software package (Fagan et al. 2007; Liu et al. 2012). The finite element mesh was created using the Vox-2-Vec executable file which directly converts voxels into eight-noded linear cubic elements. The model consisted of 3,712,145 finite elements.

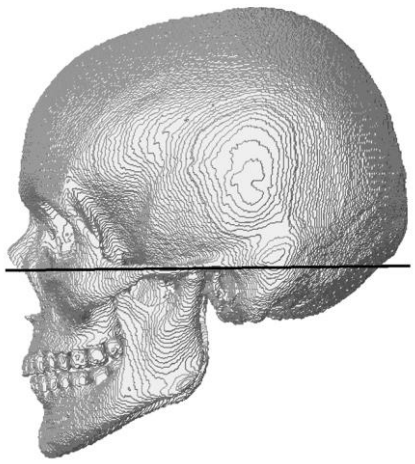

Figure 23. A surface rendering of the *H. sapiens* cranium and mandible aligned to the Frankfurt horizontal.

2.3.4. Determining the loading and boundary conditions of the model

The *H. sapiens* FE model was constructed from an anonymised CT scan, without physical access to the cadaver, meaning many of the loading and boundary conditions of the model could not be constructed from specimen-specific data. As such cranial material properties values could not be experimentally obtained, meaning the values applied to the elements of the FE model were simplified in accordance with the previously validated *H. sapiens* craniofacial FE models of Toro-Ibacache et al. (2016) and Godinho et al. (2017). This also means that the cadaver could not be dissected to obtain specimen-specific muscle internal

architecture data to calculate PCSA. While values for *H. sapiens* cadavers could be used from the literature (e.g. van Eijden et al. 1999), the CT scan used to construct the model also contained soft tissues meaning specimen-specific muscle cross-sectional area (CSA) could be used to estimate muscle force magnitude following Toro-Ibacache et al. (2015) and Toro-Ibacache and O'Higgins (2016). This was preferential to estimating muscle forces using bony proxies, owing to poor correlations between muscle CSA estimated in this manner versus muscle CSA calculated from CT scans (Toro-Ibacache et al. 2015). As the CT scan also contained the entire mandible of the specimen, the lines of action of the muscle force vectors applied to the model were also calculated following specimen-specific geometry. The following subsections outline how the loading and boundary conditions of the model were determined.

2.3.4.1. Estimating muscle force magnitude

Within humans, the muscles primarily responsible for jaw-elevator are the bilateral temporalis, masseter, and medial pterygoid (van Eijden et al. 1997), therefore the action of these six muscles were included in the loading conditions of the *H. sapiens* FE model. The magnitude of force (*f*Max) applied to each vector was estimated using a calculation of muscle CSA from the CT scan used to segment the model. The protocol used to estimate jaw-elevator muscle CSA followed Toro-Ibacache et al. (2015). Following Weijs and Hillen (1984a), these authors calculated jaw-elevator muscle CSA from sections taken of CT stacks aligned approximately perpendicular to their fibre orientations (see Table 1), and controlled for error in identifying muscle tissue from CT images by calculating the CSA of each muscle in each section three times and averaging this value, and by also recording CSA from the slices 1mm above and below the originally identified sectioning plane (Toro-Ibacache et al. 2015).

To calculate muscle CSA following Toro-Ibacache et al. (2015), the volume file of the cadaveric CT scan (containing soft tissues and bone) was rotated within Avizo until it was aligned to the orientations outlined in Table 1, using a volume render of the CT stack as a visual guide (Figure 24). Following this, muscle CSA was calculated. Voxels visually identified as the masseter, temporalis or medial pterygoid were selected and were regionally segmented, to separate

them from other surrounding soft tissues and bone. Any areas not selected as muscle tissue by the regional threshold but surrounded by four voxels regionally segmented as muscle tissue were manually added to make a more complete material. Regional segmentation was used to reduce error in how the boundaries between other soft tissues, bone and muscle were defined as this methodology is repeatable.

Table 1. Description of how the CT stack was aligned to calculate muscle CSA and which slice muscle CSA was recorded from for each jaw-elevator muscle, following Toro-Ibacache et al. (2015).

Muscle(s)	Alignment of CT stack	CT slice muscle CSA was calculated from
Temporalis	The Frankfurt horizontal	The coronal slice containing the medial most point of the infratemporal crest
Masseter and medial pterygoid	Parallel to the posterior-inferior border of the zygomatic bone	The coronal slice containing the posterior base of the mandibular lingula

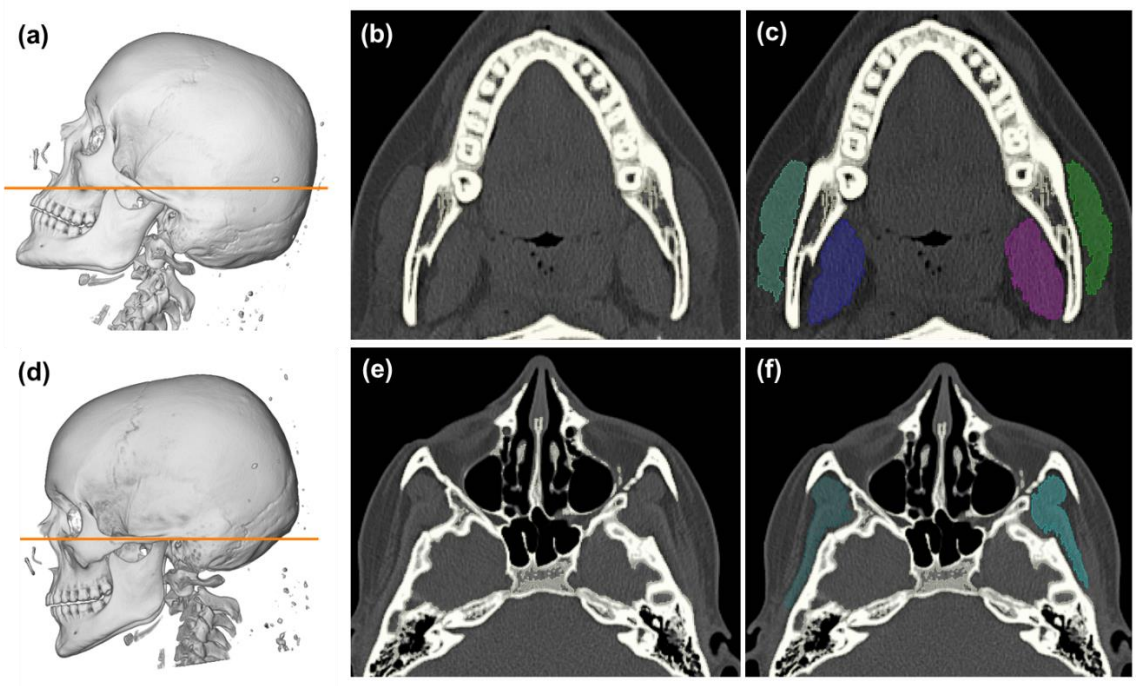

Figure 24 Visualisation of protocol for estimating masseter and medial pterygoid (a-c), as well as temporalis (d-f) CSA from the cadaveric CT scan following Toro-Ibacache et al. (2015). (a) The CT stack aligned to the inferior-posterior border of the zygomatic body. (b) The CT slice containing the posterior base of the mandibular lingula that masseter and medial pterygoid CSA was calculated from. (c) The voxels regionally segmented as the bilateral masseter (green and teal) and medial pterygoid (purple and pink). (d) The CT stack aligned to the Frankfurt plane. (e) The CT slice containing the medial-most point of the infratemporal crest that temporalis CSA was calculated from. (f) The voxels regionally segmented as bilateral temporalis (blue).

Further muscle CSA calculations were taken from slices approximately 1mm above and below the CT slices outlined within Table 1, using the same regional thresholds for all muscles across all slices. The material statistics module within Avizo was used to calculate the area of each

slice occupied by the materials segmented as the cross sections of the jaw-elevator muscles. The measurements of CSA for each jaw-elevator muscle from each slice were averaged to calculate an estimate of their CSA. The muscle CSA values calculated for this individual fall within the range reported by Toro-Ibacache et al. (2015) for the masseter and temporalis, and the values calculated for the medial pterygoid fall within the range identified by Weijs and Hillen (1984a).

The estimate of CSA for each muscle was then multiplied by 37 N/cm^2 to estimate *f*Max (Equation 1 and Table 2). This value was chosen as it is a previously estimated value of the muscle stress constant of the human masticatory musculature (Weijs and Hillen 1985), and has been used to estimate muscle *f*Max for previous *Homo sapiens* craniofacial FE models (Toro-Ibacache and O'Higgins 2016; Toro-Ibacache et al 2016; Godinho et al. 2018). Table 2 contains the average CSA of each bilateral muscle and its estimated *f*Max.

Equation 1. The equation used to estimate the maximum force produced by the masticatory muscles.

$$f\text{Max} = \text{CSA X } 37 \text{ N/cm}^2$$

Table 2. Average CSA of the jaw-elevator muscles and their estimated *f*Max.

Masticatory Muscle	Average CSA (cm^2)	*f*Max (N)
R. Masseter	2.98	110.31
L. Masseter	3.42	126.46
R. Medial pterygoid	3.48	128.55
L. Medial pterygoid	3.34	123.69
R. Temporalis	3.60	133.07
L. Temporalis	4.10	150.34

The estimated *f*Max was averaged bilaterally for each muscle, symmetrising the forces applied to the model (Table 3). The model was initially loaded assuming 100% activation of the jaw elevator muscles, owing to the lack of information surrounding the relative activation patterns of the specimen. While this is not a physiologically realistic loading scenario, previous sensitivity studies on *H. sapiens* craniofacial FE models have demonstrated that this is a reasonable modelling simplification to make in the absence of specimen specific muscle activation data (Toro-Ibacache and O'Higgins 2016). However, the sensitivity of the model to

these assumptions in the modelling muscle activation patterns was investigated as part of objective 3 of this chapter (see section 2.5.1).

Table 3. The symmetrised *f*Max estimates applied to the muscle force vectors of the model.

Masticatory Muscle Pair	*f*Max (N)
Masseter	118.39
Medial pterygoid	126.12
Temporalis	141.70

2.3.4.2. Modelling muscle lines of action within Vox-Fe

To simulate masticatory loading within FE models, force vectors representing the jaw elevator musculature are applied to FE models (Dumont et al. 2005; Strait et al. 2005). The lines of actions of the jaw-elevator musculature can be approximated on cranial FE models by applying force vectors oriented towards the insertion of these muscles to nodes within the origin sites of the muscles on the surface of a cranial model (Grosse et al. 2007). As such, within Vox-Fe nodes within the origin sites of the bilateral temporalis, masseter and medial pterygoid were selected as nodes that force vectors representing the lines of actions of these muscles were applied to (Table 4 and Figure 25).

To determine the orientation of the force vectors representing the action of the bilateral masseter, temporalis and medial pterygoid, landmarks were placed on a surface file of the mandible of the specimen within Avizo in locations approximating the insertion of these muscles (Table 4). The mandible was positioned so that the teeth were in occlusion and the condyles were in the glenoid fossae prior to the placement of these landmarks. The coordinates of these landmarks were used to orient the line of action of each vector within Vox-Fe by defining their end points.

Table 4. Descriptions of the nodes that the force vectors representing bilateral temporalis, masseter, and medial pterygoid were applied to, and the location of the landmarks placed on the mandible of the *H. sapiens* specimen that used to define the end points of these vectors.

Masticatory muscle	Description of nodes selected to approximate muscle origins	Position of the landmark used to determine force vector end point
Masseter	Nodes on the inferior border of the zygomatic arches from the anterior to the slope of the articular eminence to the outer corner of the zygomatic process on the maxilla	The widest part of the mandibular angle on the lateral aspect of the mandibular ramus
Medial pterygoid	Nodes on the medial surface of the lateral pterygoid plates of the sphenoid bone	The widest part of the mandibular angle on the medial aspect of the mandibular ramus
Temporalis	Nodes on the lateral walls of the frontal, sphenoid, temporal and parietal bones contained within the superior temporal lines, zygomatic arch and infratemporal crest	Superior most point on the coronoid process of the mandible

All the force vectors were modelled as 'area' forces, meaning that their magnitude was distributed equally over the nodes which they were applied to. The bilateral masseter and medial pterygoid were modelled as 'parallel' forces, meaning that the individual force vectors applied to each node selected within their origin sites (Table 4) ran parallel to the line of actions of these muscles, as defined by the position of their end point (Table 4). This reflects the rectangular shape of these muscles with broad origin and insertion sites (Gaudy et al. 2000; El Haddioui et al. 2007). The temporalis was modelled as a 'point' force meaning that the force vectors applied to each individual node selected within the origin site of temporalis (Table 4) converged upon its end point (Table 4). This reflects the fan shaped temporalis with its large origin in the temporal fossa, and a small insertion on the coronoid process (Hylander and Johnson 1985; Gaudy et al. 2002; El Haddioui et al. 2007).

The lines of action of the jaw-elevator muscles as described above were defined from a jaw-closed position, however as the jaw opens, these lines of actions will change (Herring and Herring 1974; Herring et al. 1979; Thockmorton and Dean 1994; Koolstra 2002). Therefore, to simulate bites at gape, as this thesis aims to do, the orientation of the force vectors applied to the FE model will need altering to reflect these changes (Bourke et al. 2008; Dumont et al. 2011; McIntosh and Cox 2016; Chatar et al. 2022). Because of this, the sensitivity of the models to alterations in the orientation of muscle force vectors was addressed (see section 2.5.2).

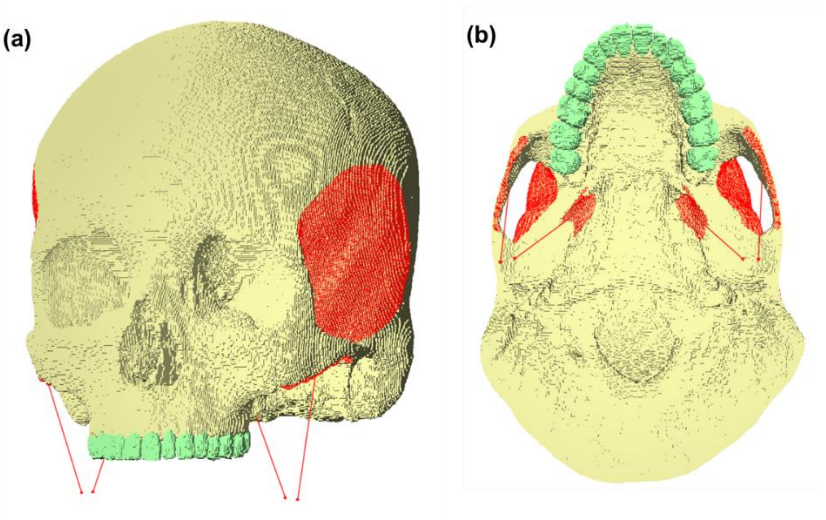

Figure 25. The selection of nodes within the origin sites of the jaw-elevator muscles and their lines of action within Vox-Fe. (a) Oblique view. (b) Inferior view.

2.3.4.3. Constraining the model

To prevent a model from rigid body movement during the solution phase, nodes are selected as constraints to prevent the model from moving in a particular dimension. As Vox-Fe is an orientation dependent FEA software package, the constraints applied to models prevent its movement in the direction of a defined axis (Fagan et al. 2007). Therefore, to simulate a vertical bite force vector, the model was constrained in all three axes (X,Y,Z) at both glenoid fossae and in the vertical (Y) axis at the maxillary dentition. Toro-Ibacache and O'Higgins (2016) and Godinho et al. (2017) report that reducing the number of axes of constraint at each joint for their human craniofacial FE model (also constructed in Vox-Fe) allowed rigid body movement during solution so it was decided to not assess the sensitivity of the model to changes in this input parameter. For each joint, 175 nodes were selected as constraints on the articular surface of the most anterior and superior parts of each mandibular fossa. However, during jaw opening the mandibular condyles rotate and anterior-inferiorly translated over articular eminences (Lindauer et al. 1995; Koolstra 2002; Hylander 2006), therefore to model bites at different gapes the location of the constraints at each temporomandibular joint will need altering (Dumont et al. 2011). As such the sensitivity of the model to this was addressed (see section 2.5.3).

Nodes on the inferior-most surfaces of the cusps of the bilateral P^3s and M^1s were selected as constraint (33 for the LP^3, 34 for the RP^3, 41 for the LM^1, and 46 for the RM^1). 36 nodes on the central incisal surface of both I^1s were selected to simulate an incisor bite due to their close apposition (Cox et al. 2011). Figure 26 visualises the model with all the applied loading and boundary conditions. While Figure 26 and this description refers to all the teeth being selected, the loading scenarios simulated only had one tooth constrained for each simulation sent for solving.

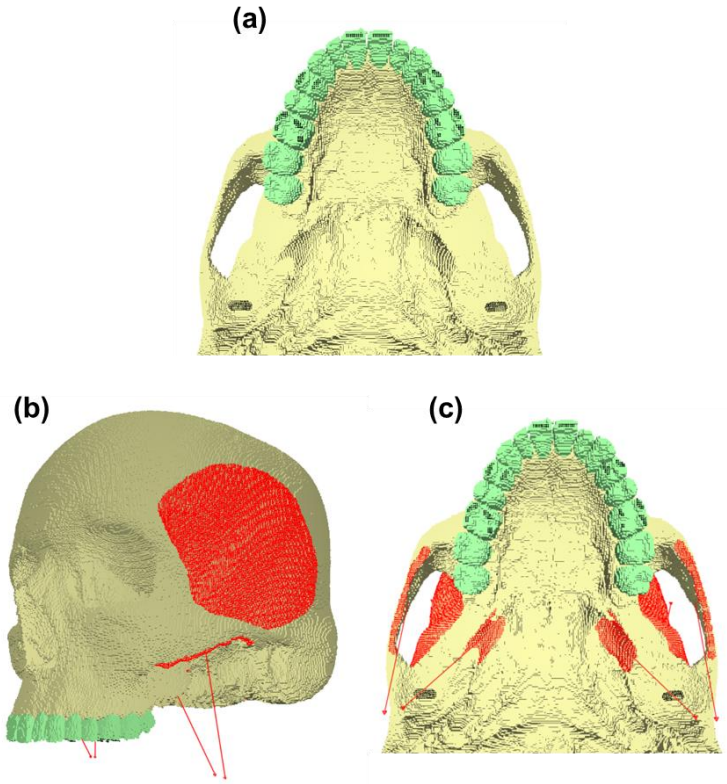

Figure 26. The nodes selected as the loading and boundary conditions of the model. (a) Inferior view of the nodes selected as constraints (black) at both glenoid fossae and the I^1s, LP^3, RP^3, LM^1 and RM^1. (b-c) The muscle force vectors (red) and constraints (black) of the model from a (b) oblique and a (c) inferior view. Only one tooth was constrained for each script sent for solving.

2.3.4.4. Material properties

Only two materials were included within the model: bone and teeth (see section 2.3.2). Each was modelled as isotropic and linearly elastic with a Poisson's ratio of 0.3, following previously validated human craniofacial FE models (Szwedowski et al. 2011; Toro-Ibacache et al. 2016; Godinho et al. 2017). A Young's modulus of 17 GPa was assigned to bone, approximating the

heterogeneity in material properties observed within the human cranium (Peterson and Dechow 2002, 2003; Peterson, Wang and Dechow 2006). An Young's modulus of 50 GPa was assigned to teeth, approximating the wide range of values reported for human dental tissues (Meredith et al. 1996; Habelitz et al. 2001; Cuy et al. 2002; He and Swain 2007). These are the same values that have previously been used in other validated human craniofacial FE models (Toro-Ibacache et al. 2016; Godinho et al. 2017), who experimentally ratified the material properties assigned to their model via nanoindentation and similar values have been reported for *Macaca fascicularis* specimens which have applied to validated craniofacial FE models (Kupczik et al. 2007, 2009; Fitton et al. 2012, 2015). Given that these material properties have produced valid predictions for models of both *H. sapiens* and *M. fascicularis* crania (Fitton et al. 2015; Toro-Ibacache et al. 2016; Godinho et al. 2017), it was decided that assessing sensitivity of the model to varying its material properties was not necessary. These values will apply to all subsequent models.

2.3.5. Model solution and data analysis

Once created, each set of loading and boundary conditions was exported as a script file and submitted for solving using PARA-BMU (the model solver of the Vox-Fe FEA software package) on Viking, a high-performance computing cluster provided by the University of York. This generates a series of simultaneous equations that are solved to calculate nodal displacements of a model based on the material properties of its elements and the loading and boundary conditions applied to it (Richmond et al. 2005; Rayfield 2007). These nodal displacements are used to interpolate strains, and stresses are calculated from the calculations of strain and the Young's modulus values of elements (Richmond et al. 2005; Rayfield 2007). As static loading scenarios are simulated, the reaction forces experienced at the constraints of the model required to prevent rigid body movement (by balancing its moments and maintaining the model in equilibrium) can be extracted.

2.3.5.1. Expressing strain distributions and magnitudes

Following the solution phases, predicted nodal displacements can be used to calculate and visualise a range of different output parameters including stresses and strains in the form of colour maps within Vox-Fe. Owing to the importance of strain in regulating the response of bone to mechanical load (Currey 2012), global strain maps representing von Mises strain were produced for each simulated bite point. 18 anatomical areas were chosen as sites to export average strain magnitudes (Figure 27), allowing absolute differences in strain magnitudes between different simulations to be quantified and compared. The specific areas chosen to extract strain magnitudes from were developed from those used within Ledogar et al. (2016) and Smith et al. (2015). However, as I^1 bites were simulated in this thesis, strains were also extracted from the subnasal region as this is directly superior to the premaxillary region containing the central incisors. To ensure that the alveolar region was evenly sampled, strains were also extracted from the infratemporal surface of the maxilla superior to the M^3s. Between 123 and 220 nodes were selected on the surface of the model within Vox-Fe in the areas described within Table 5, allowing strain magnitudes to be extracted following the loading of nodal displacements into Vox-FE and the calculation of strains.

Table 5. The name of anatomical regions that strain magnitudes were extracted from, their landmark number and their description

Name of Area	Region number	Description
Glabella	1	Midline point on the metopic suture between the supraciliary arches
Right supraorbital	2	Lateral to the frontal notch and medial to the supraorbital foramen on the right supraciliary arch
Left supraorbital	3	Lateral to the frontal notch and medial to the supraorbital foramen on the left supraciliary arch
Right postorbital junction	4	Along the angle formed between the temporal and frontal processes on the lateral aspect of the right zygomatic bone
Left postorbital junction	5	Along the angle formed between the temporal and frontal processes on the lateral aspect of the left zygomatic bone
Right zygomatic arch	6	Inferior half of the lateral surface of the temporal process of the right zygomatic bone anterior to the zygomaticotemporal suture
Left zygomatic arch	7	Inferior half of the lateral surface of the temporal process of the left zygomatic bone anterior to the zygomaticotemporal suture
Right zygomatic root	8	Articulation between the zygomatic and alveolar process of right maxilla, superior to the boundary between the M^1-M^2
Left zygomatic root	9	Articulation between the zygomatic and alveolar process of left maxilla, superior to the boundary between the M^1-M^2
Right infraorbital	10	Inferior to the right infraorbital foramen
Left infraorbital	11	Inferior to the left infraorbital foramen
Right nasal margin	12	Lateral most point on the inferior border of the nasal cavity on the right side
Left nasal margin	13	Lateral most point on the inferior border of the nasal cavity on the left side

Right zygomatic body	14	Superior to the lateral most corner of the zygomatic process of the right maxilla
Left zygomatic body	15	Superior to the lateral most corner of the zygomatic process of the left maxilla
Nasoalveolar clivus	16	Midline point between the incisive alveolar process and the anterior nasal spine
Right infratemporal maxilla	17	Immediately superior to the superior border of the alveolar process containing the right M^3
Left infratemporal maxilla	18	Immediately superior to the superior border of the alveolar process containing the left M^3

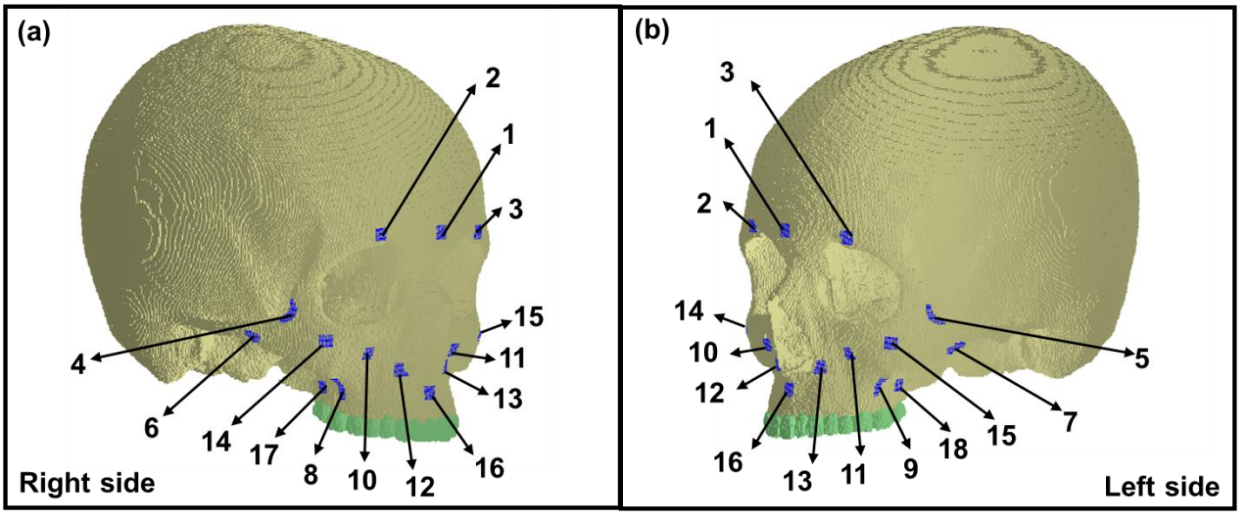

Figure 27. Right (a) and left view (b) of the FE model with the nodes selected in the locations where average strain magnitudes were extracted from (blue). The regions correspond to those outlined within Table 5.

2.3.5.2. Reaction forces and bite force efficiency

Maximal bite force and temporomandibular joint reaction forces are key metrics of masticatory performance. In craniofacial FE models simulating masticatory loads, calculating the reaction forces experienced at constraints on the maxillary dentition can act as a proxy for bite force and calculating the reaction forces experienced by constraints at the glenoid fossae or articular eminences are proxies for joint reaction forces (Dumont et al. 2005; Strait et al. 2005).

As the nodes at each biting tooth are constrained in the Y-axis only, reaction forces experienced will be in this axis. Therefore, the magnitude of reaction force experienced in the Y-axis at each constrained node on the surface of the constrained tooth for each simulation was summed to calculate bite force predictions (Godinho et al. 2018), this is referred to as

'bite force magnitude' henceforth. As the glenoid fossae were constrained in the X, Y, and Z directions, the constraints will experience a reaction force in all axes. Therefore, the magnitude of reaction force experienced at the constrains of each fossa was calculated using Equation 2, which will be referred to as the 'joint reaction force magnitude'.

Equation 2. Calculation of joint reaction force magnitude, where x, y, and z equal the sum of the reaction forces experienced in each axis by all the nodes constrained at one glenoid fossa.

$$\sqrt[2]{x^2 + y^2 + z^2}$$

Another key metric of masticatory performance is the efficiency of which muscle force is converted into bite reaction force (i.e. bite force efficiency; O'Connor et al. 2005). Within lever-mechanical analyses of the hominin masticatory apparatus, bite force efficiency has been calculated as the ratio of predicted bite force to the total applied muscle force (Anton 1990; O'Connor et al. 2005; Eng et al. 2013). This measure has also been used in hominin craniofacial FEA studies (Godinho et al. 2018), and has been termed mechanical advantage by some authors (including: Ledogar et al. 2016, 2017; Wroe et al. 2018; Cook et al. 2021). However, in this thesis the ratio of bite force magnitude to total applied muscle force is termed 'bite force efficiency', as it refers to the efficiency of the jaw-elevator muscles collectively, rather than the efficiency of individual muscles (O'Connor et al. 2005).

To calculate bite force efficiency the total input force of the model was calculated. This is the magnitude of the resultant vector of the jaw-elevator muscles and can be calculated from script files (which detail the magnitude and orientation of the forces applied to selected nodes) using Equation 2, where x, y and z are the sum of the force magnitude applied to the model in each axis. The ratio of bite force magnitude (calculated as described above) to total input force was used as a measure of bite force efficiency for each simulated bite.

2.3.5.3. Accounting for differences in bite force between models

While in the subsequent objectives of this chapter (objectives 2 and 3; see section 2.2), the model is of the same size and shape, in Chapter 3 the zygoma region of the model will be

altered to resemble that of a *Homo ergaster* fossil. As both size and shape are influential in determining the response of a structure to mechanical loading (Dumont et al. 2009), researchers have adopted different approaches to make the outputs of FE models of different shapes and sizes comparable. For example Ledogar et al. (2016) scaled their FE models of *H. sapiens* crania to have equal force: surface area ratios, following the recommendations of Dumont et al. (2009). Others, such as Toro-Ibacache et al. (2016), Fitton et al. (2012), and Godinho et al. (2018), have scaled the deformations predicted by their models to have equivalent bite forces. This is possible due to the relationship between the deformation of linearly elastic materials and magnitude of applied force (or Hooke's law; see section 1.1.4), meaning that the magnitude of deformation predicted by a model can be scaled to a pre-determined bite force while retaining the mode of deformation (Fitton et al. 2012; Toro-Ibacache et al. 2016). This approach was used within this thesis, with both strain distribution maps and the magnitudes extracted from the regions outlined within Table 5 (see section 2.3.5.1) being scaled to the deformations that would occur at pre-determined bite forces.

Therefore, the loading and boundary conditions of the model were determined following previously reported protocols used to construct *H. sapiens* craniofacial FE models in Vox-Fe (Toro-Ibacache et al. 2016; Godinho et al. 2018). Following their application to the model, a series of script files simulating a range of bites (I^1s, LP^3, LM^1, RP^3 and RM^1) were exported and sent for solving to assess whether the predictions of the model were in line with expectations.

2.4. Objective two: assessing the behaviour of the *Homo sapiens* FE model

As with any biomechanical models, many simplifications have been made in the construction of this craniofacial FE model. As such, it is important to assess that its predictions are reasonable and in line with biomechanical expectations (Rayfield 2007; Anderson et al. 2011). However, as the cadaver from which the model was constructed is physically unavailable for *ex vivo* strain analyses, the validity of its predictions were assessed against previously reported *Homo sapiens* craniofacial FE models and other biomechanical principles.

Firstly, the input force of a FE model should be equal in magnitude to the combined magnitude of reaction forces experienced at the constrained nodes, i.e. the output force of a model (Herbst et al. 2021). Secondly, lever mechanical models of the masticatory system predict that bite force magnitude increases as the bite point moves posteriorly along the dental row as length of the out-lever compared to the length of the in-lever decreases, increasing the mechanical advantage (MA) of the masticatory muscles (Hylander 1975). Therefore, as the muscle forces applied to the model were equal for all the simulated bites, bite force magnitude should increase as the bite point moves posteriorly. Further, when bites away from the midline are simulated, non-FE models that assume equal activation between the biting (working) and contralateral (balancing) jaw-elevator muscles predict that that the balancing joint experiences a reaction force greater than that experience at the working side (Smith 1978). Additionally, previously published *H. sapiens* craniofacial FE models have demonstrated that while strain magnitudes vary, strain distributions under masticatory loads are similar between individuals (Ledogar et al. 2016a), and models produce reasonably symmetrical strain distributions when bites on the same tooth on contralateral dental rows are simulated (Toro-Ibacache and O'Higgins 2016). Therefore, the predictions of the model will be assessed against the following 4 hypotheses:

H1. The input force magnitude of the model will be equal to the total output force magnitude of the model.

H2. Bite force magnitude will increase posteriorly along the dental row.

H3. Working joint reaction force magnitude will be lower than balancing joint reaction force magnitude.

H4. Strain distributions will be more comparable between bites simulated at the same tooth on contralateral dental rows, than to strain distributions for bites at different teeth on the same dental row.

If the model is behaving as expected then these hypotheses should be supported.

2.4.1. H1: The input force magnitude of the model will be equal to the total output force magnitude of the model

Theoretically, the force input into the model should be equal in magnitude to the sum of the reaction forces experienced at the nodes of constraint, as together these should prevent rigid body movement of the model during solution (Herbst et al. 2021). This can be assessed by calculating the total input force of the model (see section 2.3.5.2) and the total output forces of the model which can be calculated using Equation 2 where x, y and z represent the sum of the reaction forces experienced at all the constrained nodes in each axis. As such, to assess whether the input and output forces of the model were of an equal magnitude, a script file simulating an I^1 bite was exported and solved. This loading scenario (as well as the M^1 bites) was chosen as it would allow a direct comparison between this FE model and previously a validated *H. sapiens* crania modelled in Vox-FE by Toro-Ibacache et al. (2016) and Godinho et al. (2018).

The results of this I^1 bite predicted relative strain distribution comparable to the previously published models of *H. sapiens* crania simulating the same bite (Figure 28). This provided a preliminary indication that the model was behaving as expected. However, the input force magnitude and output force magnitude calculated for this simulation were not equal. Table 6 demonstrates that 33.58 N of force was lost during the model solution phase, meaning it was not in equilibrium. Therefore, H1 could not be accepted as true at this stage.

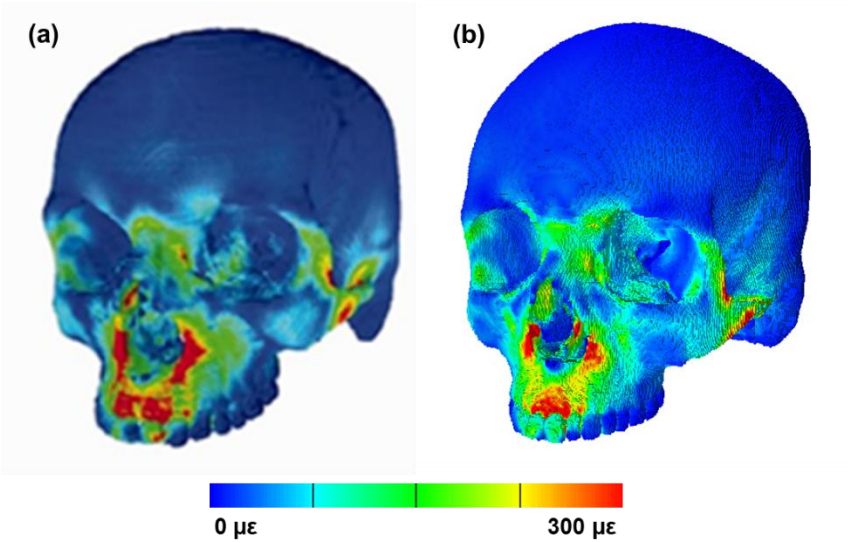

Figure 28. Global Von Mises strain maps produced from human craniofacial FE models simulating incisive bites. (a) The strain maps produced by Toro-Ibacache and O'Higgins (2016). (b) The strain map produced by the model constructed within this thesis.

Table 6. Comparison of input and output force magnitude for the first simulation of an I^1 bite.

	Magnitude (N)
Input Force	627.83
Output Force	594.25

Closer inspection of the model within Vox-Fe revealed that some of the nodes that left temporalis force vectors were applied to were not attached to nodes on the surface of the model (Figure 29). This explains the discrepancy between the input force and output force magnitudes as the forces attributed to these nodes were included within the calculation of input force magnitude, but the force applied to these nodes did not contribute to the reaction forces experienced at the model's constraints.

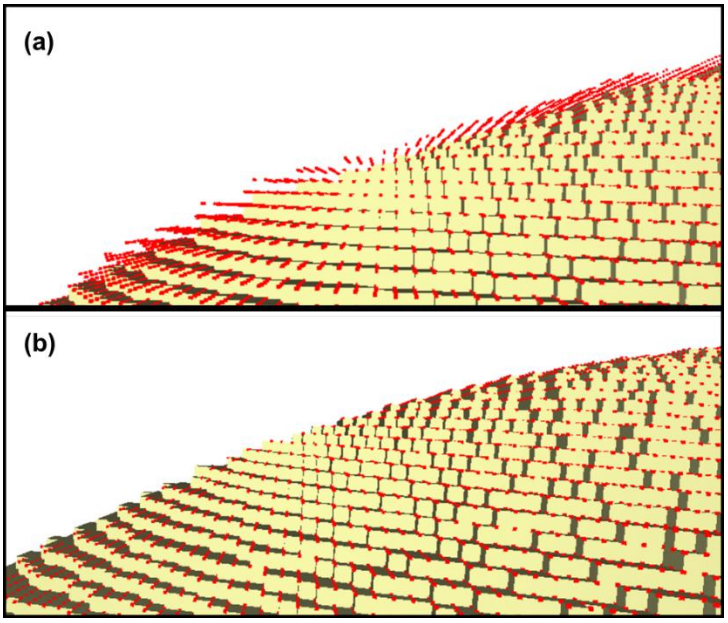

Figure 29. Comparison of the nodes selected as left temporalis between (a) the originally defined loading and boundary conditions and (b) the redefined loading and boundary conditions.

To resolve this, the boundary and loading conditions applied to the model were re-selected. Careful attention was given to ensure nodes not attached to the surface of the model were not selected, and in instances where this occurred the selection of nodes was restarted. Once the error was corrected the model was re-solved. The input force magnitude and output force magnitude were calculated and compared (Table 7) which demonstrated that the model was in equilibrium. To further confirm this, script files simulating the other bites (LP^3, RP^3, LM^1 and RM^1) were exported and sent for solving, and their respective input and output force magnitudes were calculated. Table 7 demonstrates that these values are equal to all seven simulations, therefore H1 is supported for this FE model.

Table 7. Input and output force magnitudes for the simulated bites using the revised boundary and loading conditions. The minor differences in the values can be attributed to error in rounding.

Bite Point	Input Force Magnitude (N)	Output Force Magnitude (N)
I^1	623.00	622.98
LP^3	623.00	623.01
LM^1	623.00	622.96
RP^3	623.00	623.00
RM^1	622.97	622.99

2.4.2. H2: Bite force magnitude will increase posteriorly along the dental row

Two-dimensional, biomechanical models of the human masticatory system predict that the maximum bite force magnitude produced should increase as the biting point moves posteriorly along the dental row, owing to the increasing MA of the jaw-elevator muscles (Hylander 1975). However, this is not reflective of biological reality, as most *H. sapiens* individuals can produce maximal bites forces at the M^1, explainable by the constrained lever model of jaw biomechanics (see section 1.1.2; Greaves 1978; Spencer 1999; Edmonds and Glowacka, 2020). As the muscle forces applied to the model within this subsection assume 100% activation for all the simulated bites, it is expected that bite force magnitude will continue to increase as the bite point moves posteriorly along the dental row.

To confirm that this FE model meets biomechanical expectations based on its input parameters, bite force magnitudes were calculated for each simulated bite. Table 8 demonstrates that along both sides of the dental arcade, bite force magnitude increases as the bite point moves posteriorly. Thus, H2 is supported for this FE model.

Table 8. Bite force magnitudes and TMJ reaction force magnitudes for all simulated bite points.

Bite Point	Bite Force Magnitude (N)	Left joint Reaction Force Magnitude (N)	Right joint Reaction Force Magnitude (N)
I^1	269.24	191.44	207.04
RP^3	323.47	222.39	133.76*
LP^3	317.54	146.61*	211.34
RM^1	394.2	215.56	109.2*
LM^1	390.67	109.69*	209.30

***Denotes the working joint for the bite simulated.**

While these results meet the expectations for models loaded with 100% muscle activation for each simulated bite, this is not physiologically realistic (see above and section 1.1.2). Sensitivity studies in the following section (chapter objective 2) explore the impacts that altering the force magnitudes applied to the model to reflect a more physiologically accurate muscle activation pattern have upon its predictions (see section 2.5.1).

2.4.3. H3: Working joint reaction force magnitude will be lower than balancing joint reaction force magnitude

Non FE biomechanical models of the human masticatory system that assume equal activation between the working and balancing side jaw-elevator muscles predict that the balancing joint experiences a reaction force greater than that experienced at the working side, during bites away from the midline (Smith 1978). As the FE models considered in this subsection are loaded with equal muscle forces, it is expected that the joint reaction force magnitude predicted at the working joint will be lower than that of the balancing side for all bites away from the midline. As mentioned, the next section will consider the sensitivity of the predictions of the model to alterations in muscle activation patterns (see sections 2.5.1 and 2.5.2).

To test hypothesis three, joint reaction force magnitudes were calculated for both the working and balancing joint for each simulated bite away from the midline (RP^3, LP^3, RM^1 and LM^1). Table 8 shows that the balancing joint reaction force magnitudes are higher than the working joint reaction force magnitudes for all bites simulated. This demonstrates that H3 is supported for this FE model.

2.4.4. H4: Strain distributions will be more comparable between bites simulated at the same tooth on contralateral dental rows, than to strain distributions for bites at different teeth on the same dental row

Different bites induce different strain distributions in the craniofacial skeleton. Previously published craniofacial FE models have demonstrated that while strain magnitudes vary, strain distributions under masticatory loads are similar between individuals (Ledogar et al. 2016a), and models produce reasonably symmetrical strain distributions when bites on the same tooth on contralateral dental rows are simulated (Toro-Ibacache and O'Higgins 2016), while strain distributions vary more when bites at different point on the same dental row are simulated (Fitton et al. 2012). To test hypothesis four, the strains predicted by this model simulating I^1, LP^3, LM^1, RP^3 and RM^1 bites were visually inspected to assess whether strain

distributions were more comparable between bites simulated at the same tooth on contralateral dental rows, than between bites at different teeth on the same dental row.

Firstly, the global strain distributions predicted by this model (Figure 30) simulating I^1 and LM^1 bites are a visual match to the validated models of Toro-Ibacache et al. (2016) and Godinho et al. (2018) that were also modelled using Vox-Fe and were constructed following similar protocols to the model created for this thesis (Figure 28, see section 2.4.1). This is indicative that the distributions of strain predicted by this model for the bites simulated are as expected for a *H. sapiens* cranium under masticatory loads. Further comparisons of strain and reaction force magnitude between these models cannot be made due to uncontrollable differences in loading and boundary conditions.

Figure 30 demonstrates that the global strain distribution plots vary more between bites at different points along the dental row, compared to equivalent bites on contralateral dental row. The regions local to the origins of the jaw-elevator musculature demonstrate consistently high strains between the biting simulations. The mandibular fossae also experienced high strains during each biting scenario. Aside from the I^1 bite during which strains across the glenoid fossae were reasonably equally distributed, the fossae experiencing the highest strains varied depending on which side of the cranium was working or balancing. Through all biting scenarios, the supraorbital region strains little. During the I^1 bite, strain is distributed from the biting point through the facial skeleton along an inferior-superior gradient about the midline; the regions experiencing the highest strains are the subnasal region, the lateral borders of the nasal aperture, and the frontal process of the maxilla, and the anterior palate.

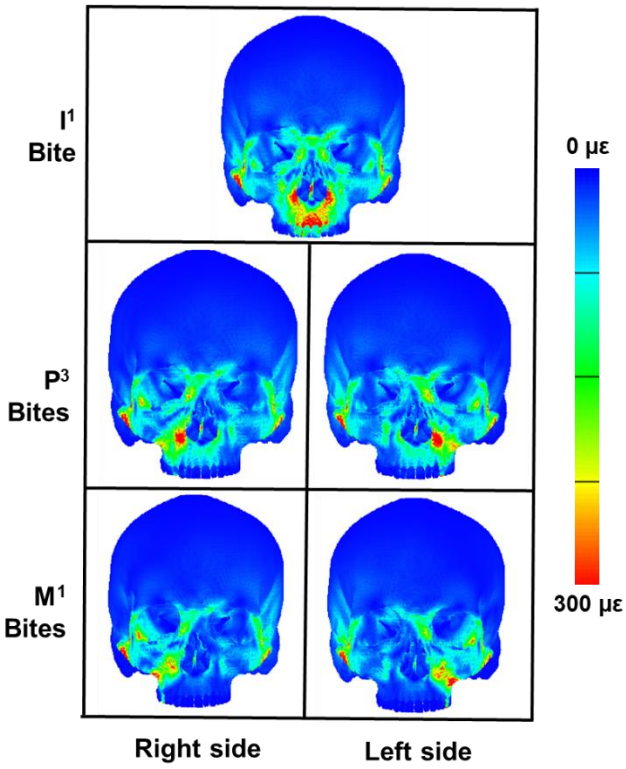

Figure 30. Global distribution of von Mises strains for all simulated bites (I^1, LP^3, RP^3, LM^1, RM^1). The incisor bite falls in-between the left and right columns as the bite point lies on the midline.

As the biting point moves to the P^3 the areas experiencing the highest strains move away from the midline and concentrate on the working side of the face, again through the zygomatic root, lateral nasal margin, and the frontal process of the maxilla. Although for this bite the subnasal region and balancing lateral nasal margin still experienced elevated strains. When M^1 bites are simulated, strains are more concentrated on the working side of the face, again through the zygomatic roots, and the frontal process of the maxilla. The elevated strains in the subnasal and bilateral nasal margins seen in more anterior bites are not observed. Overall, the global strain maps produced by bites at the same tooth on contralateral dental rows appear to mirror one another relatively closely, yet differences in strain distribution are more apparent between different bite locations (Figure 30). This demonstrates that H4 is supported for this model.

As all four hypotheses can be accepted as true, it can be said that the model is behaving as expected. Therefore, the model can be used in the subsequent zygoma region morphology form-function analysis of this thesis.

2.5. Objective three: assessing the sensitivity of the *H. sapiens* model

An important part of constructing biomechanical models is quantifying how sensitive their output parameters are to altered input parameters, allowing assessments of the robusticity of the predictions made by a model (Sellers and Crompton 2004; Gröning et al. 2012). As one of the aims of this thesis is to simulate bites at submaximal and maximal jaw gapes, this may require altering a range of input parameters (including: relative muscle activation patterns, the location of the nodes constrained at the glenoid fossae, and the orientation of the muscle vectors), to account for mandibular rotation and translation during jaw opening and how muscle activation patterns change as the jaw is opened (Bourke et al. 2008; Dumont et al. 2011; McIntosh and Cox 2016; Chatar et al. 2022). Understanding how these changes may influence the predictions of the model is important to contextualise the results of simulations with altered input parameters, and to establish what input parameters need altering to simulate bites at submaximal and maximal gapes.

2.5.1. Sensitivity Study One: sensitivity of the FE model to modelling different muscle activation patterns

In vivo EMG experiments recording jaw elevator muscle activity have demonstrated that the relative activation patterns of these muscles' changes for bites at different stages of jaw opening. Typically, during bites performed at the early stages of jaw opening a decrease in muscle activity is seen, whereas an increase is seen as the jaw reaches the maximal stages of opening to compensate for the decrease in muscle force that occurs as the jaw-elevator muscles are stretched beyond their optimal lengths (see sections 1.1.1 and 1.1.3; Manns et al. 1979; Mackenna and Turker 1983; Lindauer et al. 1993; Pröschel et al. 2008; Koc et al. 2012). Altering the symmetry and heterogeneity of applied muscle force to a FE model has been demonstrated to impact predicted reaction force magnitudes, as well as the magnitude and distribution of strains local to the attachments of the masticatory musculature, due to

alterations in the magnitude of the force input into the model and the relative amount of force applied to each vector (Ross et al. 2005; Fitton et al. 2015; Toro-Ibacache and O'Higgins 2016). While previous sensitivity studies have demonstrated that not loading models with a physiologically realistic muscle activation pattern meaningfully approximates global strain distributions (Ross et al. 2005; Fitton et al. 2012; Toro-Ibacache and O'Higgins 2016), these studies were not simulating bites at different gapes. Thus, the sensitivity of this model to altering muscle activation patterns was considered.

To assess this, the sensitivity of the model's predictions was assessed by comparing the predictions of a simulation loaded assuming 100% activation for each muscle and a simulation loaded where a more physiologically realistic muscle activation is modelled. It is hypothesized that while the predictions of reaction force and global strain magnitudes will be sensitive to variations in applied muscle force, predictions of strain distributions will remain comparable.

2.5.1.1. Modelling different muscle activation patterns

As no *in vivo* EMG data could be obtained for the specimen, previously recorded and published EMG data was used to scale the *f*Max values originally applied to the model (see section 2.3.4.1) to an activation pattern more reflective of physiological reality during a LM^1 bite at a closed jaw position. The EMG signals used to scale masseter and temporalis were the average standardised EMG readings from Spencer (1998), and the EMG readings for medial pterygoid were taken from MacDonald and Hannam (1984). Table 9 denotes the scaling factors used to for each muscle force vector modelled for the simulations included within this sensitivity test. Script files simulating a LM^1 bite loaded assuming 100% muscle activation (simulation 1) and simulating an LM^1 bite loaded with a physiological activation pattern (simulation 2) were exported and sent for solving. The predicted deformations were scaled to a 500 N bite as this falls within the range of voluntary maximum unilateral clenching force that *H. sapiens* females can generate under experimental conditions (Waltimo and Könönen, 1993).

Table 9. Masticatory muscle force at 100% activation and the scaled forces that represent a more physiological activation pattern for each muscle during a closed jaw LM^1 bite.

	Muscle Force (N)					
	Temporalis		Masseter		M. pterygoid	
	Left	Right	Left	Right	Left	Right
***f*Max (100% activation)**	141.70	141.70	118.39	118.39	126.12	126.12
Scaling factor[a]	0.8	0.68	0.6	0.7	0.75	0.5
Scaled muscle force magnitude	113.36	96.36	71.03	82.87	94.59	63.06

[a]These scaling factors were calculated from the EMG values reported by Spencer (1998) for masseter and temporalis, and MacDonald and Hannam (1984) for medial pterygoid.

2.5.1.2. Results from modelling different muscle activation patterns

Altering the relative activation patterns of muscle force applied to the model had an appreciable effect on the reaction force magnitudes predicted by the model (Table 10). Firstly, there was a 130.38 N decrease in bite force magnitude between the simulation 1 and the simulation 2 (Table 10). A similar trend is observed for joint reaction force magnitudes, with a 74.32 N decrease at the balancing joint and a 43.06 N decrease at the working joint; this further demonstrates the sensitivity of joint reaction forces to applied muscle forces previously identified by Toro-Ibacache and O'Higgins (2016). These observations are likely a product of the difference in the overall input force magnitude between the two models (205.9 N).

Table 10. The input force magnitude, and reaction force magnitudes predicted for a LM[1] bite when the model is loaded assuming 100% activation for each muscle (simulation 1), versus when the model is loaded with a more physiologically accurate muscle activation pattern (simulation 2).

Simulation	Input Force Magnitude (N)	Reaction Force Magnitudes (N)		
		Bite	Right TMJ	Left TMJ
1	622.96	390.67	209.3	109.69
2	417.06	261.29	134.98	66.63

As expected, the biggest impacts of altering the heterogeneity and symmetry of applied muscle force was upon the strain magnitudes predicted by the model. Figure 31 and Figure 32 demonstrate that when differences in bite force are not controlled for, simulation 1 predicted higher strain magnitudes globally. Once the differences in bite force are controlled for by scaling strains to a 500 N bite, minor differences in strain magnitude local to the zygomatic arch can be observed visually between simulation 1 and 2, reflecting the impacts of altering the force applied to the masseter. For example, at region 6 (the right zygomatic arch) simulation 1 predicted lower strain magnitudes (338.06με) than simulation 2

(355.49με), however at region 7 (the left zygomatic arch) simulation 1 predicted higher strain magnitudes (264.39με) than simulation 2 (235.49με). A similar trend is observable at the post-orbital junctions (regions 4 and 5; Figure 32). These observations are expected and are consistent with previous sensitivity studies such as Kupczik et al. (2007), Fitton et al. (2012) and Toro-Ibacache and O'Higgins (2016) who also note the sensitivity of the zygomatic region of FE models of macaques and modern humans to varying the heterogeneity and symmetry of applied force.

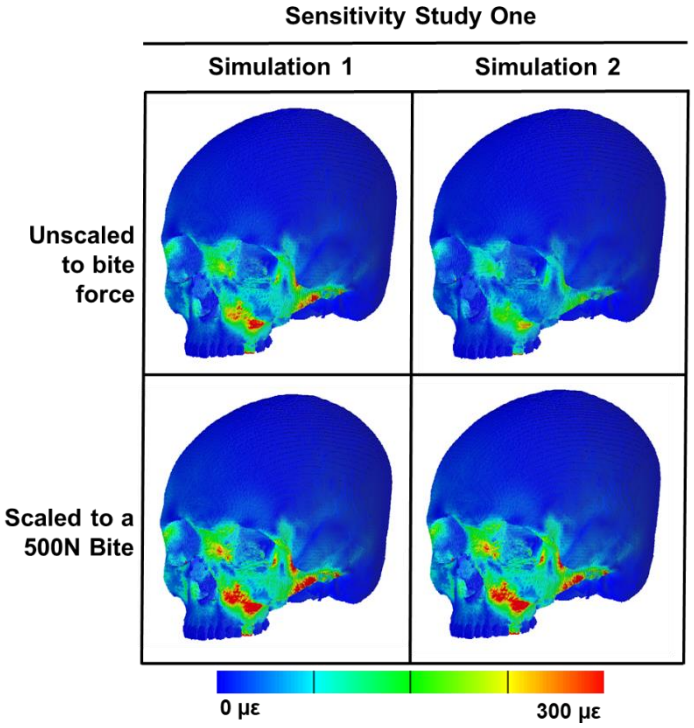

Figure 31. von Mises global strain distribution maps for a LM[1] bite when the model is loaded assuming 100% activation for each muscle (simulation 1; left column), versus when the model is loaded with a more physiologically accurate relative muscle activation pattern (simulation 2; right column). Distributions both unscaled to a given bite force (top row) and scaled to a 500 N bite (bottom row) are shown.

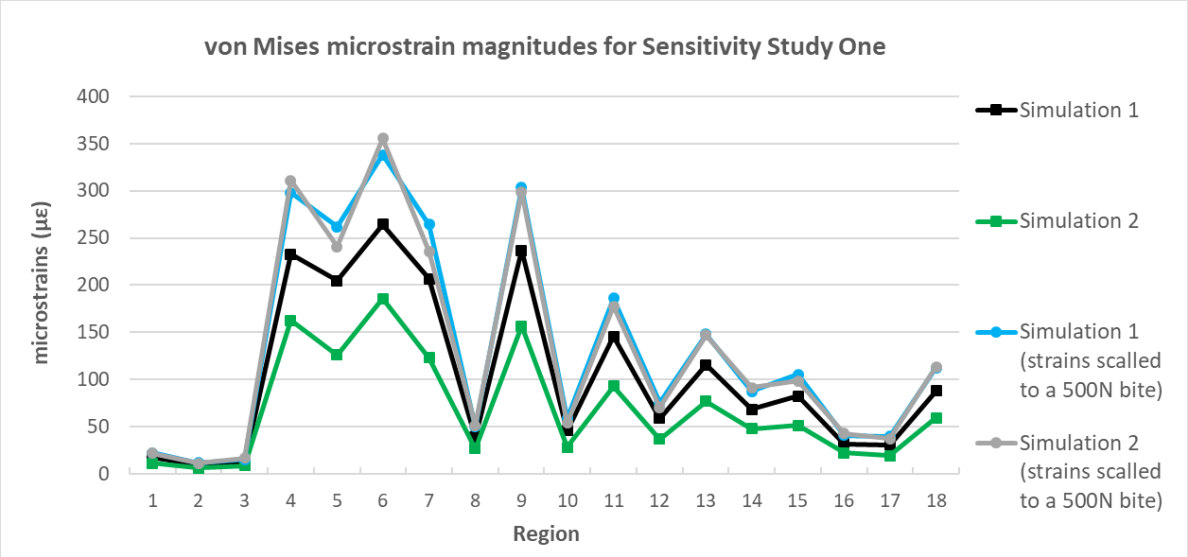

Figure 32. Average von Mises strain magnitudes for a LM[1] bite when the model is loaded assuming 100% activation for each muscle (simulation 1), versus when the model is loaded with a physiological muscle activation pattern (simulation 2). Magnitudes unscaled to a given bite force (green and black lines) and scaled to a 500 N bite (blue and grey lines) are shown.

The results of this sensitivity study demonstrate that the reaction force predictions and strain magnitudes will vary between models loaded with different total input force magnitudes, however once these differences for are controlled for, global strain distributions vary little. Therefore, the hypothesis pertaining to this sensitivity study (see section 2.5.1) can be accepted.

As experimental limitations prevent the inclusion of the medial pterygoid in many EMG studies, the values reported by MacDonald and Hannam (1984) are the only *in vivo* medial pterygoid relative activation data available for *H. sapiens,* but this did not include bites at different gapes. As such, the activation patterns of this muscle during bites at different gapes would either need to be estimated, or not scaled to a relative activation at all. Given this, and the limited impacts that simulating physiologically realistic muscle activation patterns had upon predictions of craniofacial strain, assuming 100% activation for each jaw-elevator muscle is a reasonable simplification to make in the loading of this model in the absence of suitable relative activation pattern data, as has been suggested by Toro-Ibacache and O'Higgins (2016) for other *H. sapiens* cranial FE models. Going forwards, 100% muscle activation will be assumed for every biting scenario simulated, and to make results of different

simulations more comparable, strain distribution plots and extracted magnitudes will be scaled to the same bite forces.

2.5.2. Sensitivity Study Two: sensitivity of the FE model to altering muscle vector orientation

As the mandible opens, the spatial positioning of the jaw-elevator muscle insertions also change, altering their line of action, mechanical advantage and thus force production capabilities (Thockmorton and Dean 1994; Koolstra 2002). As such, when bites at gape have been simulated on mammalian cranial and mandibular FE models muscle force vector orientations are altered to reflect how their lines of action change as the mandible opens (Bourke et al. 2008; Dumont et al. 2011; McIntosh and Cox 2016; Chatar et al. 2022). Changing the mechanical advantage and the lines of actions of the muscle force vectors applied to a cranial FE model therefore has the potential to substantially impact predictions of reaction forces and craniofacial strains. Because of this, the sensitivity of the model to altering the orientation of muscle force vectors was investigated.

To investigate this, a series of models were created in which the lines of actions of the masseter and medial pterygoid vectors were altered by re-defining the location of their end points. It is hypothesized that while the predictions of reaction force and strain distributions local to the zygoma will be sensitive to variations in the orientation of the masseter and medial pterygoid vectors, predictions of global strain distributions will remain consistent.

2.5.2.1. Altering the orientation of the masseter and medial pterygoid vectors

The decision was made to address the sensitivity of the model to alterations in the orientation of the masseter and medial pterygoid vectors as they both have wide areas of insertion on the mandibular ramus, meaning they have multiple possible lines of action (Godinho et al. 2018). To test the sensitivity of the model to alterations in the orientation of these force vectors, two new sets of landmarks approximating the insertions of the masseter and medial pterygoid force vectors were placed on the surface file of the mandible of the *Homo sapiens* specimen in Avizo (Table 11). The landmarks were placed bilaterally on the medial and lateral

aspects of the mandibular angle at its anterior and posterior most limits (Figure 33), approximating the limits of the insertion sites of these muscles (Gaudy et al. 2000; El Haddioui et al. 2007; Godinho et al. 2018). The coordinates of these landmarks were used to redefine the end points of the force vectors of the masseter and medial pterygoid within Vox-Fe, changing their orientation. To assess the sensitivity of the model to the orientation of masseter and medial pterygoid force vectors, the results of three simulations were compared (Table 11). All other loading and boundary conditions remained consistent with previous simulations. Script files simulating LM^1 bites were exported and solved. Again, the deformations predicted by the three simulations were scaled to a 500 N bite (see section 2.3.5.3).

Table 11. Description of the landmarks used to define the masseter and medial pterygoid force vector end points for simulations 1, 2 and 3 of sensitivity study two.

Simulation	Location of masseter end point	Location of M. pterygoid end point
1	Anterior limit of the mandibular angle on its lateral aspect	Anterior limit of the mandibular angle on its medial aspect
2	The widest part of the mandibular angle on its lateral aspect	The widest part of the mandibular angle on its medial aspect
3	Posterior limit of the mandibular angle on its lateral aspect	Posterior limit of the mandibular angle on its medial aspect

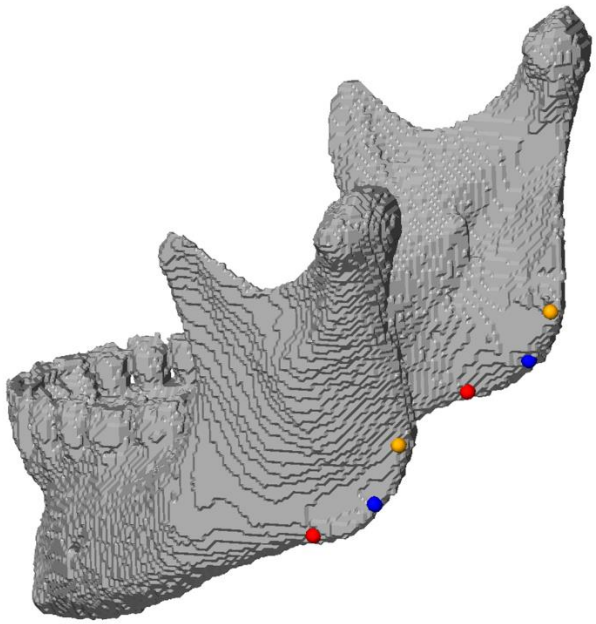

Figure 33. The landmarks used to define the masseter and medial pterygoid force vector end points for sensitivity study two, simulation 1 (red), simulation 2 (blue), and simulation 3 (orange).

2.5.2.2. Results of altering the orientation of the masseter and medial pterygoid vectors

The results of this sensitivity test indicate that the reaction force predictions of the model were sensitive to changes in the orientation of the masseter and medial pterygoid force vectors. Table 12 indicates that this had a pronounced impact on the magnitude of total input force, with values ranging from 614.59 N with for simulation 3 to 679.70 N for simulation 1. This is consistent with the observations of Stansfield et al. (2018) for their model of a human mandible.

This variation in input force magnitude impacted the reaction force magnitudes predicted by the model. While the bite force predictions between the simulations are consistent and only vary by 7.43 N between simulations 1, 2 and 3 (Table 12), larger impacts were apparent for joint reaction force magnitudes, and particularly how symmetrically this was distributed between the working and balancing joints. For example, simulation 1 predicts the largest disparity between reaction force magnitudes at the right and left joints (134.08 N).

Table *12*. The input force magnitude and the reaction force magnitudes for a LM[1] bite where end points of the bilateral masseter and medial pterygoid vectors were defined by landmarks placed on the anterior most (simulation 1), central (simulation 2) and posterior most (simulation 3) limits of the mandibular angle (see Table 11).

Simulation	Input force magnitude (N)	Reaction force magnitudes (N)		
		Bite force	Right joint	Left joint
1	679.70	388.85	232.17	98.09
2	649.89	395.23	215.45	93.02
3	614.59	387.81	208.52	117.71

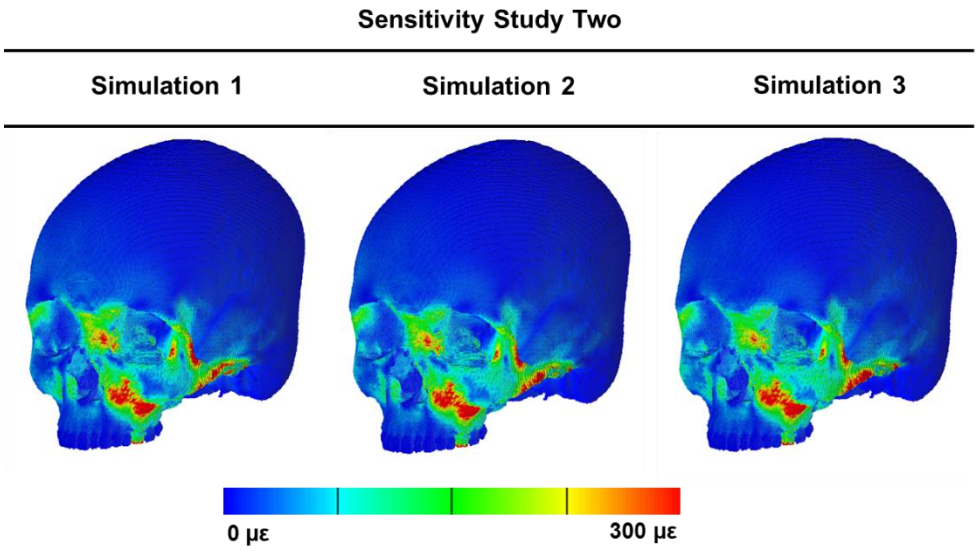

Figure 34. Global Von Mises strain distribution for a LM[1] bite where end points of the bilateral masseter and medial pterygoid vectors were defined by landmarks placed on the anterior most (simulation 1), central (simulation 2) and posterior most (simulation 3) limits of the mandibular angle (see Table 11). All are scaled to a 500 N bite.

The differences in strain distribution (Figure 34) and magnitude (Figure 35) between simulations 1, 2 and 3 were mostly concentrated locally to the zygoma. The global differences in strain distribution were minimal, aside from some slight differences in strain magnitude in the interorbital and glabella regions where simulation 1 predicted the highest magnitudes and simulation 3 predicted the lowest magnitudes (Figure 34). Most of the differences in strain predictions between simulations 1, 2 and 3 are localised zygoma region (Figure 34 and Figure 35). For example, at the postorbital junctions, simulation 3 predicted the lowest strains (287.12με at region 4 and 255.00με at region 5), whereas simulation 1 predicted the highest strains (358.62με and 331.01με). The reverse of this observed in the zygomatic arches, where simulation 1 predicted the lowest strains (253.41 με at region 6 and 212.14με at region 7) and simulation 3 predicted highest strains (353.95με and 266.74με). Simulation 1 also predicted the lowest strains at the zygomatic bodies (52.09με at region 14 and 71.76με at region 15), whereas simulation 3 predicted the highest strains (94.86με and 107.69με). There was less difference in magnitude between the simulations 1, 2 and 3 in the other regions of the facial skeleton. These results are in correspondence of previous researchers who have investigated the sensitivity mammalian craniofacial FE models to altering muscle force vector orientation (Bright and Rayfield 2011; Cox et al. 2011; Cox et al. 2015; Godinho et al. 2018).

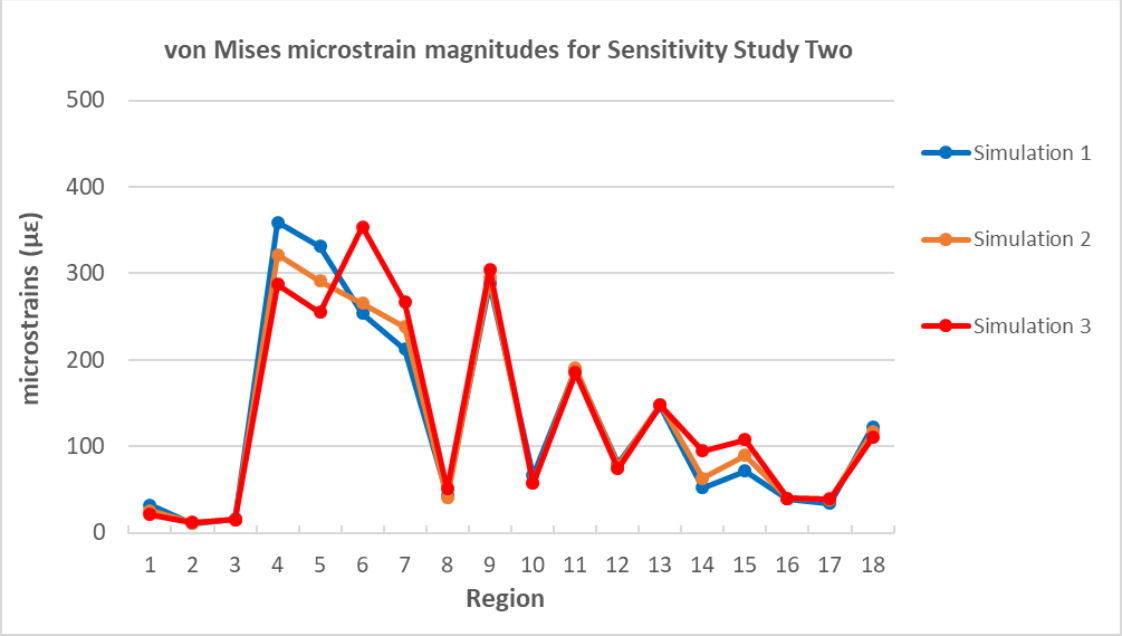

Figure 35. Average von Mises strain magnitudes for a LM[1] bite where end points of the bilateral masseter and medial pterygoid vectors were defined by landmarks placed on the anterior most (simulation 1; blue line), central (simulation 2; orange line) and posterior most (simulation 3; red line) limits of the mandibular angle (see Table 11). All magnitudes are scaled to a 500 N bite.

Overall, the hypothesis regarding this sensitivity test (see section 2.5.2) cannot be accepted fully. This is because while the predictions of joint reaction force did vary considerably between simulations 1, 2 and 3, the predictions of bite force magnitude remained similar between the simulations. Furthermore, although strain distributions local to the zygoma did vary between simulations 1, 2 and 3, global strain distributions were not wholly unaffected by the changes in masseter and medial pterygoid force vector orientation. Going forwards, although the vector orientation of the masseter will change due to changes to the zygoma region of the FE model (see Chapter 3), the orientation of the other force vectors will remain consistent between the unmodified and modified models to ensure the predictions of the two models are comparable, and the changes to masseter force vector orientation are isolated. Furthermore, these results will provide insightful in interpreting the predictions of the unmodified and modified FE models when simulating bites at gape, where muscle force vector orientation will be altered to reflect how their lines of action change as the mandible opens.

2.5.3. Sensitivity Study Three: sensitivity of the model to temporomandibular joint constraint position

Jaw opening is facilitated by the rotation of the mandibular condyles, their anterior translation over the articular eminences, and depression of the mandible (Koolstra 2002; Hylander 2006). Dumont et al. (2011) simulated bites at gape in their tamarin and marmoset FE models by changing muscle force vector orientation and the position of their TMJ constraints to account for condylar translation. Changing the position of these constrains may impact the reaction force predictions of the model as changing the position of the fulcrum impacts the lever-mechanics of the masticatory system, which may in turn influence predictions of craniofacial strain. As such, the sensitivity of the FE model to changes in the position of TMJ constraints was assessed. It is hypothesized that that moving the position of the TMJ constraints will not impact global strain distributions but will impact predictions of joint reaction force and bite force magnitudes.

2.5.3.1. Altering the position of the temporomandibular joint constraints

As the condyles translate anterior-inferiorly as the mandible is opened, the TMJ constraints were altered to reflect the changes to the location of the mandibular condyles that may occur during submaximal and maximal gapes. As such, nodes were selected as constraints at different positions on the articular surfaces on the temporal bone (Figure 36); 175 nodes were selected on the posterior slope of the articular eminence (simulation 2), and at the anterior limit of the articular eminence (simulation 3). The position of the nodes selected for simulations 2 and 3 were determined following the translation of the mandible of the *H. sapiens* specimen within Avizo in accordance with the mandibular kinematic data used to redefine the loading and boundary conditions of the model to simulate bites at different gapes (see section 3.5.1.1). The predictions of simulations 2 and 3 are compared to the predictions of a simulation where the TMJ constraints were positioned at the superior-anterior limit of the glenoid fossae (simulation 1). All other loading and boundary conditions remained consistent with previous simulations. Script files simulating LM^1 bites were exported and sent for solving and the deformations predicted by the three simulations were scaled to a 500 N bite.

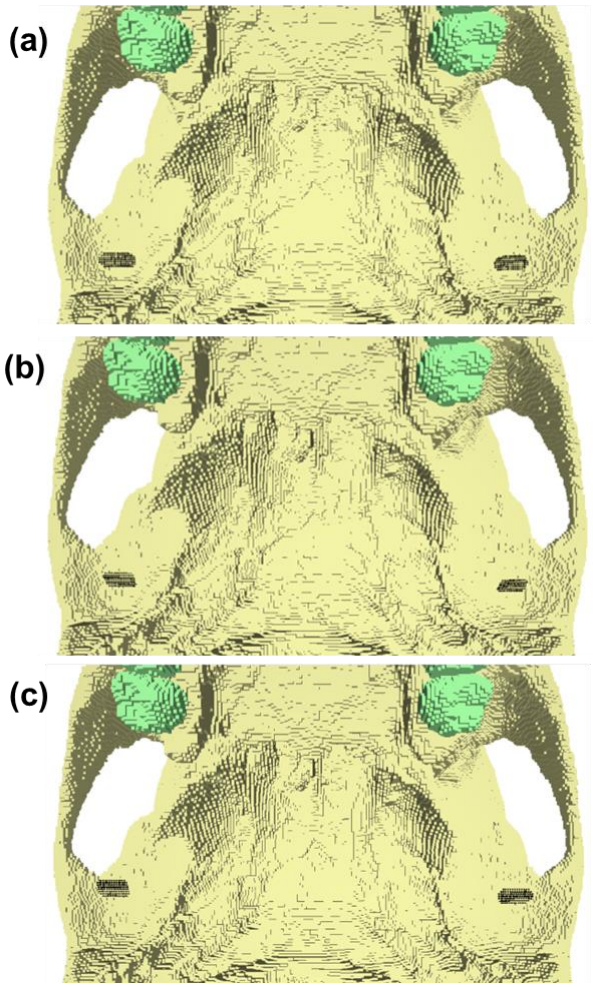

Figure 36. The position of the TMJ constraints for sensitivity study three. (a) constraints positioned at the superior-anterior limit of the glenoid fossae (simulation 1), (b) on the posterior slope of the articular eminence (simulation 2), and (c) at the anterior limit of the articular eminences (simulation 3).

2.5.3.2. Results of altering the position of the TMJ constraints

The results of this sensitivity test show that the reaction force predictions of the model were significantly impacted by the position of TMJ constraints (Table 13). The predictions of bite force varied by 48.69 N between simulations 1, 2 and 3, decreasing as the TMJ constraints moved anterior-inferiorly. Joint reaction force predictions were less sensitive than bite force predictions, varying by 9.94 N at the left joint and by 11.81 N at the right joint between simulations 1, 2 and 3, increasing as the TMJ constraints moved anterior-inferiorly. These findings are likely a consequence of how this interacts with the relative lengths of the in and out levers of the muscle force vectors.

Table 13. The reaction force magnitudes predictions for a LM[1] bite where the TMJ constraints are positioned at the superior-anterior limit of the glenoid fossae (simulation 1), on the posterior slope of the articular eminence (simulation 2), and at the anterior limit of the articular eminence (simulation 3).

Simulation	Reaction force magnitudes (N)		
	Bite force	Left Joint	Right Joint
1	390.67	109.69	209.30
2	372.07	113.51	214.89
3	341.98	119.63	221.11

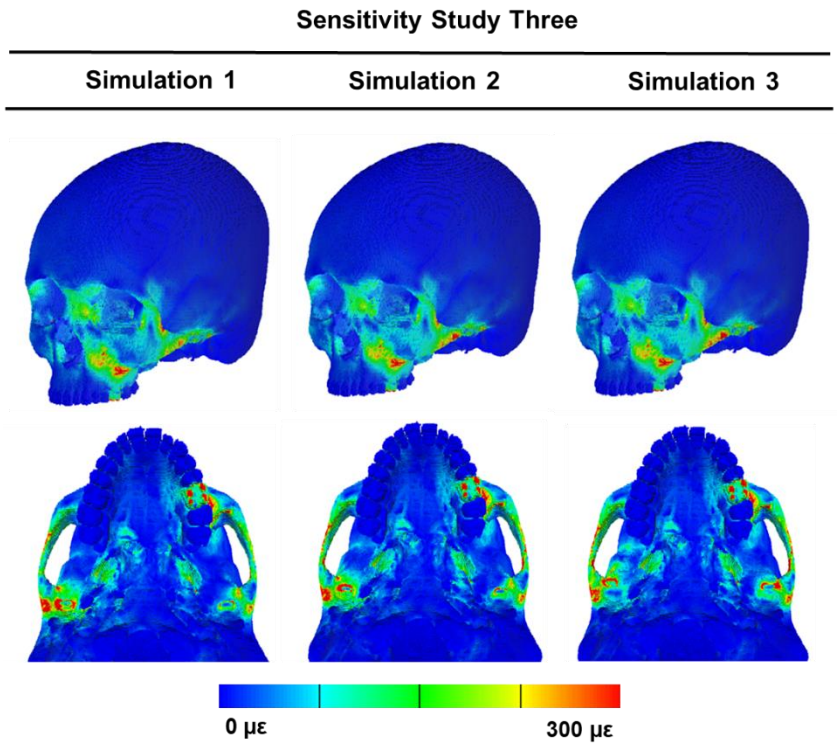

Figure 37. Global von Mises strain distribution maps for a LM[1] bite where the TMJ constraints are positioned at the superior-anterior limit of the glenoid fossae (simulation 1), on the posterior slope of the articular eminence (simulation 2), and at the anterior limit of the articular eminence (simulation 3). All are scaled to a 500 N bite.

There were differences in global strain distributions (Figure 37) and magnitudes (Figure 38) between simulations 1, 2 and 3. Reflecting the changing position of the constraints, the distribution of strain local to the glenoid fossae varied between simulations 1, 2 and 3. There were more global impact on strain distributions in the neurocranium between simulations 1, 2 and 3, where strain magnitudes on the balancing side increase in the squamous temporal and sphenoid bones as the constrains are positioned more anterior-inferiorly. Strain distributions local to the zygoma were also impacted, with simulation 1 predicted the lowest magnitudes in this region and simulation 3 predicted the highest magnitudes (Figure 37 and

Figure 38). For example, at the postorbital junctions, simulation 1 predicted the lowest strains (297.70με at region 4 and 261.89με at region 5), whereas simulation 3 predicted the highest strains (312.62με and 283.88με). The same is apparent in the zygomatic arches (simulation 1 predicted 338.05με and 264.39με at regions 6 and 7 and compared to 364.13με and 291.31με for simulation 3) and the zygomatic bodies (simulation 1 predicted 87.32με and 105.25με at regions 15 and 16 compared to 101.17με and 118.235με for simulation 3). Differences in magnitude between simulations 1, 2 and 3 in the other regions of the facial skeleton were minimal. Therefore, there were slight global and local differences in strain distribution and magnitude between simulations 1, 2 and 3 which likely reflect the impacts of changing the position of the TMJ constraints (e.g. strain increasing in the neurocranium as the constraints move anterior-inferiorly).

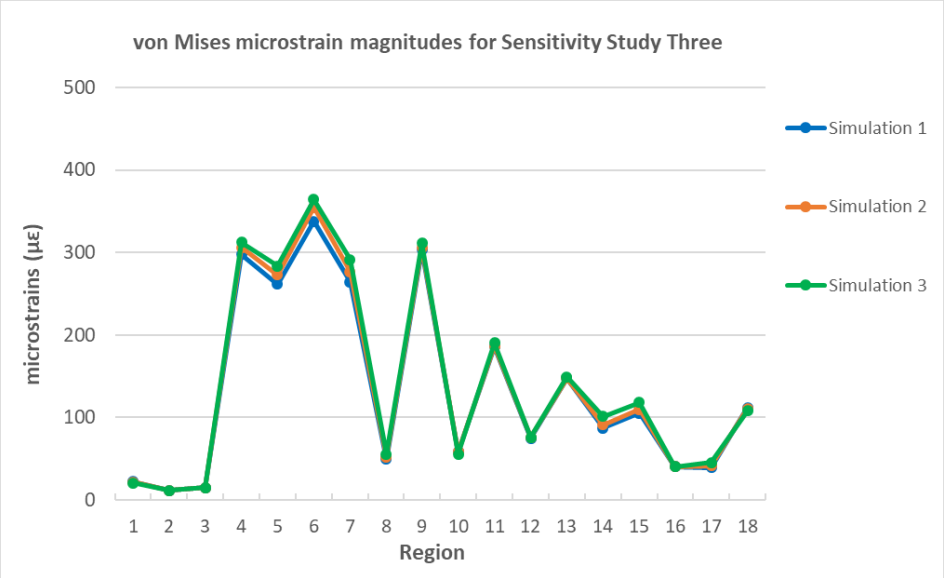

Figure 38. Average von Mises regional strain magnitudes for a LM[1] bite where the TMJ constraints are positioned at the superior-anterior limit of the glenoid fossae (simulation 1; blue line), on the posterior slope of the articular eminence (simulation 2; orange line), and at the anterior limit of the articular eminence (simulation 3; green line). All magnitudes are scaled to a 500 N bite.

Overall, the hypothesis pertaining to this sensitivity study (see section 2.5.3) can be rejected. This is because, while the predictions of joint reaction force and bite force magnitudes varied between simulations 1, 2 and 3, the strains predicted by these simulations also varied globally, particularly in the neurocranium and the zygoma. Going forwards therefore, when the zygoma region of the model is modified to resemble *H. ergaster* (see chapter 3), the position

of the TMJ constraints will remain consistent between the modified and unmodified models to ensure that their predictions are comparable. Furthermore, these results will provide insightful in interpreting the predictions of the unmodified and modified FE models when simulating bites at gape, where the position of the TMJ constraints will be altered to reflect condylar translation during jaw opening.

2.6. Chapter Conclusion

In conclusion, this chapter has created a working voxel-based FE model of a modern *Homo sapiens* female crania. As the model was constructed using a low-resolution medical CT scan, many input parameters were simplified following previously validated *H. sapiens* cranial FE models also constructed for use within Vox-Fe (Toro-Ibacache et al. 2016; Godinho et al. 2017). Therefore, the geometry of the model was reconstructed to preserve fine cortical bone structures, retain major air spaces, and separate tooth roots from alveolar bone (Fitton et al. 2015; Toro-Ibacache et al. 2016; Godinho et al. 2017). However, cortical bone and trabecular bone were modelled as a bulk material, as were enamel, pulp and dentine; both bulk materials were given Young's modulus and Poisson's ratio values previously applied to validated human and non-human primate craniofacial FE models (Fitton et al. 2015; Toro-Ibacache et al. 2016; Godinho et al. 2017). The muscle forces applied to the model assumed homogenous and symmetrical 100% activation, and their magnitudes were estimated from the CT of the specimen following previously reported protocols (Toro-Ibacache et al. 2015; Toro-Ibacache and O'Higgins 2016), and the lines of actions of the muscles were estimated based on specimen-specific geometry. Overall, the model constructed will not produce accurate predictions of strain magnitude, but reasonably approximates relative strain distributions, which is an acceptable level of resolution for the aims of this research.

The validity of the predictions of the model was assessed against the predictions of previously published *H. sapiens* craniofacial FE models simulating masticatory loading of Toro-Ibacache et al. (2016), Toro-Ibacache and O'Higgins (2016), and Godinho et al. (2018). The visual similarity of global strains predicted by these models and the model constructed within this thesis under similar loading scenarios are indicative of the validity of this model. Furthermore,

the series of hypotheses that the results of the model were tested against further confirm that its predictions are in line with biomechanical expectations. Thus, the working cranial FE model was subsequently used in form-function investigations, pertaining to the relationship between gracilisation in the zygoma region within *H. sapiens* and masticatory loading.

One of the aims of this thesis is to simulate bites at a range of gapes, which may require changes to input parameters including relative muscle activation patterns, muscle force vector orientation and the position of the TMJ constraints (Bourke et al. 2008; Dumont et al. 2011; McIntosh and Cox 2016; Chatar et al. 2022). As such, the sensitivity of the FE model was assessed to isolated changes in each of these input parameters. This demonstrated that predictions of reaction force and strain magnitudes were sensitive to changes in how muscle forces were modelled, both relative activation patterns and vector orientation, owing to the changes in the magnitude of applied force. Once these differences were controlled for, only strains local to the zygoma were sensitive to how muscle forces were modelled. This is consistent with previous craniofacial FE model sensitivity studies (Kupczik et al. 2007; Fitton et al. 2012; Toro-Ibacache and O'Higgins 2016). In line with expectations, altering the position of the TMJ constraints had localised impacts on joint reaction force predictions and strains proximate to the glenoid fossae, however unexpectedly changes in this input parameter had more global impacts on strains in the zygomatic region. Overall, these sensitivity studies have demonstrated the types of changes in strain and reaction force predictions may occur when these input parameters are changed in combination. Thus, a framework to simulate bites at gape can now be implemented for the *H. sapiens* FE model and the hypothetical FE model this will be used to create (see Chapter 3), to assess how the craniofacial skeleton globally and the zygoma region locally responds to bites at different gapes.

3. Chapter 3: Investigating the Functional Importance of Zygoma Region Morphology on Craniofacial Strain and Bite Force Production

The zygomatic region is a key component of the masticatory apparatus. This region hosts the origin of the masseter, meaning its spatial position is important in determining bite force capabilities because of how this interacts with the mechanical advantage of this muscle (Ward and Molnar 1980; Weber and Krenn 2017; Ledogar et al. 2017). Furthermore, as a part of the midface the form of the zygoma region is important in resisting strains induced by bite reaction forces and the contraction of the masseter (Herring et al. 2001; Prado et al. 2016). Owing to these reasons, many authors have hypothesized as to the functional significance of the form of zygoma region within fossil hominins, including australopithecines and the Neanderthals (see section 1.5 for a more detailed review on the zygoma region functional morphology in hominins; Rak and Hylander 2003; Rak and Marom 2017).

The zygoma region of *Homo ergaster* however has not been investigated. The zygoma region of *H. ergaster* is robust, relatively large and wide, projects anteriorly, has a flattened infraorbital surface, and an anteriorly positioned masseter origin (Howells 1980; Rightmire 1988; Pope 1991; Rightmire 1992, 1998; Antón 2003; Freidline et al. 2012a; Rightmire 2013). Comparatively, the zygoma region of *Homo sapiens* is gracile and smaller in all dimensions, is non-projecting and has a more concave infraorbital profile owing to the presence of a canine fossa (Lieberman 1995; Lieberman et al. 2002; Maddux and Franciscus 2009; Lieberman 2011; Lacruz et al. 2019; Trafí et al. 2022).

These anatomical changes between the two species coincide with changes in the archaeological record that indicate an intensification of complex food processing behaviours (e.g. cooking) with the evolution of *H. sapiens,* resulting in a less mechanically demanding diet compared to ancestral *Homo* (see section 1.2.1; Zink et al 2014; Zink and Lieberman 2016). Within modern *Homo sapiens*, populations that consume more mechanically demanding diets have been demonstrated to have more robust facial skeletons with larger and wider zygomatic regions containing more anteriorly positioned and larger masticatory muscle

attachments (see section 1.3.2; von Cramon-Taubadel 2017; Eyquem et al. 2019). This is due to increased selective pressures on bites force production increasing the size and mechanical advantage of the masticatory musculature and more frequent exposures to higher craniofacial strain increasing bone modelling in the facial skeleton (Lieberman et al. 2004; von Cramon-Taubadel 2017; Katz et al. 2017; Eyquem et al. 2019). Given the archaeological evidence for decrease to the mechanical challenge posed by dietary objects throughout the evolution of the genus *Homo*, the more robust facial skeletons and zygomatic regions of early *Homo* species could be a consequence of the previously described processes (Demes and Creel 1988; Lieberman et al. 2004; Lieberman 2011; Eng et al. 2013; Ledogar et al. 2016a). It follows that the gracile zygoma region morphology of *H. sapiens* may be poorly configured to produce and resist high bite forces, and to resist high muscle force magnitudes, whereas the robust zygoma region morphology of *H. ergaster* may be better suited to these functional demands.

With the increase in the complexity of food processing behaviours with the evolution of *H. sapiens*, it is reasonable to assume that the size of dietary items placed into the oral cavity would be reduced (Zink et al. 2014; Zink and Lieberman 2016). Prior to this, *H. ergaster* may have consumed larger food items, and the australopithecines may have consumed food items even larger still, prior to the habitual use of stone tools to process dietary resources. As such, the gracile zygoma region of *H. sapiens* may also be poorly suited to resisting bites performed at larger gapes, compared to the more robust zygoma region morphology of *H. ergaster.*

3.1. Investigating the functional significance of morphological variability within hominin cranial fossils

To investigate these predictions, finite element analysis (FEA) can be used (see section 1.4.1 and 2.1 for more detailed reviews of FEA and its use within paleontological research). Combined, FEA and geometric morphometrics have been used to investigate the biomechanical consequences of shape differences between biological structures (see section 1.6 for further details; O'Higgins et al. 2011; 2012; 2019). This can involve the use of thin plate splines (TPSs) to create hypothetical models to address form-function research questions by

changing isolated anatomical features of a model to contain the corresponding isolated feature of another digitised specimen (O'Higgins et al. 2011).

For TPS deformations to change an isolated anatomical feature, multiple different landmark datasets are required, containing information surrounding the form of the reference specimen (the surface to be deformed) and the target specimen (the specimen that the reference surface will be warped into; O'Higgins et al. 2011). Firstly, a set of landmarks used to 'lock' areas of the reference surface to needs to be created, which involves placing a dense mesh of landmarks over the surface of the specimen in the areas where change is undesirable (O'Higgins et al. 2011). Two more landmark datasets are needed which contain the landmarks used to deform the surface of a reference specimen into the homologous configuration of a target specimen (O'Higgins et al. 2011). These two landmark sets function as the 'warping' landmarks and are placed on the region of interest on the reference and target specimens. Following this, the first, second and third sets of landmarks are combined, to produce two new landmark datasets for use in TPS surface deformation (i.e. the warp). This first of these is the reference landmark dataset used in the TPS warp, which contains the locking landmarks in combination with the warping landmarks placed on the reference surface (O'Higgins et al. 2011). The second is the target landmark dataset used in the TPS warp, containing the locking landmarks in combination with the warping landmarks placed on the target specimen (O'Higgins et al. 2011). Between the reference and target landmark configurations used in the TPS warp, only the landmarks from the region of interest differ in their spatial position, as such only these areas of the reference surface are deformed (O'Higgins et al. 2011).

Using TPSs to deform models is not without limitations. This pertains to how the deformations impact the internal morphology of biological structures (Sigal et al. 2008; Stayton 2009; O'Higgins et al. 2011, 2012). Within warps of crania, this can result in the deformation of cortical bone thickness, tooth roots, sinus walls, etc, into forms not reflective of either the reference or target specimens (O'Higgins 2011; 2012; 2019). If these issues are accounted for in experimental design, then the use of TPS warping provides a robust and controllable methodology to address form-function hypotheses (O'Higgins et al. 2011).

FEA in combination with TPS warping has previously been used to investigate the functional significance of zygoma region morphology in fossil hominins, however this research has focused on the australopithecines (see section 1.5; Fitton et al. 2009; Ledogar et al. 2017). Collectively, this research has demonstrated that changing features in isolation impact how the craniofacial skeleton responds globally to masticatory loads (Fitton et al. 2009; Ledogar et al. 2017), and that the zygoma region is key in determining craniofacial strains and bite force capabilities. Therefore, it is important to investigate the functional significance of changes to the zygoma region during the evolution of the genus *Homo*, and how having a larger and more robust zygoma (and the larger masseter force associated with this) impacts craniofacial strains in the entire facial skeleton, which could explain other areas of increased robusticity within *H. ergaster*.

However, no early Pleistocene *Homo* fossils have been included within FEA research involving hominin fossils and the functional significance of *H. ergaster*-type zygoma region morphology is yet to be investigated. This is because fossils of the complete facial skeleton of *H. ergaster* are rare (Antón and Middleton 2023). While specimens like the Nariokotome fossil (KNM-WT 170000) preserve the necessary anatomy, this specimen is a juvenile meaning that bite force production and response of the crania to masticatory loading may be impacted by changes to facial skeleton during ontogeny (Kupczik et al. 2009; Zollikofer 2012; Cobb et al. 2015; Edmonds and Glowacka 2020). The 5 skulls from the Dmanisi sample could also be suitable candidates, however the taxonomic status of this assemblage is contended (Rosas and Bermúdez De Castro 1998; Gabunia et al. 2000; Rightmire et al. 2006; Jiménez-Arenas et al. 2011; Dembo et al. 2015; Rightmire et al. 2019). While not as well preserved as KNM-WT 17000 or the Dmanisi sample, KNM-ER 3733 is a specimen confidently attributed to *H. ergaster* (Wood 1992; Wood and Collard 1999a, 1999b) that preserves the necessary anatomy to investigate the functional importance of the zygoma region in early *Homo.*

3.1.1. The use of finite element analysis to assess adaptations to large object feeding in hominin fossils

As discussed, the increased use of complex extra-oral food processing technologies throughout the evolution of the genus *Homo* may have impacted the mechanical loading of the cranium by decreasing the size of food objects placed within the oral cavity. Comparatively, the consumption of larger dietary objects in earlier hominin species may have placed different functional demands upon the cranium (Strait et al. 2009; Zink et al. 2014; Zink and Lieberman 2016). Therefore, using FEA to simulate bites at gape on hominin fossil cranial FE models could be important in understanding adaptations to the consumption of food items of different sizes.

The ability of fossil hominin crania to consume large food items has been addressed by researchers using FEA (Strait et al. 2009, 2010; Smith et al. 2015b; Ledogar et al. 2016b). However, no research has directly addressed how the performance of these models are impacted by the simulation of bites at different gapes, meaning the experimental design of these authors limit conclusions surrounding adaptations for large object feeding in fossil hominins (see section 1.4.2). Thus, there is currently a gap in the questions being addressed by FEA when investigating the dietary adaptations within fossil hominins.

As the mandible opens, the lines of action of the jaw-elevator musculature change, as do their relative activation patterns and the position of the mandibular condyles relative to the articular eminences (Koolstra 2002; Hylander 2006). When bites at gape have been simulated on FE models of non-hominin taxa, the loading and boundary conditions of models are altered to reflect these changes (Bourke et al. 2008; Dumont et al. 2011; McIntosh and Cox 2016; Chatar et al. 2022). In these investigations it is reported that these alterations impact predictions of reactions forces and strains (Bourke et al. 2008; Dumont et al. 2011; McIntosh and Cox 2016; Chatar et al. 2022), demonstrating how performing bites at different gapes can impact the mechanical loading of the cranium

It therefore stands that simulating bites at gapes on hominin cranial FE models offers a more systematic approach to assess adaptations to the consumption of food objects of different sizes. While other features of hominins have been suggested to be functionally important for increasing gape (e.g. subnasal prognathism and reduced canine heights; Hylander 2013), the form of the zygoma region may also be important in this, owing to impacts that the position of the origin of the masseter has on the gape capacity of an organism (Herring and Herring 1974; Hylander 2013; Terhune et al. 2015b; Fricano and Perry 2019).

3.2. Chapter aims, objectives, and hypotheses

The aim of this chapter is to investigate the functional importance of the zygoma region morphology in *H. ergaster* during various bite scenarios. To do this the previously constructed *H. sapiens* FE model (see Chapter 2) will be modified using TPS warping to contain the zygoma region morphology of KNM ER 3733. A series of FE models will be run, with and without modified zygoma regions, and their performance (quantified by bite force, bite force efficiency, and craniofacial strains) during different bite scenarios will be compared, including bites at submaximal and maximal gapes. To account for the larger masseter of *H. ergaster* the models will also be loaded with *H. ergaster*-like masseter forces for some bite scenarios. This chapter is divided into three objectives with specific testable hypotheses (see below); the materials and methods detailing how each objective was achieved are outlined, as well as the accompanying FEA results. The key results will then be synthesized and discussed in relation to the hypotheses of this chapter to consider the relationship between gracilisation in the zygoma region within *H. sapiens* and masticatory loading.

Objective One: Investigate the impacts of modifying the zygoma region of *Homo sapiens* FE model to resemble the zygoma region of *Homo ergaster* on craniofacial strain and bite force production

Modifying the zygoma region in a controlled manner and keeping all other input-parameters identical allows the investigation of how changes to the form of this region alter the

mechanical advantage and force vector of the masseter, and the subsequent impact that these changes have on craniofacial strains, both locally and globally to the zygoma. Therefore, the following hypotheses will be tested:

H1: A Homo sapiens cranium with Homo ergaster-like zygoma regions will increase the mechanical advantage of the masseter and subsequently increase bite forces during anterior and posterior bites

H. ergaster has a masseter origin more anteriorly positioned than *H. sapiens* (Pope 1991; Lieberman 1995). Therefore, the *H. sapiens* FE model with the *H. ergaster*-like zygoma regions should predict higher bite reaction forces for both anterior and posterior bite as these modifications should increase the mechanical advantage of the masseter.

H2: A Homo sapiens cranium with Homo ergaster-like zygoma regions will result in decreased craniofacial strain magnitudes locally to the zygoma region and more globally during anterior and posterior bites

The zygoma region of *H. ergaster* is larger and more robust than that of *H. sapiens* (Pope 1991). It is predicted that strain locally to the zygoma should decrease for the *H. sapiens* FE model with the *H. ergaster*-like zygoma regions due to an absolute increase in size of this region, but on a global level the new position of the zygomatic arches and roots may change the path of load through the rest of the craniofacial skeleton and subsequently reduce strains on a global level.

Objective Two: Investigate the impacts of loading the unmodified and modified *Homo sapiens* FE models with *Homo ergaster*-like masseter muscle forces on craniofacial strain and bite force production

Using FEA to simulate masticatory loads allows the investigation of how increasing muscle force impacts predictions of bite force and strains in the *H. sapiens* model and the *H. sapiens* model with *H. ergaster*-like zygoma regions. Therefore, the following hypothesis will be tested:

H3: A Homo sapiens cranium with Homo ergaster-like zygoma regions and Homo ergaster-like masseter muscle force magnitudes will further increase bite force, which will increase craniofacial strain magnitudes globally, but lower strains are still predicted locally to the zygoma region

As *H. ergaster* likely had a more forceful masseter than *H. sapiens*, the zygoma region of this species should be adapted to resist this. As such, the *H. sapiens* FE model with the *H. ergaster* zygoma like regions loaded with *H. ergaster-like* masseter muscle forces should predict lower strain magnitudes locally to the zygoma region. However, due to the predicted increased bite force, it is predicted that globally strain magnitudes will increase in regions shown to be more robust in *H. ergaster*.

Objective Three: Investigate the impacts of simulating bites at submaximal and maximal gapes on craniofacial strains and bite force production for the unmodified and modified *Homo sapiens* FE models

The lines of action of the jaw-elevator musculature, and the position of the temporomandibular joint constraints of a FE model can be altered to replicate the changes to these variables that occur when the mandible opens, thus allowing bites at different gapes to be simulated. The changes to the predictions of reaction forces and craniofacial strains within cranial FE models that occur when these input parameters are altered may offer insights in the ability of an organism to

withstand bites at different gapes. Therefore, the following hypotheses will be tested:

H4: A Homo sapiens cranium with Homo ergaster-like zygoma regions will increase bite forces during anterior and posterior bites at submaximal and maximal gapes

Following the modifications to the zygoma region of the *H. sapiens* FE model, the origins of the masseter will be more anteriorly positioned as observed within the zygoma region morphology of *H. ergaster* (Pope 1991; Lieberman 1995). Thus, even when the loading and

boundary conditions of the models are altered to simulate bites at different gapes, the masseter should have a higher mechanical advantage for the *H. sapiens* FE model with the *H. ergaster*-like zygoma region, meaning this model should predict higher bite reaction forces for both anterior and posterior bites.

H5: Global craniofacial and local zygoma strain magnitudes will be relatively lower during bites at maximal gapes and submaximal gapes in the Homo sapiens cranium with Homo ergaster-like zygoma regions compared to the unmodified Homo sapiens cranium

The zygoma region of *H. ergaster* may be better suited to producing and withstanding bites at submaximal and maximal gapes, while the zygoma region of *H. sapiens* may be poorly configured to produce and withstand bites at larger gapes. Accordingly, the *H. sapiens* FE model with the *H. ergaster*-like zygoma regions should demonstrate lower global and local strain magnitudes when simulating bites at submaximal and maximal gapes than those recorded in the unmodified *H. sapiens* FE model.

3.3. Objective One: Investigate the impacts of modifying the zygoma region of *Homo sapiens* FE model to resemble the zygoma region of *Homo ergaster* on craniofacial strain and bite force production

Previous researchers have used thin plate spline (TPS) deformations to modify finite element (FE) models to investigate form-function relationships (Stayton 2009; Sigal et al. 2008; 2010; O'Higgins et al. 2011; Gröning et al. 2011; O'Higgins et al. 2012; Ledogar et al. 2017; O'Higgins et al. 2019). The first section of this objective details how TPS warping was used to modify the zygoma region of the previously constructed *Homo sapiens* cranial FE model to resemble that of *Homo ergaster.* Following this, the impacts that this geometrical change had upon bite force predictions, the mechanical advantage of the masseter and craniofacial strain during masticatory loads are outlined.

3.3.1. Objective One: materials and methods

The morphology of the zygoma region of the *H. sapiens* cranial FE model was modified to resemble that of a *H. ergaster* fossil using TPS warping. Before this could occur however, a digitised specimen of a *H. ergaster* fossil suitable for use as a target specimen needed to be produced. As such, this section outlines how a *H. ergaster* fossil was digitally reconstructed for use as the target specimen in the TPS warp used to produce a *H. sapiens* FE model containing *H. ergaster*-like zygoma regions. Before this model could be solved however, the force vector of the masseter needed to be redefined owing to the insertion of this muscle changing with the TPS warp. Therefore this subsection also details how the loading and boundary conditions of the modified model were redefined following the changes to the geometry of the zygoma regions.

3.3.1.1. Reconstruction of KNM-ER 3733

The *H. ergaster* fossil used as the target specimen to modify the zygoma region of the *H. sapiens* specimen was KNM-ER 3733 (see section 3.1). Access to a CT scan of KNM-ER 3773 was granted by the Department of Earth Sciences of the National Museum of Kenya. Firstly, the image stack of the CT scan of KNMER-3733 (voxel resolution of 0.302734 x 0.302734 x 0.5

mm^3) was loaded into Avizo 9.2.0 (FEI, Thermofisher Scientific), saved as a volumetric file and segmented via semi-automatic thresholding. All the voxels selected by the semi-automatic thresholding algorithm were added to one homogenous material (the cranium; Figure 39).

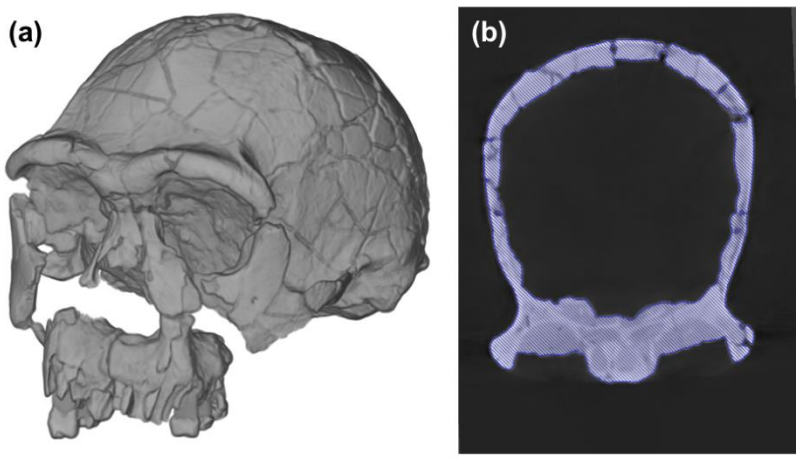

Figure 39. The segmentation of the CT stack of KNM-ER 3733. (a) Rendering of the volumetric file prior to semi-automatic thresholding. (b) The material segmented as cranium.

Following this, the cranium was manually symmetrised owing to the post-depositional deformations of the fossil (Gunz et al. 2009). This was achieved by aligning the midline of the cranium to be parallel to the global Y axis (Figure 40). Following this, the voxels within the sagittal slice falling on the midline were removed. This allowed the two halves of the cranium to be added to two new materials, and the right side of the cranium was reflected and merged with the non-reflected right side using the resample module within Avizo. The right side of the cranium was chosen as this region preserved more zygoma region morphology. This produced a symmetrised version of KNM-ER 3733 (Figure 41).

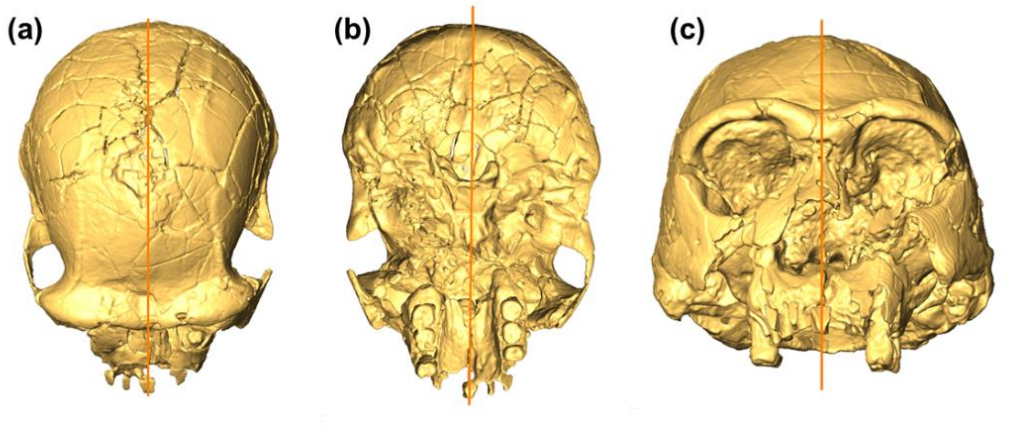

Figure 40. Alignment of the cranial midline of KNM-ER 3733 to the global Y axis. (a) Superior view. (b) Inferior view. (c) Frontal view.

Only the left side of KNM-ER 3733 preserves the zygomatic root (Figure 39). As such, this feature was reconstructed using manual virtual object manipulation and segmentation techniques (Gunz et al. 2009). To achieve this, all the voxels segmented on the left side of the cranium lateral to the buccal most extent of the post-canine dental arcade were added to a new material representing the left zygomatic-alveolar region of KNM-ER 3733, which was translated and rotated until it was appropriately positioned on both sides of the cranium of the symmetrised version of KNM-ER 3733. The resample module within Avizo was then used to combine the repositioned left zygomatic-alveolar regions with the symmetrised cranium. Following this, manual segmentation was used to join the zygomatic roots and the alveolar regions to the cranium in areas where these materials did not fully connect. This process produced a symmetrised KNM-ER 3733 with reconstructed zygomatic roots (Figure 41; henceforth KNM-ER 3733).

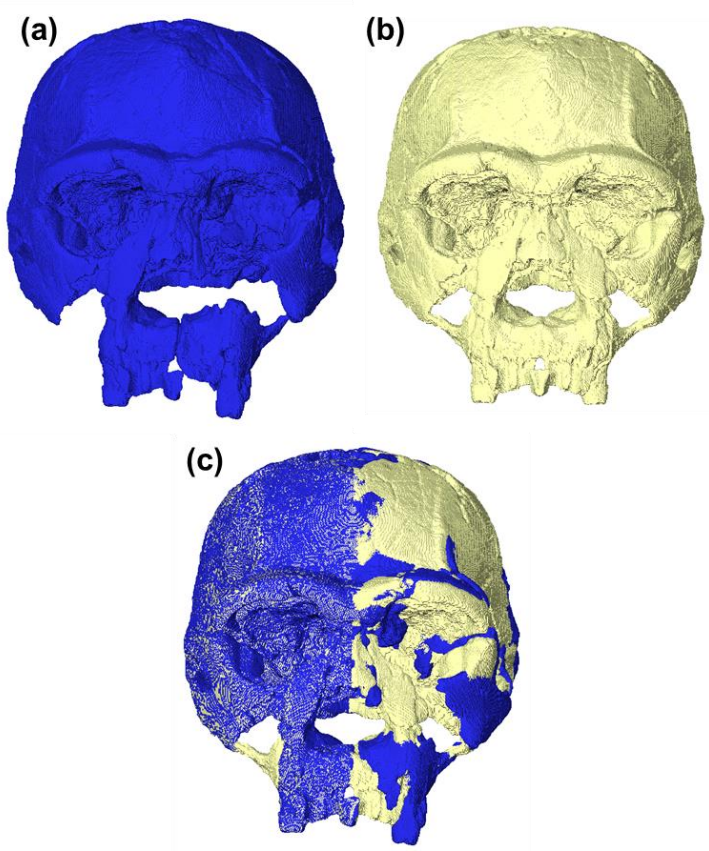

Figure 41. The correspondence between KNM-ER 3733 prior to reconstruction and KNM-ER 3733 following reconstruction. (a) KNM-ER 3733 prior to reconstruction (blue). (b) KNM-ER 3733 following reconstruction (cream). (c) KNM-ER 3733 following reconstruction overlaying KNM-ER 3733 following reconstruction.

This reconstruction process ensured that the target surface used to produce the modified FE model preserved all the necessary anatomy to alter the zygoma region of the *H. sapiens* specimen, while lessening the impacts that asymmetries may have on the deformed surface produced by the TPS warp (O'Higgins et al. 2011). Yet, differences between the size and spatial positioning of the reference and target specimen still needed accounting for.

3.3.1.2. Scaling and aligning the reference and target specimens

To aid the TPS warping, any differences in the size and spatial position of the reference and target specimens were minimised (O'Higgins et al. 2011). Within Avizo, the 'rigid alignment and scale' landmark surface warp module was used scale a surface file of KNM-ER 3733 to the centroid size of a surface of the *H. sapiens* specimen, based on a landmark dataset containing 22 landmarks placed on both surfaces (Table 14 and Figure 42). This produced a surface file of KNM-ER scaled to the same size as the *H. sapiens* specimen.

Table 14. The landmarks used to scale KNM-ER 3733 to the centroid size of the *H. sapiens* specimen.

Landmark	Number	Definition
Glabella	1	The most anterior point on the midline of frontal bone between the supraciliary arches
Frontomalar-orbitale	2,3	Point on the orbital rim marked by the zygomaticofrontal suture
Inion	4	Midline point between the superior nuchal lines at the external occipital protuberance
Mastoid processes	5,6	Most inferior point on the mastoid processes bilaterally
Orbitale	7,8	Most inferior point on the orbital rim
Lambda	9	Convergence between the lambdoid and sagittal sutures
Bregma	10	Intersection between the sagittal and coronal sutures
Prosthion	11	Midline point between the I^1s on the maxillary alveolar margin
Nasospinale	12	Midline point at the opening of the nasal cavity
Pterion	13,14	Meeting between the greater wings of the sphenoid, temporal and parietal bones
Frontotemporal	15,16	Most anterior-medial point on the temporal line on the zygomatic process of the frontal bone
Porion	17,18	Central point on the superior margin of the external auditory meatus
Basion	19	Midline point on the anterior rim of the foramen magnum
Zygion	20,21	Most laterally projecting point on the zygomatic arch
Rhinion	22	Rostral most point on the internasal suture

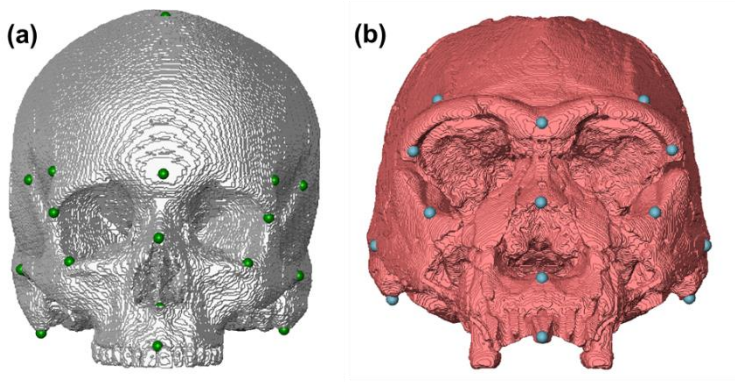

Figure 42. The 22 landmarks (see Table 14) used to scale KNM-ER 3733 to the same size as the *H. sapiens.* (a) The landmarks (green) placed on the surfaces the *H. sapiens* specimen. (b) The landmarks (blue) placed on the surfaces the KNM-ER 3733.

Following this, the scaled surface of KNM-ER 3733 was manually aligned to the infraorbital margin of the *H. sapiens* specimen using the transform editor within Avizo (Figure 43). This alignment was chosen as the TPS warp aimed to modify the zygoma region morphology of the *H. sapiens* specimen. These preparatory steps minimised any artefacts introduced into the warped surface because of asymmetries, size differences and misalignments between the reference and target specimen (O'Higgins et al. 2011).

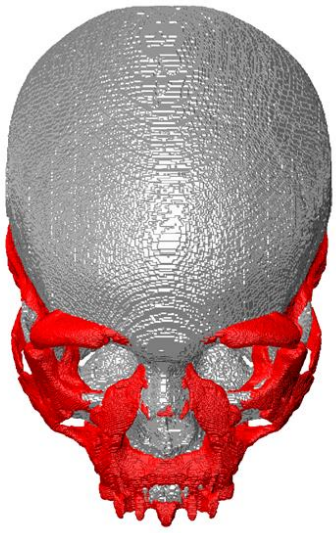

Figure 43. Alignment of KNM-ER 3733 (red) to the infraorbital rim of the *H. sapiens* (silver) specimen.

3.3.1.3. Using TPS warping to modify the zygoma region of the *H. sapiens* specimen

The 'Bookstein landmark surface warp' module within Avizo was used to perform the TPS warp that modified the zygoma region of the *H. sapiens* specimen to contain the zygoma region morphology of KNM-ER 3733. The results of TPS warps are heavily dependent on the choice of landmarks (Gunz et al. 2009; O'Higgins et al. 2011; 2019; Shui et al 2023), therefore the warp was performed multiple times using different combinations, placements and numbers of warping and locking landmarks in the reference and target landmark datasets (see Appendix 1 for further details). In total 14 warping landmarks were placed on both the zygoma regions of the reference and target surfaces (7 on each side; Figure 44), while a dense mesh of 1399 locking landmarks were placed on other regions of the cranium of the reference surface (Figure 44) to prevent any unwanted deformations, particularly around the maxillary dentition, glenoid fossae, the lateral walls of the skull within the temporal fossae, and the pterygoid processes of the sphenoid bone as to maintain the spatial position of the constraints of the FE model and the nodes that medial pterygoid and temporalis force vectors were applied to. Figure 45 shows the correspondence between the deformed surface produced by the TPS warp (henceforth the modified *H. sapiens* specimen) and KNM-ER 3733,

and Figure 46 shows this between the deformed surface and the unmodified *H. sapiens* specimen.

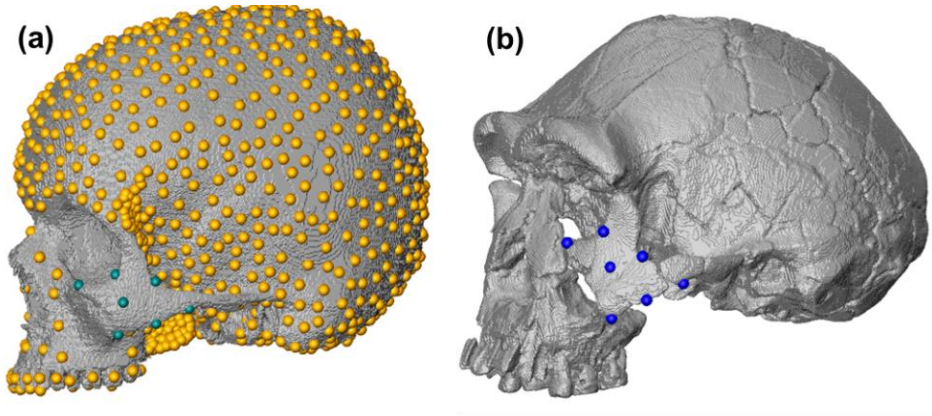

Figure 44. The combination of warping and locking landmarks used in the TPS warp that created the modified *H. sapiens* specimen. (a) The locking (yellow) and warping landmarks (teal) placed on the reference specimen. (b) The warping landmarks (dark blue) placed on the target specimen.

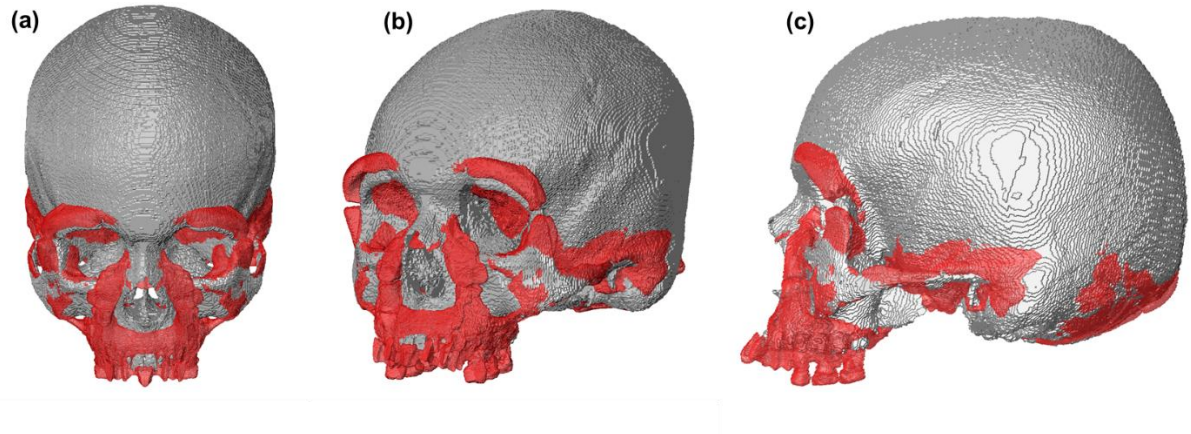

Figure 45. The modified *H. sapiens* specimen (silver) and its correspondence to KNM-ER 3733 (red). (a) Superior view (a). (b) Oblique view. (c) Lateral view.

The TPS warp altered the zygomatic region of the *H. sapiens* specimen, as such the zygomatic bodies and arches have become as laterally flaring, anteriorly projecting, superior-inferiorly as tall as observed within KNM-ER 3733 (Figure 46). The warp did not artificially thin the anterior walls of the maxillary sinus, reducing any error that may be introduced into the predictions of the modified FE model because of differences in cortical bone thickness (see Appendix 1; Szwedowski et al. 2011; Toro-Ibacache et al. 2016). The anterolateral orientation of the frontal process of the zygoma of KNM-ER 3733 could not be reflected in the modified *H. sapiens* specimen (see Appendix 1) because the spatial position of the post-orbital

attachment of the temporalis needed to remain identical between the models to isolate the impacts of changing the vector of the masseter. Compared to the unmodified model, the frontal process is slightly more anterolateral oriented, but not to the extent seen within KNM-ER 3733 (Figure 45 and Figure 46). As the zygoma region KNM-ER 3733 is superiorly-inferiorly taller than that of the *H. sapiens* specimen, warping this in isolation of the height of the maxilla decreased the angle of the zygomatic root (Figure 46). The form of this structure in the warped surface therefore differs from that of KNM-ER 3733, however the origins of the masseter have become more anterior-inferiorly positioned (Figure 46). The modified FE model will therefore investigate how altering the spatial position of the origin of the masseter, and how having a zygoma region as laterally flaring and as superior-inferiorly tall as KNM-ER 3733 impacts reaction force predictions and distributions of craniofacial strains in a *H. sapiens* FE model.

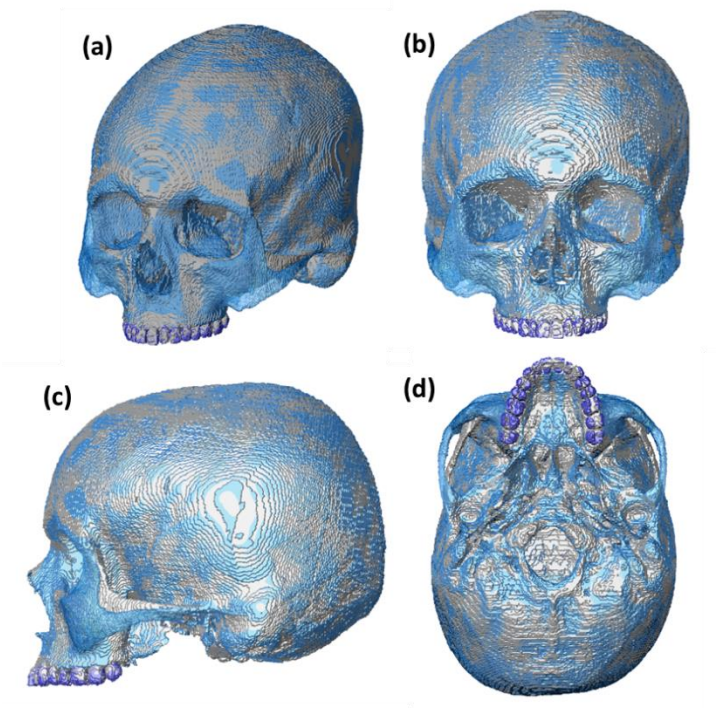

Figure 46. The modified *H. sapiens* specimen (blue) and its correspondence to the unmodified *H. sapiens* specimen (silver). (a) Oblique view. (b) Frontal view. (c) Lateral view. (d) Inferior view.

3.3.1.4. Creating a FE model from the warped surface

A voxel-based FE model of the unmodified *H. sapiens* specimen had already been created (see Chapter 2), however the for the same to be created for the modified *H. sapiens* specimen, the deformed surfaced produced by the TPS warp first needed converting into a volumetric file

suitable for conversion into a voxel-based FE mesh (Fagan et al. 2007; Liu et al. 2012). The deformed surface was converted into an isometric volume file with the same resolution as the volume file of the unmodified *H. sapiens* specimen (0.566507 x 0.566507 x 0.566507 mm^3), using the 'scan surface to volume' module within Avizo. This new volumetric file contained the same two materials as the unmodified FE model (see section 2.3.2), being the bulk material representing all the cortical and trabecular bone of the cranium (bone), and the material representing all the dental tissues of the maxillary tooth crowns and roots (tooth). The label field containing the warped cranium was exported as a .bmp stack and converted into a voxel-based FE mesh via direct voxel conversion using the Vox-2-Vec executable (Fagan et al. 2007; Liu et al. 2012). The modified model consisted of 3,760,344 eight-noded linear cubic elements.

3.3.1.5. The loading and boundary conditions of the modified *Homo sapiens* FE model

The unmodified *H. sapiens* model was loaded to simulate masticatory loading, therefore the muscle force vectors applied to the model included the bilateral masseter, temporalis and medial pterygoid, and it was constrained at bilaterally at the glenoid fossae, and at maxillary dentition. However, as the TPS warp changed the zygoma region morphology of the *H. sapiens* specimen, the nodes that the masseter force vectors were applied to within the origin sites of this muscle on the modified *H. sapiens* FE model needed re-defining. As such, in Vox-Fe the nodes on the inferior border of the zygomatic arches between the anterior slope of the articular eminence and the outer corners of the zygomatic process of the maxilla on the modified FE model were selected as the new nodes to apply the masseter force vectors to (Figure 47).

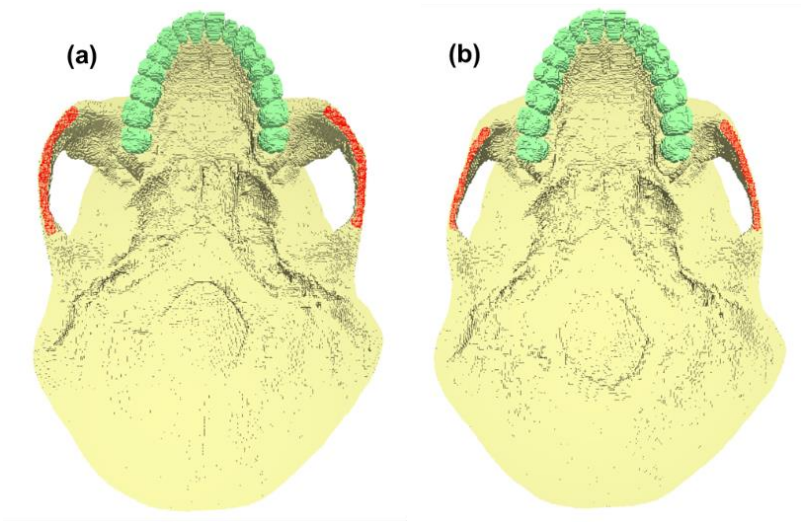

Figure 47. The nodes that the masseter force vectors were applied to (red selected areas) on the modified (a) and unmodified (b) models.

The locking landmarks used for the TPS warp (Figure 44; see section 3.3.1.3) ensured that the spatial position of the glenoid fossae, maxillary dentition and the origin sites of the temporalis and medial pterygoids were unaltered. As such, only the nodes that the masseter force vectors were applied to varied between the unmodified and modified *H. sapiens* FE models (Figure 48). The same landmark coordinates that defined the end points of the muscle force vectors of the unmodified FE model (see section 2.3.4.2) were used to define the end points of the muscle force vectors applied to the modified FE model. For this analysis, both the unmodified and modified FE models were loaded with the muscle force magnitudes originally estimated for the unmodified *H. sapiens* specimen (Table 15 and see section 2.3.4.1), which assumed 100% activation for each muscle as the sensitivity studies of the unmodified model (see section 2.5.1) and previous craniofacial FEA sensitivity studies have demonstrated this is a reasonable modelling simplification to make in the absence of specimen-specific relative activation data (Toro-Ibacache and O'Higgins 2016). The elastic properties applied to the two materials of the modified model were the same as those applied to the unmodified FE model (see section 2.3.4.4).

Table 15. *f*Max estimates applied to the muscle force vectors modelled for both the unmodified and modified *H. sapiens* FE models.

Jaw-elevator muscle	*f*Max (N)*
Masseter	118.39
Medial pterygoid	126.12
Temporalis	141.70

***see section 2.1.4.1 for how these values were estimated.**

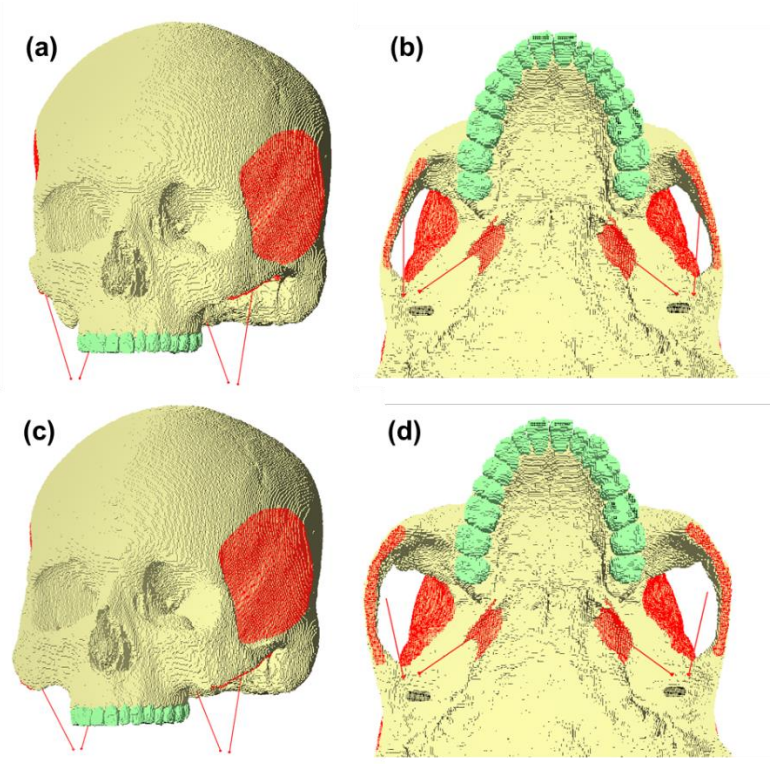

Figure 48. The loading and boundary conditions of the unmodified and unmodified *H. sapiens* FE models. The nodes to which the force vectors representing the bilateral masseter, medial pterygoid and temporalis were applied are selected in red. The constraints applied to the model (at the I^1s, LM^1s and both glenoid fossae) are selected in black, although for each simulation only one tooth was constrained. (a) Oblique view of the unmodified FE model. (b) Inferior view of the unmodified FE model. (c) Oblique view of the modified FE model. (d) Inferior view of the modified FE model.

3.3.1.6. Model solution and data analysis

Following the application of the loading and boundary conditions to the modified and unmodified *H. sapiens* FE models script files simulating an I^1 and an LM^1 bite were exported and solved, using PARA-BMU (the model solver for Vox-Fe), via Viking (a high-performance computing cluster provided by the University of York). Following the solution phase, the predicted nodal displacements were used to display colour maps representing principal strain 1 (PS1) and principal strain 3 (PS3) distributions for each simulation. Maximum and minimum principal strains were chosen due to the importance of strain in regulating the adaptation of bone to mechanical load (Skerry, 2008). Bite force magnitudes were extracted by summing the reaction forces recorded at the constrained nodes on the biting tooth, and joint reaction

force values were also extracted by calculating the reaction force magnitude recorded at the nodes constrained at each glenoid fossa (see section 2.3.5.2). The global strain distribution plots could also then be scaled to a given bite force at the constrained tooth, allowing strain predictions to be compared in light of geometric differences between the models (see section 2.3.5.3), rather than the impacts that the changes to the form of zygoma region may have upon the bite forces predictions and the craniofacial strains associated with this (which is considered in section 3.4; chapter objective two). The deformations predicted by the models were scaled to represent a 500 N bite at the $I^{1\prime}$s and an 800 N at the $LM^{1\prime}$s.

Strain magnitudes were also extracted from different anatomical regions (Figure 49). The regions from which strain magnitudes were extracted from for the unmodified model were described within section 2.3.5.1; corresponding locations were identified on the surface of the modified FE model and the same number of nodes were selected for each region (Figure 49).

Bite force efficiencies were also calculated as described within section 2.3.5.2. The differences in predictions for this output parameter (as well as the reaction force predictions) will solely be a product of the changes to the origin and vector of the masseter, as this is the only loading condition to vary between the unmodified and modified FE models. Table 16 lists the simulations performed to address the impact that modifying the *H. sapiens* FE model to have a zygoma region like *H. ergaster* had upon predictions of craniofacial strain and bite force when loaded with estimates of human muscle force.

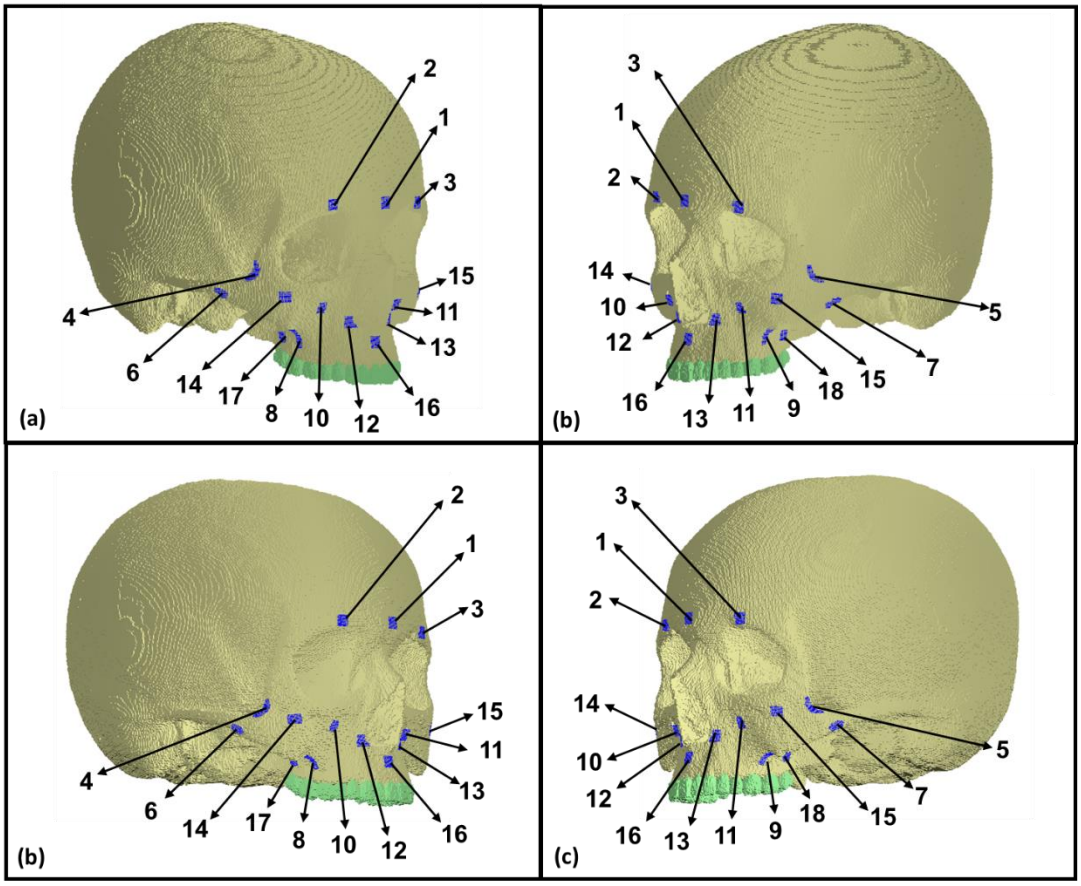

Figure 49. The regions (blue) where strain magnitudes will be extracted from on the unmodified (a and b) and modified (c and d) models. See section 2.1.5.1 for descriptions of these regions.

Table 16. The simulations performed (and a description of their loading and boundary conditions) to address H1 and H2

Simulation Number	Model	Bite Point	Gape	Muscle forces
1	Unmodified Model	I^1	Occlusion	Human Muscle Forces*
2	Modified Model	I^1	Occlusion	Human Muscle Forces*
3	Unmodified Model	LM^1	Occlusion	Human Muscle Forces*
4	Modified Model	LM^1	Occlusion	Human Muscle Forces*

***Human muscle forces magnitudes can be found within Table 15**

3.3.2. Objective One Results (H1): reaction force predictions and bite force efficiencies

Table 17 contains the reaction force and bite force efficiency predictions for I^1 and LM^1 bites for the unmodified and modified *H. sapiens* FE models loaded with human muscle force magnitudes. For both the I^1 and the LM^1 bites, the modified model (simulations 2 and 4) predicted slightly higher bite force magnitudes, mostly lower joint reaction forces, and higher

bite force efficiencies (Table 17) compared to the unmodified model (simulations 1 and 3). For the I^1 bites (simulations 1 and 2), the predicted bite force for the modified model is only 4.84 N higher that the prediction of the unmodified model, equating to a negligible (0.01) increase in bite force efficiency between the models. The predictions of joint reaction force for the modified model are only slightly lower than for the unmodified model, with a 6.84 N lower reaction force occurring at the left joint and a 4.83 N decrease occurring at the right. For the LM^1 bites, the modified model had a higher bite force efficiency than unmodified model (0.51 compared to 0.63), while predicting a bite force increase of 7.54 N. The joint reaction force magnitudes predicted for both are comparable at the balancing side joint, and there was a small decrease in magnitude predicted at the working side (4.29 N) for the modified model.

Table 17. Reaction force predictions and bite force efficiency for the modified and unmodified *H. sapiens* FE models simulating an I^1 (simulations 1 and 2) and a LM^1 bite (simulations 3 and 4).

Simulation Number	Model	Bite Point	Bite Force Magnitude (N)	Bite force efficiency	Left joint reaction force (N)	Right joint reaction force (N)
1	Unmodified *H. sapiens*	I^1	272.43	0.42	220.89	197.83
2	Modified *H. sapiens*	I^1	277.27	0.43	214.05	193.00
3	Unmodified *H. sapiens*	LM^1	395.23	0.51	93.02	215.45
4	Modified *H. sapiens*	LM^1	402.77	0.63	93.06	210.58

3.3.3. Objective One results (H2): global and local strain distributions

The craniofacial strain predictions of the modified and unmodified *H. sapiens* FE models loaded with human jaw-elevator muscle force magnitudes are presented below, and the results are split according to the loading scenario simulated.

3.3.3.1. I^1 bites

Figure 50 visualises global PS1 and PS3 distributions for the unmodified (simulation 1) and unmodified models (simulating 2) during I^1 bites. The overall distribution of strains resembles expected strain distributions for an I^1 bite; strains are highest in regions close to the bite

reaction force like the subnasal regions and the lateral nasal margins and are distributed through the facial skeleton superior-inferiorly about the midline. The regions local to the attachment of the masticatory muscles also demonstrate elevated strains, while the supraorbital region demonstrates low magnitudes for both simulations.

Globally, strain magnitudes vary little between the modified and unmodified models (Figure 50 and Figure 51). One exception to this is the left lateral nasal margin (region 13; Figure 51) where PS3 magnitudes were higher for the modified model (-491.12με for the modified model compared to -449.48με for the unmodified model), although magnitudes are more comparable at the contralateral nasal margin (region 12; Figure 51). Another interesting exception to this is that strain magnitudes at the greater wing of the sphenoid and the squamous temporal bone superior to the glenoid fossae are higher for the unmodified model (Figure 50), however strain magnitudes proximate to the TMJ itself were comparable for both models. Strains are comparable in all other global regions aside from these areas (Figure 50 and Figure 51).

The main differences in strain distribution and magnitude between the modified and unmodified models are concentrated in the zygomatic regions (Figure 50 and Figure 51). While at the zygomatic bodies (inferior to the lateral corner of the orbit; Figure 50) the modified model predicted elevated PS1 and PS3 magnitudes (e.g. at region 14 the modified model predicted 109.20με and -83.19με compared to 87.47με and -55.08με for the unmodified model), strain magnitudes in some other areas of the zygoma region are decreased (e.g. along the infraorbital rims; Figure 50). Strains along the zygomatic arch for the modified model are more widely distributed across the structure, compared to the unmodified model where they are concentrated through a smaller, more posterior portion of the arch (Figure 50); while PS1 magnitudes are similar at regions 6 and 7 (the left and right zygomatic arches) for both the models (Figure 51), the modified model predicted higher PS3 magnitudes (e.g. at region 7 the unmodified model predicted -307.33με and the modified model predicted -334.88με). However, at the postorbital regions strain magnitudes are lower for the modified model (e.g. at region 4 the modified model predicted magnitudes of

362.26με and -138.42με whereas the unmodified model predicted 550.06με and -194.86με). There are small differences between strains in other regions local to the zygoma (e.g. the infraorbital region and the zygomatic roots; Figure 50 and Figure 51). At the left zygomatic root, PS3 magnitudes are lower for the modified model (region 9; the modified model predicted -29.74με and the unmodified model predicted -62.16με), although again at the contralateral zygomatic root both models predict similar magnitudes (Figure 51).

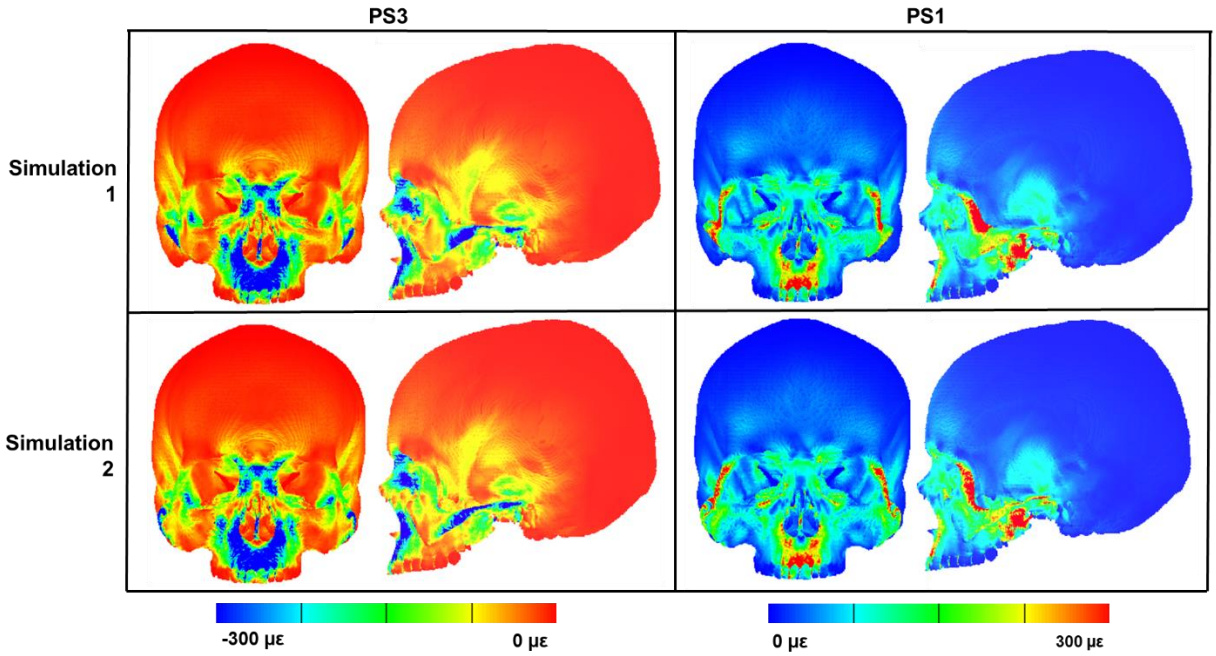

Figure 50. Global PS1 and PS3 strain distributions during I^1 bites for the unmodified (simulation 1) and modified models (simulation 2), scaled to a 500 N bite.

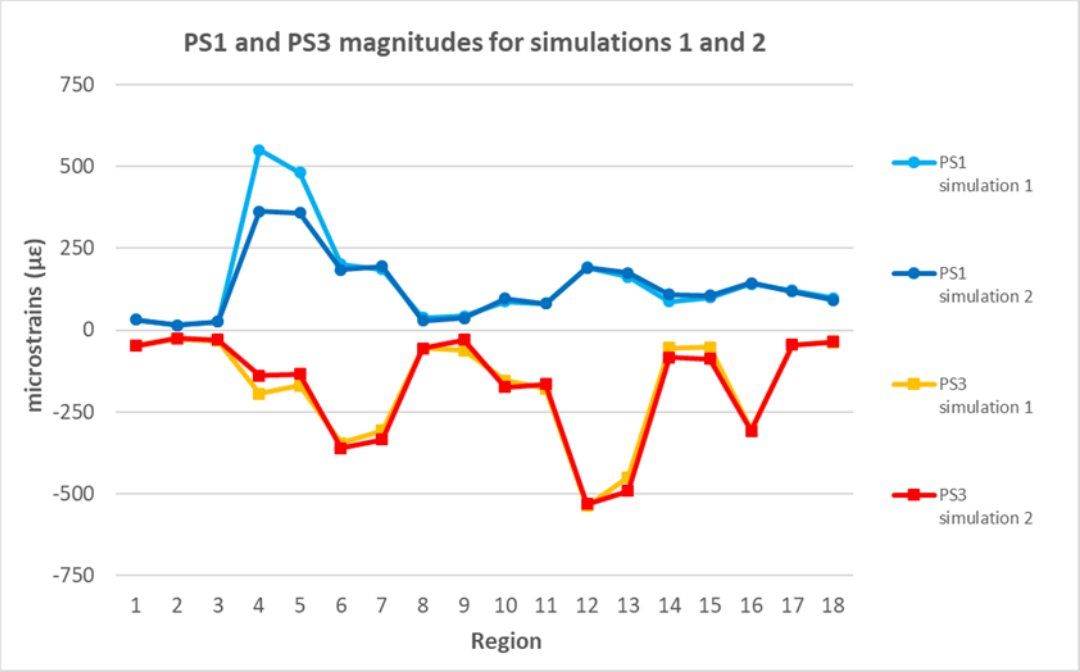

Figure 51. Average PS1 and PS3 magnitudes during I^1 bites for the unmodified (simulation 1) and modified models (simulation 2), scaled to a 500 N bite. See sections 3.3.1.6 for a description and visualisation of the numbered regions.

3.3.3.2. LM^1 bites

Figure 52 visualises global PS1 and PS3 distributions for the unmodified (simulation 3) and unmodified models (simulation 4) during LM^1 bites. The overall distribution of strains for both models resemble those expected for an LM^1 bite, meaning strains are the highest close to the occlusal plane and are elevated on the working (left) side of the face for both models, as well as regions local to the attachment of the masticatory muscles bilaterally while the supraorbital region for both show low strain magnitudes.

Like the results of simulations 1-2, the differences in magnitude and distribution of strain are mostly in regions local the zygoma during molar bites (Figure 52 and Figure 53). Again, PS1 and PS3 magnitudes at the zygomatic bodies inferior to the lateral corner of the orbit bilaterally are elevated for the modified model (e.g. at region 15 the modified model predicted -73.18με and the unmodified model predicted -47.59με). Again, strains in the zygomatic arch for the modified model are more widely distributed across the structure, and PS3 magnitudes are higher (e.g. at region 7 the modified model predicted -361.29με

compared to -343.01με). Likewise, the modified model predicted lower strain magnitudes at the frontal process of the zygoma and the postorbital regions (e.g. at region 4 the modified model predicted 361.41με and -135.45με whereas the unmodified model predicted 469.64με and -166.80με). In most other regions local to the zygoma are comparable between the models on the working side of the face, while magnitudes on the balancing side of the face are elevated in the rest of the zygomatic bodies, zygomatic roots and in the infraorbital region for the modified model (Figure 52). For PS1 however, magnitudes in the working and balancing infraorbital regions are reduced for the modified model, while magnitudes are higher more laterally in the balancing zygomatic body and along both infraorbital rims (Figure 52).

As seen for the incisor bites, the differences in global strain distributions and magnitude between the models are minimal (Figure 52 and Figure 53). A notable global difference includes lower strain magnitudes for both PS1 and PS3 in the neurocranium for the modified model although this is only apparent on the balancing side (Figure 52), however again strain magnitudes proximate to the itself were comparable for both models. The only other global difference is the higher PS3 magnitudes predicted by the modified model at the left lateral nasal margin (region 13; the modified model predicted -241.16με compared to -212.93με).

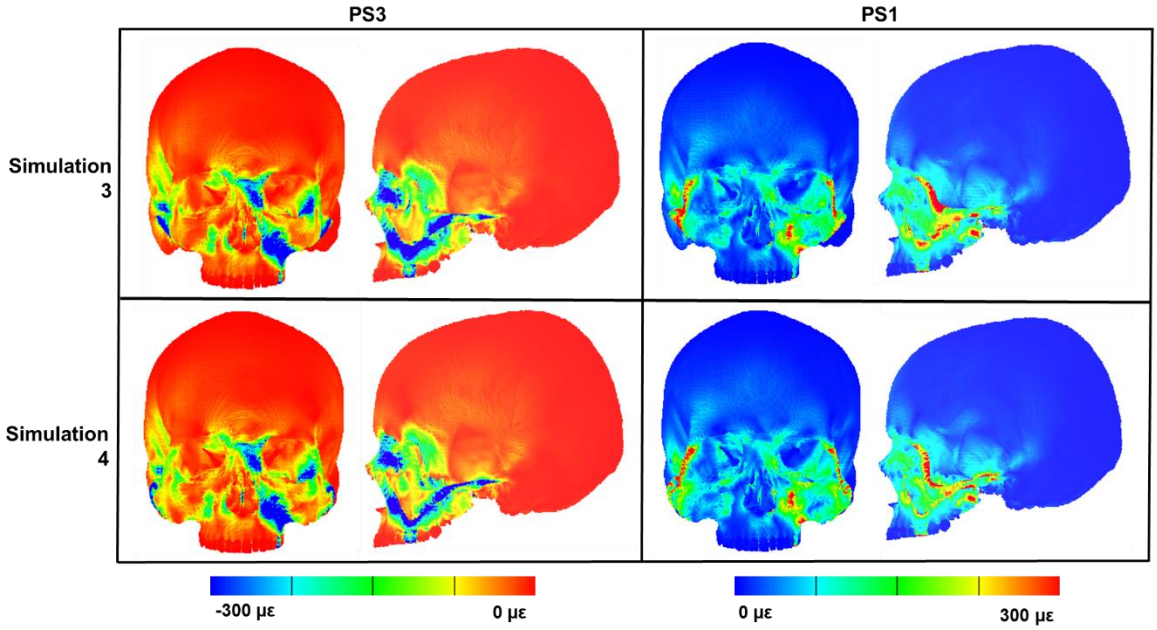

Figure 52. Global PS1 and PS3 strain distributions during LM[1] bites for the unmodified (simulation 3) and modified models (simulation 4), scaled to an 800 N bite.

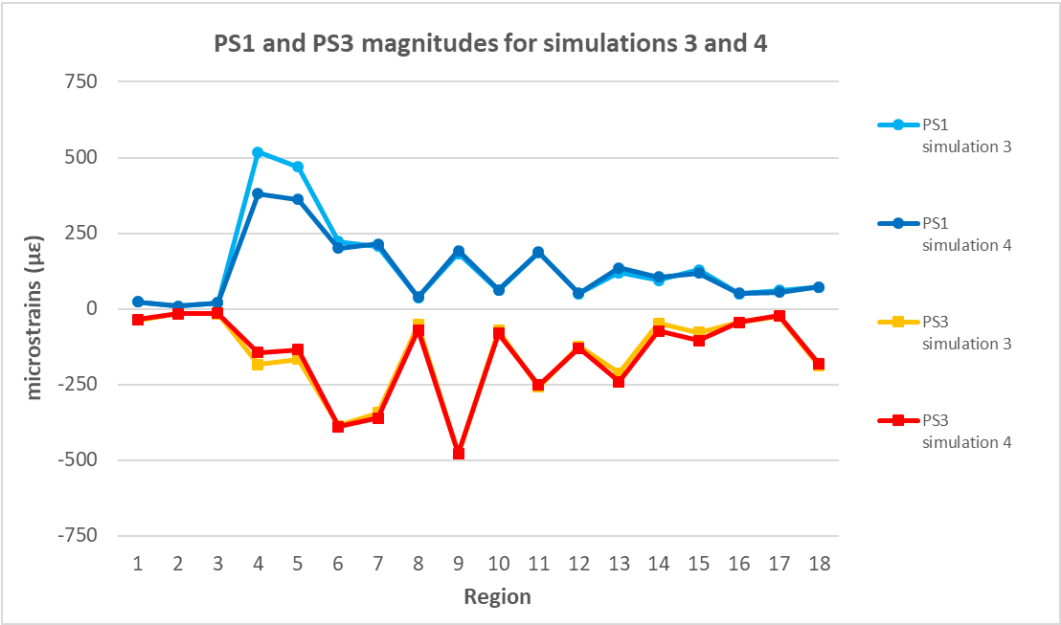

Figure 53. Average PS1 and PS3 magnitudes during LM[1] bites for the unmodified (simulation 3) and modified models (simulation 4), scaled to an 800 N bite.

3.4. Objective Two: investigate the impacts of loading the unmodified and modified *H. sapiens* FE models with *H. ergaster*-like masseter muscle forces on craniofacial strain and bite force production

The warp increased the width of the zygoma region and the size of the masseter muscle attachments. As facial width has been correlated with an increase in masseter cross-sectional area (CSA) within modern *Homo sapiens* (Weijs and Hillen 1986; Hannam and Wood 1989; Raadsheer et al. 1999; Rohila et al. 2012), the wide zygoma region of *H. ergaster* indicates a larger and thus more forceful masseter compared to *H. sapiens* (Demes and Creel 1988). While the previous subsection outlined the predictions of the modified and unmodified FE models when loaded with estimates of human jaw-elevator muscle force, H3 could only be addressed by re-estimating masseter CSA and *f*Max values for the modified *H. sapiens* specimen. This subsection details how this was achieved, and the impacts this change to the loading conditions of the modified and unmodified *H. sapiens* FE models had upon their predictions.

3.4.1. Objective two: materials and methods

The magnitude of force applied to both models was re-estimated to reflect how an increasing the width of the face may increase the CSA of the masseter (Weijs and Hillen 1986b; Hannam and Wood 1989; Raadsheer et al. 1996; Rohila et al. 2012). This subsection details how masseter CSA and *f*max values were re-estimated with the increased width of the zygoma region following the warp.

3.4.1.1. Re-estimation of masseter force

The modified specimen is hypothetical and has no associated medical imaging visualising soft tissues. Therefore, it was necessary to re-estimate masseter CSA via bony proxies, despite the poor correspondence between muscle CSA estimated via bony proxies and muscle CSA recorded from medical imaging for the same individuals (Toro-Ibacache et al. 2016).

To re-estimate the CSA of the masseter for the modified *H. sapiens* cranium, the mediolateral distance between a centroidal point on the mandibular insertion of the masseter and the

lateral extent of the zygomatic arch was multiplied by the length of the origin site of the masseter on the inferior border of the zygomatic arch (Anton 1990; O'Connor et al. 2005; Eng et al. 2013; Toro-Ibacache et al. 2015). To do this, the length of the origin site of the masseter on the inferior border of the zygomatic arch was firstly calculated. The surface file of the modified crania was converted into a .ply file and loaded into 3D slicer (Fedorov et al. 2012), where two semilandmark curves (each with 10 semilandmarks) were created along the origin site of the masseter bilaterally (Figure 54). The length of each of these curves was recorded at 5.60cm, which is consistent with previous measurements of the length of the masseteric scar of KNM-ER 3733 (Demes and Creel 1988).

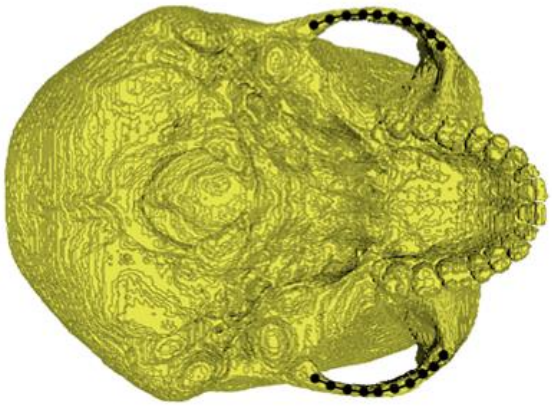

Figure 54. Calculation of the length of the origin site of the masseter bilaterally using semi-landmark curves in 3D slicer.

Following this, the mediolateral distance between the lateral edge of the zygomatic arch and the mandibular ramus was calculated bilaterally (Figure 55). Following the protocol of Toro-Ibacache et al. (2015), the surface files of the modified crania and the mandible were loaded into Avizo and landmarks were placed on most posterior point at the base of the mandibular lingula bilaterally, which were then translated onto the lateral surface of the mandibular ramus (becoming landmark 1; Figure 55). Following this, another landmark was placed on the lateral edge of the zygomatic arch with the same coordinates in an anterior-posterior (global Z) dimension as the landmark on the lateral surface of the mandibular ramus (landmark 2; Figure 55). Subsequently, the landmark on the mandibular ramus was translated to have the

same coordinates in a medio-lateral dimension (global X) as the landmark on the zygomatic arch (landmark 2) and was saved as a new ascii file (becoming landmark 3). The difference in the X axis coordinates between landmarks 1 and 3 were calculated, providing a measure of the mediolateral distance between the insertion of the masseter on the mandibular ramus and lateral edge of the zygomatic arch (Figure 55). This protocol was repeated on each side of the crania for landmarks placed 1 mm above and below landmarks 1 and 2, producing six estimates of the mediolateral distance between the mandibular rami and lateral edge of the zygomatic arches overall.

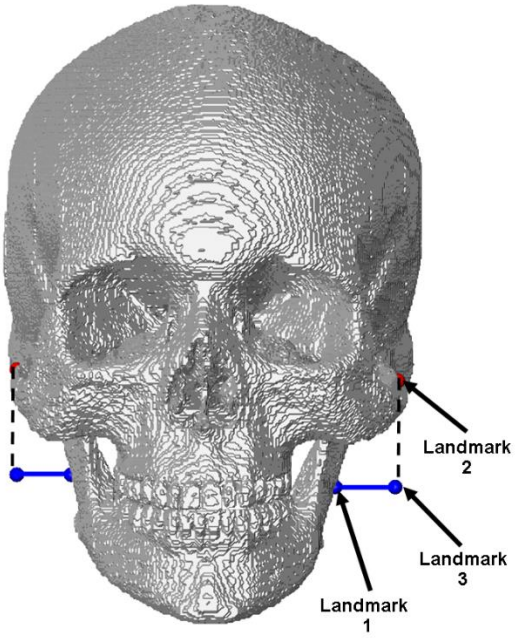

Figure 55. Calculation of the mediolateral distance between the mandibular ramus and the zygomatic arch (blue line), using landmarks 1, 2 and 3 (see text for a description of how their position was determined).

Following this, the calculations of the mediolateral distance between the mandibular ramus and the lateral aspect of the zygomatic arch were multiplied by the calculations of the length of the origin site of the masseter to provide new estimates of masseter CSA (Table 18). Once the six re-estimates of masseter CSA were calculated, the values were averaged, and this average was multiplied by 37 N/cm^2 to provide an estimation of *H. ergaster*-like masseter *f*Max (i.e. *f*Max for the modified H. sapiens specimen; Table 19).

Table 18. Estimated values of masseter CSA for the modified *H. sapiens* crania.

	Left masseter section number			Right masseter section number			Average CSA (cm^2)
	1	**2**	**3**	**1**	**2**	**3**	
CSA (cm^2)*	11.94	11.66	12.08	10.81	10.68	10.68	11.31

***Calculated via bony proxies following the protocol of Toro-Ibacache et al. (2015).**

Table 19. The estimation of masseter *f*Max for the modified *H. sapiens* crania compared to the *f*Max estimate for the unmodified *H. sapiens* cranium.

	Masseter *f*Max (N)
Unmodified *H. sapiens*[a]	118.38
Modified *H. sapiens*[b]	418.47

[a] Calculated via bony proxies (see above)

[b] Calculated from the specimen-specific CT scan (see section 2.3.4.1)

3.4.1.2. Model solution and data analysis

Following the estimation of masseter *f*Max for the modified *H. sapiens* specimen, the magnitude of force applied to the masseter of both the modified and unmodified FE models were altered in Vox-Fe, and script files simulating I^1 and LM^1 bites for both models were exported and solved. Aside from the alterations to the force magnitude of the masseter, the loading and boundary conditions remained consistent with previous simulations (see section 3.3.1.5). The strain distribution colour maps, bite force magnitude, joint reaction force magnitude and bite force efficiency predictions of each simulation are presented as outlined within section 3.3.1.6. However, to examine H3 the strain colour maps and regional strain magnitudes extracted from the model were not scaled to a given bite force to allow investigation into how the increase in bite force that arises due to an increase to masseter force magnitude impacts craniofacial strains locally to the zygoma and globally. Table 20 lists all the simulations performed to investigate the impact that increasing the force applied to the masseter had upon predictions of craniofacial strain and bite force for both the modified and unmodified FE models.

Table 20. The simulations performed (and a description of their loading and boundary conditions) to address H3.

Simulation Number	Model	Bite Point	Gape	Muscle Forces
5	Unmodified *H. sapiens*	I^1	Occlusion	Masseter – modified human *f*Max[a] M. pterygoid – human *f*Max[b] Temporalis – human *f*Max [b]
6	Modified *H. sapiens*	I^1	Occlusion	Masseter – modified human *f*Max[a] M. pterygoid – human *f*Max[b] Temporalis – human *f*Max [b]
7	Unmodified *H. sapiens*	LM^1	Occlusion	Masseter – modified human *f*Max[a] M. pterygoid – human *f*Max[b] Temporalis – human *f*Max [b]
8	Modified *H. sapiens*	LM^1	Occlusion	Masseter – modified human *f*Max[a] M. pterygoid – human *f*Max[b] Temporalis – human *f*Max [b]

[a] **Re-estimated masseter *f*Max can be found in Table 19**

[b] **Human *f*Max values can be found in Table 15**

3.4.2. Objective Two results (H3): reaction force predictions and bite force efficiencies

Table 21 contains the reaction force and bite force efficiency predictions for I^1 and LM^1 bites for the unmodified and modified *H. sapiens* FE models, when loaded with a *H. ergaster*-like masseter force magnitudes. For the I^1 bites (simulations 5 and 6), the modified model predicted a 17.33 N higher bite force than the unmodified model, while bite force efficiency only increased marginally (0.02), and joint reaction force is lower bilaterally (12.17 N at the left joint and 7.38 N at the right joint). For the LM^1 bites (simulations 7 and 8), the modified model has a higher bite force efficiency than unmodified model (0.68 compared to 0.59) as well as a 90.8 N higher prediction of bite force magnitude. The predictions of joint reaction force for the modified model are marginally higher than the predictions for the unmodified model bilaterally (4.85 N at the left joint and 7.17 N at the right joint).

Table 21. Reaction force predictions and bite force efficiency for the modified and unmodified *H. sapiens* FE models simulating an I^1 (simulations 5 and 6) and a LM^1 bite (simulations 7 and 8) when loaded with *H. ergaster*-like masseter force magnitudes.

Simulation Number	Model	Bite Point	Bite Force Magnitude (N)	Bite force efficiency	Left Joint reaction force (N)	Right Joint reaction force (N)
5	Unmodified *H. sapiens*	I^1	542.16	0.45	399.05	384.99

6	Modified *H. sapiens*	I^1	559.49	0.47	386.88	377.61
7	Unmodified *H. sapiens*	LM^1	719.72	0.59	256.32	403.60
8	Modified *H. sapiens*	LM^1	810.52	0.68	261.17	410.77

3.4.3. Objective Two results (H3): Global and local strain distributions

The craniofacial strain predictions of the modified and unmodified *H. sapiens* FE models loaded with *H. ergaster*-like masseter muscle force magnitudes are presented below, and the results are split according to the bite simulated.

3.4.3.1. I^1 bites

Figure 56. visualises the global PS1 and PS3 distributions for the unmodified (simulation 5) and modified (simulation 6) *H. sapiens* FE models loaded with *H. ergaster*-like masseter force magnitudes during an I^1 bite. The global predictions are expected for a I^1 bite (see section 3.3.3.1). Compared to previous simulations loaded with human muscle forces (see section 3.3.3.1), both models predicted a global increase in strain magnitude, particularly in regions local to the attachment of the masseter (the zygomatic arches) and in regions proximate to the bite reaction force (Figure 56). This is observable for PS1 in the entire supraorbital region and PS3 in the glabella region, where both the models show elevated magnitudes compared to previous simulations (see section 3.3.3.1). Compared to the unmodified model, PS1 magnitudes at the lateral supraciliary arches for the modified model are marginally higher compared to unmodified model, as are PS3 magnitudes at the glabella and interorbital regions (Figure 56). Another global difference in strain magnitude is that the modified model demonstrates lower strain magnitudes for both PS1 and PS3 at the greater wing of the sphenoid bone and around the squamous temporal bone superior to the glenoid fossae (Figure 56), while strains were comparable more locally to the TMJ for both models. Globally, in regions local to the bite reaction force the modified model predicted higher strain magnitudes than the unmodified model (Figure 56 and Figure 57). For example, at the left

lateral nasal margin (region 13; the modified model predicts a PS3 magnitude of -532.42με compared to -470.00με for the unmodified model).

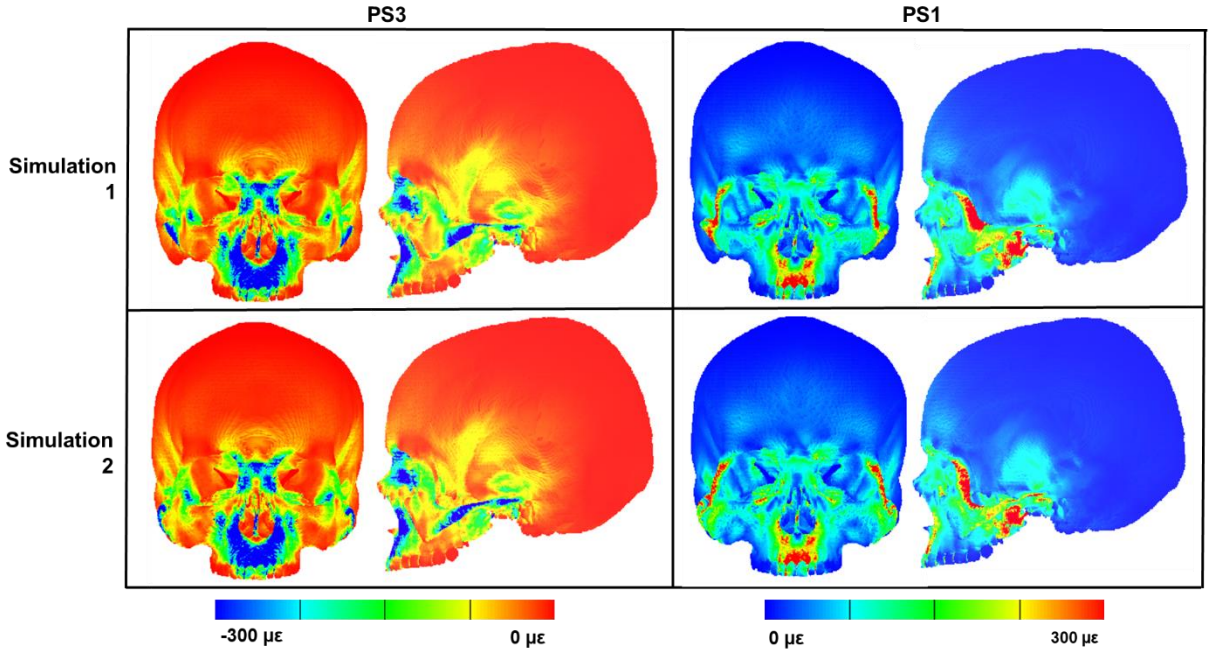

Figure 56. Global PS1 and PS3 strain distributions during I^1 bites for the unmodified (simulation 5) and modified models (simulation 6) loaded with *H. ergaster*-like masseter force magnitudes.

As identified in section 3.3.3.1, most of the differences in magnitude and distribution of strain between the models are local the zygoma. In many regions local to the zygoma (for example regions 8-11; Figure 57) the modified model predicts marginally higher PS1 and PS3 magnitudes than the unmodified model, which is most likely a product of the higher bite force magnitude prediction. As previously identified for the modified FE model, the strains in the zygomatic bodies are concentrated inferiorly to the lateral corner of the orbit (Figure 56). This is also apparent from the unscaled to bite force extracted strain magnitude data (Figure 57) where the modified model predicted higher PS3 values (-156.45με for the modified model compared to -90.33με for the unmodified). Again, strains are more widely distributed along the zygomatic arch of the modified model although both PS1 and PS3 magnitudes are comparable between simulations 5 and 6 (Figure 57). The modified model also predicted higher strain magnitudes (particularly for PS3) in other regions local to the zygoma, for example at the infraorbital regions (e.g. at region 10 the unmodified model predicted -144.72με compared to for the unmodified model -173.12με), as well as at the zygomatic roots

and zygomatic processes of the maxilla (Figure 56). While PS1 magnitudes in these regions appear lower for the modified model, tensile strains are instead more concentrated laterally towards the zygomatic bodies. However, both PS1 and PS3 magnitudes are lower for the modified model in the postorbital region (e.g. at region 4 the modified model predicted 680.47με and -259.25με whereas the unmodified model predicted 958.62με and -340.56με).

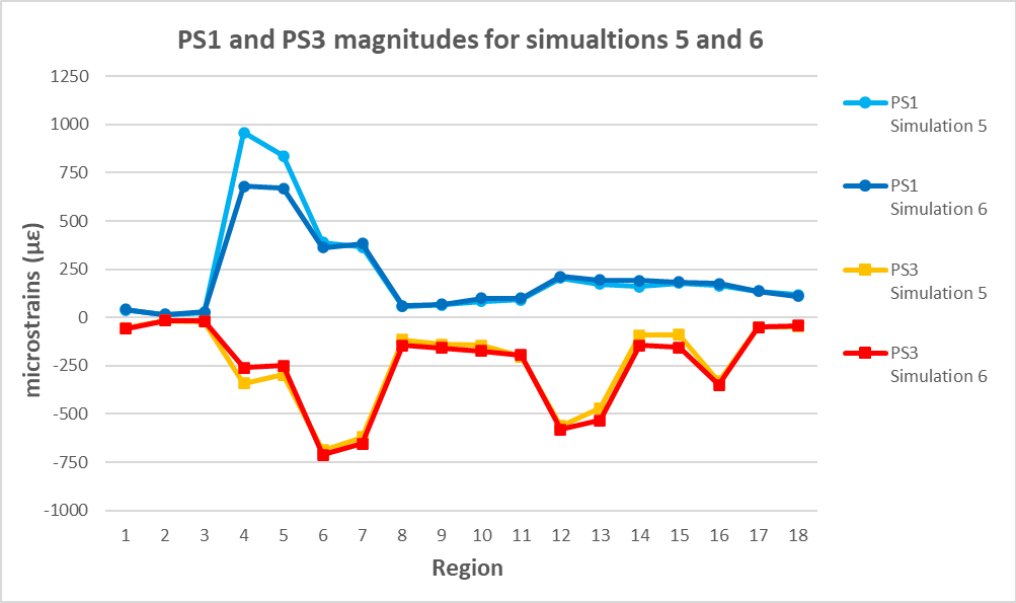

Figure 57. Average PS1 and PS3 magnitudes during I^1 bites for the unmodified (simulation 5) and modified models (simulation 6), loaded with *H. ergaster*-like masseter force magnitudes See section 3.3.1.6 for a description and visualisation of the numbered regions.

3.4.3.2. LM^1 bites

Figure 58 visualises the global PS1 and PS3 distributions for the unmodified (simulation 7) and modified (simulation 8) *H. sapiens* FE models loaded with *H. ergaster*-like masseter force magnitudes during an LM^1 bite. The global predictions are expected for a LM^1 bite (see section 3.3.3.2). Compared to previous simulations (see section 3.3.3.2), both models again predict a global increase in strain magnitude. This is observable for PS1 in the lateral supraciliary arches and PS3 in the glabella region, however the modified model demonstrates slightly lower magnitudes than the unmodified model, particularly in the interorbital area (Figure 58). Again, another notable global difference in strain distribution again includes lower strain magnitudes for both PS1 and PS3 in the neurocranium for the modified model, with this again being mostly apparent on the balancing side of the cranium (Figure 58). As seen for the incisor

bites, in regions local to the bite reaction force the modified model predicted higher strain magnitudes than the unmodified model (Figure 58 and Figure 59). For example, at the working (left) nasal margin, PS3 magnitudes are higher for the modified model (region 13; the modified model predicted -243.42με compared to -203.50με); this is also apparent at the working zygomatic root (e.g. at region 9 the modified model predicted -584.47με compared to -563.44με).

As identified previously, most of the differences in magnitude and distribution of strain between the models are local the zygoma. However, despite a 90.8 N higher prediction of bite force, the modified model predicts comparable strain magnitudes to the unmodified model (Figure 59). At the zygomatic bodies on both sides of the face, strain magnitudes are higher for the modified model (e.g. at region 15 the unmodified model predicted -108.58με compared to -162.48με for the modified model), and visually this is again concentrated around the inferior-lateral corner of the orbit. On the working side of the face the modified model demonstrates higher strain magnitudes (particularly for PS3) in regions including the zygomatic bodies and infraorbital regions (e.g. region 10 the modified model predicted -89.78με compared to -69.21με), as well as at the zygomatic process of the maxilla (Figure 58). While PS1 magnitudes in the working zygomatic body are higher for the modified model, magnitudes are slightly lower in the infraorbital regions, but are also higher along the infraorbital rim itself (Figure 58). On the balancing side of the face, PS1 magnitudes are again lower in the infraorbital regions but are concentrated more laterally in the zygomatic bodies and are again higher along the infraorbital rim for the modified model (Figure 58), while PS3 magnitudes are higher in these regions especially around the zygomatic root and zygomatic process of the maxilla (e.g. at region 8 the modified model predicted -154.45με compared to -110.58με)

Owing to the increased force applied to the masseter, both models demonstrate high strain magnitudes through both the frontal process of the zygoma and the zygomatic arches (Figure 58 and Figure 59). Although the absolute values are predicted at the postorbital regions are lower for the modified model (e.g. at region 4 the modified model predicted 663.06με and -

252.09με compared to 871.51με and -309.35με). The absolute magnitudes predicted by both models at the zygomatic arches are comparable, however again strains are visually distributed along a larger proportion of the structure (Figure 58 and Figure 59).

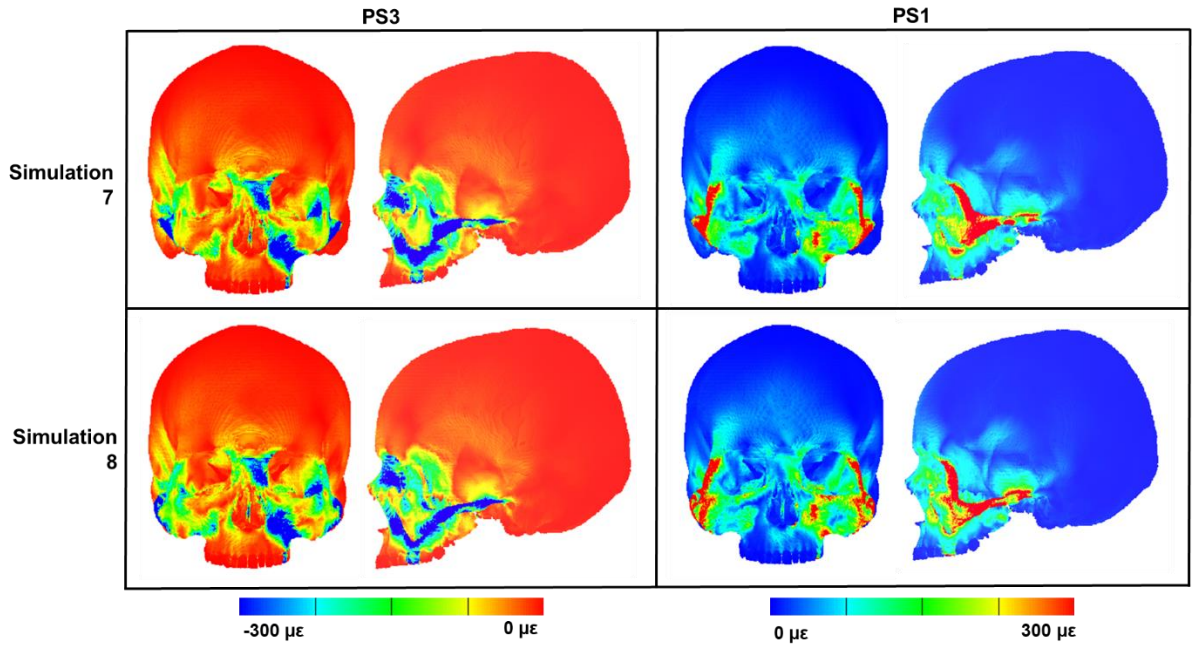

Figure 58. Global PS1 and PS3 strain distributions during LM[1] bites for the unmodified (simulation 7) and modified models (simulation 8) loaded with *H. ergaster*-like masseter force magnitudes.

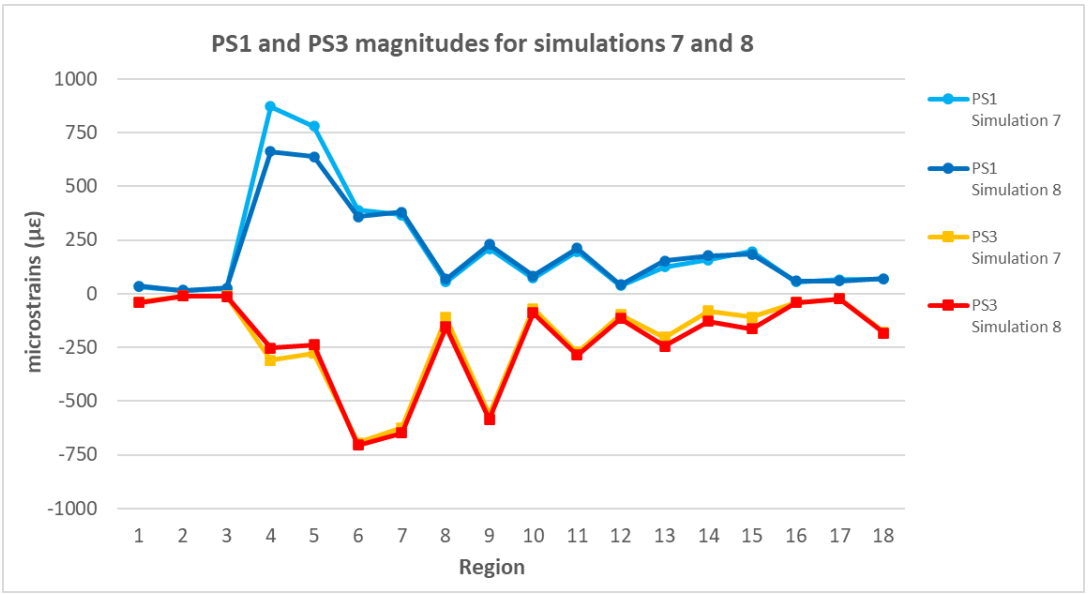

Figure 59. Average PS1 and PS3 magnitudes during LM[1] bites for the unmodified (simulation 7) and modified models (simulation 7), loaded with *H. ergaster*-like masseter force magnitudes.

3.5. Objective Three: investigate the impacts of simulating bites at submaximal and maximal gapes on craniofacial strains and bite force production for the unmodified and modified *Homo sapiens* FE models

To simulate a bite at gape, the loading and boundary conditions of a FE model need altering to reflect condylar translation and rotation, and the re-orientation of muscle force vectors (Dumont et al. 2011). The previous chapter assessed the sensitivity of the *H. sapiens* FE model to individually altering the input parameters necessary to simulate bites (see section 2.5). This demonstrated that the model was relatively insensitive to how muscle activation patterns are modelled (see section 2.5.1.2), however changes to the orientation of the masseter and medial pterygoid force vectors and position of the TMJ constraints impacted predictions of reaction forces and strains local to the zygoma (see sections 2.5.2.2 and 2.5.3.2).

This sections details how the loading and boundary conditions of the unmodified and modified FE models were altered to simulate bites at a range of gapes, and the impacts these changes have upon reaction force predictions and craniofacial strains during I^1 and LM^1 bites for both models. This facilitates the investigation as to whether the zygoma region morphology of *H. ergaster* is better adapted to bites at larger gapes, relative to a *H. sapiens* specimen.

3.5.1. Objective Three: materials and methods

To simulate bites at different gapes, the loading and boundary conditions of the models were altered reflect the anterior-inferior translation and rotation of the mandible during jaw opening, and the accompanying changes to the lines of action of the jaw-elevator musculature. This following subsection describes how the loading and boundary conditions of both models were modified in combination to simulate bites at gape.

3.5.1.1. Determining the spatial position of TMJ constraints and orientation of muscle force vectors

The *H. sapiens* FE model was constructed from an anonymous cadaveric CT scan (see section 2.3). As such, the maximal jaw opening capacity of the *H. sapiens* specimen used to construct the FE model from is unavailable. Gapes of 20mm and 40mm of incisal separation were chosen to represent submaximal and maximal gapes as these distances encompass the range size range of many large hard food objects (e.g. the *Sacoglottis gabonensis* seeds fed on by *Cercocebus atys* are on average 24 mm long on their minor axis and 32 mm long on their major axis; Daegling et al. 2011), and fall within the range of maximal jaw-opening capacities reported for *H. sapiens* (Muto et al. 1994; Lindauer et al. 1995; Travers et al. 2000; Lewis et al. 2001). In the absence of specimen-specific mandibular kinematic data, the rotation and translation of the mandible required to obtain these interincisal distances needed to be established. Baird (unpublished data and via personal communication) recently collected some *in vivo* data of maximum jaw opening and recorded mandibular positions via structure light scanning of teeth in a *H. sapiens* individual. After gaining permission to use this kinematic data, the mandibular rotation and translation data used to produce 20mm and 40mm of interincisal separation were applied to the model within this thesis (see Table 22). The surface file of the mandible, and associated landmarks used to approximate the jaw-elevator muscle insertions (see Table 4 in section 2.3.4.2), were translated, and rotated using this pre-determined translation and rotation data.

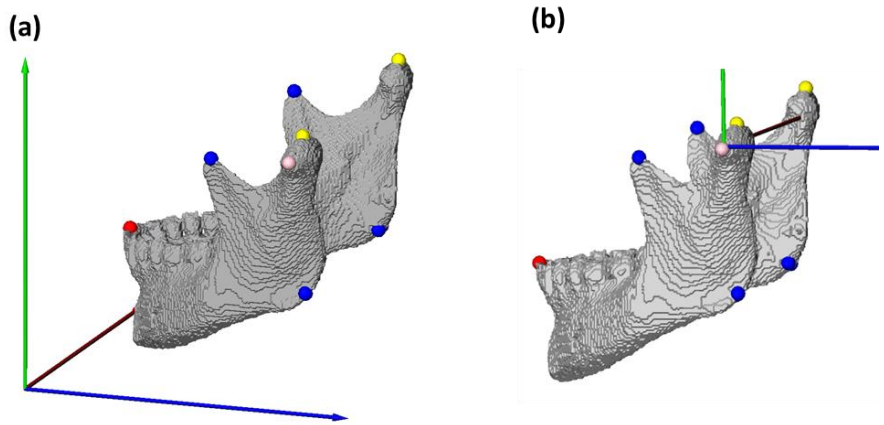

Figure 60. The surface of the *H. sapiens* mandible in its original spatial position (a) and aligned to the global X axis (b). The landmarks used to redefine the end points of the muscle force vectors (blue), the position of the

TMJ constraints (yellow), as well as the landmarks used to align the surface of the mandible and these landmarks to the global x axis (pink) and to calculate inter-incisal separation following rotation and translation (red) are also shown.

Before the transformation of the landmarks approximating the insertions of the jaw-elevator musculature could take place, some additional landmarks were created (Figure 60). Firstly, two landmarks were placed on the centre of the occlusal surfaces of the mandibular and maxillary central incisors (Figure 60) which were subsequently used to calculate inter-incisal separation following the rotation and translation of the mandible. Additionally, two new landmarks were placed on the superior-most point of each mandibular condyle to help redefine the position of the TMJ constraints in the Vox-Fe models (Figure 60). However, before the mandible could be rotated in Avizo it was necessary to translate the surface file so that the global X-axis passed through both the mandibular condyles (Figure 60), to establish a rotational axis. To do this another landmark was placed on a central point on the left condyle in lateral view and both the mandible and landmarks were translated so that this landmark had a global position of (0,0,0) (Figure 60). The landmarks could then be rotated about the X-axis, approximating the rotation of the condyles during jaw opening (Figure 61). The transformation matrixes used at this step were recorded so that it could be inversed to move the landmarks back to their original spatial position.

Table 22. Translation matrices applied to the landmarks used to define the loading and boundary conditions of the model to simulate bites at different gapes.

Targeted Interincisal separation (mm)	Rotation (deg) [a]	Anterior Translation (mm) [a]	Interincisal separation (mm) [b]
20	-10.03	1.41	19.00
40	-22.38	4.32	41.01

[a] the values were derived from Baird (unpublished). The mandibular rotation and anterior translation data taken from Baird produced 20mm and 40mm of interincisal separation in their work.

[b] the interincisal separation produced by applying these kinematic values to the mandible of the *H. sapiens* specimen within this thesis did not result in exactly 20mm and 40mm but the values are close.

Following this, the landmarks and surface file of the mandible were rotated about the X-axis, and then anteriorly translated along the Z-axis, depending on whether a submaximal or maximal gape was to be simulated (using the values within Table 22; Figure 61). Next, the original translation matrix was inverted, moving the translated and rotated landmarks back

to their original position (Figure 62). After this, the position of the mandible and landmarks in relation to the cranium was checked. If the landmarks on the superior surface of the mandibular condyles penetrated the surface of the articular eminence (i.e. they were too superior), the landmarks were translated inferiorly until these landmarks were bilaterally visible on the surfaces of the articular eminences.

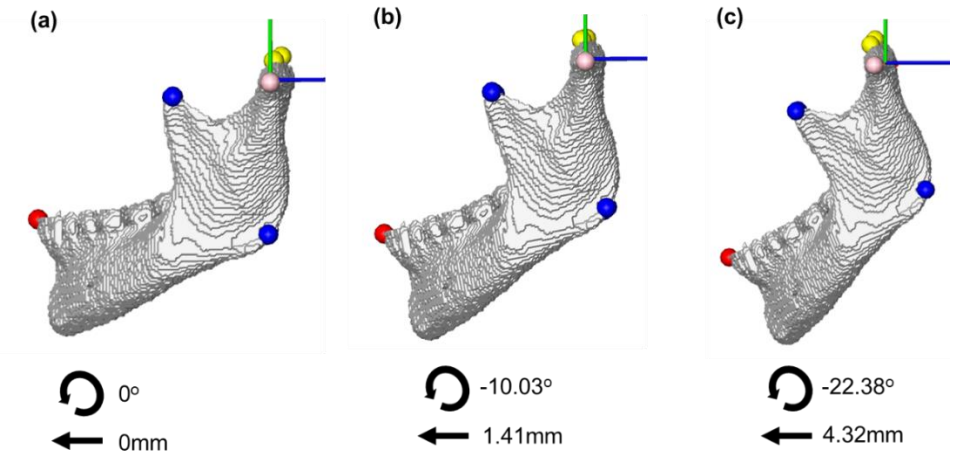

Figure 61. The application of the mandibular rotation and translation data of Baird (Unpublished) to the landmarks and the surface of the mandible following their alignment to the global X axis. (a) Lateral view of the mandible and landmarks aligned to the global X axis prior to translation and rotation. (b) The mandible and landmarks following their rotation and translation to produce a submaximal gape. (c) The mandible and landmarks following their rotation and translation to produce a maximal gape. See Figure 60 for a description of the landmark colour correspondences.

After this, the coordinates of the landmarks placed on the mandibular and maxillary central incisors (Figure 62) were used to calculate the interincisal distances that the applied condylar rotations and translations produced for this specimen (Table 22). The correspondence between the targeted and produced inter-incisal separation (Table 22) is indicative that the mandibular kinematic pathway used to re-locate the loading and boundary conditions of the model is feasible within biological reality.

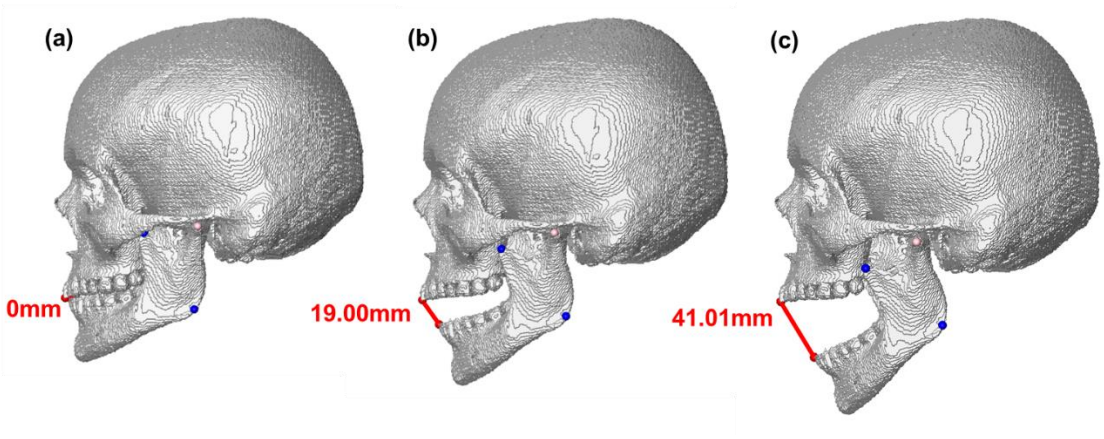

Figure 62. The unmodified *H. sapiens* crania, mandible, and mandibular landmarks following the inversion of the translation matrix used to align them to the global X axis. (a) Lateral view of the mandible, cranium, and landmarks in their original spatial position (included for comparison). (b) The position of the mandible and landmarks in relation to the cranium during a submaximal gape. (c) The position of the mandible and landmarks in relation to the cranium during a maximal gape. See figure 60 for a description of the landmark colour correspondences.

3.5.1.2. Altering the loading and boundary conditions of both FE models within Vox-Fe

The rotated and translated mandibular landmark sets were used to redefine the loading boundary and conditions of the unmodified and modified *H. sapiens* models in Vox-Fe to simulate bites at submaximal and maximal gapes. Firstly, the coordinates of the landmarks defining the end points of the jaw-elevator muscle force vectors were used to re-define the orientation of each vector (Figure 63) within Vox-Fe. The magnitudes applied to the force vectors are outlined in Table 15, which assumed 100% activation for each muscle and are the *f*Max estimates for the unmodified *H. sapiens* specimen. Although this is not a physiologically accurate muscle relative activation pattern for bites performed at different gapes, the sensitivity studies of this model (see section 2.5.1) and other *H. sapiens* cranial FE models demonstrate that loading models in this manner is a reasonable simplification in the absence of specimen specific relative activation data (Toro-Ibacache and O'Higgins 2016).

The new landmarks on the superior most points of the mandibular condyles were also imported into Vox-Fe to reposition the TMJ constraints on the unmodified *H. sapiens* model (Figure 63). The number of nodes selected at each joint for each simulation remained identical to previous simulations (175). As the form of the articular surfaces of the temporal bones

remained identical between both models, the spatial position of the TMJ constraints were altered for the modified FE model by copying the coordinates of the nodes selected as TMJ constraints for bites at both gapes from script files of the unmodified model and pasting them into script files detailing the other loading and boundary conditions applied to the modified model. This ensures that the results of the models would be comparable, as the *H. sapiens* model was sensitive to alterations in the spatial position of the TMJ constraints (see section 2.5.3.2). Thus, aside from the changes to the line of action of the masseter because of the changes to the zygoma region, both the unmodified and modified models simulating bites at submaximal or maximal gapes were loaded identically.

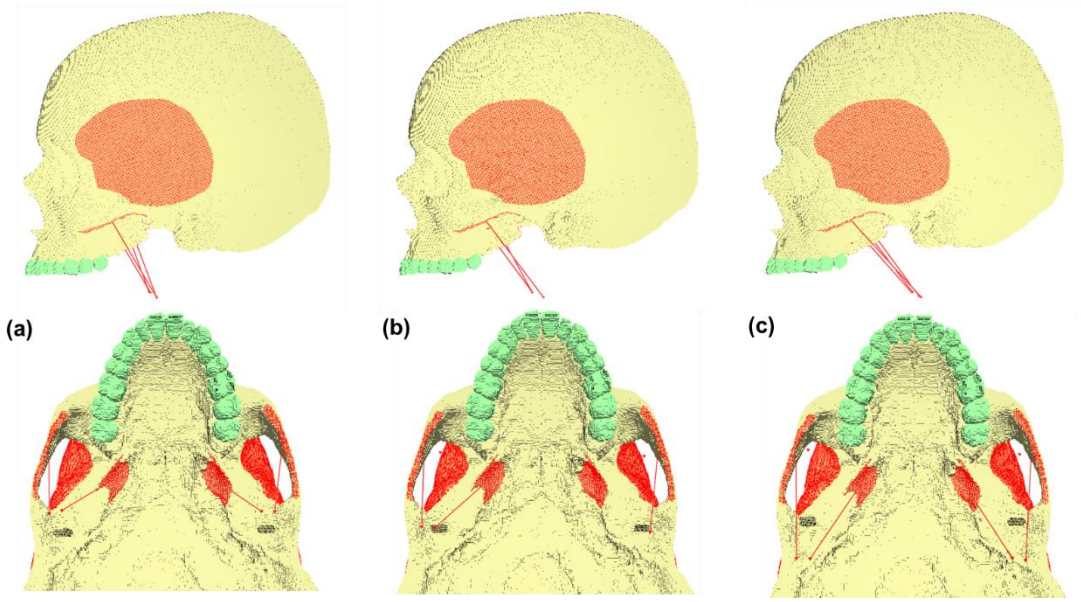

Figure 63. The constraints (black) and muscle force vectors (red lines) applied to *H. sapiens* FE model to simulate bites at different gapes. (a) Occluded bite. (b) Bite at a submaximal gape. (c) Bite at a maximal gape.

3.5.1.3. Model solution and Data analysis

Once the force vector orientations and TMJ constraints had been altered, script files simulating a I^1 and a LM^1 bite at submaximal and maximal gapes for both the unmodified and modified models were created and solved. The strain distribution, strain magnitude, bite force magnitude, joint reaction force magnitude and bite force efficiency predictions of each simulation are presented as outlined within section 3.4.1.2. The global distribution plots will again be scaled given bite force at the constrained tooth, allowing the strain predictions following the changes to the loading conditions of the models to be compared rather than

the indirect impacts that these changes may have upon strain magnitudes predicted by the models due to differences in bite force predictions as moving the positions of the TMJ constraints impacted the reaction forces predicted by the unmodified model considerably (see section 2.5.3.2). The deformations predicted by the models were scaled to represent a 500 N bite at the I^1s and an 800 N at the LM^1. Table 23 all the simulations performed to compare to performance of the unmodified and modified models during bites at submaximal and maximal gapes.

Table 23. The simulations ran (and a description of their loading and boundary conditions) to address H4 and H5.

Simulation Number	Model	Bite Point	Gape	Muscle Vector Magnitudes
9	Unmodified *H. sapiens*	I^1	Submaximal	Human muscle forces*
10	Unmodified *H. sapiens*	I^1	Maximal	Human muscle forces
11	Unmodified *H. sapiens*	LM^1	Submaximal	Human muscle forces
12	Unmodified *H. sapiens*	LM^1	Maximal	Human muscle forces
13	Modified *H. sapiens*	I^1	Submaximal	Human Muscle Forces
14	Modified *H. sapiens*	I^1	Maximal	Human Muscle Forces
15	Modified *H. sapiens*	LM^1	Submaximal	Human Muscle Forces
16	Modified *H. sapiens*	LM^1	Maximal	Human Muscle Forces

***Human muscle forces magnitudes can be found within Table 15.**

3.5.2. Objective Three results: bites at submaximal gapes

The results (reaction force predictions, bite force efficiencies, and strain predictions) of the modified and unmodified *H. sapiens* FE models during I^1 and LM^1 bites at submaximal gapes (simulations 9, 13, 11, and 15) are presented below.

3.5.2.1. Reaction force predictions and bite force efficiencies (H4)

For both the I^1 and the LM^1 bites at submaximal gapes, the modified model (simulations 13 and 15) predicted slightly higher bite force magnitudes, lower joint reaction forces and has higher bite force efficiencies than the unmodified model (Table 24) compared to the unmodified model (simulations 9 and 13). However, the bite force predictions for I^1 and LM^1 bites for both models at submaximal gapes are lower than predicted for the occluded bites, while the predictions of joint reaction force are higher (see section 3.3.2).

For the I^1 bites (simulations 9 and 13), the prediction of bite force for the modified model is only 5.93 N higher that the prediction of the unmodified model, equating to a negligible 0.02 increase in bite force efficiency between the models. The predictions of joint reaction force for the modified model are only slightly lower than for the unmodified model for the I^1 bite, with a 6.73 N lower reaction force occurring at the left joint and a 5.00 N decrease occurring at the right. For the LM^1 bites, the modified model predicted a bite force 8.29 N higher than the unmodified model, having a bite force efficiency 0.02 higher. The joint reaction force magnitudes predicted for both models are comparable at the working joint (left side), and there is a small decrease in magnitude predicted at the working side (4.81 N) for the modified model.

Table 24. Reaction force predictions and bite force efficiency of the modified and unmodified *H. sapiens* FE models during I^1 and LM^1 bites at submaximal gapes (simulations 9, 13, 11, and 15).

Simulation Number	Model	Bite point	Bite Force Magnitude (N)	Bite force efficiency	Left TMJ reaction force (N)	Right TMJ reaction force (N)
9	Unmodified	I^1	254.77	0.39	226.99	209.67
13	Modified	I^1	260.75	0.41	220.26	204.67
11	Unmodified	LM^1	375.15	0.58	116.82	226.11
15	Modified	LM^1	383.44	0.60	116.63	221.30

3.5.2.2. I^1 bites strain global and local strain distributions (H5)

Figure 64 visualises the global distributions of PS1 and PS3 for the unmodified (simulation 9) and modified (simulation 13) *H. sapiens* models simulating I^1 bites at submaximal gapes. The predictions of global strain distribution are mostly similar to distributions for an I^1 bite at occlusion for both models (see section 3.3.3.1 for a description of the differences between the models), however strains local to the TMJ were concentrated more anterior-inferiorly on the surfaces of the articular eminence for both models due to the translation of the constrained nodes, although magnitudes in this region were comparable between models. For the unmodified model, strain magnitudes are elevated at the zygomatic bodies, along the zygomaxillary suture and infraorbital margins, and at the zygomatic arches, compared to the I^1 bites at occlusion (Figure 64 and see section 3.3.3.1). For the modified model, there is a slight increase in strain magnitudes in the zygomatic arches and along the infraorbital rims while strain magnitudes in the zygomatic bodies and along the zygomaxillary suture remain

more comparable and increase less relative to this bites at occlusion that what is observed for the unmodified model (Figure 64 and see section 3.3.3.1).

Most of the differences between the predictions of the models when I^1 bites at submaximal gapes are simulated are again local to the zygoma (Figure 64 and Figure 65). Firstly, as previously identified (see section 3.3.3.1) strains in the postorbital regions are lower for the modified model (e.g. at region 4 the modified model predicted 358.59με and -136.89με compared to 548.19με and -193.84με for the unmodified model). For the modified model, PS3 magnitudes are still higher at the zygomatic bodies (e.g. at region 14 the modified model predicted -75.72με compared to -60.49με), however the differences in strain magnitudes predicted at these between the models is smaller compared to simulations of I^1 bites at occlusion (Figure 65 and see section 3.3.3.1). This is also apparent at the zygomatic arches where PS3 magnitudes are comparable between the modified and unmodified models (Figure 65) when previously the modified model had predicted higher magnitudes (see section 3.3.3.1), and again strains are more widely distributed along the structure in the modified model (Figure 64).

For both models, globally there is a reduction in compressive strains in the interorbital and glabella region is apparent between the bites at submaximal gape, while strains increase in the neurocranium in the squamous temporal immediately superior to the glenoid fossae and at the sphenoid bone, compared to the bites at occlusion (Figure 64 and see section 3.3.3.1). While strain magnitudes in the interorbital and glabella regions are consistent between the models for I^1 bites at a submaximal gape (Figure 64), as identified previously strain magnitudes in the neurocranium for the modified model are lower (see section 3.3.3.1). In all other regions strain magnitudes are comparable between the models (Figure 64 and Figure 65).

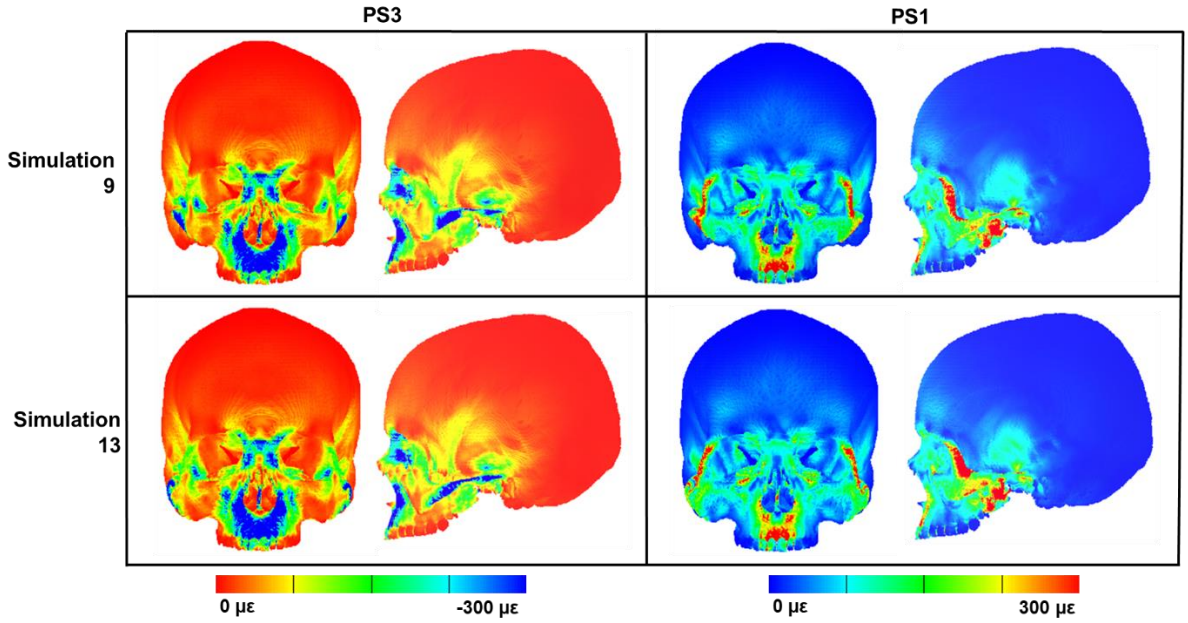

Figure 64. Global PS1 and PS3 strain distributions during I^1 bites at a submaximal gape for the unmodified (simulation 9) and modified models (simulation 13), scaled to a 500 N bite.

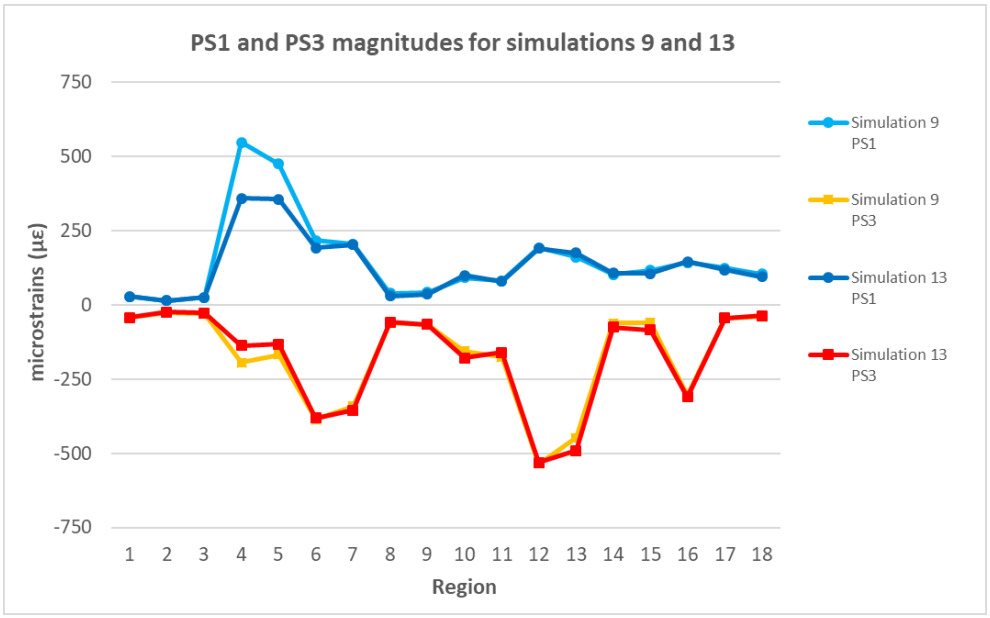

Figure 65. Average PS1 and PS3 magnitudes during I^1 bites at a submaximal gape for the unmodified (simulation 9) and modified models (simulation 13), scaled to a 500 N bite. See sections 3.3.1.6 for a description and visualisation of the numbered regions.

3.5.2.3. LM^1 bites strain global and local strain distributions (H5)

Figure 66 visualises the global distributions of PS1 and PS3 for the unmodified (simulation 11) and modified (simulation 15) *H. sapiens* models simulating LM^1 bites at submaximal gapes. Overall, the pattern of strain for both models is as expected for an LM^1 bite (see section

3.3.3.2 for a description of the difference between the models), except for locally to the TMJ were strains were focused more anterior-inferiorly on the surfaces of the articular eminence for both models, although comparable magnitudes in this region were predicted for both models. For the modified model, strain magnitudes are again increased at the zygomatic bodies, along the zygomaxillary suture and infraorbital margins, and at the zygomatic arches, compared to the LM^1 bites at occlusion (Figure 66 and see section 3.3.3.2). For the modified model, while strain magnitudes have increased along both infraorbital margins and in the zygomatic body on the working side of the face, on the balancing side strain magnitudes decrease in regions including the zygomatic process of the maxilla and the zygomatic bodies, relative to LM^1 bites at occlusion (Figure 66 and see section 3.3.3.2).

Many of the differences between the predictions of the models for LM^1 bites at submaximal gapes are local to the zygoma (Figure 66 and Figure 67). Interestingly at the zygomatic bodies, while PS3 magnitudes are still marginally higher for the modified model (e.g. at region 15 the modified model predicted -100.96με compared to -82.18με), PS1 magnitudes are now lower (e.g. at region 15 the modified model predicted 120.07με compared to 143.68με). In line with previous predictions (see section 3.3.3.2), strain magnitudes in the postorbital regions are lower for the modified model compared to the modified model (e.g. at region 5 the modified model predicted 354.81με and -132.21με compared to 460.67με and -163.70με for the unmodified model). This is also apparent at the zygomatic arches where the modified model predicted lower or comparable PS1 and PS3 values compared to the unmodified model (e.g. at region 6 the modified model predicted 205.74 and -405.18 compared to 235.71 and -425.36); strains are more widely distributed along the structure in the modified model as seen for other loading scenarios (see section 3.3.3.2).

Globally, compared to the bites at occlusion (see section 3.3.3.2), there is again a reduction in compressive strains in the interorbital and glabella region is apparent between the bites at submaximal gape for both models, while strains increase in the neurocranium superior to the working glenoid fossae (Figure 66). As identified previously, strain magnitudes in the neurocranium for the modified model are lower (Figure 66 and see section 3.3.3.2), while strain magnitudes in the interorbital and glabella regions are consistent between the models

for LM[1] bites at a submaximal gape (Figure 66). In all other regions strain magnitudes are comparable between the models (Figure 66 and Figure 67).

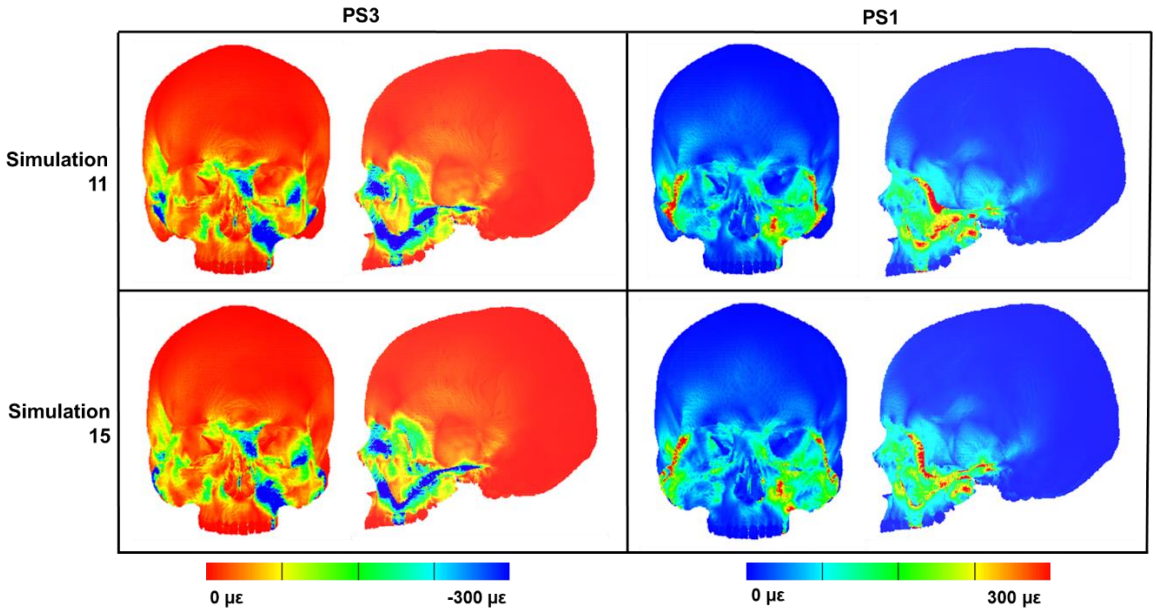

Figure 66. Global PS1 and PS3 strain distributions during LM[1] bites at a submaximal gape for the unmodified (simulation 11) and modified models (simulation 15), scaled to an 800 N bite.

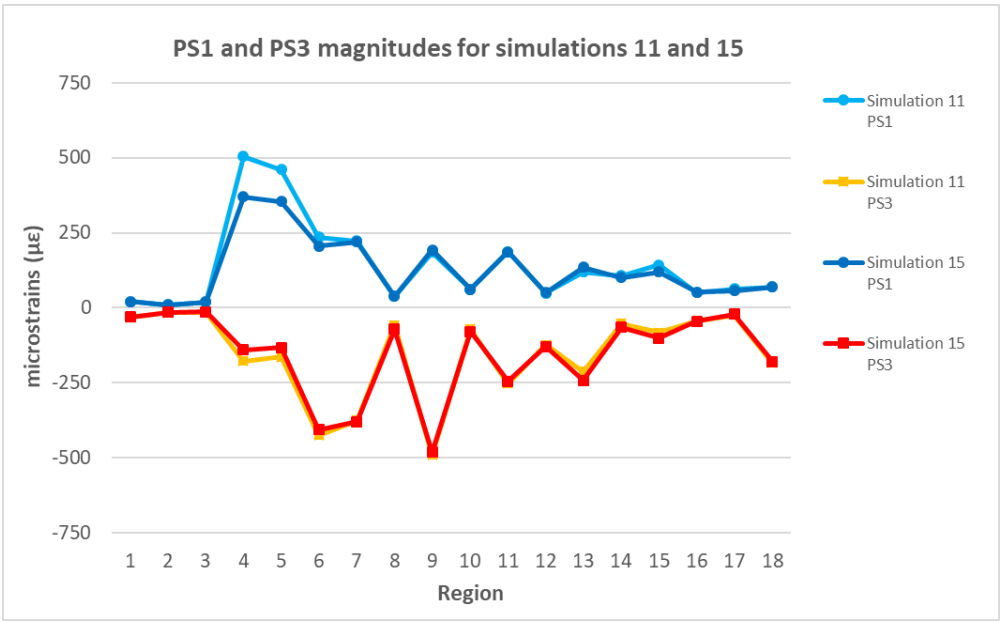

Figure 67. Average PS1 and PS3 magnitudes during LM1[1] bites at a submaximal gape for the unmodified (simulation 11) and modified models (simulation 15), scaled to an 800 N bite.

3.5.3. Objective Three results: bites at maximal gapes

The results (reaction force predictions, bite force efficiencies, and strain predictions) of the modified and unmodified *H. sapiens* FE models during I^1 and LM^1 bites at maximal gapes (simulations 10, 14, 12, and 16) are presented below.

3.5.3.1. Reaction force predictions and bite force efficiencies (H4)

For both the I^1 and the LM^1 bites at maximal gapes, the modified model again (simulations 14 and 16) predicted slightly higher bite force magnitudes, mostly lower joint reaction forces and has higher bite force efficiencies than the unmodified model (Table 25) compared to the unmodified model (simulations 10 and 12). However, the bite force predictions for I^1 and LM^1 bites for both models at maximal gapes are lower than predicted for the bites at submaximal gapes and occluded bites, while the predictions of joint reaction force are higher than these loading scenarios (see section 3.3.2 and 3.5.2.1).

For the I^1 bites (simulations 10 and 14), the prediction of bite force for the modified model is 6.87 N higher that the prediction of the unmodified model, again equating to a negligible 0.02 increase in bite force efficiency between the models. Interestingly, the modified model predicted an 8.09 N increase in left joint reaction force and a 19.14 N decrease in reaction force magnitude at the contralateral joint. For the LM^1 bites, the modified model predicted a bite force 9.72 N higher than the unmodified model, with a negligible increase in bite force efficiency of 0.02. The joint reaction force magnitudes predicted by the modified model are marginally lower at both the working and balancing joints (a decrease of 1.42 N at the left joint and 3.99 N decrease at the right).

Table 25. Reaction force predictions and bite force efficiency of the modified and unmodified *H. sapiens* FE models during I^1 and LM^1 bites at maximal gapes (simulations 10, 14, 12, and 16).

Simulation Number	Model	Bite point	Bite Force Magnitude (N)	Bite force efficiency	Left TMJ reaction force (N)	Right TMJ reaction force (N)
10	Unmodified	I^1	223.88	0.34	221.33	236.38
14	Modified	I^1	230.75	0.36	229.42	217.24
12	Unmodified	LM^1	337.12	0.52	143.11	239.05

16	Modified	LM^1	346.84	0.54	141.69	235.09

3.5.3.2. I^1 bites global and local strain distributions (H5)

Figure 68 visualises the global distributions of PS1 and PS3 for the unmodified (simulation 10) and modified (simulation 14) *H. sapiens* models simulating I^1 bites at maximal gapes. The predictions of global strain distribution are mostly similar to distributions for an I^1 bite for both models (see section 3.3.3.1 for a description of the difference between the models), aside from locally to the TMJ where strains were instead concentrated towards the limits of the articular eminence and onto the preglenoid plane due to the anterior translation of the constraints, however both models predicted similar strain magnitudes in this region. For the unmodified model, strain magnitudes at the zygomatic bodies increase further, as do magnitudes along the zygomaxillary suture and infraorbital margins, and at the zygomatic arches, compared to the I^1 bites at occlusion and submaximal gapes (Figure 68 and see sections 3.3.3.1 and 3.5.2.2). For the modified model, compared to the I^1 bites at occlusion and submaximal gapes, there is a further increase in strain magnitudes in these regions but to a lesser degree than what is apparent for the unmodified model (Figure 68 and see sections 3.3.3.1 and 3.5.2.2).

Many of the differences between the predictions of the models when I^1 bites at maximal gapes are localised to the zygoma (Figure 68 and Figure 69). Strain magnitudes at the zygomatic bodies of the modified model are reduced or comparable to those predicted by the unmodified model (e.g. at region 14 the modified model predicted magnitudes of 109.63με and -81.16με compared to 135.12με and -68.29με predicted by the unmodified model), while in previous simulated loading scenarios magnitudes have always been higher (see sections 3.3.3.1 and 3.5.2.2). The strain magnitudes at the zygomatic arches also follow this trend, where the modified model predicted lower or comparable values to the unmodified model (e.g. at region 7 the modified model predicted 214.14με and -431.16με compared to 243.51με and -434.96με), while appearing more widely distributed along the structure (as has been previously identified for other loading scenarios; Figure 68, and see sections 3.3.3.1 and 3.5.2.2). As previously identified, strain magnitudes in the postorbital regions are lower for

the modified model (e.g. at region 5 the modified model predicted 364.01με and -133.77με compared to 469.39με and -166.68με for the unmodified model).

For both models, globally there is again a reduction in compressive strains in the interorbital and glabella region between the bites at occlusion and a submaximal gape, while strains further increase in the neurocranium immediately superior to the glenoid fossae (Figure 68 and see sections 3.3.3.1 and 3.5.2.2). As seen for the I^1 bites at submaximal gapes and at occlusion (Figure 68 and see sections 3.3.3.1 and 3.5.2.2), strain magnitudes in the neurocranium for the modified model are lower. In all other regions strain magnitudes are comparable between the models (Figure 68 and Figure 69).

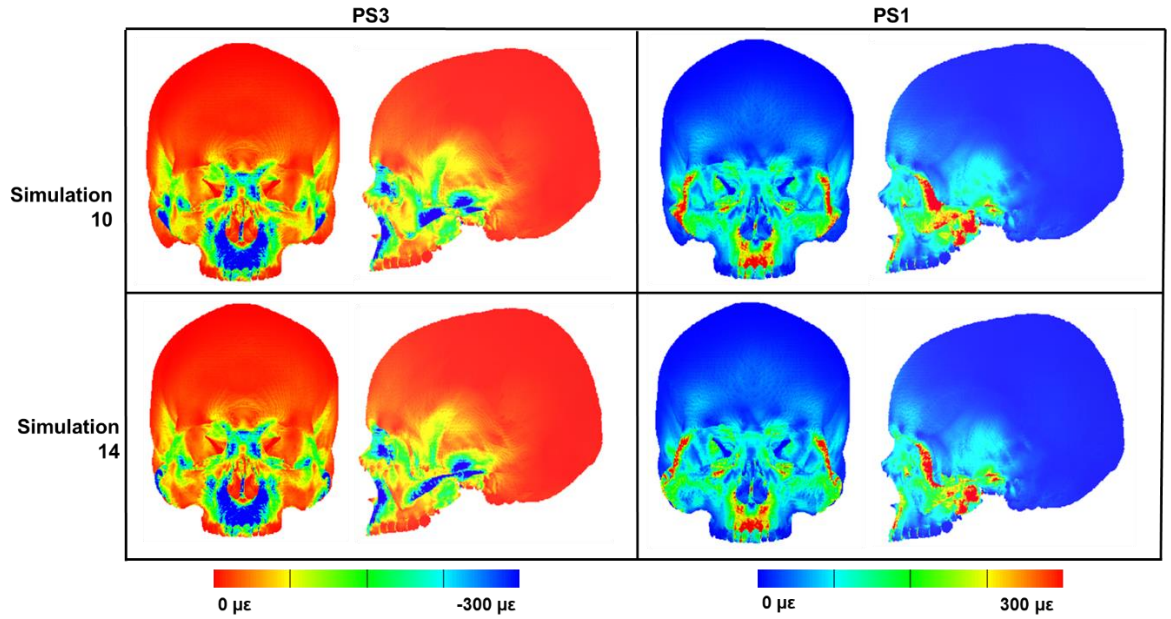

Figure 68. Global PS1 and PS3 strain distributions during I^1 bites at a maximal gape for the unmodified (simulation 10) and modified models (simulation 14), scaled to a 500 N bite.

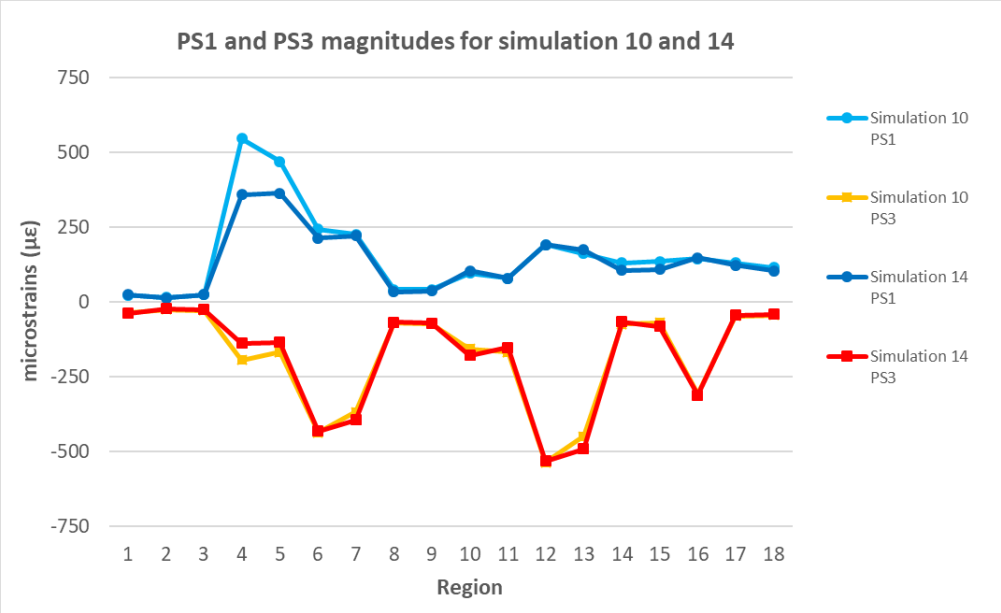

Figure 69. Average PS1 and PS3 magnitudes during I^1 bites at a maximal gape for the unmodified (simulation 10) and modified models (simulation 14), scaled to a 500 N bite. See sections 3.3.1.6 for a description and visualisation of the numbered regions.

3.5.3.3. LM^1 bites global and local strain distributions (H5)

Figure 70 visualises the global distributions of PS1 and PS3 for the unmodified (simulation 12) and modified (simulation 16) *H. sapiens* models simulating LM^1 bites at maximal gapes. The overall distribution of strains predicted by both models is as expected for an LM^1 bite (see section 3.3.3.2 for a description of the difference between the models), except for locally to the TMJ where strains were focused towards the anterior limits of the articular eminence and onto the preglenoid plane, despite this both models predicted comparable strain magnitudes in this region. For the unmodified model, relative to the LM^1 bites at occlusion and submaximal gapes (see sections 3.3.3.2 and 3.5.2.3), strain magnitudes are further increased at the zygomatic bodies, along the zygomaxillary suture and infraorbital margins, and at the zygomatic arches (Figure 70). For the modified model, compared to the bites at occlusion and submaximal gapes (see sections 3.3.3.2 and 3.5.2.3), while strain magnitudes have further increased along both infraorbital margins and in the working zygomatic body, on the balancing side of the face strain magnitudes have further decreased in regions including the zygomatic process of the maxilla and the zygomatic bodies (Figure 70).

As identified previously, most of the differences between the predictions of the models for LM^1 bites at maximal gapes are local to the zygoma (Figure 70 and Figure 71). In line with previous predictions (see section 3.3.3.2), strain magnitudes in the postorbital regions are lower for the modified model compared to the modified model (e.g. at region 4 the modified model predicted 360.14με and -136.31με compared to 489.19με and -172.49με for the unmodified model); strain magnitudes at the zygomatic arches for the modified model are now lower or comparable to those of the unmodified model (e.g. at region 7 the modified model predicted 233.87με and -411.35με compared to 243.11με and -402.75με), and again strains are more widely distributed along the structure in the modified model as seen for other loading scenarios (see section 3.3.3.2 and 3.5.2.3). The modified model predicts lower strain magnitudes at the zygomatic bodies, particularly for PS1 (e.g. at region 14 the modified model predicted magnitudes of 96.48με and -53.90με compared to 134.15με and -63.56με).

Globally, compared to the bites at occlusion and at submaximal gape (see sections 3.3.3.2 and 3.5.2.3), there is again a reduction in compressive strains in the interorbital and glabella region is apparent between the bites at submaximal gape and occlusion for both models, however the modified model predicts slightly higher magnitudes in these regions relative to the modified model when bites at maximal gape are simulated (Figure 70). While strains increase in the neurocranium superior to the working glenoid fossae for both models relative to bites at occlusion and at a submaximal gape, strain magnitudes in the neurocranium for the modified model are lower as has been identified in previous loading scenarios (Figure 70 and see sections 3.3.3.2 and 3.5.2.3). In all other regions strain magnitudes are comparable between the models (Figure 70 and Figure 71).

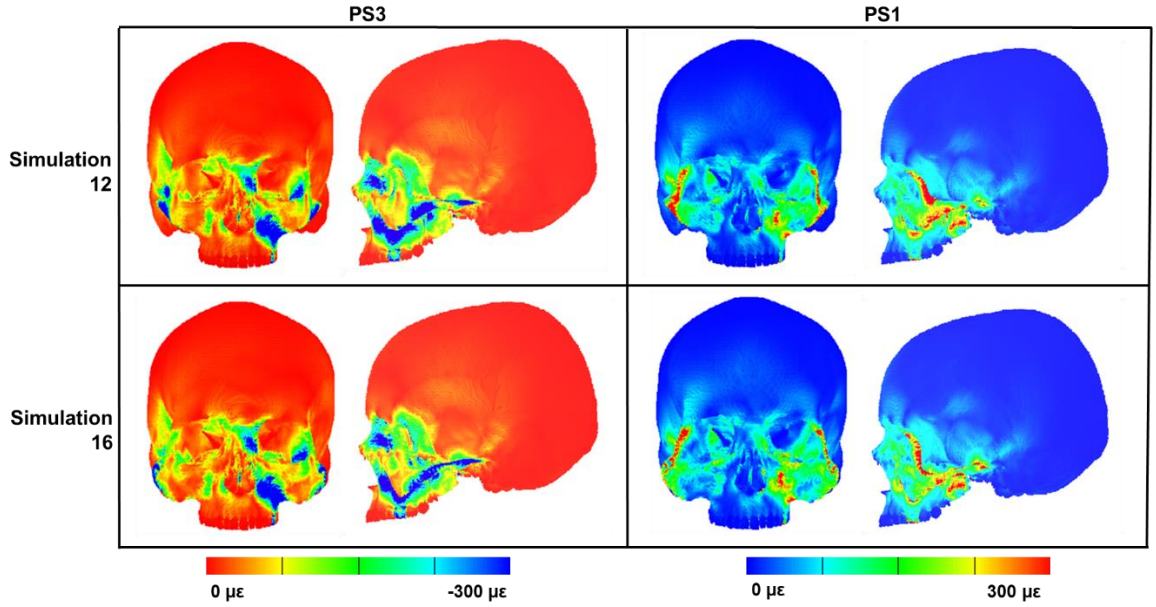

Figure 70. Global PS1 and PS3 strain distributions during LM[1] bites at a maximal gape for the unmodified (simulation 12) and modified models (simulation 16), scaled to an 800 N bite.

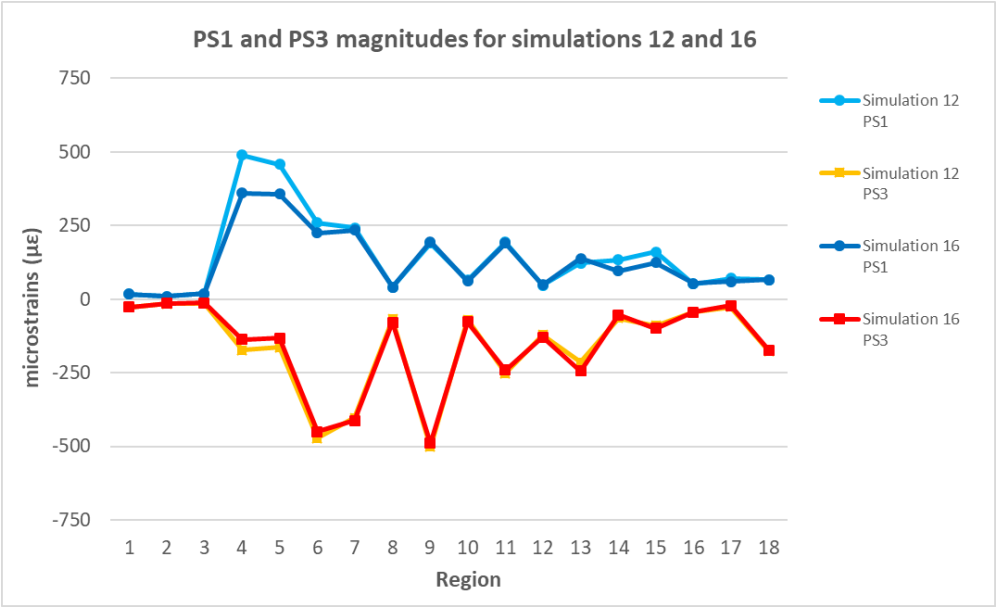

Figure 71. Average PS1 and PS3 magnitudes during LM1[1] bites at a maximal gape for the unmodified (simulation 12) and modified models (simulation 16), scaled to an 800 N bite.

3.6. Discussion of the experimental FEA results

This chapter has reported how modifying the geometry of a *Homo sapiens* FE model to contain *Homo ergaster-like* zygoma region morphology impacts predictions of strain distribution and bite force under different masticatory loads, including anterior and posterior bites (chapter objective one), loading both models with *H. ergaster*-like masseter muscle forces (chapter objective two), and bites at submaximal and maximal gapes (chapter objective three). Accordingly, this required a wide range of loading scenarios to be simulated, generating a wealth of interesting results that have been reported in detail in sections 3.3.2, 3.3.3, 3.4.2, 3.4.3, 3.5.2, and 3.5.3. The major findings pertaining to the hypotheses of this chapter have been synthesized within Table 26 and the discussion following this synthesis will consider the implications of the results of this chapter, assessing whether they provide support for the five hypotheses of the chapter.

3.6.1. Synthesis of key findings

The following table (Table 26) synthesises the most important results relating to the hypotheses of this chapter outlined within section 3.2. These results were previously presented in sections 3.3.2, 3.3.3, 3.4.2, 3.4.3, 3.5.2, and 3.5.3.

Table 26. Synthesis of the most important results relevant to the five hypotheses of the chapter originally outlined in section 3.2. The results are presented in full in sections 3.3.2 (chapter objective one; findings relevant for H1), 3.3.3 (chapter objective one; findings relevant for H2), 3.4.2 (chapter objective two; findings relevant for H3), 3.4.3 (chapter objective two; findings relevant for H3), 3.5.2 (chapter objective three; findings relevant for H4 and H5), and 3.5.3 (chapter objective three; findings relevant for H4 and H5).

Hypothesis	Key Findings
H1: A Homo sapiens cranium with Homo ergaster-like zygoma regions will increase the mechanical advantage of the masseter and subsequently increase bite forces during anterior and posterior bites	• Both models had a similar bite force efficiency for a I^1 bite. • The modified model had a higher efficiency than the unmodified model for a LM^1 bite.
	• The modified model predicted slightly higher bite force magnitudes than the unmodified model for both bites.
H2: A Homo sapiens cranium with Homo ergaster-like zygoma regions will result in decreased craniofacial strain magnitudes (local to the	• Global strain magnitudes were comparable in most regions for both bites for both models.
	• The modified model did not predict consistently lower strain magnitudes locally to the zygoma region for both bites.

zygoma region and globally) during anterior and posterior bites	• While varying between I^1 and LM^1 bites, local strain magnitudes increased in some regions and decrease in others.
H3: A Homo sapiens cranium with Homo ergaster-like zygoma regions and Homo ergaster-like masseter muscle force magnitudes will further increase bite force, which will increase craniofacial strain magnitudes globally, but lower strains are still predicted locally to the zygoma region	• The modified model predicted higher bite forces than the unmodified model for both bites.
	• Global strain magnitudes were elevated for both models for both bites particularly in regions close to the bite reaction force. • Magnitudes were consistently higher for the modified model in these regions.
	• The modified model predicted higher strain magnitudes than the unmodified model in most regions local to the zygoma, particularly in regions proximate to the bite reaction force and insertion of the masseter.
H4: A Homo sapiens cranium with Homo ergaster-like zygoma regions will increase bite forces during anterior and posterior bites at submaximal and maximal gapes	• For both bites at a submaximal gape the modified model predicted higher bite forces. • The bite forces predicted by both models for both bites were lower than bites at occlusion.
	• For the bites at a maximal gape the modified model predicted higher bite forces. • The bite forces predicted by both models for both bites were lower than bites at a submaximal gape and occlusion.
H5: Global craniofacial and local zygoma strain magnitudes will be relatively lower during bites at maximal gapes and submaximal gapes in the Homo sapiens cranium with Homo ergaster-like zygoma regions compared to the unmodified Homo sapiens cranium	• The modified model did not consistently predict lower global strain magnitudes than the unmodified model during bites at larger gapes. • Magnitudes were higher in some regions and lower in others depending on the bite simulated.
	• Locally to the zygoma, strain magnitudes increased with gape for both models. • Comparatively less of an increase occurred for the modified model for I^1 bites. • Strains decreased as gape increased from submaximal to maximal for the modified model for LM^1 bites, while magnitudes increased for the unmodified model.

3.6.2. Objective One: The impacts of modifying the zygoma region of the *Homo sapiens* FE model to resemble the zygoma region of *Homo ergaster* on craniofacial strains and bite force production

The large, robust and projecting zygoma region morphology of early *Homo* is suggested to be a product of both selective pressures maintaining features advantageous for withstanding and producing high bite forces, and the increased craniofacial modelling that would consequently occur due to the consumption of a mechanically challenging diet prior to the habitual use of complex food processing technologies (Demes and Creel 1988; Lieberman et al. 2004; Lieberman 2008, 2011; Ledogar et al. 2016a; Zink and Lieberman 2016). As such, it was predicted that modifying the zygoma region of the *Homo sapiens* FE model to resemble the zygoma region of *Homo ergaster* would increase bite force predictions while reducing craniofacial strains during masticatory loading.

However, the differences between the reaction force predictions of the modified model and the predictions of the unmodified model were only marginal. For the incisor bites there was a negligible increase in bite force efficiency, however for the molar bites there was a more noticeable increase despite bite force only increasing marginally. As the modifications to the model included an anterior movement of the origin of the masseter, this is likely responsible for the increase in bite force and bite force efficiency for both bites. These results are consistent with the results of other researchers investigating the impacts of changes to the zygoma region morphology of hominin fossils (Ledogar et al. 2017). Taken together, these results could suggest that a more anteriorly positioned masseter origin within *H. sapiens* facilitates the production of higher bite forces, as has been suggested by other researchers (e.g. Noback and Harvati 2015a, 2015b). Considering that *H. ergaster* has more pronounced subnasal prognathism than *H. sapiens* (Norman 1999; Spoor et al. 2005; Lesciotto et al. 2016), which decreases the mechanical advantage of the jaw elevator muscles (Ledogar et al. 2016a; Godinho et al. 2018), the more anteriorly positioned masseter origin could alternatively be an adaptation to maintaining bite forces on the anterior dentition. These results therefore indicate that the *H. ergaster* zygoma region morphology was not specialised to produce high anterior bite forces. Similar interpretations have been made regarding the zygoma region morphology of the Neanderthals (O'Connor et al 2005; Wroe et al. 2018).

Contrary to predictions, strains local to the zygoma were not uniformly lower during either biting scenario for the modified model, and globally strain magnitudes varied little between models. For both bites, strains were higher in the zygomatic bodies, and were either comparable in magnitude to the unmodified model, or were higher in other regions local to the zygoma. These results therefore indicate that the large and projecting zygoma region of *H. ergaster* is not directly associated with reducing craniofacial strains during masticatory loads, opposing common suggestions within paleoanthropological literature (Demes and Creel 1988; Lieberman et al. 2004; Lieberman 2008, 2011; Ledogar et al. 2016a; Zink and Lieberman 2016).

Many researchers have emphasised the importance of the zygomatic root in reinforcing the hominin facial skeleton against masticatory forces (Rak 1983; Demes 1987; Ledogar et al. 2017). The more angular profile of the zygomatic root in the modified model could explain the increase in strains reported for the modified model in regions such as the zygomatic processes of the maxilla. Similarly to this thesis, Ledogar et al. (2017) demonstrated that gracile australopithecine FE models with more curved zygomatic roots predict higher strain magnitudes locally to the zygoma compared to models with straight and steep roots. Thus, the shape differences between the zygomatic roots of the two models within this thesis could explain why the modified model predicted higher strain magnitudes in some regions local to the zygoma. This indicates the presence of more curved zygomatic roots increases strains in the zygomatic region within the facial skeleton of members of the genus *Homo*. Consequently, this may have selected for other craniofacial adaptations, and on a plastic level increased bone formation, in order to reduce elevated strains potentially explaining the present of features such as the taller facial skeleton and flat infraorbital profile of *H. ergaster* (Lieberman 2008, 2011). Consistent with the suggestions of Ledogar et al. (2017, 2022) in regards to the evolution of the facial skeleton within the australopithecines, this points towards the importance of mechanical compensations in the evolution and development of craniofacial form within *H. ergaster*, being the selection for and plastic development of strain-reducing traits as a consequence of adaptations that increase bite force production, but simultaneously increase craniofacial strain.

Previous researchers have reported that modifying the cross sectional shape of the zygomatic arch has minimal impacts on global strain distributions (Smith and Grosse 2016). In this thesis, where the lateral position of the zygomatic arch in relation to the cranium differed between models, appreciable differences in strain predictions local to the zygoma were apparent. In addition to the changes to strain in the zygomatic bodies, the zygomatic arches of the modified models also showed a different strain distribution pattern and slightly higher strain magnitudes relative to the unmodified. These differences may reflect the combined impacts of factors including changes to the lateral positioning of the zygomatic arches, increasing its length, and the alterations to the orientation of the masseter force vector. The result of this thesis therefore indicate that changes to the spatial position of the zygomatic arch in relation to the cranium, and the impacts this has upon the masseter force vector, have a considerable impact on the response of the cranium to masticatory load. This may be more impactful on craniofacial strains than changes to the cross-sectional shape of this structure.

It has been suggested that the width of the upper facial skeleton and the frontal process of the zygoma is important in resisting the inferior pull of the masseter on a laterally positioned zygomatic arch within australopithecines (Rak 1983; Rak and Marom 2017). Interestingly, the modified model predicted lower strains in the these regions compared to the unmodified model. This could suggest that the increased lateral projection of the upper facial skeleton within *H. ergaster* and more anterolaterally oriented frontal process (Antón and Middleton 2023), may also be an adaptation to reinforce the facial skeleton against the contraction of the masseter on a laterally flaring zygomatic arch.

Thus, while global differences between the models were minimal, modifying the zygoma region of the *H. sapiens* model to resemble *H. ergaster* did not consistently decrease strains locally to the zygoma region for either anterior or posterior bite. As the zygoma region was altered in isolation, other anatomical features of *H. ergaster* may be more influential in reducing craniofacial strain under masticatory load than increasing the width and height of the zygomatic region. Therefore, these results provide support for H1: "*A H. sapiens cranium with H. ergaster-like zygoma regions will increase the mechanical advantage of the masseter and subsequently increase bite forces during anterior and posterior bites*". This is because

while the impact was minimal, bite force did increase for both incisor and molar bites. However, these results do not provide evidence to either support or reject H2: "*A H. sapiens cranium with H. ergaster-like zygoma regions will result in decreased craniofacial strain magnitudes locally to the zygoma region and globally during anterior and posterior bites*". This is because during both bites, the differences in global craniofacial strains between the models were minimal, while strain magnitudes local to the zygoma increased in some areas and decreased in others.

3.6.3. Objective Two: the impacts of increasing masseter force magnitude on craniofacial strain and reaction force predictions

Previous researchers have emphasised the selective importance of producing high bite forces in shaping the form of the hominin craniofacial skeleton, both through the need to maintain jaw-elevator musculature with large cross-sectional areas and the need to resist the increase in strain associated with larger bite forces and more powerful muscles (Demes and Creel 1988; Lieberman 2008, 2011; Eng et al. 2013). It has previously been demonstrated that *Homo ergaster* may have had a more forceful masseter than *Homo sapiens* (Demes and Creel 1988; Eng et al. 2013), therefore the zygoma region of this species should be better adapted to resisting this increased masseter force and the accompanying increased bite force a larger masseter may produce. Thus, it was predicted that the *H. sapiens* FE model with the *H. ergaster*-like zygoma regions loaded with *H. ergaster*-like masseter muscle forces should predict lower strain magnitudes locally to the zygoma region, while strain magnitudes globally in regions shown to be more robust in *H. ergaster* were predicted to be elevated as a consequence of an increase in predicted bite force.

As predicted, increasing the magnitude of force applied to the masseter increased the reaction force predictions of both the unmodified and modified models, while the modified model predicted higher bite forces than the unmodified model for both molar and incisive bites. Interestingly, the modified model predicted a substantially higher bite force for the molar bite compared to the unmodified model. These results support that the laterally flaring zygoma region, which facilitates the larger masseter, combined with a more anteriorly

positioned masseter origin could reflect adaptations to maintaining high bite forces in *H. ergaster* generally. Indeed, this combination of features may be an adaptation to maintaining bite forces on the anterior dentition owing to the more pronounced subnasal prognathism of *H. ergaster* compared to *H. sapiens* (Norman 1999; Spoor et al. 2005; Lesciotto et al. 2016). The more apparent increase in molar bite force when the magnitude of force applied to the masseter was increased could supports findings that for *H. ergaster*, high posterior bite forces were produced primarily through possessing larger jaw-elevator muscles rather than increasing their mechanical efficiency (Eng et al. 2013). This is suggestive that bony morphologies that increase the CSA of the masseter, like the width of the zygoma region, may have been adaptively important in generating high bite forces on the posterior dentition in early member of the genus *Homo*, as has been suggested for earlier hominin species (Demes and Creel 1988).

While these results indicate that the wide zygoma region within *H. ergaster* may represent an adaptation to increasing bite forces by facilitating a larger masseter, the craniofacial skeleton of this species equally needed to be adapted to resisting this increased bite and muscle force. It has been suggested that the large zygoma region of *H. ergaster* could be an adaptation to resisting increased masticatory strains (Lieberman 2008, 2011). However, strains were elevated in zygoma region for the modified model compared to the unmodified model for both bites. These results are indicative that although the zygoma region morphology of *H. ergaster* may increase bite force magnitudes via increasing the anterior positioning of the origin of the masseter and increasing its CSA, this morphology is not simultaneously an adaptation to resist increased strains associated with having a larger masseter muscle and the increase in bite force associated with this. Similar conclusions have been reach surrounding adaptations to increase bite force in the australopithecine face (Ledogar et al. 2017, 2022). Consequently, other anatomical features of *H. ergaster*, such as the superior-inferior height of the facial skeleton and the flat infraorbital profile, may be more influential in reducing craniofacial strains under masticatory load. Such features may have been selected for, and developed plastically due to the increased strains in the midfacial skeleton. This is indicative that mechanical compensations were important in the evolution of craniofacial form within *H. ergaster.*

The zygomatic root is frequently described as an important feature in reinforcing the facial skeleton against masticatory forces, including resisting the contraction of the masseter (Rak 1983; Demes 1987; Ledogar et al. 2017). As mentioned, the modified model predicted higher strain magnitudes in many regions locally to the zygoma, particularly around the zygomatic roots and other nearby structures including the zygomatic process of the maxilla and infraorbital regions. Ledogar et al. (2017) reported that when the zygomatic roots of gracile australopithecine FE models were moved more anteriorly and bite force increased consequently, strains in these regions local to the zygoma region also increased. Thus, the increase in strain in these regions predicted by the unmodified model could be a consequence of the absolute increase in bite force.

Equally, the shape differences between the zygomatic roots of the unmodified and modified models could also explain this increase in strain in these regions. Ledogar et al. (2017) reported that increasing the curvature of the zygomatic root caused higher strains to be predicted in the previously mentioned regions for gracile australopithecine FE models. The results of this thesis are consistent with this, demonstrating that a more curved zygomatic root provides poorer resistance to higher masseter and bite reaction forces, as previously argued by researchers including (Rak 1983; Demes 1987). Thus, both the increase in bite force and more curved zygomatic roots could explain the increased strains in many regions local to the zygoma predicted by the modified model loaded with *H. ergaster*-like masseter forces; these elevated strains may have necessitated the selection for and plastic development of features seen in *H. ergaster* like a taller facial skeleton and flatter infraorbital region. These results therefore emphasise the importance of the form of the zygomatic roots in not only producing bite forces, but also resisting the contractile force of the masseter and transmitting bite reaction forces through the facial skeleton.

The width of the upper facial skeleton is also suggested to be important in resisting the inferior pull of the masseter on a laterally positioned zygomatic arch, particularly when the forces of this is muscle is increased owing to this lateral flare (Rak 1983; Rak and Marom

2017). Again, the postorbital regions and frontal processes of the zygoma were some of the only regions local to the zygoma where the modified model predicted lower strains than the unmodified model when loaded with *H. ergaster*-like masseter forces. This indicates that increased width of the upper face of *H. ergaster* in relation to *H. sapiens* may be an adaptation to reinforce the facial skeleton against the contraction of a more forceful masseter on a laterally flaring zygomatic arch, itself a bony adaptation that facilitates increased masseter force. Similar interpretations have been made regarding the upper facial morphology of the robust australopithecines (Rak 1983; Rak and Marom 2017).

One region of the craniofacial skeleton within *H. ergaster* (and other fossil hominins) that is considerably more robust than *H. sapiens* is the supraorbital region (Athreya 2009, 2012). Interestingly, the global areas most affected for both models by increasing the force applied to the masseter were the supraorbital, glabella and interorbital regions, where strain magnitudes were elevated for both models compared to previous simulations loaded with human muscle force estimates. For the incisor bites, strain magnitudes in these regions were higher for the modified model, whereas during the molar bites strain magnitudes in these regions were higher for the unmodified model. These results could suggest that anterior bites combined with a forceful masseter may have contributed to the increased supraorbital and glabella robusticity in fossil hominin species. As strain magnitudes in these regions also increased in the unmodified model when the force applied to the masseter increased, the more pronounced supraorbital robusticity in *H. sapiens* populations that consume mechanically demanding diets could therefore also partially be a product of having a more forceful masseter. Therefore, in line with the suggestions of many researchers (such as: Endo 1970; Oyen et al. 1979; Russell et al. 1985; Endo and Adachi 1988; Hilloowala and Trent 1988; Baab et al. 2010), having a larger and more forceful masseter may contribute towards increased supraorbital robusticity in modern humans and other hominins. These findings are contrary to researchers that are critical of connections between masticatory loading and supraorbital robusticity (such as: Hylander et al. 1991; Hylander and Johnson 1992; Lahr and Wright 1996; Ravosa et al. 2000; Godinho et al. 2018).

Therefore, the overall increase to muscle force and the consequential increase in bite reaction force did increase global craniofacial strains for both models, and interestingly in some regions known to be more robust within *H. ergaster.* However, while the zygoma region morphology of *H. ergaster* may have facilitated this increase in bite force by increasing masseter cross-sectional area, this zygoma region morphology does not appear well adapted to resisting this increased masseter force, as the modified model predicted higher strain magnitudes in most regions locally to the zygoma when the force applied to the masseter was increased. Overall, these results only partially support H3: "*A H. sapiens cranium with H. ergaster-like zygoma regions and H. ergaster-like masseter muscle force magnitudes will further increase bite force, which will increase craniofacial strain magnitudes globally, but lower strains are still predicted locally to the zygoma region*". As while the modified model loaded with increased masseter forces did predict higher bite forces for incisor and molar bites consequently increasing global strain magnitudes, strain magnitudes locally to the zygoma region were not consistently lower.

3.6.4. Objective Three: comparing the performance of the unmodified and modified FE models during bites at gape

The habitual use of extra-oral processing technologies to prepare dietary items may have reduced the size of food objects consumed by hominins throughout the evolution of the genus *Homo* (Zink et al. 2014; Zink and Lieberman 2016). This means that the facial skeleton of *Homo ergaster* may be better adapted to withstand the differential mechanical loading of the cranium associated with performing bites at larger gapes than that of *Homo sapiens,* due to the more frequent consumption of larger food items. Therefore, it was predicted that the *H. sapiens* FE model with the *H. ergaster*-like zygoma regions would predict lower global and local strain magnitudes when bites at submaximal and maximal gapes were simulated, relative to the unmodified *H. sapiens* FE model. As the modifications to the model included moving the origins of the masseter more anteriorly, it was also predicted that this model should produce higher bite reaction forces for both anterior and posterior bites as the leverage of the masseter would be increased.

In line with predictions, when both molar and incisor bites at submaximal and maximal gapes are simulated, the predictions of bite force magnitude and efficiency are always slightly higher for the modified model than the unmodified models. However, overall bite force for both bites decreased while joint reaction forces increased as gape increased for both models which indicates that the overall efficiency of the masticatory system decreased as inter-incisal separation increased for both models. The higher bite force predictions of the modified model are likely due to the more anteriorly positioned masseter origin, which could indicate that the zygoma region morphology of *H. ergaster* was better adapted to producing higher bite forces at wider gapes than that of *H. sapiens*. However, it is important to appreciate that physiologically this may preclude the production of high bite forces at large gapes due to the increased stretch of the superficial masseter that would occur with a more anteriorly positioned origin (Herring and Herring 1974). As has been suggested for other primates (Terhune et al. 2015b; Hylander 2013; Fricano and Perry 2019), the increased subnasal prognathism of *H. ergaster* may reflect an adaptation to increase gape capacities at the incisors while reducing muscle stretch to maximise bite forces during anterior bites at gape.

As discussed, debate exists as to whether supraorbital robusticity within fossil hominins is a consequence of masticatory loading or other mechanisms (Athreya 2012). While the previously discussed results provided one masticatory-based explanation for supraorbital robusticity within the genus *Homo*, when bites at larger gapes were simulated strains in the glabella and interorbital regions decreased as gape increased for both models. For the incisor bites at submaximal and maximal gapes, strains in these regions are comparable for both the models, however for the molar bites the modified model predicted slightly higher strain magnitudes in these regions, especially during bites at maximal gape. These results may point to a connection between the performance of molar bites at submaximal and maximal gapes, and glabella robusticity within *H. ergaster* due to the increased bone formation that would occur with elevated strains in this region. Thus, gracilisation of the supraorbital region within *H. sapiens* could be a consequence of this species performing molar bites at larger gapes less frequently than *H. ergaster*. However other mechanisms such as allomeric scaling (Lahr and Wright 1996; Freidline et al. 2012a, 2012b), or as a by-product of the facial skeleton projecting from the anterior cranial fossa (Moss and Young 1960; Hylander et al. 1991; Ravosa et al.

2000), that have been suggested to explain supraorbital robusticity within archaic *Homo* cannot be ruled out based on the results of this thesis alone.

While previously unexplored for members of the genus *Homo*, aside from the suggestions of Rak and Hylander (2003) relating to gape capacity adaptations within the craniofacial skeleton of *Homo neadnerthalensis*, the results of the simulations of bites at gape offer interesting insights into the ability of the zygoma region of *H. sapiens* and *H. ergaster* to withstand such loading regimes. Overall, strains in most regions local to the zygoma were lower for the modified model relative to the unmodified model for both anterior and posterior bites at submaximal and maximal gapes. For the unmodified model, as gape increased for both bites, strains increased considerably in most regions local to the zygoma. On the contrary, for the modified model there was less of an increase in zygoma regions strains for incisor bites, and for molar bites strains decreased as gape increased. Taken together, these results suggest that the zygoma region morphology of *H. sapiens* is poorly adapted to withstanding bites at large gapes, while the zygoma region morphology of *H. ergaster* is better adapted to this.

Therefore, these results provide support for H4: "*A H. sapiens cranium with H. ergaster-like zygoma regions will increase bite forces during anterior and posterior bites at submaximal and maximal gapes*". This is because while bite force decreased for both models as gape increased, the modified model consistently predicted higher bite forces than the unmodified model for both incisor and molar bites. These results also mostly support H5: "*Global craniofacial and local zygoma strain magnitudes will be relatively lower during bites at maximal gapes and submaximal gapes in the H. sapiens cranium with H. ergaster-like zygoma regions compared to the unmodified H. sapiens cranium*". This is because aside from strain magnitudes in the interorbital region being higher for the modified model during molar bites at maximal gapes, strain magnitudes in other global regions were lower for the during both anterior and posterior bites at submaximal and maximal gapes, as well as being lower in regions locally to the zygoma, especially during molar bites at maximal gapes.

3.7. Chapter Conclusion: the functional significance *Homo ergaster* zygoma region morphology and its gracilisation within *Homo sapiens*

Some researchers have suggested that the reduction in the size and increased gracilisation of the zygoma region morphology of *H. sapiens* is a consequence of a reduction in selective pressures to produce and withstand high bite forces because of the increased use of complex food processing behaviours with the evolution of this species (Demes and Creel 1988; Lieberman 2008, 2011; Ledogar et al. 2016a). The results of this chapter have demonstrated that the larger and wider zygoma region morphology of *H. ergaster* could be adaptation to increasing molar bite forces by increasing the force of the masseter by increasing its cross-sectional area rather than improving its mechanical efficiency, consistent with previous biomechanical analyses of the hominin masticatory apparatus (Eng et al. 2013). This demonstrates the selective importance of producing high bite forces through having larger muscles of mastication in determining craniofacial form in early *Homo,* as has been suggested by previous research (Demes and Creel 1988). Thus, the zygoma region morphology of *H. ergaster* may reflect adaptations to the consumption of a hard dietary objects due to the optimisation of bite force production on the most mechanically efficient position along the dental row.

However, the cranium must also suitably resist the mechanical forces it is loaded with, and the strains that this induces. It has also been suggested that the projecting, wide and tall and overall robust zygoma regions of archaic *Homo* may represent adaptations to reducing masticatory strains (Lieberman 2008, 2011). The results presented within this chapter do not support these suggestions, as the zygoma region morphology of *H. ergaster* did not on the whole decrease strains locally or globally, and in many regions strain magnitudes increased. This indicates that other craniofacial traits of *H. ergaster*, such as a flat infraorbital region and a taller maxilla, may function to reduce strain under masticatory loads, and may have been developed plastically or selected for to reduce the elevated strains associated with producing a higher bite forces, and the accompanying shape changes to the zygoma region that facilitate this increase in bite force. This points to the importance of mechanical compensations in the evolution of craniofacial form within early *Homo,* as has been suggested for the australopithecines (Ledogar et al. 2022).

The selective importance of the consumption of large, hard dietary items within hominin fossils is frequently suggested (Strait et al. 2009; Daegling et al. 2011; Strait et al. 2013; Ledogar et al. 2016b), but rarely systematically evaluated. The results of this chapter however have demonstrated that the zygoma region morphology of *H. ergaster* may be an adaptation to producing higher bite forces and reducing zygoma-region strains during bites at large gapes, especially during molar bites at maximal gapes. Therefore, the zygoma region morphology of *H. ergaster* may also reflect adaptations to the consumption of a diet with larger food items due to the reduction in local strains seen during bites at larger gapes. This emphasises the influence that large object feeding may have had on craniofacial form in early *Homo*.

Therefore, the results of this chapter support that craniofacial gracilisation within *H. sapiens* could have occurred due a release on selective pressures to produce high bite forces facilitating a decrease in the size of the jaw-elevator muscles and thus the zygoma-region, following the habitual use of complex food processing technologies (Zink et al. 2014; Zink and Lieberman 2016). These results could also indicate that the decreased size and robusticity of this region may have been further facilitated by a reduced need to withstand bites at large gapes following the reduction of the size of food items. However, these results also infer that zygoma region gracilisation within *H. sapiens* may be less of a consequence of a reduction in masticatory strains directly or a reduction in selective pressures maintaining features that reduce masticatory strain, as little evidence was found to indicate that the zygoma region morphology of *H. ergaster* lowered craniofacial strains uniformly. Overall then, gracilisation of the zygoma region within *H. sapiens* may be more directly associated with the less frequent performance of bites at large gapes, and critically reduced selective pressures maintaining large jaw-elevator musculature, rather than being a consequential reduced exposure to masticatory strains or a release of selective pressures maintaining adaptations that reduce craniofacial strains.

4. Chapter 4: Thesis Conclusion

In summary, this thesis has used finite element analysis (FEA) and thin plate spline (TPS) warping to investigate the relationship between gracilisation in the zygoma region within *Homo sapiens* and masticatory loading. To investigate this, in Chapter 2 a voxel-based cranial FE model of a modern *H. sapiens* female was constructed in line with previously reported protocols (objective 1 of the thesis; Toro-Ibacache et al. 2016; Toro-Ibacache and O'Higgins 2016; Godinho et al. 2017). Subsequently, the validity of the model's predictions were assessed against previously published *H. sapiens* cranial FE models and other biomechanical assumptions (included within objective 1 of the thesis), and the sensitivity of the model to changes in a range of input parameters were considered (objective 2 of the thesis). The sensitivity tests were specifically chosen as these input parameters were identified as those that needed changing to simulate bites at submaximal and maximal gapes (objective 4 of the thesis). Following this, in Chapter 3 the zygoma region of the *H. sapiens* FE model was modified using TPS warping following O'Higgins et al. (2011) to contain the zygoma region morphology of KNM-ER 3733, a *Homo ergaster* fossil (objective 3 of the thesis). After re-defining the loading and boundary conditions of this modified FE model, its predictions were compared to those of the unmodified FE model for a range of masticatory loading scenarios in Chapter 3 (objective 4 of the thesis).

Although the functional significance of australopithecine zygoma morphology has been investigated using FEA (Fitton et al. 2009; Ledogar et al. 2017), this thesis is the first instance in which the importance of changes to the zygoma region in the genus *Homo* have been considered. This demonstrated that while the zygoma region morphology of *H. ergaster* may represent an adaptation to increasing bite forces through increasing the cross-sectional area of the masseter, the bony adaptations that facilitate this subsequently increase strains elsewhere in the zygoma region and craniofacial skeleton. This emphasises the selective importance of producing high bite forces in shaping the facial skeleton of early *Homo,* while also indicating that the development and selection for other strain-reducing features may have been equally as important in this regard. On the whole, the results of this thesis are contrary to previous predictions from paleoanthropological literature surrounding the functional morphology of the facial skeleton of early *Homo,* which typically assert that the

large, projecting, and robust zygomatic regions are the product of selection pressures maintaining anatomical features for withstanding high masticatory forces and of the increase in bone formation that would occur consequentially to this (Demes and Creel 1988; Lieberman et al. 2004; Lieberman 2008, 2011; Ledogar et al. 2016a; Zink and Lieberman 2016). However, the results are consistent with arguments that the need to produce high bite forces were selectively important in determining craniofacial form in early *Homo,* but that this was principally achieved via having larger muscles of mastication relative to modern *H. sapiens* (Demes and Creel 1988; Eng et al. 2013). As argued by Ledogar et al. (2022) for the australopithecines, this points to the significance of mechanical compensations in shaping the form of the facial skeleton of early *Homo*. These interpretations are suggestive that gracilisation of the zygoma region of *H. sapiens* may be in part consequential to the release of selective pressures maintaining large jaw elevator musculature, rather than a direct reduction in masticatory strain exposure or a release on pressures maintaining features that reduce craniofacial strains.

Many previous studies of fossil hominin masticatory biomechanics have focused on predicting bite forces (Demes and Creel 1988; Anton 1990; O'Connor, Franciscus and Holton 2005; Eng et al. 2013), and craniofacial strains during bites at uniform gapes (Strait et al. 2009, 2010; Smith et al. 2015b; Ledogar et al. 2016b; Wroe et al. 2018; Godinho et al. 2018; Cook et al. 2021; Ledogar et al. 2022). This thesis also considered how these variables change during bites at different gapes and the implications this has for craniofacial adaptations to large object feeding within early *Homo.* While previous researchers have suggested that some hominin taxa may have had craniofacial adaptations that would facilitate producing larger gapes (Rak and Hylander 2003b; Hylander 2013), and the predictions of australopithecine FE models have been interpreted to suggest adaptations to large, hard object feeding (Strait et al. 2009, 2010; Ledogar et al. 2016b), this thesis is the first occasion where bites at different gapes have been simulated on FE models of hominin crania. The results presented in this thesis demonstrated a potential adaptive significance of the zygoma region morphology of *H. ergaster* in both producing higher bite forces and reducing zygoma-region strains during bites at large gapes, and that gracilisation of this region within *H. sapiens* may partially be a product of less frequently performing bites at large gapes.

4.1. Study limitations

One major limitation of this research was the constraints upon the ways in which TPS warping could be used to modify the zygoma region, owing to the sensitivity of the unmodified *H. sapien*s FE model to changes in its loading and boundary conditions (see Chapter 2, section 2.5). This meant that while the form of the frontal process of the zygoma, the form of the zygomatic roots and the extent of midfacial projection of the *H. sapiens* model were altered, the resulting changes were not entirely reflective of these morphologies in KNM-ER 3733, as this would require altering more input parameters than just the masseter force vector. Therefore, although previous FE and non-FE masticatory biomechanical research has emphasised the importance of these features in the ability of the hominin facial skeleton to resist and produce masticatory forces (e.g. Rak 1983, 1986; Demes 1987; Rak and Marom 2017; Ledogar et al. 2017), the functional significance of these features in *H. ergaster* was not directly addressed by this thesis. The results presented within Chapter 3 instead offer insight into how changing the form of these features to accommodate a larger and wider zygoma region impacts bite force capabilities and craniofacial strain within a *H. sapiens* cranium.

Another important limitation of this research was the unavailability of any *in vivo* muscle activation and mandibular kinematic data from the *H. sapiens* specimen used to create define the loading parameters the unmodified and modified FE models, and of muscle PCSA and internal architecture data from KNM-ER 3733. Due to this, many simplifications, approximations, and assumptions were made to the loading and boundary conditions of the models produced within this thesis, which may limit the accuracy of some of their predictions. Firstly, it is important to appreciate that while the predictions of the model were sufficiently accurate for use in a hypothetical form-function investigation, the construction and loading of the *H. sapiens* model, while following previously validated protocols (see section 2.3), precludes predictions of absolute strain magnitudes and bite forces. Thus, while the strain magnitude and the bite force predictions made by the models are not entirely reflective of physiological reality, the differences between the modified and unmodified models provide insights into how changes in zygoma region morphology may impact lever mechanics of the masticatory system and how the craniofacial skeleton deforms in response to masticatory loading.

Secondly, one of the experimental aims of this thesis was to investigate how craniofacial strain and bite force production is impacted by increasing the force applied to the masseter. The wider zygomatic regions of *Homo ergaster* indicates that they had larger muscles of mastication than *Homo sapiens,* yet muscle PCSA is unavailable for paleontological specimens, hence the increase in masseter CSA and muscle force was estimated using bony proxies. However, Toro-Ibacache et al. (2015) report that muscle CSA calculated in this manner corresponds poorly to masticatory muscle CSA recorded from CT scans. Accordingly, the *H. ergaster*-like masseter force applied to both the models is likely not reflective of the absolute muscle force that *H. ergaster* could produce. As such, the predictions made by the models in these loading scenarios, particularly those of bite force and strain magnitude, are not accurate and are potentially overestimated as Toro-Ibacache et al. (2015) reported that estimating masseter CSA via bony proxies produces values up to 100% greater than CSA recorded from CT scans. However, the results of this thesis are informative as to how a relative increase to the force applied to the masseter impacted reactions force predictions, as well as global and local craniofacial strains predicted by both models, elucidating whether the robust zygoma region of *H. ergaster* was better adapted to withstanding higher muscle forces than the gracile zygoma region of *H. sapiens*.

One of the aims of this thesis was to investigate adaptations to the consumption of large dietary objects, therefore bites at a range of gapes were simulated by altering the loading and boundary conditions of the model to reflect changes in mandibular position during jaw opening. However, the lack of available specimen specific *in vivo* data limited how accurately these loading scenarios could be simulated. Firstly, it was impossible to obtain *in vivo* data surrounding maximal gape capacity and mandibular kinematics for the *H. sapiens* individual, meaning mandibular position at arbitrary gapes had to be approximated (see section 3.5.1). Therefore, the strain predictions of the model when bites at gape were simulated may not be physiologically realistic. Unfortunately, these strain predictions could not be experimentally validated and are potentially not representative of how the crania strains during bites at different gapes.

Indeed, the bite force predictions of the model during bites at gape were inconsistent with non-specimen specific *in vivo* bite force recordings for *H. sapiens* individuals that show an increase to bite force during the early stages of jaw-opening (Manns, Miralles and Palazzi 1979; Paphangkorakit and Osborn 1997; Koc et al. 2012). This is most likely attributable to the simplifications made to the modelling of the masticatory musculature due to the absence of the necessary *in vivo* data. In the absence of specimen-specific EMG data showing how muscle activation patterns change during bites at different gapes, the same maximal, homogeneous, and symmetrical pattern was modelled for all simulated bites at gape. However, as increasing the extent of jaw opening has been reported to change muscle activation patterns within *H. sapiens* (Manns et al. 1979; Lindauer et al. 1993; Pröschel et al. 2008; Koc et al. 2012), scaling applied muscle forces to suitable EMG data may be necessary to produce more accurate predictions of bite force, strain distribution, and magnitude during bites at gape. Similar suggestions have been made regarding bites simulated at uniform jaw positions (Ross et al. 2005; Fitton et al. 2012). Additionally, in the absence of data surrounding muscle stretch during jaw opening for the *H. sapiens* individual, and knowledge surrounding the muscle internal architecture and length-tension relationships of *H. ergaster*, these factors were not considered in the estimation of applied muscle force for the simulated bites at gape. Therefore, the bite force predictions made by the models when bites at gape where simulated are likely un-realistic, reflecting solely changes to the lever mechanics of the masticatory system as the jaw opens rather than a combination of this in addition to muscle length-tension relationships and changing activation patterns.

4.2. Future directions

The results discussed within Chapter 3 provided interesting insights into the relationship between zygoma region morphology, bite force production and craniofacial strains during masticatory loading that could be enhanced by future research. As discussed, there were some limitations on the way TPS warping could be used to modify the zygoma region morphology of the *H. sapiens* specimen, therefore making additional modifications to the model would further clarify the functional importance of the zygoma region morphology of

H. ergaster. For example, while the reduced strains in the postorbital regions of the modified model were attributable to changes in the orientation of the frontal process of the zygoma, modifying this region to resemble that of *H. ergaster* could clarify the importance of upper facial width of early Pleistocene *Homo* in resisting masticatory forces. Furthermore, as the increase in strains in some areas local to the zygoma predicted by the modified model were partially attributed to changes to the zygomatic roots, comparing how predictions vary between a model where the superior-inferior height of the maxilla is also modified in addition to the height of the zygoma thus allowing the form of the zygomatic roots to become more *H. ergaster* like, would help to clarify the impacts that the shape of the zygomatic roots has upon strain magnitudes local to the zygoma region within the facial skeleton of the genus *Homo*.

As this thesis focused on the impacts of changing the in-lever of the masseter, modifying the alveolar regions of the maxilla may better clarify relationships between out lever lengths, bite force production and craniofacial strains within the facial skeleton of *Homo*. Modifying the height of the maxilla in combination with the zygoma region could clarify whether the taller faces of early *Homo* represent adaptations to reducing masticatory strains, as suggested by previous authors (Hylander 1977; Lieberman 2008; Wang et al. 2010a; Lieberman 2011). This may also be interesting for investigations surrounding adaptations to large object feeding in early *Homo*, as increasing the height of the occlusal plane in relation to the temporomandibular joint can decrease gape capacity (Herring 1972; Vinyard et al. 2003; Terhune 2011b). Investigating the impacts that increasing subnasal prognathism has upon the predictions of the *H. sapiens* FE model may also provide interesting insights into optimisations for force production and gape capacity within the craniofacial skeleton of *Homo*, as while this trait is suggested to be an adaptation that increases gape capacities (Hylander 2013), it simultaneously decreases the mechanical advantage of the masseter (Demes and Creel 1988; Godinho et al. 2018). As many of the above suggestions were beyond the scope of this thesis to investigate, performing additional TPS warps to further modify the form of the *H. sapiens* FE model would provide a clearer picture into functional integration within the masticatory apparatus and facial skeleton of the genus *Homo,* and its optimisation for producing and withstanding high bite forces, and for performing bites at larger gapes.

Incorporating other biomechanical modelling techniques alongside FEA in the investigation of the functionality of the masticatory apparatus may enhance insights into adaptations to large object feeding within the genus *Homo.* For example, as the form of the temporomandibular joint is correlated to gape capacities within other primate taxa (Wall 1999; Terhune 2011b; Fricano and Perry 2019; Terhune et al. 2022), modifying the form of the *H. sapiens* joint to resemble the shallow glenoid fossae and poorly developed articular eminences of *H. ergaster* (Terhune et al. 2007) could impact the kinematics of jaw opening. Thus, using dynamic modelling techniques with FEA (e.g. Koolstra and van Eijden 2005) could enhance investigations of changes to gape capabilities throughout human evolution, for example how the more anteriorly positioned masseter origin of *H. ergaster* may have interacted with gape capacities and bite force production, if information on muscle stretch and optimum sarcomere lengths were incorporated into such models (as within: Koolstra and van Eijden 1997; Langenbach and Hannam 1999; Peck and Hannam 2007).

Ultimately, adapting the protocol developed in this thesis to simulate bites at gape on australopithecine FE models may provide better insights into their ability to consume large hard objects versus small hard objects, and simulating such bites on *Homo Neanderthalensis* FE models could inform whether any craniofacial adaptations in this species reduce craniofacial strains during bites at different gapes, given the presence of adaptations that indicate an optimisation of gape capacity (Rak and Hylander, 2003).

4.3. Final conclusions

Overall, this thesis has demonstrated that the robust zygoma region of *H. ergaster* may represent adaptations to increasing bite forces primarily through increasing the cross-sectional area of the masseter, as well as reducing craniofacial strains during bites at large gapes. Therefore, larger object feeding and the need to maintain large jaw-elevator musculature to generate high bite forces may have been selectively important in shaping the

form of the facial skeleton in *H. ergaster* prior to the reduction in the mechanical challenge of dietary resources with complex extra-oral food processing behaviours.

However, this thesis also found little evidence to indicate that the large robust zygoma region of *H. ergaster* reduced craniofacial strain during masticatory loading, with strains increasing in some regions locally to the zygoma, especially when the force applied to the masseter increased as a product of having a wider zygoma. This indicates that the large and wide zygomatic regions of *H. ergaster* are not an adaptation for reducing strain under masticatory load. Indeed other craniofacial features of the species may have been selected for and plastically developed due the increased strains associated with having this zygomatic region morphology. Thus, mechanical compensations could have been equally as important as the need to produce high bite forces and resist bites at large gapes in influencing craniofacial form early *Homo*.

Therefore, following the reduction of the mechanical challenge posed by dietary resources, gracilisation of the zygoma region within *H. sapiens* may have been facilitated by less frequently performing bites at large gapes, and crucially reduced selective pressures maintaining large jaw-elevator musculature, rather than being a direct product of reduced exposure to masticatory strains or release of pressures maintaining adaptations that reduce craniofacial strains.

5. References

Aiello, L. C. and Wheeler, P. (1995). 'The Expensive-Tissue Hypothesis: The Brain and the Digestive System in Human and Primate Evolution'. *Current Anthropology*, 36 (2), pp.199–221.

Alemseged, Z. (2023). 'Reappraising the palaeobiology of Australopithecus'. *Nature,* 617 (7959), pp.45–54.

Alomar, X. et al. (2007). 'Anatomy of the temporomandibular joint'. *Seminars in Ultrasound, CT and MRI,* 28 (3). pp.170–183.

Anderson, P. S. L. et al. (2011). 'Models in palaeontological functional analysis'. *Biology Letters*, 8 (1), pp.119–122.

Anton, S. C. (1990). 'Neandertals and the anterior dental loading hypothesis: a biomechanical evaluation of bite force production'. *Kroeber Anthropological Society Papers*, 71 (72), pp.67–76.

Antón, S. C. (1996). 'Tendon-associated bone features of the masticatory system in Neandertals'. *Journal of Human Evolution*, 31 (5), pp.391–408.

Antón, S. C. (2003). 'Natural history of Homo erectus'. *American Journal of Physical Anthropology*, 122 (S37), pp.126–170.

Antón, S. C. and Middleton, E. R. (2023a). 'Making meaning from fragmentary fossils: Early Homo in the Early to early Middle Pleistocene'. *Journal of Human Evolution*, 179, pp.103307.

Athreya, S. (2009). 'A comparative study of frontal bone morphology among Pleistocene hominin fossil groups'. *Journal of Human Evolution*, 57 (6), pp.786–804.

Athreya, S. (2012). 'The frontal bone in the genus Homo: a survey of functional and phylogenetic sources of variation'. *Journal of Anthropological Sciences*, 90, pp. 1-22.

Attwell, L. et al. (2015). 'Fire in the Plio-Pleistocene: the functions of hominin fire use, and the mechanistic, developmental and evolutionary consequences'. *Journal of anthropological sciences*, 93, pp.1–20.

Baab, K. L. et al. (2010). 'Relationship of cranial robusticity to cranial form, geography and climate in Homo sapiens'. *American Journal of Physical Anthropology*, 141 (1), pp.97–115.

Banus, M. G. and Zetlin, A. M. (1938). The relation of isometric tension to length in skeletal muscle. Journal of Cellular and Comparative Physiology, 12 (3), pp.403–420. [Online]. Available at: doi:10.1002/jcp.1030120310.

Bastir, M. et al. (2008). 'Middle cranial fossa anatomy and the origin of modern humans'. *The Anatomical Record*, 291 (2), pp.130–140.

Bastir, M. and Rosas, A. (2016). 'Cranial base topology and basic trends in the facial evolution of Homo'. *Journal of Human Evolution*, 91, pp.26–35.

Beecher, R. M. et al. (1983). 'Craniofacial correlates of dietary consistency in a nonhuman primate'. *Journal of Craniofacial Genetics and Developmental Biology*, 3 (2), pp.193–202.

Berthaume, M. A. (2016). 'Food mechanical properties and dietary ecology'. *American Journal of Physical Anthropology*, 159 (S61), pp.79–104.

Bonakdarchian, M. et al. (2009). 'Effect of face form on maximal molar bite force with natural dentition'. *Archives of Oral Biology*, 54 (3), pp.201–204.

Bookstein, F. L. (1989). 'Principal warps: thin-plate splines and the decomposition of deformations'. *IEEE Transactions on Pattern Analysis and Machine Intelligence*, 11 (6), pp.567–585.

Bookstein, F. L. et al. (2003). 'Cranial integration in Homo: singular warps analysis of the midsagittal plane in ontogeny and evolution'. *Journal of Human Evolution*, 44 (2), pp.167–187.

Bourke, J. et al. (2008). 'Effects of gape and tooth position on bite force and skull stress in the dingo (Canis lupus dingo) using a 3-dimensional finite element approach'. *PLOS one*, 3 (5), pp.e2200.

Brace, C. L. (1991). 'What big teeth you had grandma! Human tooth size, past and present'. *Advances in Dental Anthropology*, pp. 33-57

Brace, C. L. et al. (1987). 'Gradual Change in Human Tooth Size in the Late Pleistocene and Post-Pleistocene'. *Evolution*, 41 (4), pp.705–720.

Brachetta-Aporta, N. and Toro-Ibacache, V. (2021). 'Differences in masticatory loads impact facial bone surface remodeling in an archaeological sample of South American individuals'. *Journal of Archaeological Science: Reports*, 38, pp.103034.

Bright, J. A. (2012). 'The importance of craniofacial sutures in biomechanical finite element models of the domestic pig'. *PLOS one*, 7 (2), pp.e31769.

Bright, J. A. (2014). 'A review of paleontological finite element models and their validity'. *Journal of Paleontology,* 88 (4), pp.760–769.

Bright, J. A. and Gröning, F. (2011). 'Strain accommodation in the zygomatic arch of the pig: A validation study using digital speckle pattern interferometry and finite element analysis'. *Journal of Morphology*, 272 (11), pp.1388–1398.

Bright, J. A. and Rayfield, E. J. (2011). 'Sensitivity and ex vivo validation of finite element models of the domestic pig cranium'. *Journal of Anatomy*, 219 (4), pp.456–471.

Buchanan, T. S. (1995). 'Evidence that maximum muscle stress is not a constant: differences in specific tension in elbow flexors and extensors'. *Medical Engineering & Physics*, 17 (7), pp.529–536.

Burkholder, T. J. and Lieber, R. L. (2001). 'Sarcomere Length Operating Range of Vertebrate Muscles During Movement'. *Journal of Experimental Biology*, 204 (9), pp.1529–1536.

Campbell, K. M. and Santana, S. E. (2017). 'Do differences in skull morphology and bite performance explain dietary specialization in sea otters?'. *Journal of Mammalogy*, 98 (5), pp.1408–1416.

Carlson, D. S. (1977). 'Condylar translation and the function of the superficial masseter muscle in the rhesus monkey (M. mulatta)'. *American Journal of Physical Anthropology*, 47 (1), pp.53–63.

Carlson, D. S. and Van Gerven, D. P. (1977). 'Masticatory function and post-pleistocene evolution in Nubia'. *American Journal of Physical Anthropology*, 46 (3), pp.495–506.

Chalk, J. et al. (2011). 'A finite element analysis of masticatory stress hypotheses'. *American Journal of Physical Anthropology*, 145 (1), pp.1–10.

Chamoli, U. and Wroe, S. (2011). 'Allometry in the distribution of material properties and geometry of the felid skull: why larger species may need to change and how they may achieve it'. *Journal of Theoretical Biology*, 283 (1), pp.217–226.

Chatar, N. et al. (2022). 'Many-to-one function of cat-like mandibles highlights a continuum of sabre-tooth adaptations'. *Proceedings of the Royal Society B*, 289 (1988), pp.20221627.

Chazan, M. (2017). 'Toward a Long Prehistory of Fire'. *Current Anthropology*, 58 (S16), pp.S351–S359.

Cheverud, J. M. (1982). 'Phenotypic, Genetic, and Environmental Morphological Integration in the Cranium'. *Evolution*, 36 (3), pp.499–516.

Ciochon, R. L. et al. (1997). 'Dietary consistency and craniofacial development related to masticatory function in minipigs'. *Journal of Craniofacial Genetics and Developmental Biology*, 17 (2), pp.96–102.

Cobb, S. et al. (2015). 'The Ontogeny of Mechanical Advantage in the Masticatory System'. *The FASEB Journal*, 29 (1), pp.865.

Cook, R. W. et al. (2021). 'The cranial biomechanics and feeding performance of Homo floresiensis'. *Interface Focus*, 11 (5), pp.20200083.

Cox, P. G. et al. (2011). 'Finite element modelling of squirrel, guinea pig and rat skulls: using geometric morphometrics to assess sensitivity'. *Journal of Anatomy*, 219 (6), pp.696–709.

Cox, P. G. et al. (2015). 'Predicting bite force and cranial biomechanics in the largest fossil rodent using finite element analysis'. *Journal of Anatomy*, 226 (3), pp.215–223.

von Cramon-Taubadel, N. (2011). 'Global human mandibular variation reflects differences in agricultural and hunter-gatherer subsistence strategies'. *PNAS*, 108 (49), pp.19546–19551

von Cramon-Taubadel, N. (2014). 'Evolutionary insights into global patterns of human cranial diversity: Population history, climatic and dietary effects'. *Journal of Anthropological Sciences*, 92, pp.43–77.

von Cramon-Taubadel, N. (2017). 'Measuring the effects of farming on human skull morphology'. *PNAS*, 114 (34), pp.8917–8919.

Cuff, A. R. et al. (2015). 'Validation experiments on finite element models of an ostrich (Struthio camelus) cranium'. *PeerJ*, pp.e1294.

Currey, J. D. (2003a). 'How Well Are Bones Designed to Resist Fracture?'. *Journal of Bone and Mineral Research*, 18 (4), pp.591–598.

Currey, J. D. (2003b). 'The many adaptations of bone'. *Journal of Biomechanics*, 36 (10), pp.1487–1495.

Currey, J. D. (2006). *Bones: Structure and Mechanics*. Princeton University Press, New Jersey.

Currey, J. D. (2012). 'The structure and mechanics of bone'. *Journal of Materials Science*, 47 (1), pp.41–54.

Custodio, W. et al. (2011). 'Occlusal force, electromyographic activity of masticatory muscles and mandibular flexure of subjects with different facial types'. *Journal of Applied Oral Science*, 19, pp.343–349.

Cuy, J. L. et al. (2002). 'Nanoindentation mapping of the mechanical properties of human molar tooth enamel'. *Archives of Oral Biology*, 47 (4), pp.281–291.

Daegling, D. J. et al. (2011). 'Hard-object feeding in sooty mangabeys (Cercocebus atys) and interpretation of early hominin feeding ecology'. *PLOS One*, 6 (8), pp.e23095.

Dembo, M. et al. (2015). 'Bayesian analysis of a morphological supermatrix sheds light on controversial fossil hominin relationships'. *Proceedings of the Royal Society B*, 282 (1812), pp.20150943.

Demes, B. (1982). 'The resistance of primate skulls against mechanical stresses'. *Journal of Human Evolution*, 11 (8), pp.687–691.

Demes, B. (1987). 'Another look at an old face: biomechanics of the neandertal facial skeleton reconsidered'. *Journal of Human Evolution*, 16 (3), pp.297–303.

Demes, B. and Creel, N. (1988). 'Bite force, diet, and cranial morphology of fossil hominids'. *Journal of Human Evolution*, 17 (7), pp.657–670.

Diez-Martin, F. et al. (2010). 'New insights into hominin lithic activities at FLK North Bed I, Olduvai Gorge, Tanzania'. *Quaternary Research*, 74 (3), pp.376–387.

Dominy, N. J. et al. (2008). 'Mechanical Properties of Plant Underground Storage Organs and Implications for Dietary Models of Early Hominins'. *Evolutionary Biology*, 35 (3), pp.159–175.

Du Brul, E. L. (1977). 'Early hominid feeding mechanisms'. *American Journal of Physical Anthropology*, 47 (2), pp.305–320.

Dumont, E. et al. (2009). 'Requirements for comparing the performance of finite element models of biological structures'. *Journal of Theoretical Biology*, 256 (1), pp.96–103.

Dumont, E. R. et al. (2011). 'Finite element analysis of performance in the skulls of marmosets and tamarins'. *Journal of Anatomy*, 218 (1), pp.151–162.

Dumont, E. R. and Herrel, A. (2003). 'The effects of gape angle and bite point on bite force in bats'. *Journal of Experimental Biology*, 206 (13), pp.2117–2123.

Dumont, E. R. et al. (2005). 'Finite-element analysis of biting behavior and bone stress in the facial skeletons of bats'. *The Anatomical Record*, 283 (2), pp.319–330.

Edgar, H. et al. (2020). New Mexico decedent image database. Office of the Medical Investigator, University of New Mexico: Albuquerque, NM, USA.

Edmonds, H. M. and Glowacka, H. (2020). 'The ontogeny of maximum bite force in humans'. *Journal of Anatomy*, 237 (3), pp.529–542.

van Eijden, T. et al. (1997). 'Architecture of the human jaw-closing and jaw-opening muscles'. *The Anatomical Record*, 248 (3), pp.464–474.

El Haddioui, A. et al. (2007). 'Anatomical study of the arrangement and attachments of the human medial pterygoid muscle'. *Surgical and Radiologic Anatomy*, 29 (2), pp.115–124.

Endo, B. (1965). 'Distribution of stress and strain produced in the human facial skeleton by the masticatory force'. *Journal of the Anthropological Society of Nippon*, 73 (4), pp.123–136.

Endo, B. (1970). 'Analysis of stresses around the orbit due to masseter and temporalis muscles respectively'. *Journal of the Anthropological Society of Nippon*, 78 (4), pp.251–266.

Endo, B. and Adachi, K. (1988). 'Biomechanical simulation study on the forms of the frontal bone and facial bones of the recent human facial skeleton by using a two-dimensional frame model with stepwise variable cross-section members'. *Okajimas Folia Anatomica Japonica*, 64 (6), pp.335–349.

Eng, C. M. et al. (2013). 'Bite force and occlusal stress production in hominin evolution'. *American Journal of Physical Anthropology*, 151 (4), pp.544–557.

Engström, C. et al. (1986). 'The relationship between masticatory function and craniofacial morphology. II A histological study in the growing rat fed a soft diet'. *European Journal of Orthodontics*, 8 (4), pp.271–279.

Enlow, D. H. and McNamara, J. A. (1973). 'The neurocranial basis for facial form and pattern'. *The Angle Orthodontist*, 43 (3), pp.256–270.

Eyquem, A. P. et al. (2019). 'Normal and altered masticatory load impact on the range of craniofacial shape variation: An analysis of pre-Hispanic and modern populations of the American Southern Cone'. *PLOS ONE*, 14 (12), pp.e0225369.

Fagan, M. J. et al. (2007). 'Voxel-based finite element analysis - Working directly with microCT scan data'. *Journal of Morphology*, 268 (12), pp.1071–1071.

Farella, M. et al. (2008). 'Masticatory muscle activity during deliberately performed oral tasks'. *Physiological Measurement*, 29 (12), pp.1397

Fedorov, A. et al. (2012). '3D Slicer as an image computing platform for the Quantitative Imaging Network'. *Magnetic Resonance Imaging*, 30 (9), pp.1323–1341.

Ferrara, T. L. et al. (2011). 'Mechanics of biting in great white and sandtiger sharks'. *Journal of Biomechanics*, 44 (3), pp.430–435.

Ferrario, V. F. et al. (1993). 'Electromyographic activity of human masticatory muscles in normal young people. Statistical evaluation of reference values for clinical applications'. *Journal of Oral Rehabilitation*, 20 (3), pp.271–280.

Ferrario, V. F. et al. (2004).' Maximal bite forces in healthy young adults as predicted by surface electromyography'. *Journal of Dentistry*, 32 (6), pp.451–457.

Ferraro, J. V. et al. (2013). 'Earliest Archaeological Evidence of Persistent Hominin Carnivory'. *PLOS ONE*, 8 (4), pp.e62174.

Favreau, J. (2023). 'Sourcing Oldowan and Acheulean stone tools in Eastern Africa: Aims, methods, challenges, and state of knowledge'. *Quaternary Science Advances*, 9, pp.100068

Fitton, L. et al. (2009). 'Biomechanical Significance of Morphological Variation Between the Gracile Australopithecus Africanus (STS5) and Robust Australopethicus Boisei (OH5)'. *Abstract of Papers from the 57th Symposium of Vertebrate Palaeontology and Comparative Anatomy, Journal of Vertebrate Paleontology*, 29 (S3), pp. 96

Fitton, L. et al. (2012). 'Masticatory loadings and cranial deformation in Macaca fascicularis: a finite element analysis sensitivity study'. *Journal of Anatomy*, 221 (1), pp.55–68.

Fitton, L. C. et al. (2015). 'The Impact of Simplifications on the Performance of a Finite Element Model of a M acaca fascicularis Cranium'. *The Anatomical Record*, 298 (1), pp.107–121.

Freidline, S. E. et al. (2012a). 'A comprehensive morphometric analysis of the frontal and zygomatic bone of the Zuttiyeh fossil from Israel'. *Journal of Human Evolution*, 62 (2), pp.225–241.

Freidline, S. E. et al. (2012b). 'Middle Pleistocene human facial morphology in an evolutionary and developmental context'. *Journal of Human Evolution*, 63 (5), pp.723–740.

Fricano, E. E. I. and Perry, J. M. G. (2019). 'Maximum Bony Gape in Primates'. *The Anatomical Record*, 302 (2), pp.215–225.

Frost, H. M. (1987). 'Bone "mass" and the "mechanostat": a proposal'. *The Anatomical Record*, 219 (1), pp.1–9.

Frost, H. M. (2003). 'Bone's mechanostat: A 2003 update'. *The Anatomical Record*, 275 (2), pp.1081–1101.

Gabunia, L. et al. (2000). 'Earliest Pleistocene Hominid Cranial Remains from Dmanisi, Republic of Georgia: Taxonomy, Geological Setting, and Age'. *Science,* 288 (5468), pp.1019–1025.

Galland, M. et al. (2016). '11,000 years of craniofacial and mandibular variation in Lower Nubia'. *Scientific Reports*, 6 (1), pp.31040.

Gaudy, J. F. et al. (2000). 'Functional organization of the human masseter muscle'. *Surgical and Radiologic Anatomy*, 22, pp.181–190.

Gaudy, J.-F. et al. (2002). 'Functional anatomy of the human temporal muscle'. *Surgical and Radiologic Anatomy*, 23 (6), pp.389–398.

Giuliodori, M. J. et al. (2009). 'Hooke's law: applications of a recurring principle'. *Advances in Physiology Education*, 33 (4), pp.293–296.

Godinho, R. M. et al. (2017). 'Finite element analysis of the cranium: validity, sensitivity and future directions'. *Comptes Rendus Palevol*, 16 (5–6), pp.600–612.

Godinho, R. M. et al. (2018). 'The biting performance of Homo sapiens and Homo heidelbergensis'. *Journal of Human Evolution*, 118, pp.56–71.

Godinho, R. M. and O'Higgins, P. (2018). 'The biomechanical significance of the frontal sinus in Kabwe 1 (Homo heidelbergensis)'. *Journal of Human Evolution*, 114, pp.141–153.

Godinho, R. M. et al. (2018). 'Supraorbital morphology and social dynamics in human evolution'. *Nature Ecology & Evolution*, 2 (6), pp.956–961.

González-José, R. et al. (2005). 'Functional-cranial approach to the influence of economic strategy on skull morphology'. *American Journal of Physical Anthropology*, 128 (4), pp.757–771.

Gordon, A. M. et al. (1966). 'The variation in isometric tension with sarcomere length in vertebrate muscle fibres'. *The Journal of Physiology,* 184 (1), pp.170–192.

Greaves, W. (1978). 'The jaw lever system in ungulates: a new model'. *Journal of Zoology*, 184 (2), pp.271–285.

Greaves, W. S. (1985). 'The mammalian postorbital bar as a torsion-resisting helical strut'. *Journal of Zoology*, 207 (1), pp.125–136.

Grine, F. E. (1988). *Evolutionary History of the 'robust' Australopithecines*. de Gruyter, New York.

Gröning, F. et al. (2011). 'Why do humans have chins? Testing the mechanical significance of modern human symphyseal morphology with finite element analysis'. *American Journal of Physical Anthropology*, 144 (4), pp.593–606.

Gröning, F. et al. (2011). 'The effects of the periodontal ligament on mandibular stiffness: a study combining finite element analysis and geometric morphometrics'. *Journal of biomechanics*, 44 (7), pp.1304–1312.

Gröning, F. et al. (2012). 'Modeling the Human Mandible Under Masticatory Loads: Which Input Variables are Important?'. *The Anatomical Record*, 295 (5), pp.853–863.

Grosse, I. R. et al. (2007). 'Techniques for modeling muscle-induced forces in finite element models of skeletal structures'. *The Anatomical Record*, 290 (9), pp.1069–1088.

Gu, Y. et al. (2021). 'Bite Force Transducers and Measurement Devices'. *Frontiers in Bioengineering and Biotechnology*, 9

Gunz, P. et al. (2004). 'Computer aided reconstruction of human crania'. *Computer Applications in Osteology,*

Gunz, P. et al. (2009). 'Principles for the virtual reconstruction of hominin crania'. *Journal of Human Evolution*, 57 (1), pp.48–62.

Gupta, S. et al. (2004). 'Development and experimental validation of a three-dimensional finite element model of the human scapula'. *Proceedings of the Institution of Mechanical Engineers*, 218, pp.127–142.

Habelitz, S. et al. (2001). 'Mechanical properties of human dental enamel on the nanometre scale'. *Archives of Oral Biology*, 46 (2), pp.173–183.

Hannam, A. and Wood, W. (1989). 'Relationships between the size and spatial morphology of human masseter and medial pterygoid muscles, the craniofacial skeleton, and jaw biomechanics'. *American Journal of Physical Anthropology*, 80 (4), pp.429–445.

Hartstone-Rose, A. et al. (2018). 'Dietary Correlates of Primate Masticatory Muscle Fiber Architecture'. *The Anatomical Record*, 301 (2), pp.311–324.

Hartstone-Rose, A. et al, (2019). 'Bite Force and Masticatory Muscle Architecture Adaptations in the Dietarily Diverse Musteloidea (Carnivora)'. *The Anatomical Record*, 302 (12), pp.2287–2299.

Hartstone-Rose, A. et al. (2012). 'Bite Force Estimation and the Fiber Architecture of Felid Masticatory Muscles'. *The Anatomical Record*, 295 (8), pp.1336–1351.

Harvati, K. et al. (2010). 'Evolution of middle-late Pleistocene human cranio-facial form: A 3-D approach'. *Journal of Human Evolution*, 59 (5), pp.445–464.

He, L. H. and Swain, M. V. (2007).' Nanoindentation derived stress–strain properties of dental materials'. *Dental Materials*, 23 (7), pp.814–821.

He, T. (2004). 'Craniofacial morphology and growth in the ferret: effects from alteration of masticatory function'. *Swedish Dental Journal,* (165), pp.1–72.

Herbst, E. C. et al. (2021). 'Modeling tooth enamel in FEA comparisons of skulls: Comparing common simplifications with biologically realistic models'. *Iscience*, 24 (11), pp.103182.

Herring, S. W. (1972). 'The Role of Canine Morphology in the Evolutionary Divergence of Pigs and Peccaries' *Journal of Mammalogy*, 53 (3), pp.500–512.

Herring, S. W. (1976). 'The dynamics of mastication in pigs'. *Archives of Oral Biology*, 21 (8), pp.473–480.

Herring, S. W. et al. (2001). 'Jaw muscles and the skull in mammals: the biomechanics of mastication'. *Comparative Biochemistry and Physiology*, 131 (1), pp.207–219.

Herring, S. W et al. (1979). 'Functional heterogeneity in a multipinnate muscle'. *American Journal of Anatomy*, 154 (4), pp.563–575.

Herring, S. W. and Herring, S. E. (1974). 'The Superficial Masseter and Gape in Mammals'. *The American Naturalist*, 108 (962), pp.561–576.

Hilloowala, R. A. and Trent, R. B. (1988). 'Supraorbital ridge and masticatory apparatus II: Humans (Eskimos)'. *Human Evolution*, 3 (5), pp.351–356.

Hinton, R. J. and Carlson, D. S. (1979). 'Temporal changes in human temporomandibular joint size and shape'. *American Journal of Physical Anthropology*, 50 (3), pp.325–333.

Hlubik, S. et al. (2019). 'Hominin fire use in the Okote member at Koobi Fora, Kenya: New evidence for the old debate'. *Journal of Human Evolution*, 133, pp.214–229.

Howells, W. W. (1980). 'Homo erectus—who, when and where: A survey'. *American Journal of Physical Anthropology*, 23 (S1), pp.1–23.

Huang, C. L. H. (2020). *Keynes & Aidley's Nerve and Muscle (5th ed)*. Cambridge, Cambridge University Press.

Hublin, J. J. et al. (2017). 'New fossils from Jebel Irhoud, Morocco and the pan-African origin of Homo sapiens'. *Nature*, 546 (7657), pp.289–292.

Huxley, A. F. and Niedergerke, R. (1954). 'Structural Changes in Muscle During Contraction: Interference Microscopy of Living Muscle Fibres'. *Nature*, 173 (4412), pp.971–973.

Huxley, H. and Hanson, J. (1954). 'Changes in the Cross-Striations of Muscle during Contraction and Stretch and their Structural Interpretation'. *Nature*, 173 (4412), pp.973–976.

Hylander, W. L. (1975). 'The human mandible: lever or link?'. *American Journal of Physical Anthropology*, 43 (2), pp.227–242.

Hylander, W. L. (1978). 'Incisal bite force direction in humans and the functional significance of mammalian mandibular translation'. *American Journal of Physical Anthropology*, 48 (1), pp.1–7.

Hylander, W. L. et al. (2005). 'Temporalis function in anthropoids and strepsirrhines: An EMG study.' *American Journal of Physical Anthropology*, 128 (1), pp.35–56.

Hylander, W. L. (2006). 'Functional anatomy and biomechanics of the masticatory apparatus'. In Laskin, D. M. et al. (eds): *Temporomandibular disorders: an evidenced approach to diagnosis and treatment*. New York, Quintessence Publishing Company.

Hylander, W. L. (2011). 'The Adaptive Significance of Eskimo Craniofacial Morphology. In: The Adaptive Significance of Eskimo Craniofacial Morphology'. *De Gruyter Mouton*. pp.129–170. [Online]. Available at: doi:10.1515/9783110807554.129 [Accessed 7 July 2023].

Hylander, W. L. (2013). 'Functional links between canine height and jaw gape in catarrhines with special reference to early hominins'. *American Journal of Physical Anthropology*, 150 (2), pp.247–259.

Hylander, W. L. and Johnson, K. R. (1985). 'Temporalis and masseter muscle function during incision in macaques and humans'. *International Journal of Primatology*, 6 (3), pp.289–322.

Hylander, W. L. and Johnson, K. R. (1992). 'Strain gradients in the craniofacial region of primates'. In Davidovitch, Z. (eds): *The Biological Mechanisms of Tooth Movement and Craniofacial Adaptation*. Ohio State University College of Dentistry, Columbus Ohio , pp.559–569.

Hylander, W. L. and Johnson, K. R. (1997). 'In vivo bone strain patterns in the zygomatic arch of macaques and the significance of these patterns for functional interpretations of craniofacial form'. *American Journal of Physical Anthropology*, 102 (2), pp.203–232.

Hylander, W. L. and Johnson, K. R. (2002). 'Functional Morphology and In Vivo Bone Strain Patterns in the Craniofacial Region of Primates: Beware of Biomechanical Stories about Fossil Bones'. In: Plavcan, J. M. et al. (Eds). *Reconstructing Behavior in the Primate Fossil Record: Advances in Primatology*. Springer US, Boston MA, pp.43–72.

Hylander, W. L. et al. (1991). 'Masticatory-stress hypotheses and the supraorbital region of primates'. *American Journal of Physical Anthropology*, 86 (1),

Iriarte-Diaz, J. et al. (2017). 'Functional correlates of the position of the axis of rotation of the mandible during chewing in non-human primates'. *Zoology*, 124, pp.106–118.

Ito, G. et al. (1988). 'Effect of soft diets on craniofacial growth in mice'. *Anatomischer Anzeiger*, 165 (2–3), pp.151–166.

Jiménez-Arenas, J. M. et al. (2011). 'A probabilistic approach to the craniometric variability of the genus Homo and inferences on the taxonomic affinities of the first human population dispersing out of Africa'. *Quaternary International*, 243 (1), pp.219–230.

de Jong, T. et al. (2017). 'The intricate anatomy of the periodontal ligament and its development: Lessons for periodontal regeneration'. *Journal of Periodontal Research*, 52 (6), pp.965–974.

Judex, S. et al. (2007). 'Low-magnitude mechanical signals that stimulate bone formation in the ovariectomized rat are dependent on the applied frequency but not on the strain magnitude'. *Journal of Biomechanics*, 40 (6), pp.1333–1339.

Jung, H. et al. (2023). 'Functional morphological integration related to feeding biomechanics in the hominine skull'. *Journal of Human Evolution*, 182, p.103401.

Kalisz, K. et al. (2016). 'Artifacts at Cardiac CT: Physics and Solutions'. *RadioGraphics*, 36 (7), pp.2064–2083.

Katsimbri, P. (2017). 'The biology of normal bone remodelling'. *European Journal of Cancer Care*, 26 (6), pp.e12740.

Katz, D. C. et al. (2017). 'Changes in human skull morphology across the agricultural transition are consistent with softer diets in preindustrial farming groups'. *PNAS,* 114 (34), pp.9050–9055.

Keeley, L. H. and Toth, N. (1981). 'Microwear polishes on early stone tools from Koobi Fora, Kenya'. *Nature*, 293 (5832), pp.464–465.

Keyak, J. H. et al. (1990). 'Automated three-dimensional finite element modelling of bone: a new method'. *Journal of Biomedical Engineering*, 12 (5), pp.389–397.

Kiliaridis, S. (1986). 'Masticatory muscle function and craniofacial morphology. An experimental study in the growing rat fed a soft diet'. *Swedish Dental Journal,* 36, pp.1–55.

Kiliaridis, S. et al. (1985). 'The relationship between masticatory function and craniofacial morphology: I. A cephalometric longitudinal analysis in the growing rat fed a soft diet'. *European Journal of Orthodontics*, 7 (4), pp.273–283.

Kiliaridis, S. and Kälebo, P. (1991). 'Masseter muscle thickness measured by ultrasonography and its relation to facial morphology'. *Journal of Dental Research*, 70 (9), pp.1262–1265.

Kimbel, W. H. and Rak, Y. (1985). 'Functional morphology of the asterionic region in extant hominoids and fossil hominids'. *American Journal of Physical Anthropology*, 66 (1).

Kimbel, W. H. et al. (1984). 'Cranial morphology of Australopithecus afarensis: A comparative study based on a composite reconstruction of the adult skull'. *American Journal of Physical Anthropology*, 64 (4), pp.337–388.

Kitai, N. et al. (2002). 'Human masticatory muscle volume and zygomatico-mandibular form in adults with mandibular prognathism'. *Journal of Dental Research*, 81 (11), pp.752–756.

Koc, D. et al. (2012). 'Effects of increasing the jaw opening on the maximum bite force and electromyographic activities of jaw muscles'. *Journal of Dental Sciences*, 7, pp.14–19.

Koc, D. et al. (2010). 'Bite force and influential factors on bite force measurements: a literature review'. *European journal of dentistry*, 4 (2), pp.223–232.

Koolstra, J. H. (2002). 'Dynamics of the Human Masticatory System'. *Critical Reviews in Oral Biology & Medicine*, 13 (4), pp.366–376.

Koolstra, J. H. and van Eijden, T. (1997). 'The jaw open-close movements predicted by biomechanical modelling'. *Journal of Biomechanics*, 30 (9), pp.943–950.

Koolstra, J. H. and van Eijden, T. (2005). 'Combined finite-element and rigid-body analysis of human jaw joint dynamics'. *Journal of Biomechanics*, 38 (12), pp.2431–2439.

Korfage, J. M. and Eijden, T. (1999). 'Regional differences in fibre type composition in the human temporalis muscle'. *The Journal of Anatomy*, 194 (3), pp.355–362.

Kupczik, K. et al. (2007). 'Assessing mechanical function of the zygomatic region in macaques: validation and sensitivity testing of finite element models'. *Journal of Anatomy*, 210 (1), pp.41–53.

Kupczik, K. et al. (2009). 'Masticatory loading and bone adaptation in the supraorbital torus of developing macaques'. *American Journal of Physical Anthropology*, 139 (2), pp.193–203.

Lacruz, R. S. et al. (2019). 'The evolutionary history of the human face'. *Nature ecology & evolution*, 3 (5), pp.726–736.

Lahr, M. M. and Wright, R. V. (1996). 'The question of robusticity and the relationship between cranial size and shape in Homo sapiens'. *Journal of Human Evolution*, 31 (2), pp.157–191.

Laird, M. F. et al. (2016). 'Spatial determinants of the mandibular curve of Spee in modern and archaic Homo'. *American Journal of Physical Anthropology*, 161 (2), pp.226–236.

Laird, M. F. et al. (2023). 'Ontogenetic changes in bite force and gape in tufted capuchins'. *Journal of Experimental Biology*, 226 (15), pp.jeb245972.

Langenbach, G. E. J. and Hannam, A. G. (1999). 'The role of passive muscle tensions in a three-dimensional dynamic model of the human jaw'. *Archives of Oral Biology*, 44 (7), pp.557–573.

Lanyon, L. E. (1993). 'Osteocytes, strain detection, bone modeling and remodeling'. *Calcified Tissue International*, 53 (1), pp.S102–S107.

Lanyon, L. E. and Rubin, C. T. (1984). 'Static vs dynamic loads as an influence on bone remodelling'. *Journal of Biomechanics*, 17 (12), pp.897–905

Ledogar, J. A. et al. (2016a). 'Human feeding biomechanics: performance, variation, and functional constraint's. *PeerJ*, pp.e2242..

Ledogar, J. A. et al. (2016b). 'Mechanical evidence that Australopithecus sediba was limited in its ability to eat hard foods'. *Nature Communications*, 7 (1), pp.10596.

Ledogar, J. A. et al. (2017). 'The Biomechanics of Bony Facial "Buttresses" in South African Australopiths: An Experimental Study Using Finite Element Analysis'. *The Anatomical Record*, 300 (1), pp.171–195.

Ledogar, J. A. et al. (2018). 'Biting mechanics and niche separation in a specialized clade of primate seed predators'. *PLOS ONE*, 13 (1), p.e0190689.

Ledogar, J. A. et al. (2022). 'Mechanical compensation in the evolution of the early hominin feeding apparatus'. *Proceedings of the Royal Society B*, 289 (1977), pp.20220711.

Lee, Y.-K. and Moon, H.-J. (2012). 'Reciprocal influence of masticatory apparatus, craniofacial structure and whole body homeostasis'. *Medical Hypotheses*, 79 (6), pp.761–766.

Lee-Thorp, J. and Sponheimer, M. (2006). 'Contributions of biogeochemistry to understanding hominin dietary ecology'. *American Journal of Physical Anthropology*, 131 (43), pp.131–148.

Lengsfeld, M. et al. (1998). 'Comparison of geometry-based and CT voxel-based finite element modelling and experimental validation'. *Medical Engineering & Physics*, 20 (7), pp.515–522.

Lesciotto, K. M. et al. (2016). 'A morphometric analysis of prognathism and evaluation of the gnathic index in modern humans'. *HOMO*, 67 (4), pp.294–312.

Lewis, R. P. et al. (2001). 'Sex differences in mandibular movements during opening and closing'. *American Journal of Orthodontics and Dentofacial Orthopedics*, 120 (3), pp.294–303.

Lieber, R. L. and Fridén, J. (2000). 'Functional and clinical significance of skeletal muscle architecture'. *Muscle & Nerve*, 23 (11), pp.1647–1666.

Lieberman, D. E. (1995). 'Testing Hypotheses About Recent Human Evolution From Skulls: Integrating Morphology, Function, Development, and Phylogeny'. *Current Anthropology*, 36 (2), pp.159–197.

Lieberman, D. E. (1998). 'Sphenoid shortening and the evolution of modern human cranial shape'. *Nature*, 393 (6681), pp.158–162.

Lieberman, D. E. et al. (2004). 'Effects of food processing on masticatory strain and craniofacial growth in a retrognathic face'. *Journal of Human Evolution*, 46 (6), pp.655–677.

Lieberman, D. E. (2008). 'Speculations about the selective basis for modern human craniofacial form'. *Evolutionary Anthropology*, 17 (1), pp 55–68.

Lieberman, D. E. (2011). *The Evolution of the Human Head*. Harvard University Press, Harvard USA.

Lieberman, D. E. et al. (2004). 'Testing hypotheses about tinkering in the fossil record: the case of the human skull'. *Journal of Experimental Zoology*, 302 (3), pp.284–301.

Lieberman, D. E. et al. (2002). 'The evolution and development of cranial form in Homo sapiens'. *PNAS*, 99 (3), pp.1134–1139.

Lieberman, D. E. et al. (2000). 'The primate cranial base: ontogeny, function, and integration'. *American Journal of Physical Anthropology*, 113 (S31), pp.117–169.

Lindauer, S. J. et al. (1995). 'Condylar movement and mandibular rotation during jaw opening'. *American Journal of Orthodontics and Dentofacial Orthopedics*, 107 (6), pp.573–577.

Lindauer, S. J. et al. (1993). 'Effect of Jaw Opening on Masticatory Muscle EMG-Force Characteristics'. *Journal of Dental Research*, 72 (1), pp.51–55.

Liu, J. et al. (2012). 'The application of muscle wrapping to voxel-based finite element models of skeletal structures'. *Biomechanics and Modeling in Mechanobiology*, 11 (1), pp.35–47.

Lucas, P. W. (2004). *Dental Functional Morphology: How Teeth Work*. Cambridge University Press, Cambridge.

MacDonald, J. W. C. and Hannam, A. G. (1984). 'Relationship between occlusal contacts and jaw-closing muscle activity during tooth clenching: Part I'. *The Journal of Prosthetic Dentistry*, 52 (5), pp.718–729.

Mackenna, B. R. and Turker, K. S. (1983). 'Jaw separation and maximum incising force'. *The Journal of Prosthetic Dentistry*, 49 (5), pp.726–730.

Maddux, S. D. and Franciscus, R. G. (2009). 'Allometric scaling of infraorbital surface topography in Homo'. *Journal of Human Evolution*, 56 (2), pp.161–174.

Manns, A. et al. (1979). 'EMG, bite force, and elongation of the masseter muscle under isometric voluntary contractions and variations of vertical dimension'. *The Journal of Prosthetic Dentistry*, 42 (6), pp.674–682.

Marcián, P. et al. (2021). 'On the limits of finite element models created from (micro) CT datasets and used in studies of bone-implant-related biomechanical problems'. *Journal of the Mechanical Behavior of Biomedical Materials*, 117, pp.104393.

Marinescu, R. et al. (2005). 'Finite-element modeling of the anthropoid mandible: the effects of altered boundary conditions'. *The Anatomical Record*, 283 (2), pp.300–309.

Maughan, R. J., Watson, J. S. and Weir, J. (1983). Strength and cross-sectional area of human skeletal muscle. The Journal of Physiology, 338 (1), pp.37–49. [Online]. Available at: doi:10.1113/jphysiol.1983.sp014658.

May, H. et al. (2018). 'Changes in mandible characteristics during the terminal Pleistocene to Holocene Levant and their association with dietary habits'. *Journal of Archaeological Science: Reports*, 22, pp.413–419.

Mazonakis, M. and Damilakis, J. (2016). 'Computed tomography: What and how does it measure?'. *European Journal of Radiology*, 85 (8), pp.1499–1504.

McHenry, H. M. (1984). 'Relative cheek-tooth size in Australopithecus'. *American Journal of Physical Anthropology*, 64 (3), pp.297–306.

McHenry, H. M. (1994). 'Tempo and mode in human evolution'. *PNAS*, 91 (15), pp.6780–6786.

McIntosh, A. F. and Cox, P. G. (2016). 'The impact of gape on the performance of the skull in chisel-tooth digging and scratch digging mole-rats (Rodentia: Bathyergidae)'. *Royal Society Open Science*, 3 (10), pp.160568.

Meakin, L. B. et al. (2014). 'The Contribution of Experimental in vivo Models to Understanding the Mechanisms of Adaptation to Mechanical Loading in Bone'. *Frontiers in Endocrinology*, 5.

Mellon, S. J. and Tanner, K. E. (2012). 'Bone and its adaptation to mechanical loading: a review'. *International Materials Reviews*, 57 (5), pp.235–255.

Menegaz, R. A. et al. (2010). 'Evidence for the Influence of Diet on Cranial Form and Robusticity'. *The Anatomical Record*, 293 (4), pp.630–641

Menéndez, L. et al. (2014). 'Effect of bite force and diet composition on craniofacial diversification of Southern South American human populations'. *American Journal of Physical Anthropology*, 155 (1), pp.114–127.

Meredith, N. et al. (1996). 'Measurement of the microhardness and young's modulus of human enamel and dentine using an indentation technique'. *Archives of Oral Biology*, 41 (6), pp.539–545.

Merletti, R. and Farina, D. (2016). *Surface Electromyography: Physiology, Engineering, and Applications*. Wiley-IEEE Press, Online.

Metzger, K. A. et al. (2005). 'Comparison of beam theory and finite-element analysis with in vivo bone strain data from the alligator cranium'. *The Anatomical Record*, 283 (2), pp.331–348.

Mitteroecker, P. and Bookstein, F. (2008). 'The Evolutionary role of modularity and integration in the Hominoid cranium'. *Evolution*, 62 (4), pp.943–958.

Mitteroecker, P. and Gunz, P. (2009).' Advances in Geometric Morphometrics'. *Evolutionary Biology*, 36 (2), pp.235–247.

Miyawaki, S. et al. (2001). 'Changes in masticatory muscle activity according to food size in experimental human mastication'. *Journal of Oral Rehabilitation*, 28 (8), pp.778–784.

Moore, C. A. (1993). 'Symmetry of Mandibular Muscle Activity as an Index of Coordinative Strategy'. *Journal of Speech, Language, and Hearing Research*, 36 (6), pp.1145–1157.

Moss, M. L. and Young, R. W. (1960). 'A functional approach to craniology'. *American Journal of Physical Anthropology*, 18 (4), pp.281–292.

Muto, T. et al. (1994). 'The position of the mandibular condyle at maximal mouth opening in normal subjects'. *Journal of Oral and Maxillofacial Surgery*, 52 (12), pp.1269–1272.

Naeije, M. et al. (1989). 'Electromyographic activity of the human masticatory muscles during submaximal clenching in the inter-cuspal position'. *Journal of Oral Rehabilitation*, 16 (1), pp.63–70

Noback, M. L. and Harvati, K. (2015a). 'Covariation in the human masticatory apparatus'. *The Anatomical Record*, 298 (1), pp.64–84.

Noback, M. L. and Harvati, K. (2015b). 'The contribution of subsistence to global human cranial variation'. *Journal of Human Evolution*, 80, pp.34–50.

Norconk, M. et al. (2009). 'Mechanical and Nutritional Properties of Food as Factors in Platyrrhine Dietary Adaptations'. In Garber, P. A. et al. (eds): *South American Primates: Perspectives in the Study of Behavior, Ecology and Conservation*. Springer, New York, pp.279–319.

Norman, B. (1999). Facial prognathism in the hominid and human species.

O'Connor, C. F. et al. (2005). 'Bite force production capability and efficiency in Neandertals and modern humans'. *American Journal of Physical Anthropology*, 127 (2), pp.129–151.

Oeschger, E. S. et al. (2020). 'Number of teeth is associated with facial size in humans'. *Scientific Reports*, 10 (1), pp.1820.

Oettlé, A. C. et al. (2017). 'Ancestral Variations in the Shape and Size of the Zygoma'. *The Anatomical Record*, 300 (1), pp.196–208.

O'Higgins, P. et al. (2011). 'Combining geometric morphometrics and functional simulation: an emerging toolkit for virtual functional analyses.' *Journal of Anatomy*, 218 (1), pp.3–15.

O'Higgins, P. et al. (2012). 'Virtual Functional Morphology: Novel Approaches to the Study of Craniofacial Form and Function'. *Evolutionary Biology*, 39 (4), pp.521–535.

O'Higgins, P. et al. (2019). 'Geometric morphometrics and finite elements analysis: Assessing the functional implications of differences in craniofacial form in the hominin fossil record'. *Journal of Archaeological Science*, 101, pp.159–168.

Oyen, O. J. et al. (1979). 'Browridge structure and function in extant primates and Neanderthals'. *American Journal of Physical Anthropology*, 51 (1), pp.83–95.

Paphangkorakit, J. and Osborn, J. W. (1997). 'Effect of Jaw Opening on the Direction and Magnitude of Human Incisal Bite Forces'. *Journal of Dental Research*, 76 (1), pp.561–567.

Parr, W. C. H. et al. (2012). 'Toward integration of geometric morphometrics and computational biomechanics: New methods for 3D virtual reconstruction and quantitative analysis of Finite Element Models'. *Journal of Theoretical Biology*, 301, pp.1–14.

Parr, W. C. H. et al. (2013). 'Finite element micro-modelling of a human ankle bone reveals the importance of the trabecular network to mechanical performance: New methods for the generation and comparison of 3D models'. *Journal of Biomechanics*, 46 (1), pp.200–205.

Paschetta, C. et al. (2010). 'The influence of masticatory loading on craniofacial morphology: A test case across technological transitions in the Ohio valley'. *American Journal of Physical Anthropology*, 141 (2), pp.297–314.

Paschetta, C. et al. (2016). 'Shifts in subsistence type and its impact on the human skull's morphological integration'. *American Journal of Human Biology*, 28 (1), pp.118–128.

Pearson, O. M. and Lieberman, D. E. (2004). 'The aging of Wolff's "law": ontogeny and responses to mechanical loading in cortical bone'. *American Journal of Physical Anthropology*, 125 (S39), pp.63–99.

Peck, C. C. and Hannam, A. G. (2007). 'Human jaw and muscle modelling'. *Archives of Oral Biology*, 52 (4), pp.300–304.

Peterson, J. and Dechow, P. C. (2002). 'Material properties of the inner and outer cortical tables of the human parietal bone'. *The Anatomical Record*, 268 (1), pp.7–15.

Peterson, J. and Dechow, P. C. (2003). 'Material properties of the human cranial vault and zygoma'. *The Anatomical Record*, 274A (1), pp.785–797.

Peterson, J. et al. (2006). 'Material properties of the dentate maxilla'. *The Anatomical Record*, 288 (9), pp.962–972.

Pierce, S. E. et al. (2008). 'Patterns of morphospace occupation and mechanical performance in extant crocodilian skulls: a combined geometric morphometric and finite element modeling approach'. *Journal of Morphology*, 269 (7), pp.840–864.

Pinhasi, R. et al. (2008). 'Evolutionary changes in the masticatory complex following the transition to farming in the southern Levant'. *American Journal of Physical Anthropology*, 135 (2), pp.136–148.

Plummer, T. W. and Bishop, L. C. (2016). 'Oldowan Hominin Behavior and Ecology at Kanjera South, Kenya'. *Journal of Anthropological Sciences*, 94

Pobiner, B. L. et al. (2008). 'New evidence for hominin carcass processing strategies at 1.5Ma, Koobi Fora, Kenya'. *Journal of Human Evolution*, 55 (1), pp.103–130.

Pope, G. G. (1991). 'Evolution of the zygomaticomaxillary region in the genus Homo and its relevance to the origin of modern humans'. *Journal of Human Evolution*, 21 (3), pp.189–213.

Prado, F. B. et al. (2016). 'Review of In Vivo Bone Strain Studies and Finite Element Models of the Zygomatic Complex in Humans and Nonhuman Primates: Implications for Clinical Research and Practice'. *The Anatomical Record*, 299 (12), pp.1753–1778.

Pröschel, P. A. et al. (2008). 'Motor control of jaw muscles in chewing and in isometric biting with graded narrowing of jaw gape'. *Journal of Oral Rehabilitation*, 35 (10), pp.722–728.

Quiudini, P. R. et al. (2017). 'Differences in bite force between dolichofacial and brachyfacial individuals: Side of mastication, gender, weight and height'. *Journal of Prosthodontic Research*, 61 (3), pp.283–289.

Raadsheer, M. et al. (1999). 'Contribution of jaw muscle size and craniofacial morphology to human bite force magnitude'. *Journal of Dental Research*, 78 (1), pp.31–42.

Raadsheer, M. C. et al. (1996). 'Masseter muscle thickness in growing individuals and its relation to facial morphology'. *Archives of Oral Biology*, 41 (4), pp.323–332.

Rak, Y. (1978). 'The functional significance of the squamosal suture in Australopithecus boisei'. *American Journal of Physical Anthropology*, 49 (1), pp.71–78.

Rak, Y. (1986). 'The Neanderthal: a new look at an old face'. *Journal of Human Evolution*, 15 (3), pp.151–164.

Rak, Y. (1988). 'On variation in the masticatory system of Australopithecus boisei'. In Grine, F (eds): *Evolutionary history of the "robust" australopithecines*. de Gruyter, New York. pp.193–198.

Rak, Y. (2014). *The Australopithecine Face*. Academic Press, New York.

Rak, Y. and Hylander, W. (2003a). 'Neandertal facial morphology and increased jaw gape'. pp.174–174.

Rak, Y. and Marom, A. (2017). 'Opposing Extremes of Zygomatic Bone Morphology: Australopithecus Boisei versus Homo Neanderthalensis'. *The Anatomical Record*, 300 (1), pp.152–159.

Ravosa, M. J. et al. (2008). 'Adaptive Plasticity in the Mammalian Masticatory Complex: You AreWhat, and How, You Eat'. In: Vinyard, C. et al. (Eds): *Primate Craniofacial Function and Biology. Developments In Primatology: Progress and Prospects*. Springer, Boston MA. pp.293–328.

Ravosa, M. J. et al. (2000). 'Stressed out: masticatory forces and primate circumorbital form'. *The Anatomical Record*, 261 (5), pp.173–175.

Rayfield, E. J. et al. (2001). 'Cranial design and function in a large theropod dinosaur'. *Nature*, 409 (6823), pp.1033–1037.

Rayfield, E. J. (2007). 'Finite element analysis and understanding the biomechanics and evolution of living and fossil organisms'. *Annual Review of Earth and Planetary Sciences*, 35 (1), pp.541–576.

Reaz, M. B. I. et al. (2006). 'Techniques of EMG signal analysis: detection, processing, classification and applications'. *Biological Procedures Online*, 8 (1), pp.11–35.

Reed, D. A. et al. (2011). 'The impact of bone and suture material properties on mandibular function in Alligator mississippiensis: testing theoretical phenotypes with finite element analysis'. *Journal of Anatomy*, 218 (1), pp.59–74.

Richmond, B. G. et al. (2005). 'Finite element analysis in functional morphology'. *The Anatomical Record*, 283 (2), pp.259–274.

Richter, D. et al. (2017). 'The age of the hominin fossils from Jebel Irhoud, Morocco, and the origins of the Middle Stone Age'. *Nature*, 546 (7657), pp.293–296.

van Rietbergen, B. et al. (1995). 'A new method to determine trabecular bone elastic properties and loading using micromechanical finite-element models'. *Journal of Biomechanics*, 28 (1), pp.69–81.

Rightmire, G. P. (1988). 'Homo Erectus and Later Middle Pleistocene Humans'. *Annual Review of Anthropology,* 17 (1), pp.239–259.

Rightmire, G. P. (1992). 'Homo erectus: Ancestor or evolutionary side branch?'. *Evolutionary Anthropology*, 1 (2), pp.43–49.

Rightmire, G. P. (1998). 'Evidence from facial morphology for similarity of Asian and African representatives of Homo erectus'. *American Journal of Physical Anthropology*, 106 (1), pp.61–85.

Rightmire, G. P. (2013). 'Homo erectus and Middle Pleistocene hominins: Brain size, skull form, and species recognition'. *Journal of Human Evolution*, 65 (3), pp.223–252.

Rightmire, G. P. et al. (2006). 'Anatomical descriptions, comparative studies and evolutionary significance of the hominin skulls from Dmanisi, Republic of Georgia'. *Journal of Human Evolution*, 50 (2), pp.115–141.

Rightmire, G. P. et al. (2019). 'Variation among the Dmanisi hominins: Multiple taxa or one species?'. *American Journal of Physical Anthropology*, 168 (3), pp.481–495.

Robinson, J. T. (1962a). 'Prehominid dentition and hominid evolution'. In: *Ideas on Human Evolution: Selected Essays, 1949–1961.* Harvard University Press. pp.257–267.

Robinson, J. T. (1962b). 'The genera and species of the Australopithecinae'. In*: Ideas on Human Evolution: Selected Essays, 1949–1961*. Harvard University Press. pp.268–278.

Rohila, A. K. et al. (2012). 'An ultrasonographic evaluation of masseter muscle thickness in different dentofacial patterns'. *Indian Journal of Dental Research*, 23 (6), p.726.

Rosas, A. and Bermúdez De Castro, J. M. (1998). 'On the taxonomic affinities of the Dmanisi mandible (Georgia)'. *American Journal of Physical Anthropology*, 107 (2), pp.145–162.

Ross, C. F. (2001). 'In vivo function of the craniofacial haft: The interorbital "pillar"'. *American Journal of Physical Anthropology*, 116 (2), pp.108–139.

Ross, C. F. (2005). 'Finite element analysis in vertebrate biomechanics'. *The Anatomical Record*, 283 (2), pp.253–258.

Ross, C. F. et al. (2005). 'Modeling masticatory muscle force in finite element analysis: sensitivity analysis using principal coordinates analysis'. *The Anatomical Record*, 283 (2), pp.288–299.

Ross, C. F. et al. (2011). 'In vivo bone strain and finite-element modeling of the craniofacial haft in catarrhine primates'. *Journal of Anatomy*, 218 (1), pp.112–141.

Ross, C. F. and Hylander, W. L. (1996). 'In vivo and in vitro bone strain in the owl monkey circumorbital region and the function of the postorbital septum'. *American Journal of Physical Anthropology*, 101 (2), pp.183–215.

Rowe, A. J. and Rayfield, E. J. (2022). 'The efficacy of computed tomography scanning versus surface scanning in 3D finite element analysis'. *PeerJ*, 10, p.e13760.

Rucci, N. (2008). 'Molecular biology of bone remodelling'. *Clinical Cases in Mineral and Bone Metabolism*, 5 (1), pp.49–56.

Ruff, C. et al. (2006). 'Who's afraid of the big bad Wolff?:"Wolff's law" and bone functional adaptation'. *American Journal of Physical Anthropology*, 129 (4), pp.484–498.

Russell, M. D. et al. (1985). 'The Supraorbital Torus: 'A Most Remarkable Peculiarity'. *Current Anthropology*, 26 (3), pp.337–360.

Santana, S. E. (2016). 'Quantifying the effect of gape and morphology on bite force: biomechanical modelling and in vivo measurements in bats'. *Functional Ecology*, 30 (4), pp.557–565.

Santana, S. E. et al. (2010). ‘Mechanics of bite force production and its relationship to diet in bats’. *Functional Ecology*, 24 (4), pp.776–784.

Sardi, M. L. et al. (2006). ‘Craniofacial morphology in the Argentine center-west: Consequences of the transition to food production’. *American Journal of Physical Anthropology*, 130 (3), pp.333–343.

Sardi, M. L. et al. (2004). ‘The Neolithic transition in Europe and North Africa: The functional craneology contribution’. *Anthropologischer Anzeiger*, pp.129–145.

Sedlmayr, J. C. et al. (2009). ‘The human temporalis muscle: Superficial, deep, and zygomatic parts comprise one structural unit’. *Clinical Anatomy*, 22 (6), pp.655–664.

Sellers, W. I. and Crompton, R. H. (2004). ‘Using sensitivity analysis to validate the predictions of a biomechanical model of bite forces’. *Annals of Anatomy - Anatomischer Anzeiger*, 186 (1), pp.89–95.

Semaw, S. et al. (2020). ‘Co-occurrence of Acheulian and Oldowan artifacts with Homo erectus cranial fossils from Gona, Afar, Ethiopia’. *Science Advances*, 6 (10), pp.eaaw4694.

Shimelmitz, R. et al. (2014). ‘’Fire at will’: The emergence of habitual fire use 350,000 years ago’. *Journal of Human Evolutio*n, 77, pp.196–203.

Shui, W. et al. (2023). ‘A Comparison of Semilandmarking Approaches in the Visualisation of Shape Differences’. *Animals*, 13 (3), p.385.

Sigal, I. A. et al. (2010). ‘Morphing methods to parameterize specimen-specific finite element model geometries’. *Journal of Biomechanics*, 43 (2), pp.254–262.

Sigal, I. A. et al. (2008). ‘Mesh-morphing algorithms for specimen-specific finite element modeling’. *Journal of Biomechanics*, 41 (7), pp.1381–1389.

Simpson, S. M. (2015). ‘Early Pleistocene Homo’. *Basics in Human Evolution*. 143-161.

Skerry, T. M. (2008). ‘The response of bone to mechanical loading and disuse: Fundamental principles and influences on osteoblast/osteocyte homeostasis’. *Archives of Biochemistry and Biophysics*, 473 (2), pp.117–123.

Smith, A. L. et al. (2015a). ‘Biomechanical Implications of Intraspecific Shape Variation in Chimpanzee Crania: Moving Toward an Integration of Geometric Morphometrics and Finite Element Analysis’. *The Anatomical Record*, 298, pp.122–144.

Smith, A. L. et al. (2015b). ‘The Feeding Biomechanics and Dietary Ecology of Paranthropus boisei’. *The Anatomical Record*, 298 (1), pp.145–167.

Smith, A. L. et al. (2021). ‘Comparative biomechanics of the Pan and Macaca mandibles during mastication: finite element modelling of loading, deformation and strain regimes’. *Interface Focus*, 11 (5), pp.20210031.

Smith, A. L. and Grosse, I. R. (2016). ‘The Biomechanics of Zygomatic Arch Shape’. *The Anatomical Record*, 299 (12), pp.1734–1752.

Smith, K. K. (1996). ‘Integration of Craniofacial Structures During Development in Mammals’. *American Zoologist*, 36 (1), pp.70–79.

Smith, R. J. (1978). ‘Mandibular biomechanics and temporomandibular joint function in primates’. *American Journal of Physical Anthropology*, 49 (3), pp.341–349.

Smith, R. J. (1984). ‘Comparative functional morphology of maximum mandibular opening (gape) in primates’. In Chivers, D. et al (eds): *Food acquisition and processing in primates*, Springer, New York, pp.231–255.

Spassov, A. et al. (2017). ‘Congenital muscle dystrophy and diet consistency affect mouse skull shape differently’. *Journal of Anatomy*, 231 (5), pp.736–748.

Spencer, M. A. (1998). 'Force production in the primate masticatory system: electromyographic tests of biomechanical hypotheses'. *Journal of human evolution*, 34 (1), pp.25–54.

Spencer, M. A. (1999). 'Constraints on masticatory system evolution in anthropoid primates'. *American Journal of Physical Anthropology*, 108 (4), pp.483–506.

Spencer, M. A. and Demes, B. (1993). 'Biomechanical analysis of masticatory system configuration in Neandertals and Inuits'. *American Journal of Physical Anthropology*, 91 (1), pp.1–20.

Spencer, M. A. and Ungar, P. S. (2000). 'Craniofacial morphology, diet and incisor use in three native American populations'. *International Journal of Osteoarchaeology*, 10 (4), pp.229–241.

Spoor, F. et al. (2005). 'Correlation of cranial and mandibular prognathism in extant and fossil hominids'. *Transactions of the Royal Society of South Africa*, 60 (2), pp.85–89.

Spronsen, P. H. et al. (1991). 'Relationships between jaw muscle cross-sections and craniofacial morphology in normal adults, studied with magnetic resonance imaging'. *European Journal of Orthodontics*, 13 (5), pp.351–361.

Stansfield, E. et al. (2018). 'A sensitivity study of human mandibular biting simulations using finite element analysis'. *Journal of Archaeological Science: Reports*, 22, pp.420–432.

Stayton, C. T. (2009). 'Application of thin-plate spline transformations to finite element models, or, how to turn a bog turtle into a spotted turtle to analyze both'. *Evolution*, 63 (5), pp.1348–1355.

Strait, D. S. et al. (2005). 'Modeling elastic properties in finite-element analysis: how much precision is needed to produce an accurate model?'. *The Anatomical Record*, 283 (2), pp.275–287.

Strait, D. S. et al. (2009). 'The feeding biomechanics and dietary ecology of Australopithecus africanus'. *PNAS*, 106 (7), pp.2124–2129.

Strait, D. S. et al. (2010). 'The Structural Rigidity of the Cranium of Australopithecus africanus: Implications for Diet, Dietary Adaptations, and the Allometry of Feeding Biomechanics'. *The Anatomical Record*, 293 (4), pp.583–593.

Strait, D. S. et al. (2013). 'Viewpoints: Diet and dietary adaptations in early hominins: The hard food perspective'. *American Journal of Physical Anthropology*, 151 (3), pp.339–355.

Szwedowski, T. D. et al. (2011). 'Sensitivity Analysis of a Validated Subject-Specific Finite Element Model of the Human Craniofacial Skeleton'. *Proceedings of the Institution of Mechanical Engineers*, 225 (1), pp.58–67.

Taylor, A. B. et al. (2009). 'The functional correlates of jaw-muscle fiber architecture in tree-gouging and nongouging callitrichid monkeys'. *American Journal of Physical Anthropology*, 139 (3), pp.353–367.

Taylor, A. B. et al. (2018). 'Jaw-Muscle Fiber Architecture and Leverage in the Hard-Object Feeding Sooty Mangabey are not Structured to Facilitate Relatively Large Bite Forces Compared to Other Papionins'. *The Anatomical Record*, 301 (2), pp.325–342.

Taylor, A. B. and Vinyard, C. J. (2013). 'The relationships among jaw-muscle fiber architecture, jaw morphology, and feeding behavior in extant apes and modern humans'. *American Journal of Physical Anthropology*, 151 (1), pp.120–134.

Teaford, M. F. et al. (2023). 'Changing perspectives on early hominin diets'. *PNAS*, 120 (7), pp.e2201421120.

Terhune, C. E. (2011a). 'Dietary correlates of temporomandibular joint morphology in New World primates'. *Journal of Human Evolution*, 61 (5), pp.583–596.

Terhune, C. E. (2011b). 'Modeling the biomechanics of articular eminence function in anthropoid primates'. *Journal of Anatomy*, 219 (5), pp.551–564.

Terhune, C. E. (2013). 'Dietary correlates of temporomandibular joint morphology in the great apes'. *American Journal of Physical Anthropology*, 150 (2), pp.260–272.

Terhune, C. E. et al. (2015). 'Jaw-muscle architecture and mandibular morphology influence relative maximum jaw gapes in the sexually dimorphic Macaca fascicularis'. *Journal of Human Evolution*, 82, pp.145–158.

Terhune, C. E. et al. (2022). 'Temporomandibular joint shape in anthropoid primates varies widely and is patterned by size and phylogeny'. *The Anatomical Record*, 305 (9), pp.2227–2248.

Terhune, C. E. et al. (2007). 'Variation and diversity in Homo erectus: a 3D geometric morphometric analysis of the temporal bone'. *Journal of Human Evolution*, 53 (1), pp.41–60.

Thockmorton, G. and Dean, J. (1994). 'The relationship between jaw-muscle mechanical advantage and activity levels during isometric bites in humans'. *Archives of Oral Biology*, 39 (5), pp.429–437.

Thomason, J. (1991). 'Cranial strength in relation to estimated biting forces in some mammals'. *Canadian Journal of Zoology*, 69 (9), pp.2326–2333.

Throckmorton, G. S. et al. (1980). 'Biomechanics of differences in lower facial height'. *American Journal of Orthodontics*, 77 (4), pp.410–420.

Tomioka, T. et al. (2009). 'Sarcomere length of torn rotator cuff muscle'. *Journal of Shoulder and Elbow Surgery*, 18 (6), pp.955–959.

Toro-Ibacache, V. et al. (2016). 'Validity and sensitivity of a human cranial finite element model: implications for comparative studies of biting performance'. *Journal of anatomy*, 228 (1), pp.70–84.

Toro-Ibacache, V. et al. (2016). 'The relationship between skull morphology, masticatory muscle force and cranial skeletal deformation during biting'. *Annals of Anatomy-Anatomischer Anzeiger*, 203, pp.59–68.

Toro-Ibacache, V. and O'Higgins, P. (2016). 'The Effect of Varying Jaw-elevator Muscle Forces on a Finite Element Model of a Human Cranium'. *The Anatomical Record*, 299 (7), pp.828–839.

Toro-Ibacache, V. et al. (2015). 'The predictability from skull morphology of temporalis and masseter muscle cross-sectional areas in humans'. *The Anatomical Record*, 298 (7), pp.1261–1270.

Trafí, F. R. et al. (2022). 'Canine fossa and evolution of the human mid-facial bones'. Acta *Anthropologica Sinica*, 41 (02), pp.193.

Travers, K. H. et al. (2000). 'Associations between incisor and mandibular condylar movements during maximum mouth opening in humans'. *Archives of Oral Biology*, 45 (4), pp.267–275.

Trinkaus, E. (2003). 'Neandertal faces were not long; modern human faces are short'. *PNAS*, 100 (14), pp.8142–8145.

Trotter, J. A. (2008). 'Functional Morphology of Force Transmission in Skeletal Muscle: A Brief Review'. *Acta Anatomica*, 146 (4), pp.205–222.

Tseng, Z. J. et al. (2011). 'Model Sensitivity and Use of the Comparative Finite Element Method in Mammalian Jaw Mechanics: Mandible Performance in the Gray Wolf'. *PLOS ONE*, 6 (4), pp.e19171.

Ungar, P. S. et al. (2006). 'Dental microwear and diets of African early Homo'. *Journal of Human Evolution*, 50 (1), pp.78–95.

Ungar, P. S. (2006). *Evolution of the Human Diet: The Known, the Unknown, and the Unknowable*. Oxford University Press, Oxford.

Ungar, P. S. and Sponheimer, M. (2011). 'The Diets of Early Hominins'. *Science*, 334 (6053), pp.190–193.

Van Casteren, A. et al. (2022). ‘The cost of chewing: The energetics and evolutionary significance of mastication in humans’. *Science advances*, 8 (33), pp.eabn8351.

Varrela, J. (1990). ‘Effects of attritive diet on craniofacial morphology: a cephalometric analysis of a Finnish skull sample’. *European Journal of Orthodontics*, 12 (2), pp.219–223.

Varrela, J. (1992). ‘Dimensional variation of craniofacial structures in relation to changing masticatory-functional demands’. *European Journal of Orthodontics*, 14 (1), pp.31–36.

Villmoare, B. et al. (2015). ‘Early Homo at 2.8 Ma from Ledi-Geraru, Afar, Ethiopia’. *Science*, 347 (6228), pp.1352–1355.

Vinckier, A. and Semenza, G. (1998). ‘Measuring elasticity of biological materials by atomic force microscopy’. *FEBS Letters*, 430 (1), pp.12–16.

Vinyard, C. J. et al. (2003). ‘Comparative functional analysis of skull morphology of tree-gouging primates’. *American Journal of Physical Anthropology*, 120 (2), pp.153–170.

Vinyard, C. J. et al. (2008). ‘Patterns of variation across primates in jaw-muscle electromyography during mastication’. *Integrative and Comparative Biology*, 48 (2), pp.294–311.

Walker, A. et al. (1997). ‘Diet and teeth: Dietary hypotheses and human evolution’. *Philosophical Transactions of the Royal Society of London*, 292 (1057), pp.57–64.

Wall, C. E. (1999). ‘A model of temporomandibular joint function in anthropoid primates based on condylar movements during mastication’. *American Journal of Physical Anthropology*, 109 (1), pp.67–88.

Waltimo, A. and Könönen, M. (1993). ‘A novel bite force recorder and maximal isometric bite force values for healthy young adults’. *European Journal of Oral Sciences*, 101 (3), pp.171–175.

Wang, Q. et al. (2010a). ‘Mechanical Impact of Incisor Loading on the Primate Midfacial Skeleton and its Relevance to Human Evolution’. *The Anatomical Record*, 293 (4), pp.607–617.

Wang, Q. et al. (2010b). ‘The Global Impact of Sutures Assessed in a Finite Element Model of a Macaque Cranium’. *The Anatomical Record*, 293, pp.1477–1491.

Ward, S. C. and Molnar, S. (1980). ‘Experimental stress analysis of topographic diversity in early hominid gnathic morphology’. *American Journal of Physical Anthropology*, 53 (3), pp.383–395.

Weber, G. W. and Krenn, V. A. (2017). ‘Zygomatic Root Position in Recent and Fossil Hominids’. *The Anatomical Record*, 300 (1), pp.160–170.

Weijs, W. A. (1989). ‘The functional significance of morphological variation of the human mandible and masticatory muscles’. *Acta morphologica Neerlando-Scandinavica*, 27 (1–2), pp.149–162.

Weijs, W. A. and Hillen, B. (1984a). ‘Relationship between the Physiological Cross-Section of the Human Jaw Muscles and Their Cross-Sectional Area in Computer Tomograms’. *Acta Anatomica*, 118 (3), pp.129–138.

Weijs, W. A. and Hillen, B. (1986a). ‘Correlations between the cross-sectional area of the jaw muscles and craniofacial size and shape’. *American Journal of Physical Anthropology*, 70 (4), pp.423–431.

Weijs, W. and Hillen, B. (1984b). ‘Relationships between masticatory muscle cross-section and skull shape’. *Journal of Dental Research*, 63 (9), pp.1154–1157.

Weijs, W. and Hillen, B. (1985). ‘Cross-sectional areas and estimated intrinsic strength of the human jaw muscles’. *Acta morphologica neerlando-scandinavica*, 23 (3), pp.267–274.

Williams, S. H. et al. (2007). ‘Masticatory motor patterns in ungulates: a quantitative assessment of jaw-muscle coordination in goats, alpacas and horses’. *Journal of Experimental Zoology* 307 (4), pp.226–240.

Wolpoff, M. H. (1974). ‘Sagittal cresting in the South African australopithecines’. *American Journal of Physical Anthropology*, 40 (3), pp.397–408.

Wood, B. (1992). ‘Origin and evolution of the genus Homo’. *Nature*, 355 (6363), pp.783–790.

Wood, B. and Collard, M. (1999a). ‘The changing face of genus Homo’. *Evolutionary Anthropology*, 8 (6), pp.195–207.

Wood, B. and Collard, M. (1999b). ‘The Human Genus’. *Science*, 284 (5411), pp.65–71.

Wood, B. and Strait, D. (2004). ‘Patterns of resource use in early Homo and Paranthropus’. *Journal of Human Evolution*, 46 (2), pp.119–162.

Wood, S. A. et al. (2011). ‘The effects of modeling simplifications on craniofacial finite element models: the alveoli (tooth sockets) and periodontal ligaments’. *Journal of biomechanics*, 44 (10), pp.1831–1838.

Wrangham, R. (2017). ‘Control of Fire in the Paleolithic: Evaluating the Cooking Hypothesis’. *Current Anthropology*, 58 (16), pp.303–313.

Wrangham, R. W. et al. (1999). ‘The Raw and the Stolen: Cooking and the Ecology of Human Origins’. *Current Anthropology,* 40 (5), pp.567–594.

Wright, B. W. (2005). ‘Craniodental biomechanics and dietary toughness in the genus Cebus’. *Journal of Human Evolution*, 48 (5),

Wroe, S. et al. (2010). ‘The craniomandibular mechanics of being human’. *Proceedings of the Royal Society B*, 277 (1700), pp.3579–3586.

Wroe, S. et al. (2018). ‘Computer simulations show that Neanderthal facial morphology represents adaptation to cold and high energy demands, but not heavy biting’. *Proceedings of the Royal Society B*, 285 (1876), pp.20180085.

Wroe, S. and Milne, N. (2007). ‘Convergence and remarkably consistent constraint in the evolution of carnivore skull shape’. *Evolution*, 61 (5), pp.1251–1260.

Yravedra, J. et al. (2020). ‘Mammal butchery by Homo erectus at the Lower Pleistocene acheulean site of Juma’s korongo 2 (JK2), bed III, Olduvai Gorge, Tanzania’. *Quaternary Science Reviews*, 249, pp.106612.

Zink, K. D. and Lieberman, D. E. (2016). ‘Impact of meat and Lower Palaeolithic food processing techniques on chewing in humans’. *Nature*, 531 (7595), pp.500–503.

Zink, K. D. et al. (2014). ‘Food material properties and early hominin processing techniques’. *Journal of Human Evolution*, 77, pp.155–166.

Zollikofer, C. P. E. (2012). ‘Evolution of hominin cranial ontogeny’. In: Hofman, M. A. and Falk, D. (Eds). *Progress in Brain Research: Evolution of the Primate Brain*. Elsevier, Amsterdam. pp.273–292.

6. Appendix 1: modifying the zygomatic region of the *Homo sapiens* specimen using TPS deformations

This appendix outlines how the landmarks (both their position and amount used) within the reference and target landmark datasets of the TPS warp that modified the zygoma region morphology of the *Homo sapiens* specimen to resemble KNM-ER 3733 were determined. This warp was performed using the 'Bookstein' landmark surface module landmark within Avizo.

6.1. TPS warp one

For the first TPS warp, 10 warping landmarks were placed on the surface of the zygoma region of the references (*H. sapiens*) and target (KNM-ER 3733) specimens (10 landmarks were placed in total, 5 on each zygoma region bilaterally; Figure 76). These were chosen to reflect the overall shape of the zygoma region of the reference and target specimen.

As the modifications of the zygoma region of the *H. sapiens* specimen required the force vector of the masseter to be redefined, it was desirable that the spatial position of the other loading and boundary conditions remained the same. Therefore, dense locking landmarks (1306) were placed on the glenoid fossae, maxillary dentition, lateral pterygoid plates of the sphenoid bone, and the temporal fossa.

The anterior face of the maxilla of the reference specimen was also locked for the first TPS warp (Figure 72). This is because much of the of the maxilla of KNM-ER 3733 is absent meaning the form of the maxillary sinus of the target specimen and importantly the thickness of the cortical bone surrounding this is unknown. If the warp thinned of the walls of the maxillary sinus reconstructing this without reference as to how thick this structure is in KNM-ER 3733 would be undesirable as previous sensitivity studies that have demonstrated the thickness of cortical bone structures in cranial and mandibular FE models can impact their predictions (Szwedowski et al. 2011; Parr et al. 2012; Fitton et al. 2015; Toro-Ibacache et al. 2016). This warp was also attempted without these landmarks (see section 6.4).

Overall, this warp produced a warped surface with poor correspondence to KNM-ER 3733 (Figure 73). While the lateral positioning of the zygomatic arch in KNM-ER 3733 was represented in the deformed surface, the zygomatic bodies were more laterally flaring and

anteriorly projecting than those of KNM-ER 3733. Additionally, the superior-inferior height of the anterior zygomatic arch of the deformed surface is greater than what is observed in KNM-ER 3733 (Figure 73). The results of this warp demonstrated that additional landmarks needed to be added to the reference and target landmark datasets to better capture the zygoma region morphology of KNM-ER 3733 in the deformed surface.

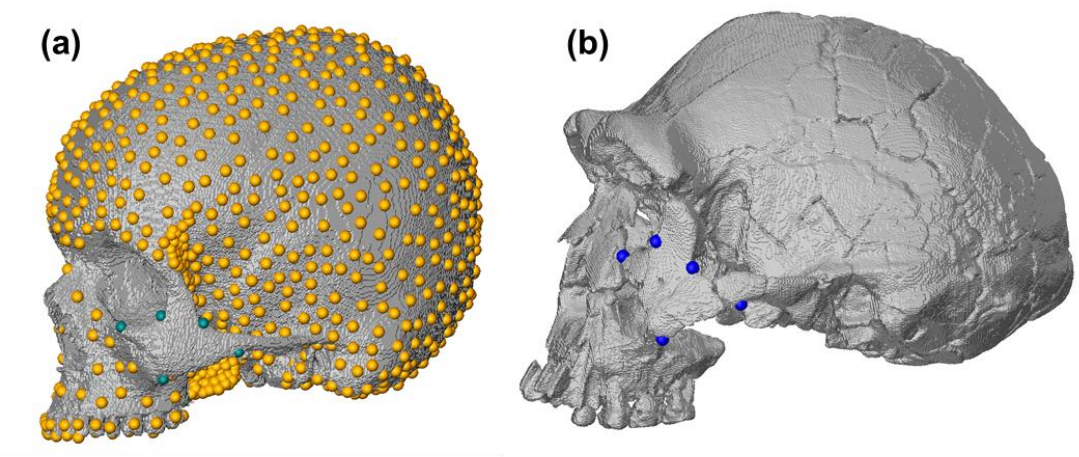

Figure 72. The locking and warping landmarks used for warp one. (a) The reference surface with the locking (orange) and reference warping (teal) landmarks. (b) The target surface with the target warping landmarks (dark blue).

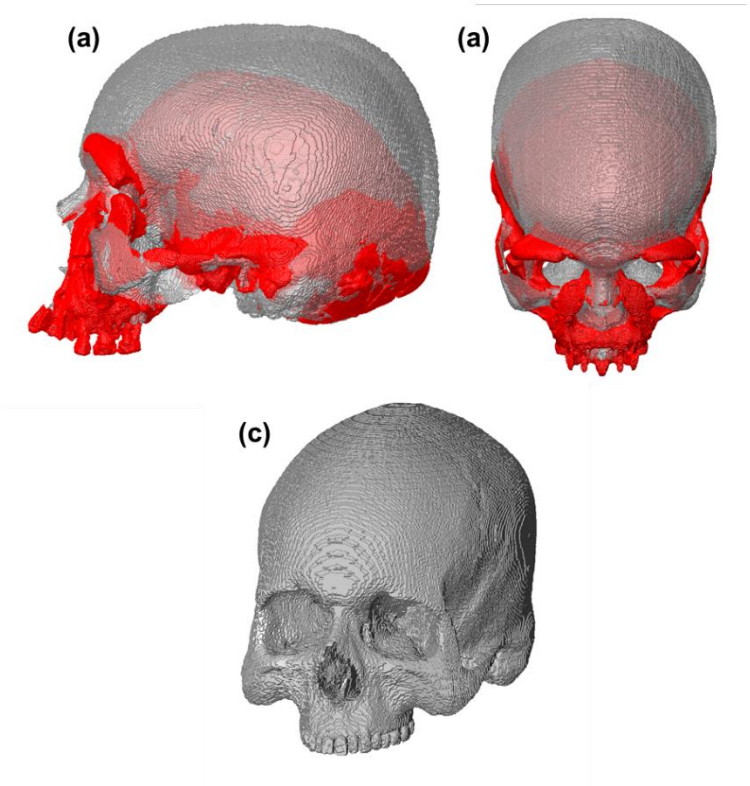

Figure 73. The deformed surface produced by TPS warp one and its correspondence to KNM-ER 3733. (a) Lateral view of the deformed surface (grey) superimposed on KNM-ER 3733 (red). (a) Superior view of the deformed surface superimposed on KNM-ER 3733. (c) Oblique view of the deformed surface.

6.2. TPS warp two

The results of the previously performed TPS warp demonstrated the need for additional warping landmarks to be added to the reference and target landmark datasets used within the TPS warp. Therefore, the warp was performed again with 4 new warping landmarks placed on the zygoma regions of the reference and target specimens (14 landmarks were placed in total, 7 on each side; Figure 74). The locking landmarks remained identical to those used in the previous warp (1306 were used in total; Figure 74). The new warping landmarks were chosen to better capture the differences in the topography, width, and height of the zygomatic bodies between the target and reference surfaces.

The addition of these landmarks to the reference and target landmark datasets used to perform the warp produced a better correspondence between the deformed surface and KNM-ER 3733 (Figure 75). The overly exaggerated lateral flare and anterior projection of the zygomatic bodies seen in the previous attempt were mostly reduced, aside from locally to the

infraorbital rims (Figure 75). The increased superior-inferior height of the anterior zygomatic arches was reduced (Figure 75).

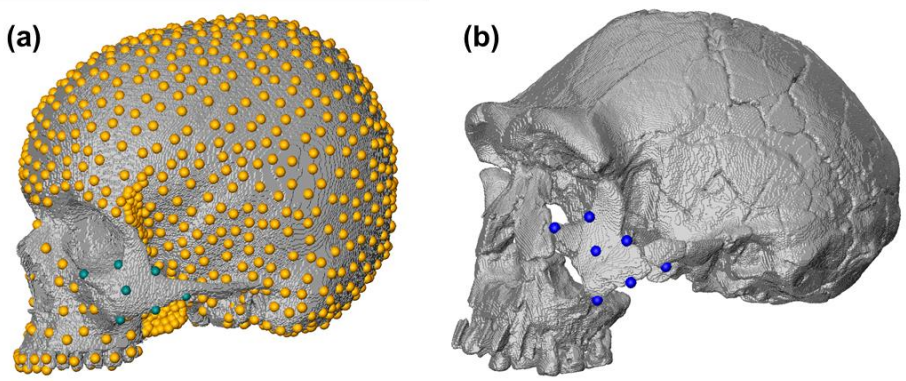

Figure 74. The locking and warping landmarks used for warp two. (a) The reference surface with the locking (orange) and reference warping (teal) landmarks. (b) The target surface with the target warping landmarks (dark blue).

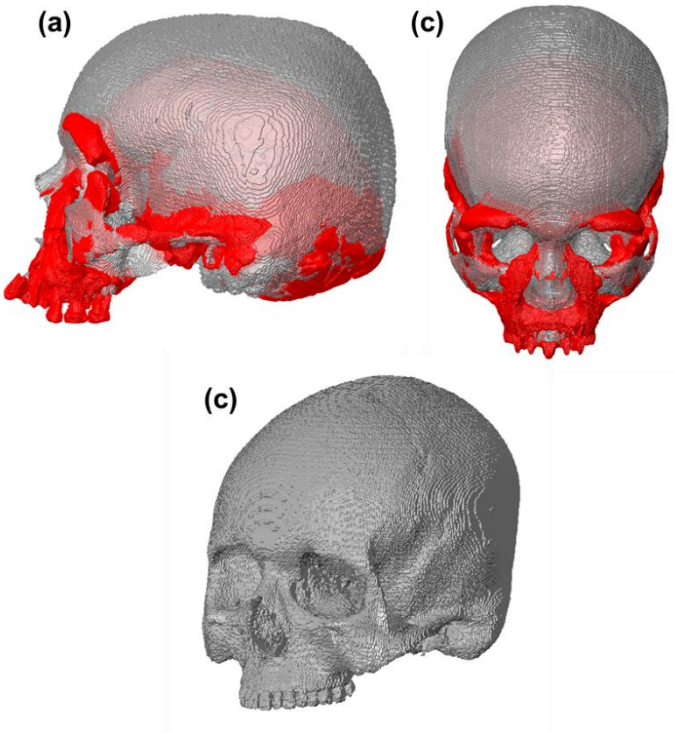

Figure 75. The deformed surface produced by TPS warp two and its correspondence to KNM-ER 3733. (a) Lateral view of the deformed surface (grey) superimposed on KNM-ER 3733 (red). (a) Superior view of the deformed surface superimposed on KNM-ER 3733. (c) Oblique view of the deformed surface.

6.3. TPS warp three: deforming the frontal process of the zygoma

The frontal process of the zygoma of KNM-ER 377 is more anterolaterally oriented than that of *H. sapiens* (Antón and Middleton 2023). As such, consideration was given as to whether this region could be modified without altering the spatial position of the post-orbital attachment of the temporalis.

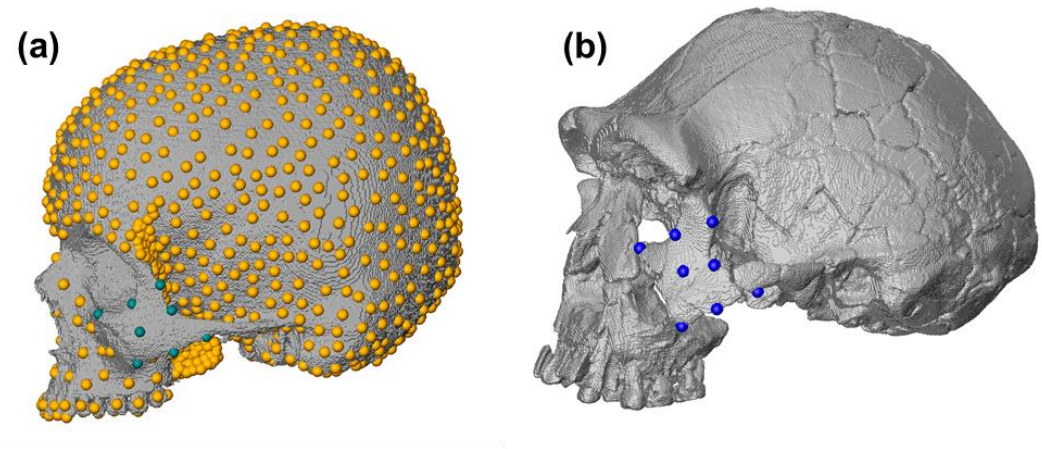

Figure 76. The locking and warping landmarks used for warp three. (a) The reference surface with the locking (orange) and reference warping (teal) landmarks. (b) The target surface with the target warping landmarks (dark blue).

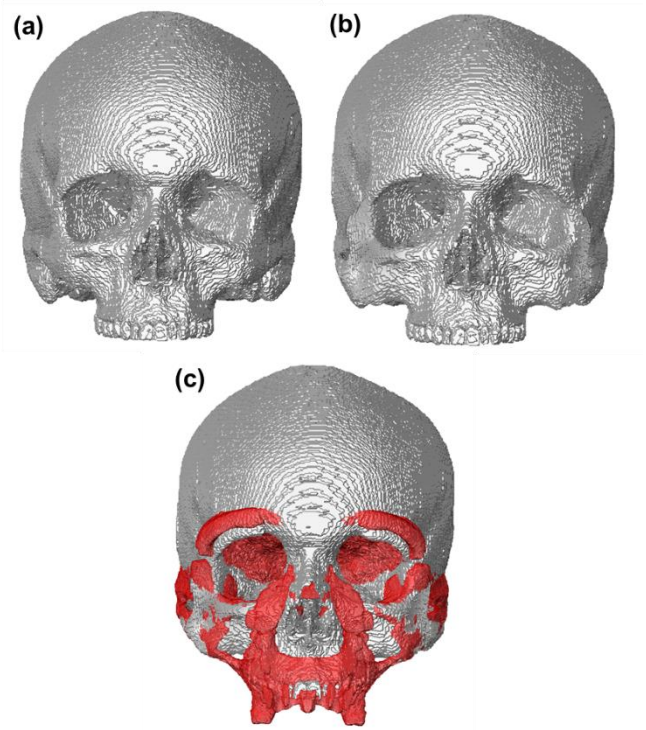

Figure 77. The deformed surface produced by TPS warp three and its correspondence to KNM-ER 3733. (a) Frontal view of the *Homo sapiens* surface. (a) Frontal view of the deformed surface. (c) Frontal view of the deformed surface superimposed on KNM-ER 3733 (red).

Therefore, the warp was attempted again, including warping landmarks to deform the frontal process of the zygoma (Figure 76). One landmark on the posterior most point of the frontal process of the zygoma bilaterally was added to the warping landmarks placed on the surface of the reference and target specimens (16 landmarks were placed in total, 8 on each side of the cranium; Figure 76). The locking landmarks remained identical to those used in the previous warps (1306 were used in total; Figure 76).

Overall, this warp produced a specimen wherein the inferior half of the frontal process of the zygoma was considerably more laterally flaring than its superior half, with the mediolateral width of the structure bottlenecking close to the frontotemporal suture (Figure 77). This was undesirable as this is not reflective of the upper facial morphology KNM-ER 3733. Therefore, the frontal process of the zygoma was not deformed directly by placing warping landmarks on this structure. However, as the zygomatic bodies of the target specimen are more laterally flaring than those of the reference specimen, the TPS warp interpolates some degree of anterolateral projection to the upper face in correspondence with the extent to this is observed within the rest of the zygomatic region as locking landmarks are not placed in this

region. This is a desirable solution as this prevented any alterations to spatial position of the postorbital attachment of the temporalis, while still allowing some degree of *Homo ergaster*-like anterolateral orientation to the frontal process of the zygoma being captured in the warped surface.

6.4. TPS warp four: assessing the impacts of locking the anterior face of the maxilla

For TPS warp two (see section 6.2), locking landmarks were placed on the anterior face of the maxilla to prevent this from being deformed due to its absence KNM-ER 3733. However, the impacts of including or excluding these locking landmarks were explored before the modified FE model was constructed. This was to assess whether the anterior projection of the midface of KNM-ER 3733 could be reflected into the warped surface.

To achieve this, the locking landmarks on the anterior face and zygomatic process of the maxilla were removed from the reference and target landmark datasets used in warp attempt 2 (Figure 78. Thus 1299 locking landmarks were used for this warp, compared to the 1306 used for warp two. The same warping landmarks as used within section 6.2 were used for this warp (14 landmarks were placed on the reference and target specimens, 7 on each side of the face; Figure 74 and Figure 78).

The differences between the warped surfaced produced by warps two and four were subtle (Figure 79). However, warp four produced a slightly flatter infraorbital profile where the anterior projection of the zygomatic bodies and anterior face of the maxilla were comparable, whereas warp two produced an infraorbital profile where the zygomatic bodies projected slightly more anteriorly than the anterior face of the maxilla (Figure 79). Furthermore, warp four reduced the overly increased anterior projection of the zygomatic bodies locally to the infraorbital margin seen in the deformed surface produced by warp two (see section 6.2). This warp (four) therefore better reflected the infraorbital flatness of *H. ergaster* than warp two (Figure 78).

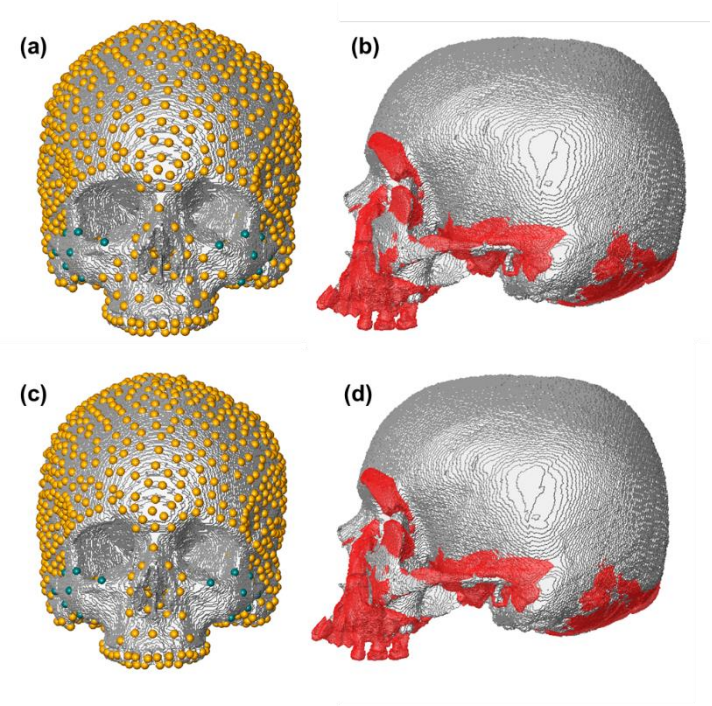

Figure 78. The locking (yellow) and reference warping (teal) landmarks used for warp two compared to those used for warp four. (a) Frontal view of the reference surface with the locking and warping landmarks used for warp two. (b) Lateral view of the deformed surface produced by warp two superimposed on KNM-ER 3733 (red). (c) Frontal view of the reference surface with the locking and warping landmarks used for warp four. (b) Lateral view of the deformed surface produced by warp four superimposed on KNM-ER 3733 (red).

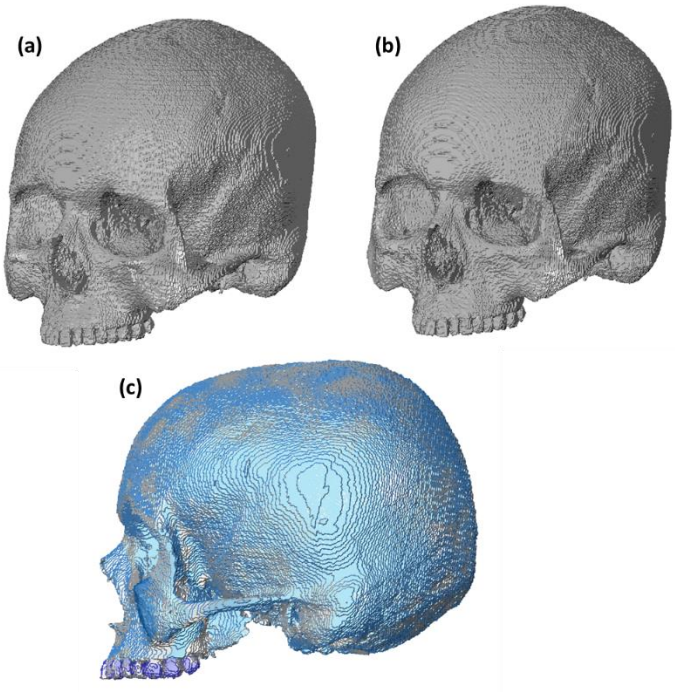

Figure 79. The deformed surfaces produced by warp attempt two versus warp attempt four. (a) Oblique view of the deformed surface produced by warp two. (b) Oblique view of the deformed surface produced by warp

four. (c) Lateral view of the deformed surface produced by warp two (blue) superimposed on the surface produced by warp four (grey).

The rationale behind locking the anterior face of the maxilla was to not alter the maxillary sinus morphology of the specimen in a manner not reflective of KNM-ER 3733, as this anatomy is absent in this fossil. To inspect if the maxillary sinus had been altered by warp attempt four, the deformed surface was converted into a volume file using the 'scan surface to volume' module within Avizo (with a voxel resolution of 0.566507 x 0.566507 x 0.566507 mm^3), and the form of the sinus was inspected within the segmentation editor. This revealed the warp had not significantly altered the shape of the maxillary sinus (Figure 80), and the walls of the maxillary sinus were not artificially thinned. Thus the potential limitations associated with reconstructing the thickness of the sinus walls without this anatomy being preserved in KNM-ER 3733 (see section 6.1) were avoided.

Thus, given that the external form of the deformed surface produced by TPS warp four produced the best correspondence to KNM-ER 3733 of the four warp attempts described above, it was decided that this was the most suitable specimen to be used to create the modified *H. sapiens* FE model used within the experimental FEA component of this thesis.

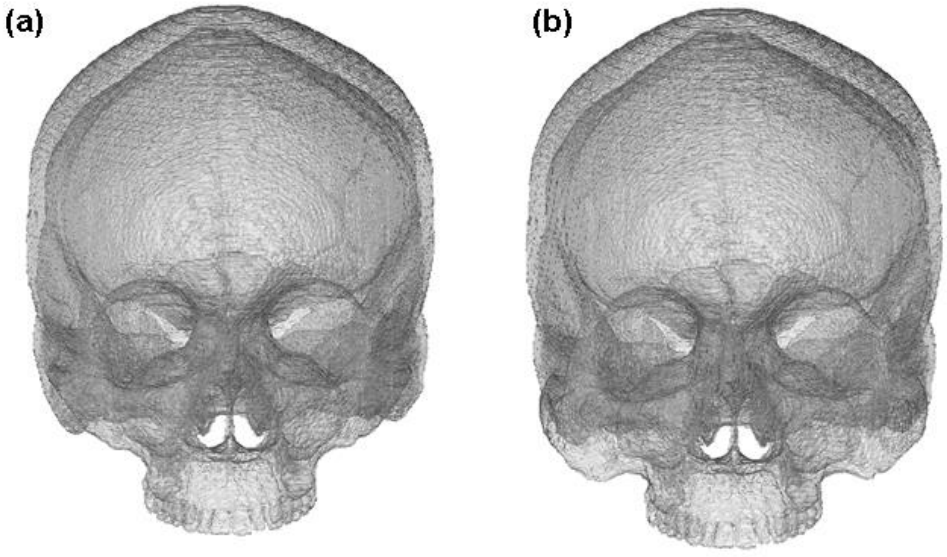

Figure 80. Partially transparent surface renderings of the surface of the *H. sapiens* specimen (a) and the deformed surface produced by TPS warp four (b).